AREVA

FINAL SAFETY ANALYSIS REPORT FOR THE NUHOMS® HD HORIZONTAL MODULAR STORAGE SYSTEM FOR IRRADIATED NUCLEAR FUEL

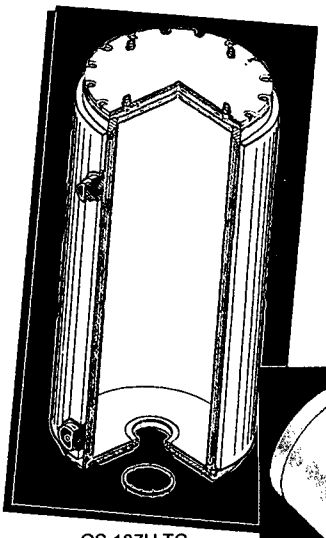

OS 187H TC

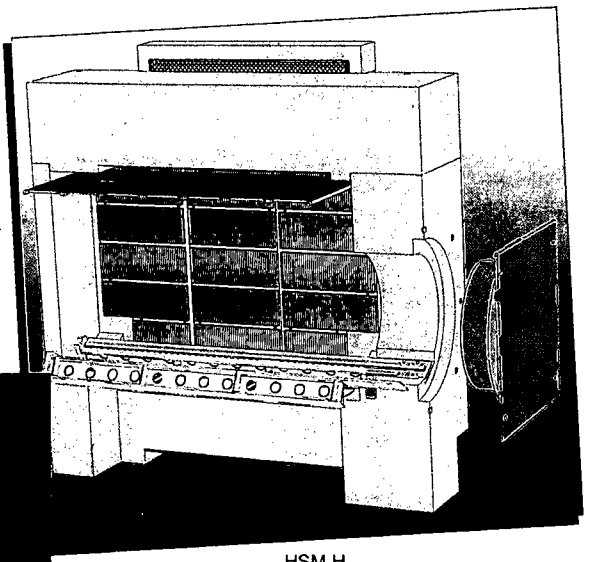

HSM-H

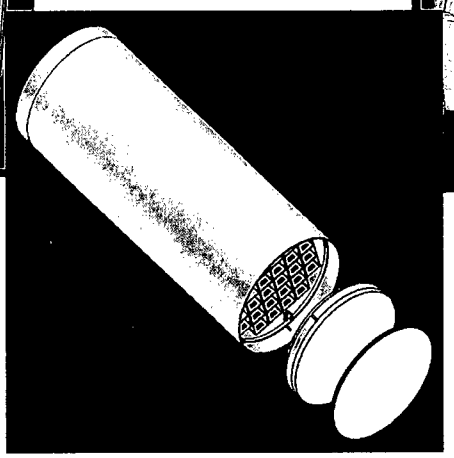

32PTH DSC

NON-PROPRIETARY

VOLUME 2 OF 3

TRANSNUCLEAR INC.

TABLE OF CONTENTS

1. GENERAL INFORMATION 1-1

1.1 Introduction 1-2

1.2 General Description of the NUHOMS® HD System 1-4

1.2.1 NUHOMS® HD System Characteristics 1-4
1.2.2 Operational Features 1-7
1.2.3 32PTH DSC Contents 1-12

1.3 Identification of Agents and Contractors 1-13

1.4 Generic Cask Arrays 1-14

1.5 Supplemental Data 1-15

1.5.1 References 1-15
1.5.2 Drawings 1-15

2. PRINCIPAL DESIGN CRITERIA 2-1

2.1 Spent Fuel to be Stored 2-1

2.1.1 Detailed Payload Description 2-1

2.2 Design Criteria for Environmental Conditions and Natural Phenomena 2-4

2.2.1 Tornado and Wind Loadings 2-4
2.2.2 Water Level (Flood) Design 2-6
2.2.3 Seismic Design 2-7
2.2.4 Snow and Ice Loadings 2-7
2.2.5 Tsunami 2-7
2.2.6 Lightning 2-7
2.2.7 Combined Load Criteria 2-8
2.2.8 Burial under Debris 2-9
2.2.9 Thermal Conditions 2-9

2.3 Safety Protection Systems 2-11

2.3.1 General 2-11
2.3.2 Protection by Multiple Confinement Barriers and Systems 2-11
2.3.3 Protection by Equipment and Instrumentation Selection 2-13
2.3.4 Nuclear Criticality Safety 2-13
2.3.5 Radiological Protection 2-14
2.3.6 Fire and Explosion Protection 2-15
2.3.7 Acceptance Tests and Maintenance 2-16

2.4 Decommissioning Considerations 2-17

2.5 Structures, Systems and Components Important to Safety 2-18

2.5.1 Dry Shielded Canister 2-18
2.5.2 Horizontal Storage Module 2-18
2.5.3 ISFSI Basemat and Approach Slabs 2-19
2.5.4 Transfer Equipment 2-19
2.5.5 Auxiliary Equipment 2-19

2.6 References 2-20

3. STRUCTURAL EVALUATION 3-1

3.1 Structural Design 3-1

3.1.1 Discussion 3-1
3.1.2 Design Criteria 3-10

3.2 Weights 3-13

3.2.1 32PTH DSC Weight 3-14
3.2.2 OS187H Transfer Cask Weight 3-15
3.2.3 HSM-H Weight 3-16

3.3 Mechanical Properties of Materials 3-17

3.3.1 32PTH DSC Material Properties 3-17
3.3.2 HSM-H Material Properties 3-18
3.3.3 OS187H Transfer Cask Material Properties 3-19

3.4 General Standards for 32PTH DSC, HSM-H, and OS187H Transfer Cask. 3-20

3.4.1 Chemical and Galvanic Reactions 3-20
3.4.2 Positive Closure 3-25
3.4.3 Lifting Devices 3-26
3.4.4 Heat 3-26
3.4.5 Cold 3.26

3.5 Fuel Rods General Standards for 32PTH DSC 3-27

3.5.1 Fuel Rod Temperature Limits 3-27
3.5.2 Fuel Assembly Thermal and Irradiation Growth 3-27
3.5.3 Fuel Rod Integrity during Drop Scenario 3-29
3.5.4 Fuel Unloading 3-32

3.6 Normal Conditions of Storage and Transfer 3-33

3.6.1 32PTH DSC Normal Conditions Structural Analysis 3-33
3.6.2 HSM-H Normal Conditions Structural Analysis 3-37
3.6.3 OS187H Transfer Cask Normal Conditions Structural Analysis 3-38

3.7 Off Normal and Hypothetical Accident Conditions 3-41

3.7.1 32PTH DSC Off-Normal and Accident Conditions Structural Analysis 3-41
3.7.2 HSM-H Off-Normal and Accident Conditions Structural Analysis 3-49

3.7.3 OS187H Transfer Cask Off-Normal and Accident Conditions Structural Analysis 3-50

3.8 References 3-54

3.9 Appendices 3-57
3.9.1 32PTH DSC (Canister and Basket) structural Analysis 3.9.1-1
3.9.2 OS187H Transfer Cask Body Structural Analysis 3.9.2-1
3.9.3 OS187H Transfer Cask Top Cover and RAM Access Cover Bolts Analyses 3.9.3-1
3.9.4 OS187H Transfer Cask Lead Slump and Inner Shell Buckling Analyses 3.9.4-1
3.9.5 OS187H Transfer Cask Trunnion Analysis 3.9.5-1
3.9.6 OS187H Transfer Cask Shield Panel Structural Analysis 3.9.6-1
3.9.7 OS187H Transfer Cask Impact Analysis 3.9.7-1
3.9.8 Damaged Fuel Cladding Structural Evaluation 3.9.8-1
3.9.9 HSM-H Structural Analysis 3.9.9-1
3.9.10 OS187H Transfer Cask Dynamic Impact Analysis 3.9.10-1
3.9.11 32PTH DSC Dynamic Impact Analysis 3.9.11-1

3.10 ASME Code Alternatives 3-58

4. THERMAL EVALUATION 4-1

4.1 Discussion 4-1

4.2 Summary of Thermal Properties of Materials 4-3

4.3 Thermal Evaluation for Normal and Off-Normal Conditions 4-9
4.3.1 Thermal Models for Normal and Off-Normal Conditions 4-9
4.3.2 Maximum Temperatures for Normal and Off-Normal Conditions 4-20
4.3.3 Minimum Temperatures for Normal and Off-Normal Conditions 4-20
4.3.4 Maximum Internal Pressures for Normal and Off-Normal Conditions 4-20
4.3.5 Maximum Thermal Stresses for Normal and Off-Normal Conditions 4-20
4.3.6 Evaluation of Thermal Performance for Normal and Off-Normal Conditions 4-20

4.4 Thermal Evaluation for Accident Conditions 4-22
4.4.1 Thermal Models for Accident Conditions 4-22
4.4.2 Maximum Temperatures for Accident Conditions 4-27
4.4.3 Maximum Internal Pressures for Accident Conditions 4-28
4.4.4 Maximum Thermal Stresses for Accident Conditions 4-28
4.4.5 Evaluation of Thermal Performance for Accident Conditions 4-28

4.5 Thermal Evaluation for Loading and Unloading Conditions 4-29
4.5.1 Vacuum Drying 4-29

4.5.2 Reflooding 4-34

4.6 Maximum Internal Pressure 4-36

4.6.1 Average Gas Temperature 4-36
4.6.2 Amount of Initial Helium Backfill 4-37
4.6.3 Free Gas within Fuel Assemblies / BPRA 4-38
4.6.4 Total Amount of Gases within DSC 4-38
4.6.5 Maximum DSC Internal Pressures 4-38
4.6.6 Maximum Pressure in Annulus 4-39

4.7 Axial Decay Heat Profile 4-40

4.8 Effective Fuel Properties 4-43

4.8.1 Discussion 4-43
4.8.2 Summary of Material Properties 4-43
4.8.3 Effective Fuel Conductivity 4-45
4.8.4 Effective Fuel Density and Specific Heat 4-46
4.8.5 Conclusion 4-47

4.9 Effective Conductivity of Fluids in the Transfer Cask 4-48

4.9.1 Effective Conductivity in the Shielding Panel 4-48
4.9.2 Effective Water Conductivity in Annulus between TC and DSC 4-50

4.10 Justification of the Assumed Hot Gap Sizes 4-52

4.10.1 Radial Gap between Basket Rails and DSC shell 4-52
4.10.2 Radial Gap between Lead and the Cask Structural Shell 4-53

4.11 Heat Transfer Coefficients 4-55

4.11.1 Total heat Transfer Coefficient to Ambient 4-55
4.11.2 Free Convection Coefficients 4-55

4.12 Effective Conductivity of Air in Closed Cavity of HSM-H 4-63

4.13 Thermal-Hydraulic Equations for the HSM-H 4-65

4.14 Thermal Evaluation of DSC Containing Damaged Fuel 4-68

4.14.1 Normal / Off-Normal Conditions 4-68
4.14.2 Accident Conditions 4-68
4.14.3 Effective Properties of Damaged Fuel 4-70
4.14.4 Evaluation of DSC Thermal Performance with Damaged Fuel 4-71

4.15 References 4-73

4.16 Appendices 4-75

5. SHIELDING EVALUATION 5-1

5.1. Discussion and Results **5-2**

5.2 Source Specification **5-3**

5.2.1 Gamma Sources 5-5
5.2.2 Neutron Source 5-5

5.3 Model Specification **5-6**

5.3.1 Description of the Radial and Axial Shielding Configurations 5-6
5.3.2 Shield Regional Densities 5-7

5.4 Shielding Evaluation **5-9**

5.4.1 Computer Programs 5-9
5.4.2 Spatial Source Distribution 5-9
5.4.3 Cross-Section Data 5.10
5.4.4 Flux-to-Dose-Rate Conversion 5.10
5.4.5 Model Geometry 5-10
5.4.6 Methodology 5-10
5.4.7. Assumptions 5-11
5.4.8 Normal Condition Models 5-12

5.5 Supplemental Information **5-15**

5.5.1 References 5-15
5.5.2 Sample Input Files 5-17

6. CRITICALITY EVALUATION 6-1

6.1 Discussion and Results **6-2**

6.2 Spent Fuel Loading **6-4**

6.3 Model Specification **6-5**

6.3.1 Description of Criticality Analysis Model 6-5
6.3.2 Package Regional Densities 6-7

6.4 Criticality Calculation **6-8**

6.4.1 Calculational Method 6-8
6.4.2 Fuel Loading Optimization 6-13
6.4.3 Criticality Results 6-22

6.5 Critical Benchmark Experiments **6-23**

6.5.1 Benchmark Experiments and Applicability 6-23
6.5.2 Results of the Benchmark Calculations 6-24

6.6 Supplemental Information **6-25**

6.6.1 References 6-25
6.6.2 KENO Input Files 6-27

7. CONFINEMENT **7-1**

7.1 Confinement Boundary 7-1

7.1.1 Confinement Vessel 7-1
7.1.2 Confinement Penetrations 7-2
7.1.3 Seals and Welds 7-2
7.1.4 Closure 7-2

7.2 Requirements for Normal Conditions of Storage 7-3

7.2.1 Release of Radioactive Material 7-3
7.2.2 Pressurization of Confinement Vessel 7-3

7.3 Confinement Requirements for Hypothetical Accident Conditions 7-4

7.3.1 Fission Gas Products 7-4
7.3.2 Release of Contents 7-4

7.4 Supplemental Data 7-5

7.4.1 Confinement Monitoring Capability 7-5
7.4.2 References 7-5

8. OPERATING PROCEDURES 8-1

8.1 Procedures for Loading the DSC and Transfer to the HSM-H 8-1

8.1.1 Narrative Description 8-1

8.2 Procedures for Unloading the DSC 8-10

8.2.1 DSC Retrieval from the HSM-H 8-10
8.2.2 Removal of Fuel from the DSC 8-11

8.3 Supplemental Information 8-14

8.3.1 Other Operating Systems 8-14
8.3.2 Operation Support System 8-14
8.3.3 Surveillance and Maintenance 8-14

8.4 References 8-15

9. ACCEPTANCE TESTS AND MAINTENANCE PROGRAM 9-1

9.1 Acceptance Criteria 9-1

9.1.1 Visual inspection and Non-Dectructive Examination (NDE) 9-1
9.1.2 Structural and Pressure tests 9-1
9.1.3 Leak Tests 9-1
9.1.4 Components 9-2
9.1.5 Shielding Integrity 9-2
9.1.6 Thermal Acceptance 9-2
9.1.7 Neutron Absorber Tests 9-3

9.2 Maintenance Program 9-5

9.2.1 Inspection 9-5
9.2.2 Tests 9-5
9.2.3 Repair, Replacement and Maintenance 9-6

9.3 Marking 9-6

9.4 Pre-Operational Testing and Training Exercise 9-6

9.5 Specification for Neutron Absorbers 9-7

9.5.1 Specification for Thermal Conductivity Testing of Neutron Absorbers . 9-7
9.5.2 Specification for Acceptance Testing of Neutron Absorbers by Neutron Transmission 9-8
9.5.3 Specification for Qualification testing of Metal Matrix Composites 9-9
9.5.4 Specification for Process Controls for Metal Matrix Composites 9-12

9.6 REFERENCES 9-14

10. RADIATION PROTECTION 10-1

10.1 Ensuring That Occupational Radiation Exposures Are As Low As Reasonably Achievable (ALARA) 10-1

10.1.1 Policy Considerations 10-1
10.1.2 Design Considerations 10-1
10.1.3 Operational Considerations 10-3

10.2 Radiation Protection Design Features 10-4

10.2.1 NUHOMS® System Design Features 10-4
10.2.2 Offsite Dose Calculations 10-4

10.3 Estimated Onsite Collective Dose Assessment 10-8

10.3.1 DSC Loading, Transfer and Storage Operations 10-8
10.3.2 DSC Retrieval Operations 10-8
10.3.3 Fuel Unloading Operations 10-9
10.3.4 Maintenance Operations 10-9
10.3.5 Doses During ISFSI Array Expansion 10-9

10.4 References 10-10

11. Accident Analysis 11-1

11.1 Introduction 11-1

11.2 Off-Normal Operation 11-2

11.2.1 Off-Normal Transfer Load 11-3

11.2.2 Extreme Temperature 11-5
11.2.3 Radiological Impact from Off-Normal Operation 11-6

11.3 Postulated Accident 11-7

11.3.1 Cask Drop 11-8
11.3.2 Earthquake 11-10
11.3.3 Tornado Wind and Tornado Missiles Effect on HSM-H 11-11
11.3.4 Tornado Wind and Tornado Missiles Effect on Transfer Cask 11-18
11.3.5 Flood 11-25
11.3.6 Blockage of HSM-H Air Inlet and Outlet Opening 11-25
11.3.7 Lightning 11-26
11.3.8 Fire/Explosion 11-27

11.4 References 11-28

12. OPERATING CONTROLS AND LIMITS 12-1

13. QUALITY ASSURANCE 13-1

13.1 Introduction 13-2

13.2 "Important-to-Safety & "Safety Related" NUHOMS® HD System Components 13-3

13.3 Description of TN 10CFR 72, Subpart G QA Program 13-5

13.3.1 Project Organization 13-5
13.3.2 QA Program 13-5
13.3.3 Design Control 13-5
13.3.4 Procurement Document Control 13-6
13.3.5 Procedures, Instructions, and Drawings 13-6
13.3.6 Document Control 13-6
13.3.7 Control of Purchased Items and Services 13-6
13.3.8 Identification and Control of Materials, Parts, and Components 13-7
13.3.9 Control of Special Processes 13-7
13.3.10 Inspection 13-7
13.3.11 Test Control 13-7
13.3.12 Control of Measuring and Test Equipment 13-7
13.3.13 Handling, Storage and Shipping 13-7
13.3.14 Inspection and Test Status 13-8
13.3.15 Control of Nonconforming Items 13-8
13.3.16 Corrective Action 13-8
13.3.17 Records 13-8
13.3.18 Audits and Surveillances 13-8

13.4 Conditions of Approval Records 13-9

13.5 Supplemental Information 13-10
13.5.1 References 13-10

14. DECOMMISSIONING **14-1**
14.1 Decommissioning Considerations **14-1**

14.2 Supplemental Information **14-4**

14.2.1 References 14-4

APPENDIX 3.9.4
OS187H TRANSFER CASK LEAD SLUMP AND INNER SHELL BUCKLING ANALYSIS

TABLE OF CONTENTS

3.9.4 OS187H TRANSFER CASK LEAD SLUMP AND INNER SHELL BUCKLING ANALYSIS 3.9.4-1

3.9.4.1 Introduction 3.9.4-1

3.9.4.2 Material Properties 3.9.4-2

3.9.4.3 Finite Element Model 3.9.4-6

3.9.4.4 FEA Results 3.9.4-11

3.9.4.5 Conclusions 3.9.4-12

3.9.4.6 References 3.9.4-13

LIST OF FIGURES

3.9.4-1 Loads and Boundary Conditions for Transfer Cask Bottom End Drop Model (Top End, 115° F Ambient Case)

3.9.4-2 Loads and Boundary Conditions for Transfer Cask Bottom End Drop Model (Bottom End, 115° F Ambient Case)

3.9.4-3 Loads and Boundary Conditions for Transfer Cask Bottom End Drop Model (Top End, -20° F Ambient Case)

3.9.4-4 Loads and Boundary Conditions for Transfer Cask Bottom End Drop Model (Bottom End, -20° F Ambient Case)

3.9.4-5 Loads and Boundary Conditions for Transfer Cask Top End Drop Model (Top End, 115° F Ambient Case)

3.9.4-6 Loads and Boundary Conditions for Transfer Cask Top End Drop Model (Bottom End, 115° F Ambient Case)

3.9.4-7 Loads and Boundary Conditions for Transfer Cask Top End Drop Model (Top End, -20° F Ambient Case)

3.9.4-8 Loads and Boundary Conditions for Transfer Cask Top End Drop Model (Bottom End, -20° F Ambient Case)

3.9.4-9 Deformed Shape of Transfer Cask for 75g Bottom End Drop (Top End, 115° F Ambient Case)

3.9.4-10 Deformed Shape of Transfer Cask for 75g Bottom End Drop (Top End, -20° F Ambient Case)

3.9.4-11 Deformed Shape of Transfer Cask for 75g Top End Drop (Bottom End, 115° F Ambient Case)

3.9.4-12 Deformed Shape of Transfer Cask for 75g Top End Drop (Bottom End, -20° F Ambient Case)

3.9.4-13 Construction of Collapse Load for Transfer Cask Bottom End Drop

3.9.4-14 Transfer Cask Top End Drop Deformation Plot

3.9.4-15 Transfer Cask Bottom End Drop Deformation Plot

3.9.4-16 Lateral Force Exerted on Inner Shell (Transfer Cask Top End Drop)

3.9.4-17 Lateral Force Exerted on Inner Shell (Transfer Cask Bottom End Drop)

3.9.4.1 Introduction

The purpose of this Appendix is to evaluate the structural adequacy of the OS187H Transfer Cask inner shell with respect to bucking, and to determine the extent of lead slump. The load considered includes lead lateral pressure and a 75*g* top and bottom end drop load in hot (115° F) ambient environments. The calculations for the component stresses and their evaluations under these loads were conducted and reported in Appendix 3.9.2 and Appendix 3.9.3 for the top cover and ram cover bolts.

During a hypothetical accident condition end drop, permanent deformation of the lead gamma shield may occur. The lead gamma shield is supported by friction between the lead and transfer cask shells, in addition to bearing at the end of the lead column.

A nonlinear finite element analysis is performed in order to quantify the amount of lead slump generated during an end drop event. A 2-dimensional axisymmetric ANSYS [1] finite element model is constructed for this purpose. The results of the finite element analysis provide both stresses and displacements generated during the end drop event. The displacement results are used in this section to determine the maximum size of the axial gap that develops between the lead gamma shield column and the structural shell of the transfer cask. The effect of this cavity size on the shielding ability of the transfer package is evaluated in Chapter 5. Both stress and displacement distributions computed by the finite element analysis are also used to perform a buckling evaluation of inner containment shell of the OS187H transfer cask.

An ANSYS elastic-plastic buckling analysis is performed for the transfer cask end drop cases. A 200*g* drop load, which is greater than the design load of 75*g*, is applied to the ANSYS model. This 200*g* drop load was ramped in small increments by many load sub-steps. The ANSYS solution was set to stop and exit at any load sub-step that fails to result in a converged solution. The failure of convergence represents the onset of buckling of the structure.

3.9.4.2 Material Properties

The maximum normal condition temperature in each transfer cask component from Chapter 4 was used to obtain the tangent modulus of the material. The following table summarizes the maximum transfer cask component temperatures taken from Chapter 4.

Cask Component	Material	Temperature Used in Analysis
Lid	SA-240 Type XM-19	300 °F
Inner Shell	SA-240 Type 304	350 °F
Top and Bottom Flanges, Ram Access Penetration Ring	SA-182 Gr. F304N	300 °F
Outer Structural Shell, Bottom Neutron Shield plate, Bottom End and Cover plates	SA-240 Type 304	300 °F
Top Lid and Bottom RAM access Cover Bolts	SA-540-Gr. B24 Cl.1	300 °F
Gamma Shield	B-29, Chemical Lead	350 °F

The following is a summary of the transfer cask material properties evaluated at the temperatures listed above.

A. Lid Material (SA-240 Type XM-19)

Temperature	Modulus of Elasticity, E (psi) [2]	Density, ρ (lb./in.3) [3]	Poisson's ratio, ν [3]
70° F	28.3×10^6	0.29	0.3
200° F	27.6×10^6	0.29	0.3
300° F	27.0×10^6	0.29	0.3
400° F	26.5×10^6	0.29	0.3

@ 300° F,

$E = 27.0\times10^6$ psi. [2]

$S_y = 43.3$ ksi. [2]

$S_u = 94.2$ ksi. [2]

Tangent Modulus, $E_T = 5\%$ of $E = 0.05 \times 27.0\times10^6$ psi $= 1.35 \times10^6$ psi

B. Inner Shell (SA-240 Type 304)

Temperature	Modulus of Elasticity, E (psi) [2]	Density, ρ (lb./in.3) [3]	Poisson's ratio, ν [3]
70° F	28.3×10^6	0.29	0.3
200° F	27.6×10^6	0.29	0.3
300° F	27.0×10^6	0.29	0.3
400° F	26.5×10^6	0.29	0.3

@ 350° F,

$E = 26.75 \times10^6$ psi. [2]
$S_y = 21.55$ ksi. [2]
$S_u = 65.1$ ksi. [2]
Tangent Modulus, $E_T = 5\%$ of $E = 0.05 \times 26.75\times10^6$ psi $= 1.34 \times10^6$ psi

C. Top and Bottom Flanges, and Ram Access Penetration Ring (SA-182 Gr. F304N)

Temperature	Modulus of Elasticity, E (psi) [2]	Density, ρ (lb./in.3) [3]	Poisson's ratio, ν [3]
70° F	28.3×10^6	0.29	0.3
200° F	27.6×10^6	0.29	0.3
300° F	27.0×10^6	0.29	0.3
400° F	26.5×10^6	0.29	0.3

@ 300° F,

$E = 27.0\times10^6$ psi. [2]
$S_y = 25$ ksi. [2]
$S_u = 76.1$ ksi. [2]
Tangent Modulus, $E_T = 5\%$ of $E = 0.05 \times 27.0\times10^6$ psi $= 1.35 \times10^6$ psi

D. Outer Structural Shell, Bottom Neutron Shield plate, Bottom End plate, and Bottom cover plate (SA-240 Type 304)

Temperature	Modulus of Elasticity, E (psi) [2]	Density, ρ (lb./in.3) [3]	Poisson's ratio, ν [3]
70° F	28.3×10^6	0.29	0.3
200° F	27.6×10^6	0.29	0.3
300° F	27.0×10^6	0.29	0.3
400° F	26.5×10^6	0.29	0.3

@ 300° F,

$E = 27.0\times10^6$ psi. [2]
$S_y = 22.4$ ksi. [2]
$S_u = 66.2$ ksi. [2]
Tangent Modulus, $E_T = 5\%$ of $E = 0.05 \times 27.0\times10^6$ psi $= 1.35 \times10^6$ psi

E. Bolts for Top Lid and Bottom RAM Access Cover (SA-54 Gr. 24 CL 1)

Temperature	Modulus of Elasticity, E (psi) [2]	Density, ρ (lb./in.3) [3]	Poisson's ratio, ν [3]
70° F	27.8×10^6	0.29	0.3
200° F	27.1×10^6	0.29	0.3
300° F	26.7×10^6	0.29	0.3
400° F	26.1×10^6	0.29	0.3

@ 300 °F,

$E = 26.7\times10^6$ psi. [2]
$S_y = 138.6$ ksi. [2]
$S_u = 165$ ksi. [2]
Tangent Modulus, $E_T = 5\%$ of $E = 0.05 \times 26.7\times10^6$ psi $= 1.335 \times10^6$ psi

F. Chemical Lead (B-29)

Temperature	Modulus of Elasticity, E (psi) [2]	Density, ρ (lb./in.3) [3]	Poisson's ratio, ν [3]
70° F	2.49×10^6	0.41	0.45
200° F	2.28×10^6	0.41	0.45
300° F	2.06×10^6	0.41	0.45
400° F	$1.78\times10^{6*}$	0.41	0.45

*Extrapolated from available Reference 4 Data.

@ 350° F,
Multi-linear Stress/Strain Curve: [4] [5]

Strain (in/in)	Stress (psi)
	350° F
0.000485	1,208*
0.030	1,500
0.100	2,100
0.300	2,400
0.500	2,700

* Values adjusted for consistence with modulus of elasticity listed in above table.

3.9.4.3 Finite Element Model

3.9.4.3.1 Approach

A 2-dimensional axisymmetric ANSYS [1] finite element model, constructed primarily from PLANE42 elements, is used in this analysis. Beam3 elements are used to model the lid and RAM port cover bolts. Contact elements are used to model the interaction between the lead gamma shield and the cask inner and outer shells. The coefficient of sliding friction for lead on mild steel varies from 0.3 for lubricated surfaces to 0.95 for dry surfaces [3]. A lower bound coefficient of static friction of 0.25 is conservatively used for this buckling analysis.

In order to determine the buckling load of the inner shell and the amount of lead slump settling, an elastic-plastic analysis is required. The material properties of the lid, bottom, inner shell and outer shell of the transfer cask are modeled with bilinear stress-strain curves, while the lead material is modeled with a multilinear stress-strain curve. Above tables list these material properties.

3.9.4.3.2 Unmodeled Components

Only the structural steel section of the top cover is modeled. The top neutron shield resin, top cover plate, and hoist ring standoffs are not modeled since they are not intended to provide any structural support. However, their inertial load is accounted for by increasing the density of the structural portion of the top cover. The weight of the unmodeled portion of the top cover assembly is as follows.

Weight of unmodeled lid components = 678 lb. (resin) + 422 lb. (cover plate) + 20 lb. (standoffs)

= 1,120 lb.

The volume and weight of the structural steel portion of the lid is 14,051 in.^{3} and 4,075 lb. respectively. Therefore the weight of the structural steel portion of the lid, ρ_l, is the following.

$$\rho_l = [1{,}120 \text{ lb.} + 4{,}075 \text{ lb.}] / 14{,}051 \text{ in.}^3 = 0.37 \text{ lb./in.}^3$$

For conservatism, the density of the top cover used in this analysis is increased 0.38 lb./in.^{3}

The radial neutron shield and shell are also not modeled, because they are not considered structural components of the transfer cask. Therefore, the density of the outer structural steel shell of the transfer cask is increased to account for the un-modeled components. The weight of the un-modeled radial neutron shield assembly is 12,746 lb.

The volume and weight of the outer structural shell is 71,895 in.^{3} and 20,850 lb. respectively. Therefore the weight of the structural steel portion of the lid, ρ_s, is the following.

$$\rho_l = [12{,}746 \text{ lb.} + 20{,}850 \text{ lb.}] / 71{,}895 \text{ in.}^3 = 0.47 \text{ lb./in.}^3$$

For conservatism, the density of the outer structural steel shell used in this analysis is increased 0.49 lb./in.^{3}

3.9.4.3.3 Attachment Bolt Modeling

The top cover and RAM access cover bolts are modeled with axisymmetric BEAM3 elements. The top cover and RAM access bolts are constructed from SA-540 grade B24 class 1 material. The element real constants are computed in the following way for the top cover and RAM access bolts.

There are 24, 1½ in - 8UN 2A bolts used to mount the transfer cask top cover. The bolt diameter used for stress analysis, D_{tc}, is computed using formulae given in Table 5.1 of Reference 6, as follows.

$$D_{tc} = 1.50 - 0.9743(1/8) = 1.378 \text{ in.}$$

The total tensile stress area for all 24 top cover bolts, A_{tc2d}, is computed as follows.

$$A_{tc2d} = (\pi/4) \times 1.378^2 \times 24 \text{ bolts} = 1.491 \times 24 \text{ bolts} = 35.793 \text{ in.}^2$$

The total moment of inertia of all 24 top cover bolts, I_{tc2d}, is,

$$I_{tc2d} = (\pi/64) \times 1.378^4 \times 24 \text{ bolts} = 4.248 \text{ in.}^4$$

The total height of the top cover bolts, H_{tc2d}, is computed assuming the following equivalent height method.

$$H_{tc2d} = \sqrt{A_{tc2d}} = \sqrt{1.491} = 1.221 \text{ in.}$$

There are 12, ½ in - 13UNC 2A bolts used to mount the transfer cask RAM access cover. The bolt diameter used for stress analysis, D_{ra}, is computed as follows.

$$D_{ra} = 0.50 - 0.9743(1/13) = 0.425 \text{ in.}$$

The total tensile stress area for all 12 RAM access cover bolts, A_{ra2d}, is computed as follows.

$$A_{ra2d} = (\pi/4) \times 0.425^2 \times 12 \text{ bolts} = 0.142 \times 12 \text{ bolts} = 1.704 \text{ in.}^2$$

The total moment of inertia of all 12 RAM access cover bolts, I_{ra2d}, is,

$$I_{ra2d} = (\pi/64) \times 0.425^4 \times 12 \text{ bolts} = 0.01922 \text{ in.}^4$$

The height of the RAM access cover bolts, H_{ra2d}, used in the model is,

$$H_{ra2d} = \sqrt{0.142} = 0.3768 \text{ in.}$$

For both the top cover bolts and the RAM access cover bolt, a bolt preload stress of 25,000 psi. is used. Since the top cover bolts and RAM access cover bolts are constructed from the same material, SA-540, type B24. Both sets of bolts are torqued to the same preload stress, and their corresponding preload strains, ε_b, used in the finite element model are computed as follows.

$$\varepsilon_b = \text{preload stress / bolt modulus of elasticity}$$

3.9.4.3.4 Contact Elements

CONTAC12 elements are places between all surfaces of the top flange and lid as well as the RAM access cover and RAM access penetration that contact each other. These contact elements are used to model the reaction forces that occur between closure surfaces.

The contact elements introduce nonlinearities in the analysis depending whether they are open or closed. Initially, at all contact surfaces, the gaps are closed. The contact element spring constant, K_n, is calculated in the following way.

$$K_n = f\,E\,h\,[7]$$

Where,

f = A factor usually between 0.01 to 100.
E = Modulus of elasticity (27.0×10^6 psi for SA-240, type 304 @ 300°F [2])
h = contact target length (i.e., the square root of target area).
Typical element length $\approx$ 1/2 in.
Typical element width $\approx$ 1 in.
Typical target length, $h = (0.5 \times 1.0)^{0.5} = 1.22$ in.

$$K_n = 27.0\times10^6 \times 1.22 \times f \approx 3.29\times10^5 \text{ to } 3.29\times10^9 \text{ lb./in}$$

Thus, there is very wide range for K_n value. For the 2-D finite element model, an upper value of 3×10^9 lb/in was used to minimize penetrations in the contact elements.

3.9.4.3.5 Bottom End Drop Boundary Conditions

The weight of the transfer cask internals (canister, basket, and fuel assemblies) is accounted for by applying equivalent pressures. The actual weights of the canister, basket, and fuel assemblies

are 28.19 kips, 29.85 kips, and 50.72 kips. respectively. Therefore, the total actual weight of the cask internals is 108.77 kips. For conservatism, the weight of the cask internals used in this analysis is increased to 115.00 kips. The transfer cask inner radius is 35.25 in., and the inner radius of the ram access penetration is 10.00 in. The inertial load of the transfer cask internals reacts against the annular surface bounded by these two radii during a bottom end drop. The area of this reaction surface, A_{bi}, is as follows.

$$A_{bi} = \pi(35.25^2 - 10.00^2) = 3{,}589.47 \text{ in}^2.$$

The pressure equivalent to the inertial load of the internals under accident conditions, P_{bi}, is,

$$P_{in} = [115{,}000 / 3{,}589.47] \times 200\ gs = 6407.63 \text{ psi}.$$

Symmetry displacement boundary conditions are applied along the y-axis of the 2-dimensionsal axisymmetric model. The bottom end of the transfer cask is held in the axial direction in order to simulate the rigid reaction force generated by the impact target. A 200 g inertial load in the positive y-direction is also applied to the model for the accident condition load case. The loading and boundary conditions are shown on Figures 3.9.4-1 to 3.9.4-4.

3.9.4.3.6 Top End Drop Boundary Conditions

The weight of the transfer cask internals (canister, basket, and fuel assemblies) is accounted for by applying equivalent pressures. The weight of the canister internals used in this analysis is 115.00 kips. The inertial load of the transfer cask internals reacts against the inside surface of the top cover assembly during a top end drop. The outer radius of the inside surface of the transfer cask top cover assembly is 35.70 in. Therefore the area of the reaction surface, A_{bi}, is as follows.

$$A_{bi} = \pi(35.70^2) = 4{,}003.93 \text{ in}^2.$$

The pressure equivalent to the inertial load of the internals under accident conditions, P_{bi}, is,

$$P_{in} = [115{,}000 / 4{,}003.93] \times 200\ gs = 5744.36 \text{ psi}.$$

Symmetry displacement boundary conditions are applied along the *y*-axis of the 2-dimensionsal axisymmetric model. The outer surface of the top cover is held in the axial direction in order to simulate the rigid reaction force generated by the impact target. A 200*g* inertial load in the negative *y*-direction is also applied to the model for the accident condition load case. The loading and boundary conditions are shown on Figures 3.9.4-5 to 3.9.4-8.

3.9.4.3.7 Thermal Loads

The temperature distributions applied to the finite element models are taken from Chapter 4.

3.9.4.4 FEA Results

- Shell Buckling

ANSYS nonlinear buckling analysis was performed. Maximum loads of 200g were applied in the following two load cases.

1. Top end drop with lateral pressure of lead in hot ambient (115°F)
2. Bottom end drop with lateral pressure of lead in hot ambient (115°F)

The automatic time stepping program option "Autots" was activated. This option lets the program decide the actual size of the load-substep for a converged solution. The program stops at the load substep when it fails to result in a converged solution. The last load step, with a converged solution, is the buckling load for the structure.

The following table summarizes the last converged load for all two load cases:

Load Cases	Last Converged Load (g)	G load calculated From Appendix 3.9.10 LS-DYNA CG Over Corner Analysis(1)	G Load Used For Cask Structural Analysis	Factor of Safety
Top End Drop (Hot)	189	15.5	75	2.52
Bottom End Drop (Hot)	178	15.5	75	2.37

Note:

1. For storage the end drop is not a creditable event. The transfer cask is transferred in the horizontal position held by the transfer trailer. In the axial direction it is possible to slide into the ground and incur a corner drop. The maximum g load calculated by the LS-DYNA as described in Appendix 3.9.10 is 15.5g. For conservatism 75g is used for inner shell buckling analysis.

The ANSYS displacement plots for the last converged load steps for the above two load cases are shown on Figures 3.9.4-14 and 3.9.4-15.

The lateral pressure of the lead vs. g load at a typical location in the middle section of the cask during the top and bottom end drops are shown in Figures 3.9.4-16 and 3.9.4-17, respectively. These figures show that the pressure load increases as the g load increases.

- Lead Slump

The ANSYS solutions have converged at different load sub-steps for each end drop as described in the above table. The lead slump at 75g load is extracted from its corresponding time in each drop solution. The calculated maximum lead slumps in each case are listed in the following table.

Load Combination	Lead Slump Cavity Length
75*g* Top End Drop, Hot Environment	0.809 in.
75*g* Bottom End Drop, Hot Environment	0.833 in.

3.9.4.5 Conclusions

The analysis indicates that the transfer cask will not buckle during 75*g* end drops. The table above shows that the maximum longitudinal gap, caused by lead slump, is 0.833 inches, and occurs during accident condition bottom end drop, in the hot environment. The effect of the gap on the shielding ability of the NUHOMS®-OS187H transfer cask is analyzed in Chapter 7.

3.9.4.6 References

1. ANSYS User's Manual, Rev 6.0

2. American Society of Mechanical Engineers, ASME Boiler and Pressure Vessel Code, Section II, Part D and Section III, Subsection NB and Appendix F, 1998, including 2000 addenda.

3. Baumeister & Marks, Standard Handbook for Mechanical Engineers, 7th Edition.

4. An Assessment of Stress-Strain Data Suitable for Finite-Element Elastic-Plastic Analysis of Shipping Containers, NUREG/CR-0481.

5. A Survey of Strain Rate Effects for some Common Structural Materials Used in Radioactive Material Packaging and Transportation Systems, U.S. Energy Research and Development Administration, Battelle Columbus Laboratories, August 1976.

6. "Stress Analysis of Closure Bolts for Shipping Casks", NUREG/CR-6007, April 1992

7. ANSYS User's Manual, Rev 5.6

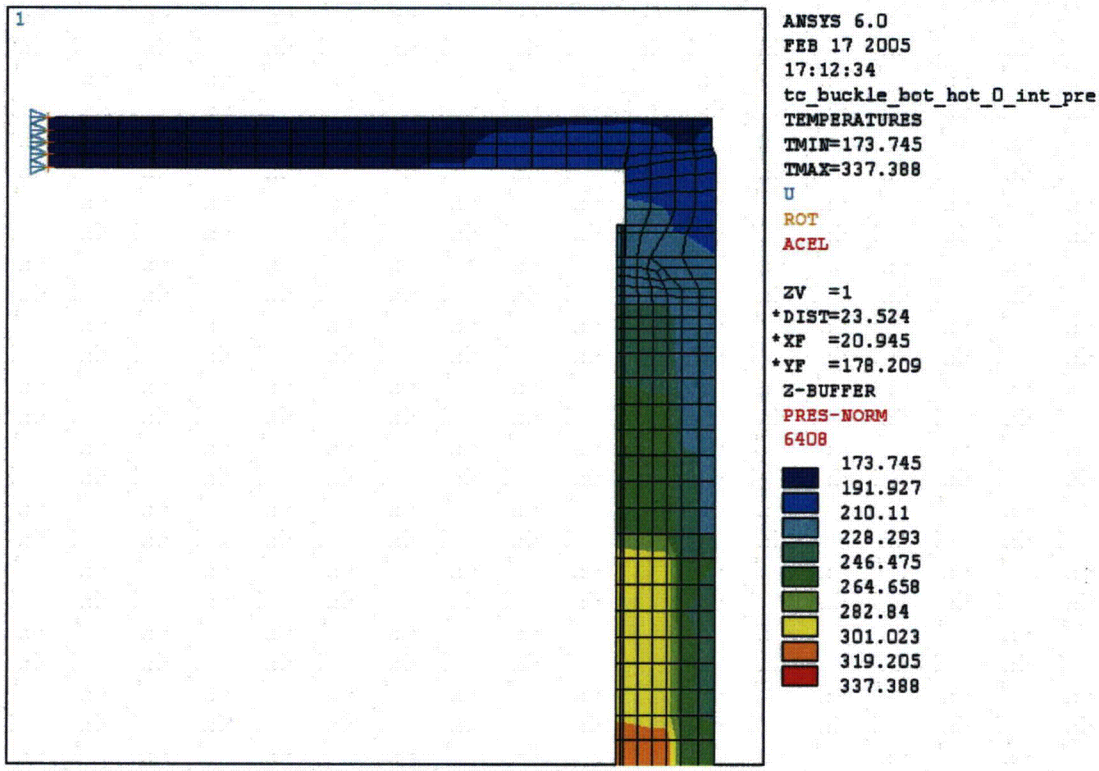

Figure 3.9.4-1
Loads and Boundary Conditions for Transfer Cask Bottom End Drop Model (Top End, 115° F Ambient Case)

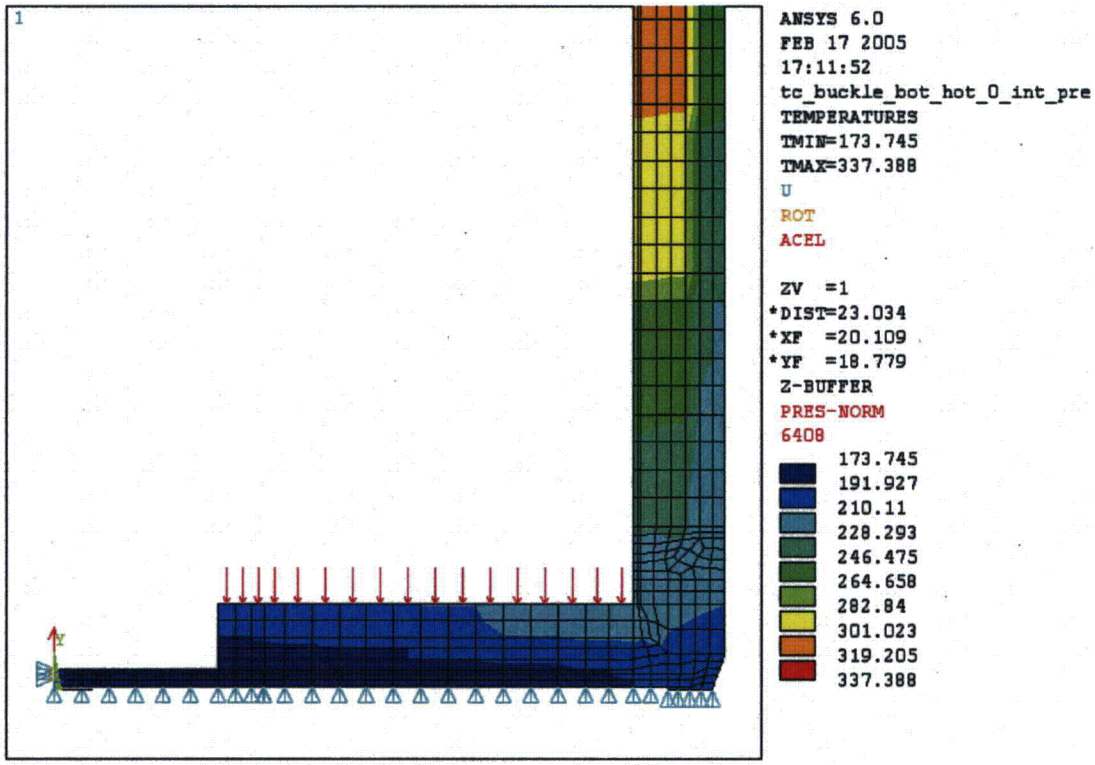

Figure 3.9.4-2
Loads and Boundary Conditions for Transfer Cask Bottom End Drop Model (Bottom End, 115° F Ambient Case)

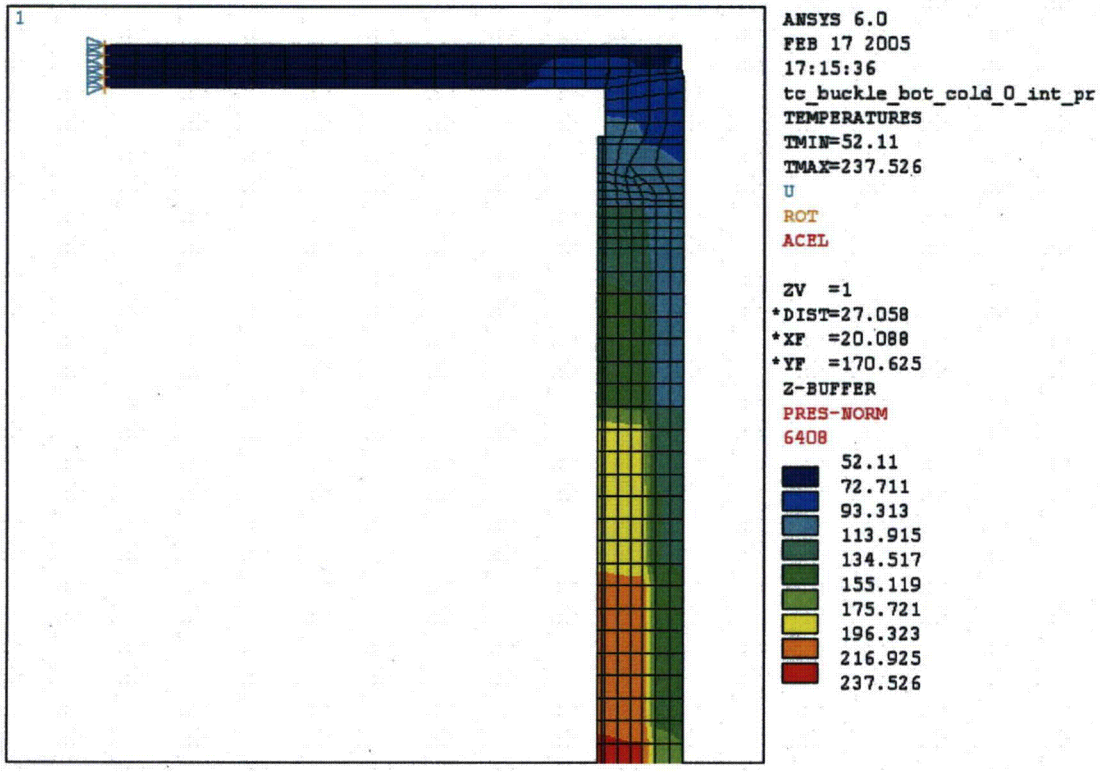

Figure 3.9.4-3
Loads and Boundary Conditions for Transfer Cask Bottom End Drop Model (Top End, -20° F Ambient Case)

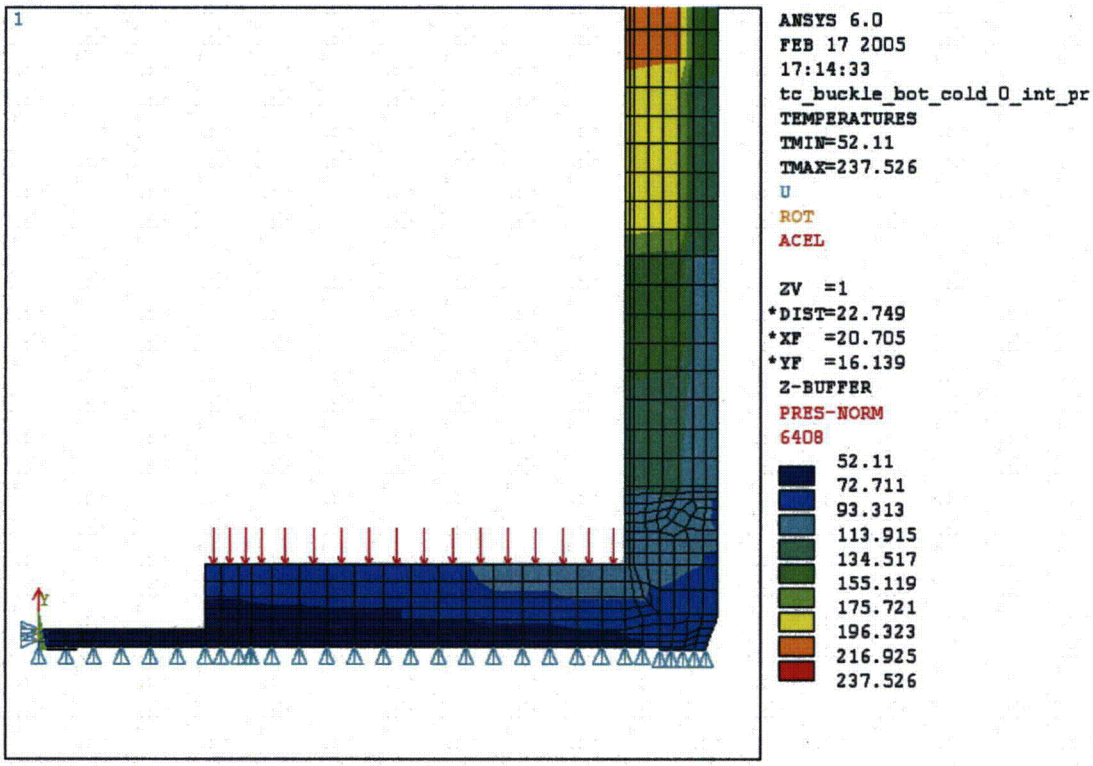

Figure 3.9.4-4
Loads and Boundary Conditions for Transfer Cask Bottom End Drop Model (Bottom End, -20° F Ambient Case)

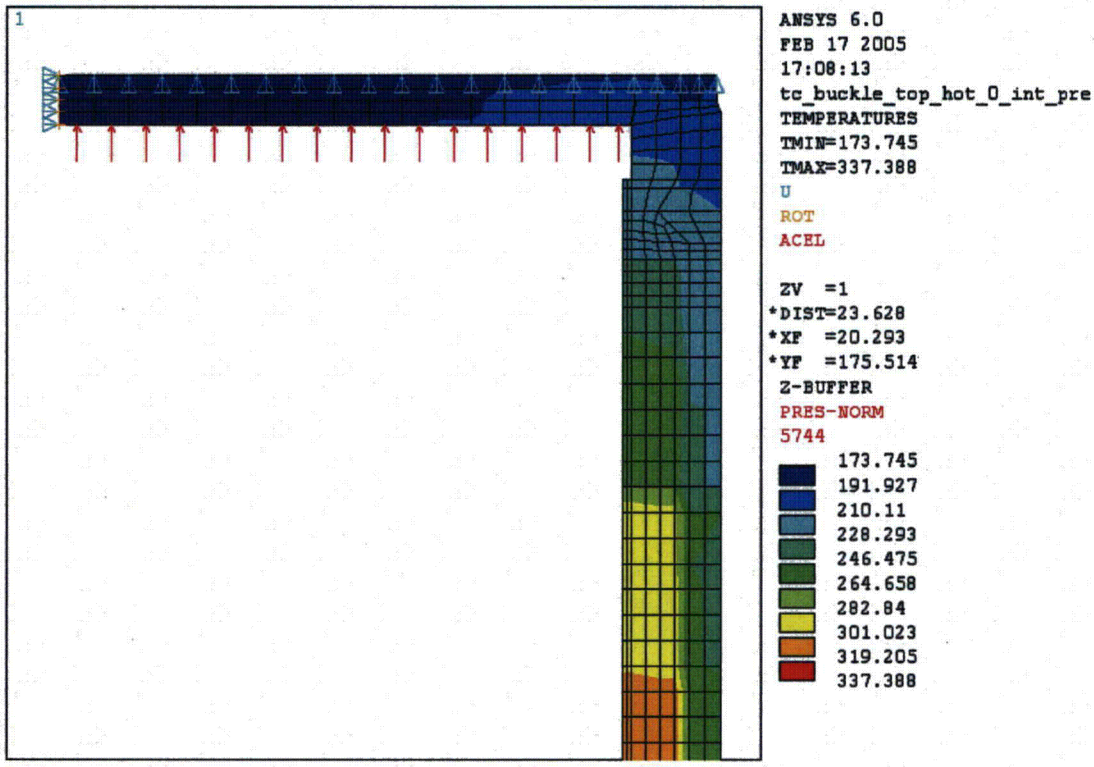

Figure 3.9.4-5
Loads and Boundary Conditions for Transfer Cask Top End Drop Model (Top End, 115° F Ambient Case)

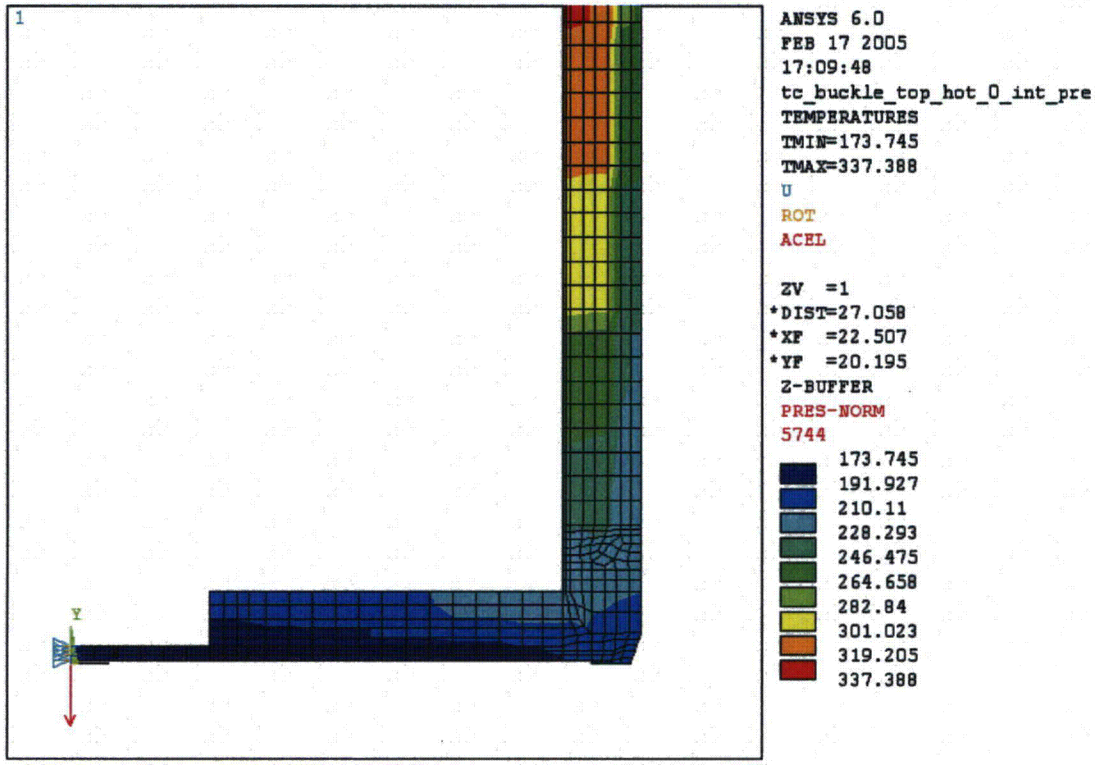

Figure 3.9.4-6
Loads and Boundary Conditions for Transfer Cask Top End Drop Model (Bottom End, 115° F Ambient Case)

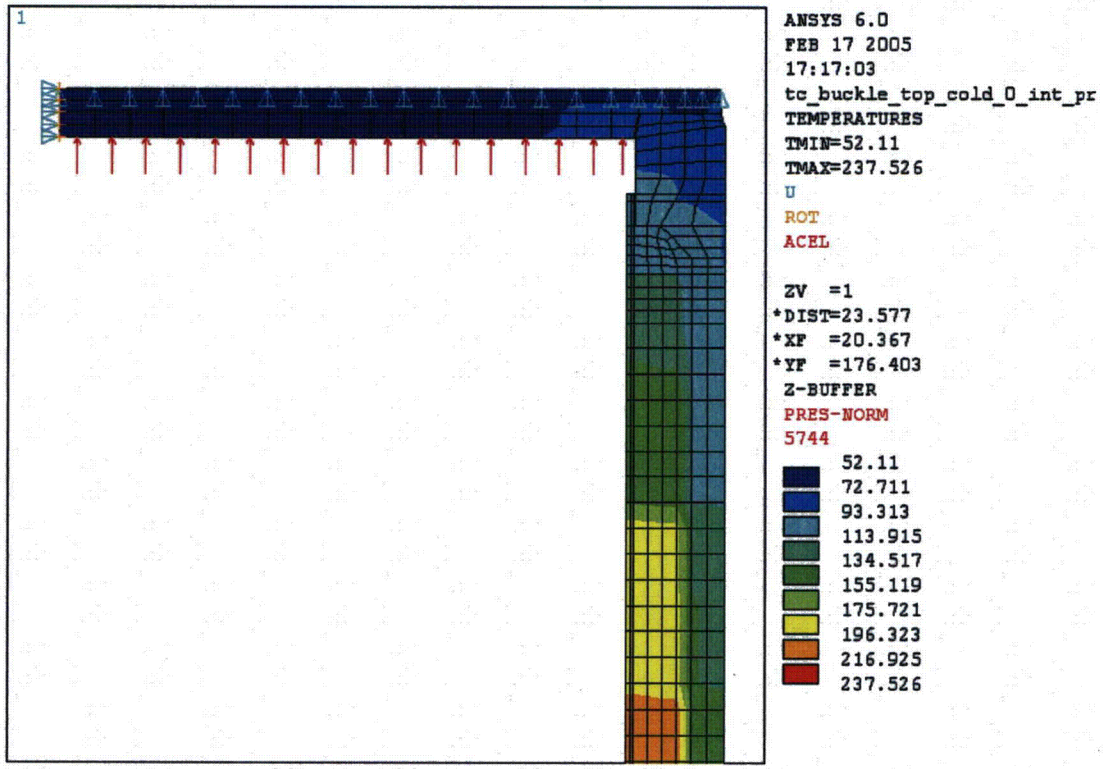

Figure 3.9.4-7
Loads and Boundary Conditions for Transfer Cask Top End Drop Model (Top End, -20° F Ambient Case)

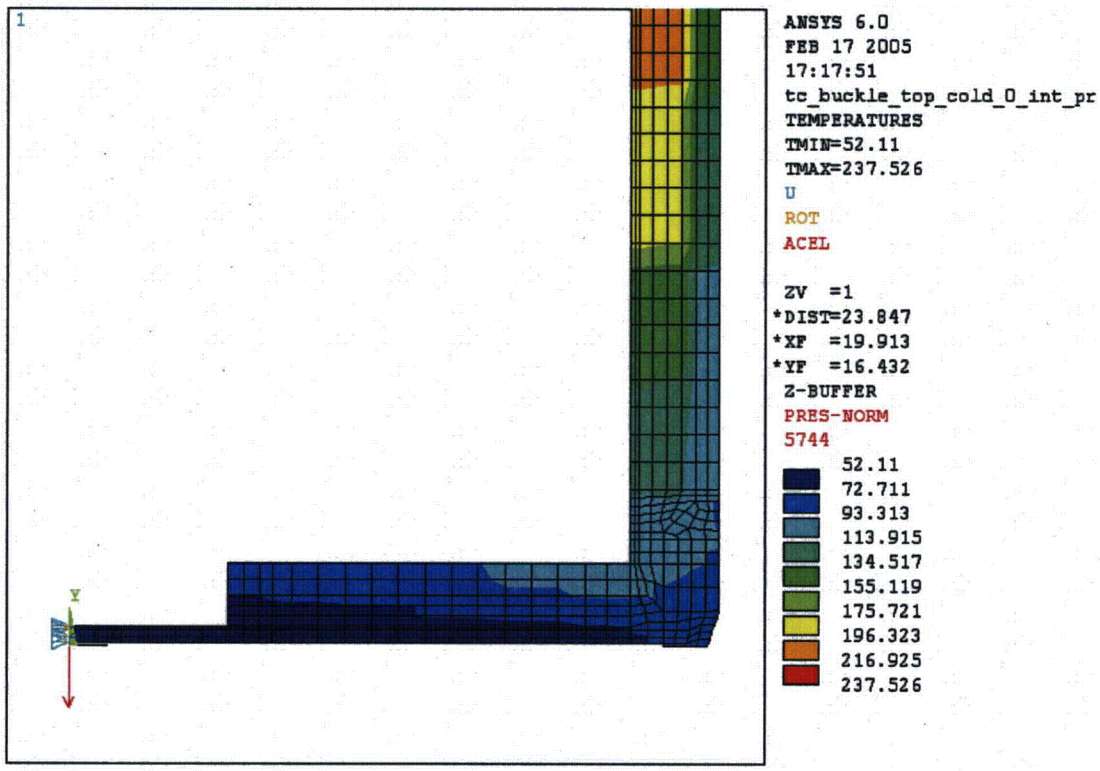

Figure 3.9.4-8
Loads and Boundary Conditions for Transfer Cask Top End Drop Model (Bottom End, -20° F Ambient Case)

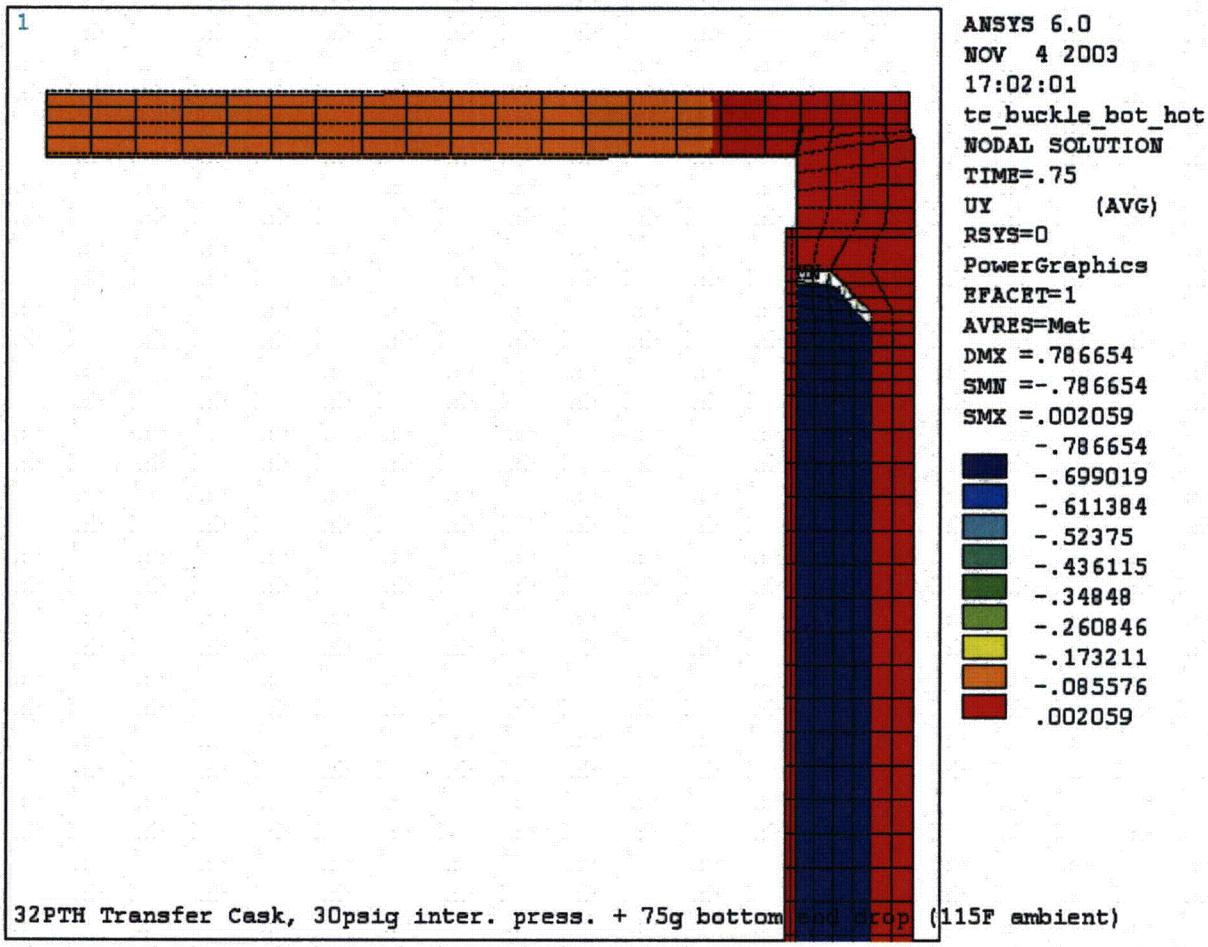

Figure 3.9.4-9
Deformed Shape of Transfer Cask for 75g Bottom End Drop
(Top End, 115° F Ambient Case)

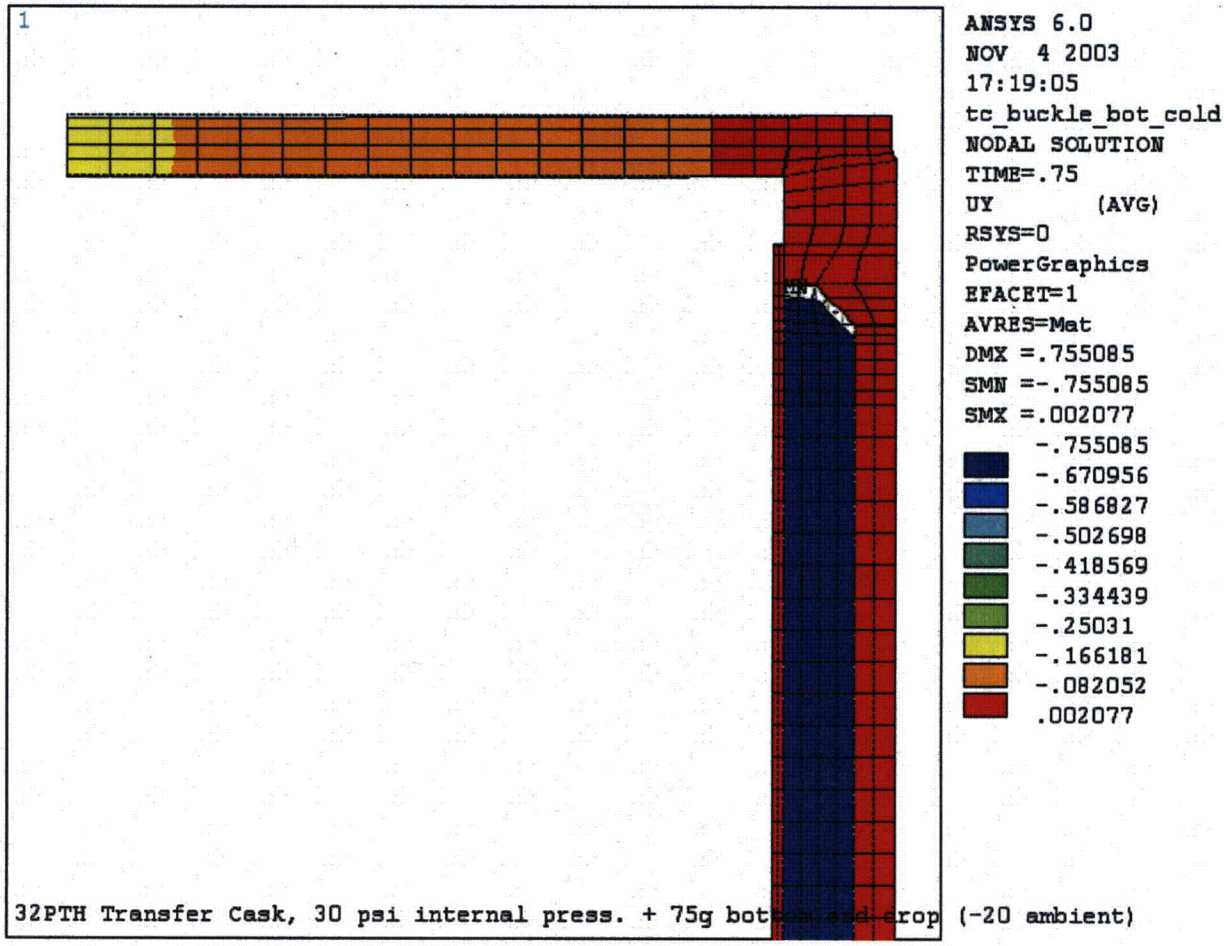

Figure 3.9.4-10
Deformed Shape of Transfer Cask for 75g Bottom End Drop
(Top End, -20° F Ambient Case)

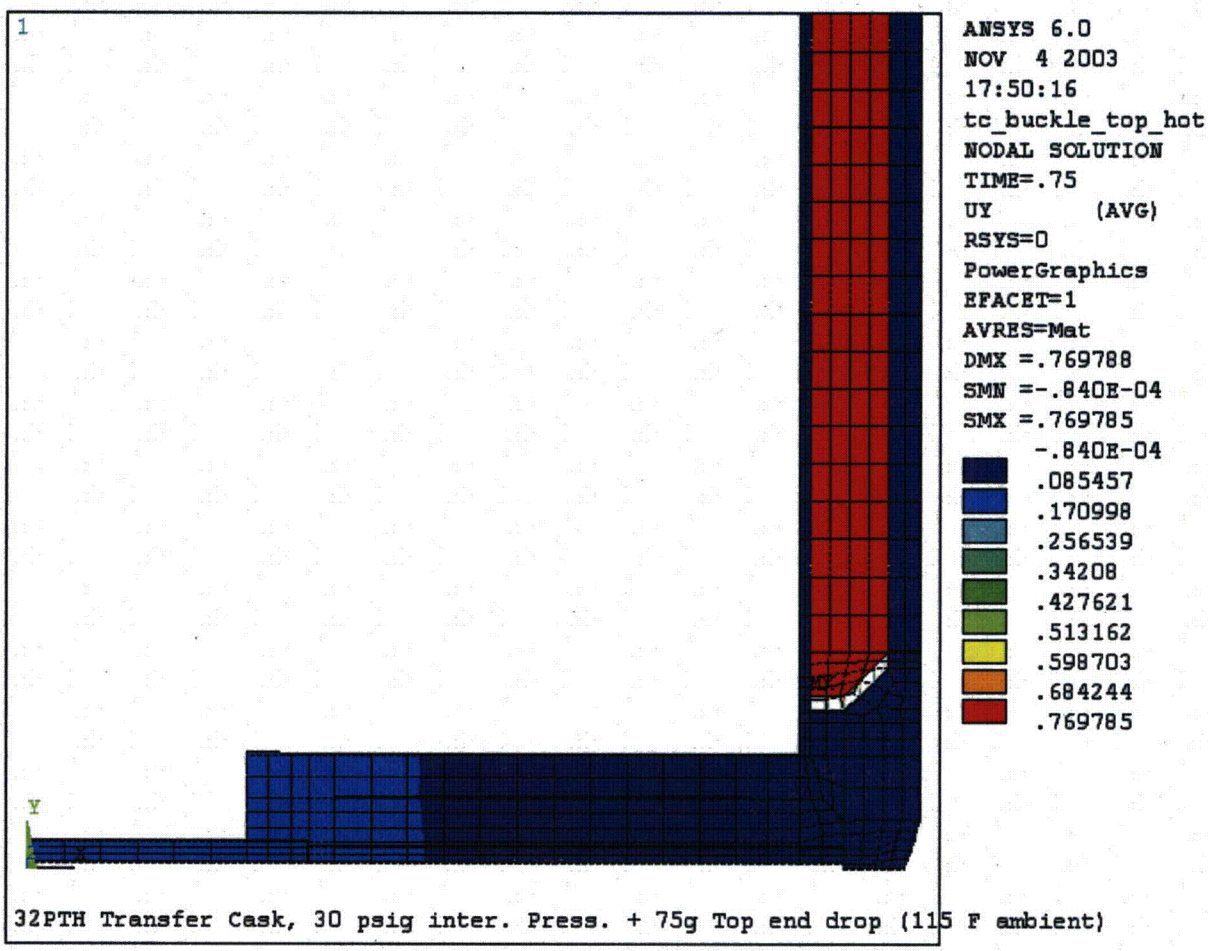

Figure 3.9.4-11
Deformed Shape of Transfer Cask for 75g Top End Drop
(Bottom End, 115° F Ambient Case)

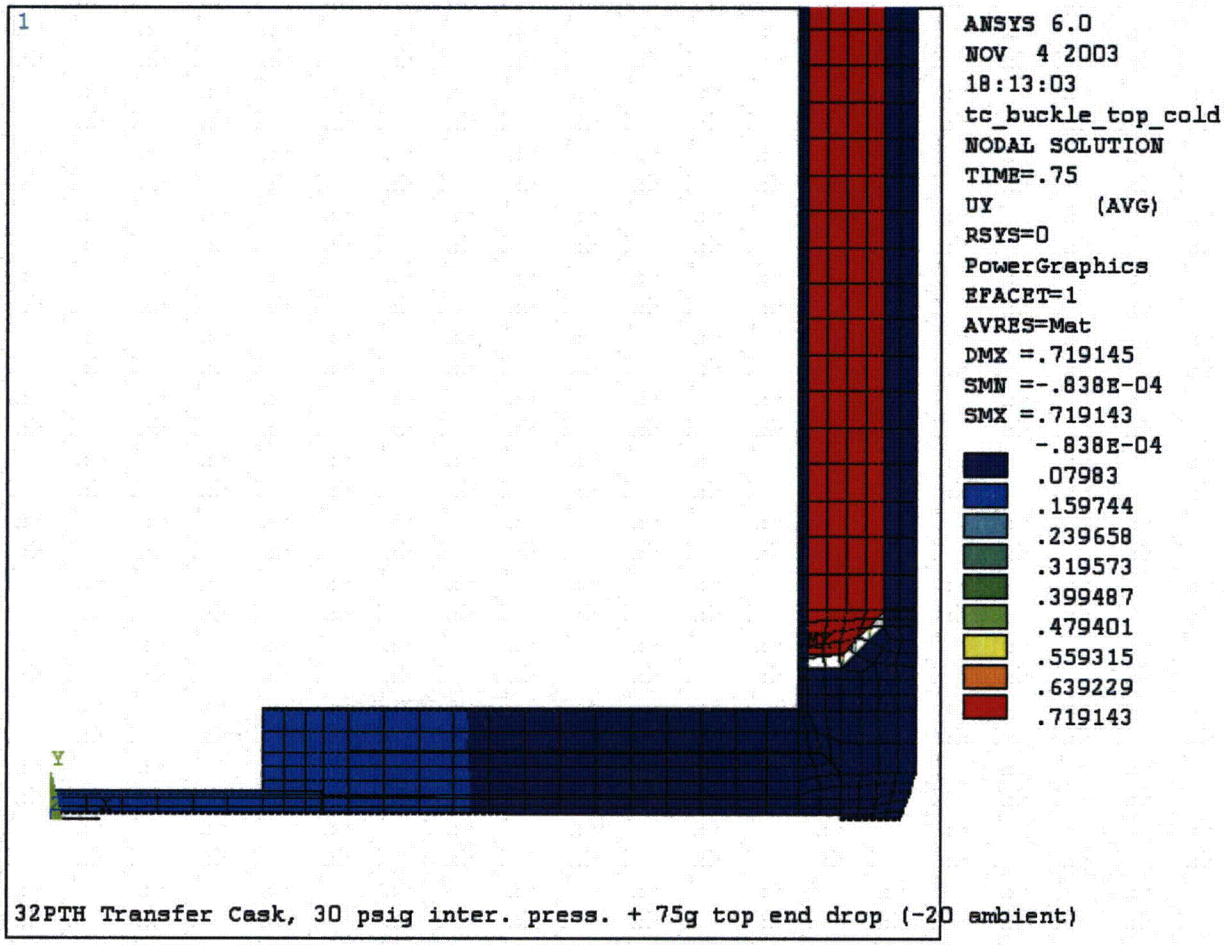

Figure 3.9.4-12
Deformed Shape of Transfer Cask for 75g Top End Drop
(Bottom End, -20° F Ambient Case)

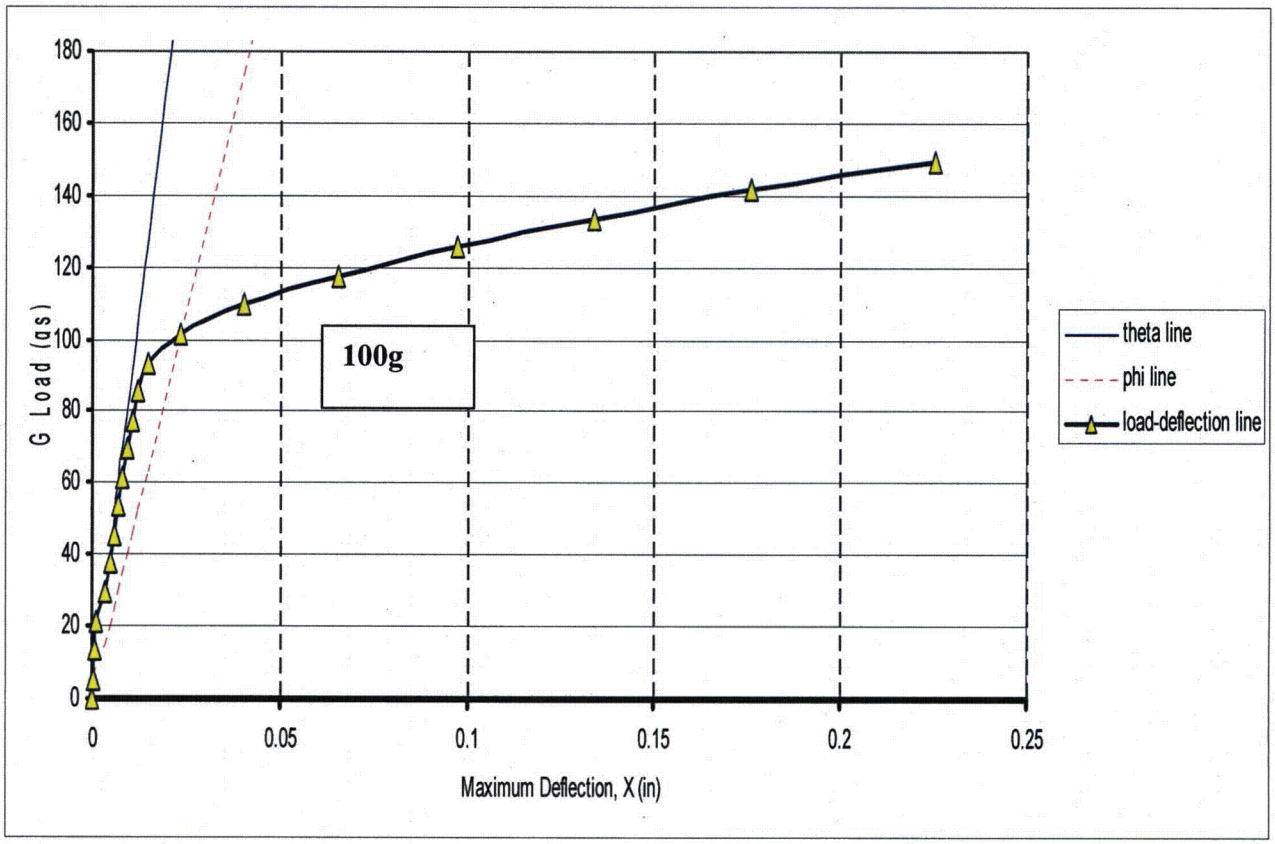

Figure 3.9.4-13
Construction of Collapse Load for Transfer Cask Bottom End Drop

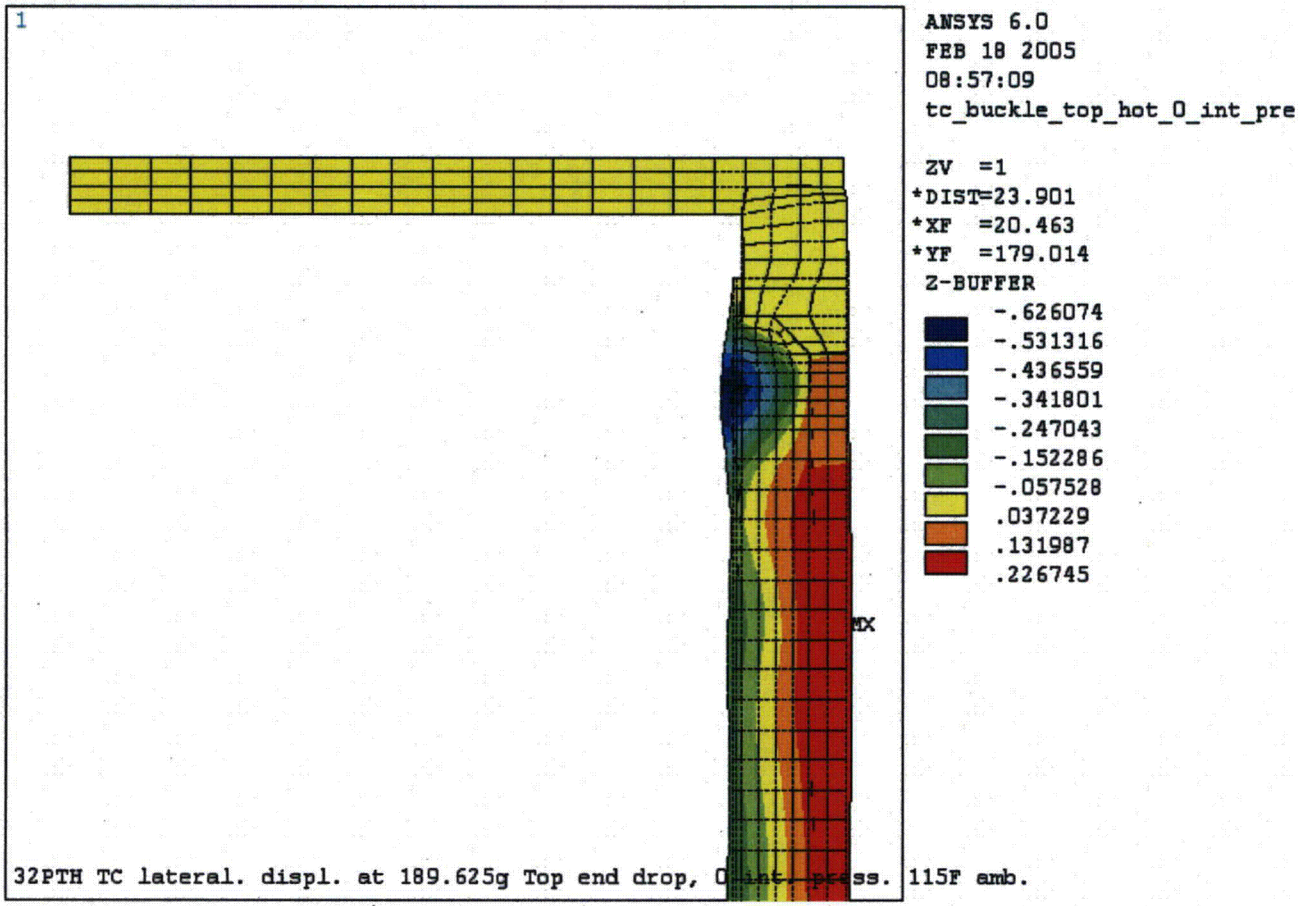

Figure 3.9.4-14
Transfer Cask Top End Drop Deformation Plot (at 189.625g)

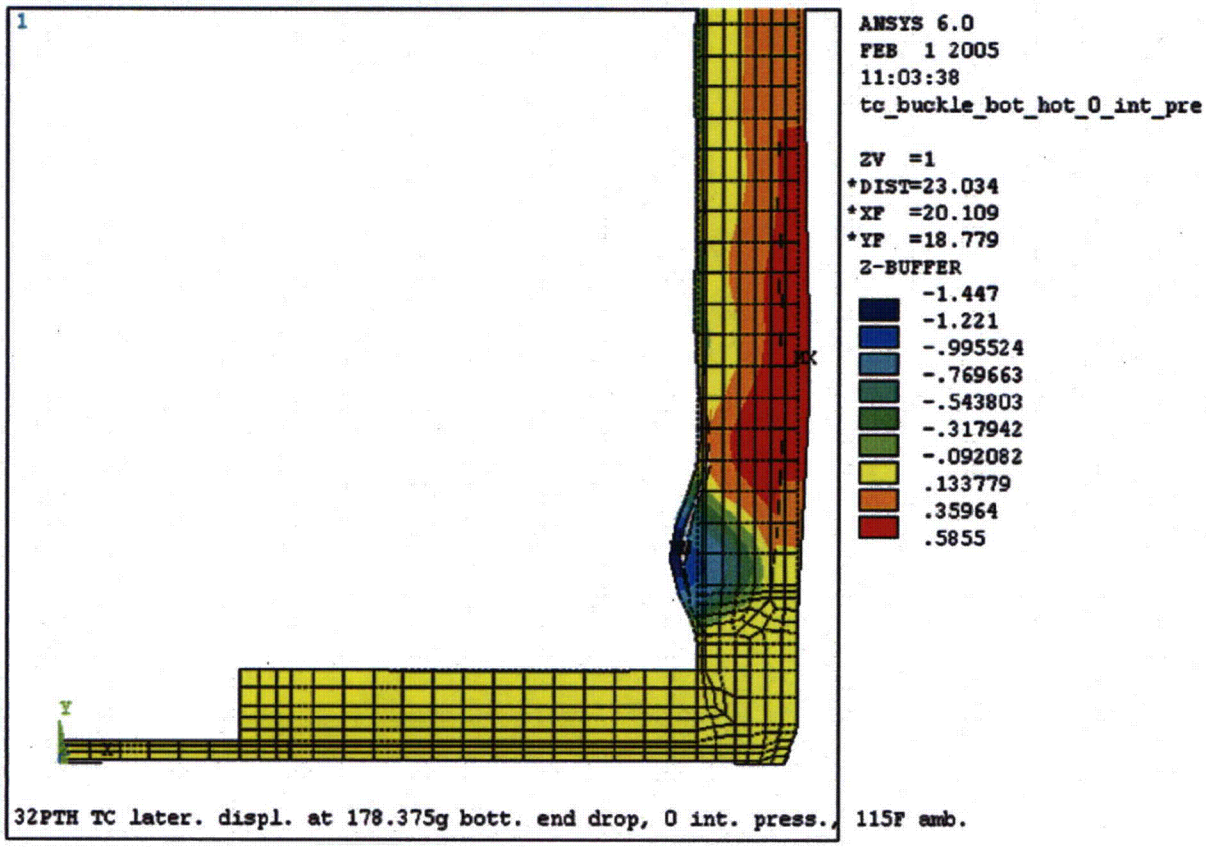

Figure 3.9.4-15
Transfer Cask Bottom End Drop Deformation Plot (at 178.375g)

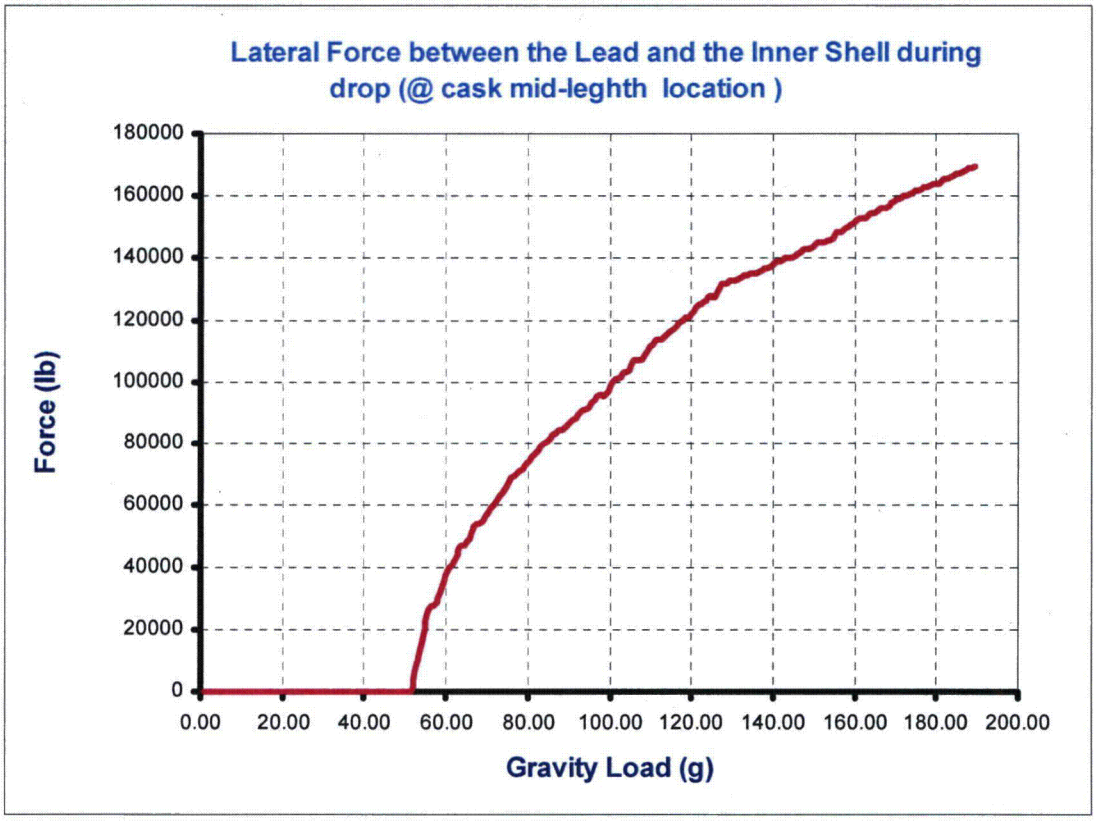

Figure 3.9.4-16
Lateral Force Exerted on Inner Shell (Transfer Cask Top End Drop)

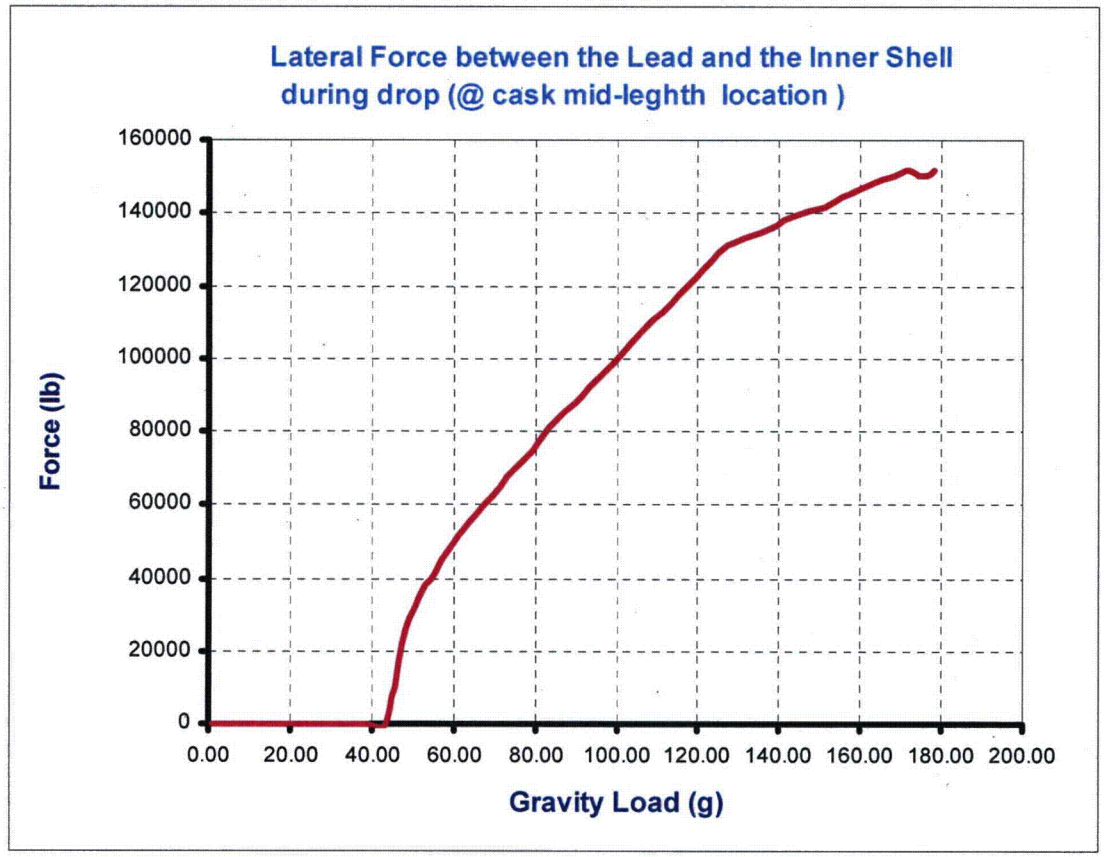

Figure 3.9.4-17
Lateral Force Exerted on Inner Shell (Transfer Cask Bottom End Drop)

APPENDIX 3.9.5
OS187H TRANSFER CASK TRUNNION ANALYSIS

TABLE OF CONTENTS

3.9.5 OS187H TRANSFER CASK TRUNNION ANALYSIS 3.9.5-1
- **3.9.5.1 Introduction 3.9.5-1**
- **3.9.5.2 Component Weights 3.9.5-2**
- **3.9.5.3 Load Cases 3.9.5-2**
- **3.9.5.4 Material Properties 3.9.5-3**
- **3.9.5.5 Stress Criteria 3.9.5-3**
- **3.9.5.6 Stress Computation 3.9.5-3**
- **3.9.5.7 Summary of Computed Stresses 3.9.5-13**
- **3.9.5.8 Conclusions 3.9.5-13**
- **3.9.5.9 References 3.9.5-14**

LIST OF TABLES

3.9.5-1 Summary of Computed and Allowable Trunnion Stresses

LIST OF FIGURES

3.9.5-1 OS187H Transfer Cask Bottom Trunnion (Top View)

3.9.5-2 OS187H Transfer Cask Top Trunnion (Top View)

3.9.5-3 Opening in the Lifting Yoke Arm Geometry

3.9.5 OS187H TRANSFER CASK TRUNNION ANALYSIS

3.9.5.1 Introduction

This appendix presents the evaluation of the NUHOMS®-OS187H Transfer Cask Trunnion stresses due to all applied loads during fuel loading and transfer operations.

NUHOMS® OS187H transfer cask has two top trunnions constructed from SA-182 Gr. FXM19 (22Cr-13Ni-5Mn Forging) and two bottom trunnions constructed from SA-182 Gr. F304. The cask shells are made of SA-240, Gr. 304 (18Cr-8Ni) stainless steel. The two top trunnions are used to first lift the cask, containing a canister and an empty basket, into a fuel pool for loading of the spent fuel. After the spent fuel has been loaded into the basket, the cask is lifted to a decontamination area. After draining and drying of the pool water, welding of the canister cover, and bolting of the cask lid, the cask is placed in a trailer for transfer to onsite HSM. The cask is vertically lifted onto the trailer and is initially supported by the bottom trunnions which are mated to transfer trailer. Then the cask is allowed to pivot about the bottom trunnions, into a horizontal position until the top trunnions rest on their supports in the trailer. Throughout the operation the maximum total load is applied to the cask top trunnions. After the cask has been placed on the trailer, it is supported by all four trunnions and is subject to a set of specified design handling loads.

The following two load cases are analyzed for the four transfer cask trunnions:

A. Lifting Loads (Cask lifted from the pool to the decontamination area and then to the trailer). The two top trunnions are analyzed for 6*g* and 10*g* vertical loads as required by ANSI N14.6 [1]. The two bottom trunnions are not used during lifting of the cask.

B. Handling Loads (Cask in a horizontal position on transfer trailer). All four trunnions rest on the supports on the trailer. The four trunnions are designed to resist the following transfer loads:

   DW (Dead Weight) + 1g Axial
   DW + 1g Transverse
   DW + 1g Vertical
   DW + ½*g* Axial + ½*g* Transverse + ½*g* Vertical

   (Directions are relative to a horizontal cask)

The transfer cask shell and trunnions are assumed to be at 300° F during transfer. This assumption is conservative based on the thermal evaluation performed in Chapter 4.

3.9.5.2 Component Weights

The weight of the NUHOMS®-OS187H Transfer Cask is 228.72 kips, including the loaded DSC (Section 3.2). However, for conservatism, a weight of 250.00 kips. is used in this analysis.

3.9.5.3 Load Cases

The following moment arms are used for the two load cases:

Load Case	*g* Load	Moment Arm Length	Reaction Support
Lifting	6g and 10g longitudinal	9.750 in.*	Top two trunnions only
Transfer Loads	DW +1*g* Axial DW+1*g* vertical DW+1*g* transverse DW + 0.5g Axial + 0.5g Vertical + 0.5g Trans.	7.135 in.**	All four top and bottom trunnions

* See Figure 3.9.5-2 (11.63"- 0.38"- 1.5" = 9.75")
** See Figure 3.9.5-1 (8.76"-1.625" = 7.135")

3.9.5.4 Material Properties

The following material properties, used for the trunnion stress analysis, are taken from Reference 2 at 300°F.

Property	SA-182, Gr. FXM-19 (Top Trunnions)	SA-182, Gr. F304 (Bottom Trunnions, t >5")
S_m	31.4 ksi	20 ksi
S_y	43.3 ksi	22.4 ksi
S_u	94.2 ksi	66.2 ksi

3.9.5.5 Stress Criteria

ANSI N14.6 requires the maximum tensile and shear stresses in the lifting trunnion due to 6*g* and 10*g* load be checked against the material yield and ultimate stresses respectively. The handling loads are normal condition (Level A) loads and are compared with the allowable stresses in ASME Code, Section III, Subsection NC [3].

3.9.5.6 Stress Computation

3.9.5.6.1 Lifting Load Stresses in Top Trunnions

The top trunnion material (SA-182 Gr. FXM19) ultimate and yield stresses at 300° F are 94,200 psi and 43,300 psi respectively. Since the ratio of two design lifting loads for each top trunnion is 1.667 (10*g* / 6*g*), is less than the ratio of the allowable stresses, 2.175 (94,200psi / 43,300 psi), it is not necessary to check stresses in the trunnions for the higher 10*g* design load.

The 6*g* Vertical load on one top trunnion, F_1, is,

$$F_1 = 250{,}000 \text{ lb} \times 6g \times 1.1 \times 1/2 = 825{,}000 \text{ lb}$$

A dynamic load factor, DLF, of 1.1 is used in this calculation.

The 2.5 inch thick lifting yoke plate is to be positioned in the middle of the 3 inch wide top trunnion groove. Therefore, the lift weight acts at the center of the 3 inch trunnion groove. (See Figure 3.9.5-2 for the load location)

A. Stresses at trunnion Section A-A (See Figure 3.9.5-2)

The cross-section area, $A_{A\text{-}A}$, and area moment of inertia, $I_{A\text{-}A}$ are the following.

$$A_{A\text{-}A} = \pi/4\ (8.75^2 - 4^2) = 47.57\ \text{in}^2$$
$$I_{A\text{-}A} = \pi/64\ (8.75^4 - 4^4) = 275.17\ \text{in}^4$$

$$M_{A\text{-}A} = F_1 \times L_{A\text{-}A} = 825{,}000\ \text{lb} \times (3 / 2) = 1{,}237{,}500\ \text{in-lb.}$$

The average shear stress, τ_{avg}, is,

$$\tau_{avg} = F_1 / A_{A\text{-}A} = 825{,}000\ \text{lb} / 47.57\ \text{in}^2 = 17{,}343\ \text{psi}$$

The maximum bending stress, σ_b, is,

$$\begin{aligned}\sigma_b &= (M_{A\text{-}A} / I_{A\text{-}A}) \times (H_{A\text{-}A} /2)\\ &= (1{,}237{,}500\ \text{in-lb} / 275.17\ \text{in}^4)\ (8.75 / 2) = 19{,}675\ \text{psi}\end{aligned}$$

The combined shear stress, τ_{max},

$$\begin{aligned}\tau_{max} &= 0.5 \times [(\sigma_b^2 + 4(\tau_{avg})^2]^{0.5}\\ &= 0.5 \times [19{,}675^2 + 4(17{,}343)^2]^{0.5}\\ &= 19{,}940\ \text{psi} < S_y\end{aligned}$$

The maximum tensile stress, σ_{max}, is the following.

$$\begin{aligned}\sigma_{max} &= \sigma_b / 2 + \tau_{max}\\ &= 19{,}675 /2 + 19{,}940 = 29{,}778\ \text{psi} < S_y\end{aligned}$$

B. Stresses at trunnion Section B-B (See Figure 3.9.5-2)

Cross-section Area, $A_{B\text{-}B}$, Area Moment of Inertia, $I_{B\text{-}B}$, are the following.

$$A_{B\text{-}B} = \pi/4\ (12^2 - 4^2) = 100.53\ \text{in}^2$$
$$I_{B\text{-}B} = \pi/64\ (12^4 - 4^4) = 1{,}005\ \text{in}^4$$

$$M_{B\text{-}B} = 825{,}000\ \text{lb} \times (3'' / 2 + 3.25'') = 3{,}918{,}750\ \text{in-lb.}$$

The average shear stress, τ_{avg}, is,

$$\tau_{avg} = F_1 / A_{B\text{-}B} = 825{,}000\ \text{lb} / 100.53\ \text{in}^2 = 8{,}207\ \text{psi}$$

The maximum bending stress, σ_b, is,

$$\sigma_b = (M_{B\text{-}B} / I_{B\text{-}B}) \times (H_{B\text{-}B} /2)$$
$$= (3{,}918{,}750 \text{ in-lb} / 1{,}005 \text{ in}^4)\ (12 / 2) = 23{,}396 \text{ psi}$$

The combined shear stress, τ_{max},

$$\tau_{max} = 0.5 \times [(\sigma_b^2 + 4(\tau_{avg})^2]^{0.5}$$
$$= 0.5 \times [23{,}396^2 + 4(8{,}207)^2]^{0.5}$$
$$= 14{,}289 \text{ psi} < S_y$$

The maximum tensile stress, σ_{max}, is the following.

$$\sigma_{max} = \sigma_b / 2 + \tau_{max}$$
$$= 22{,}396 / 2 + 14{,}289 = 25{,}987 \text{ psi} < S_y$$

C. Stresses at Section C-C (See Figure 3.9.5-2)

Cross-section Area, $A_{B\text{-}B}$, Area Moment of Inertia, $I_{B\text{-}B}$, are the following.

$$A_{C\text{-}C} = \pi/4\ (17.15^2 - 4^2) = 218.44 \text{ in}^2$$
$$I_{C\text{-}C} = \pi/64\ (17.15^4 - 4^4) = 4{,}234 \text{ in}^4$$

$$M_{C\text{-}C} = F_1 \times L_{C\text{-}C} = 825{,}000 \text{ lb} \times (11.63" - 0.38" - 3" / 2) = 8{,}043{,}750 \text{ in-lb.}$$

The average shear stress, τ_{avg}, is,

$$\tau_{avg} = F_1 / A_{C\text{-}C} = 825{,}000 \text{ lb} / 218.44 \text{ in}^2 = 3{,}777 \text{ psi}$$

The maximum bending stress, σ_b, is,

$$\sigma_b = (M_{C\text{-}C} / I_{C\text{-}C}) \times (H_{C\text{-}C} /2)$$
$$= (8{,}043{,}750 \text{ in-lb} / 4{,}234 \text{ in}^4)\ (17.15 / 2) = 16{,}291 \text{ psi}$$

The combined shear stress, τ_{max},

$$\tau_{max} = 0.5 \times [(\sigma_b^2 + 4(\tau_{avg})^2]^{0.5}$$
$$= 0.5 \times [16{,}291^2 + 4(3{,}777)^2]^{0.5}$$
$$= 8{,}979 \text{ psi} < S_y$$

The maximum tensile stress, σ_{max}, is the following.

$$\sigma_{max} = \sigma_b / 2 + \tau_{max}$$
$$= 16{,}291 /2 + 8{,}979 = 17{,}125 \text{ psi} < S_y$$

D. Bearing Stresses at Trunnion

The following dimensions refer to the Figure 3.9.5-3.

Length AO = 6.5 in., BC = 4.75 in., OC = 5 in., FC = 4.375 in.

Therefore,

$$DO = AO - AD = AO - BC = 6.5 \text{ in.} - 4.75 \text{ in.} = 1.75 \text{ in.}$$

$$\angle DCO = \sin^{-1}(DO/CO) = 20.4873°$$
$$\angle BCE = 90° - \angle DCO = 90° - 20.4873° = 69.5127°$$

During lifting, the 2.5 inch thick lifting arm plate will generate bearing stress in the outer end of the trunnion. The contact between the lifting arm plate and the trunnion is to encompass 69.51°. The projected bearing stress area, A_{br}, is,

$$A_{br} = 2 \times 4.375 \text{ in.} \times \sin 69.51° \times 2.5 \text{ in.} = 20.491 \text{ in.}^2$$

The bearing stress, σ_{br}, is then,

$$\sigma_{br} = 825{,}000 \text{ lb} / 20.491 \text{ in}^2 = 40{,}262 \text{ psi} < S_y$$

3.9.5.6.2 Handling Load Stresses

All four trunnions carry the axial and vertical loads while only one top trunnion and one bottom trunnion on the same side of the cask will carry the transverse load.

A. DW (1*g* vertical) + 1*g* Axial

At the top and bottom trunnions the *g*-loads per trunnion are:

1.0*g* (axial) / 2 sides / 2 set trunnions = 0.25*g* axial per trunnion.
1.0*g* (vertical) / 2 sides / 2 set trunnions = 0.25*g* vertical per trunnion

The bottom trunnions have a larger inner diameter (8 inch diameter of material is removed to reduce the weight, see Figure 3.9.5-1) than the top trunnions (4 inch diameter, see Figure 3.9.5-2). Also, the bottom trunnions material has lower yield and ultimate strengths relative to the top trunnions, and therefore has lower allowable stresses. Thus, the bottom trunnions are critical with respect to stress generated by the handling load. The transfer loads are therefore analyzed only for the weaker bottom trunnions, which are shown in Figure 3.9.5-1.

The vector sum of 0.25g vertical and 0.25*g* axial = $[0.25^2 + 0.25^2]^{1/2}g = 0.354g$

Therefore, the lateral load at each bottom trunnion, F_l, is,

$$F_l = 250{,}000\text{lb} \times 0.354g = 88{,}500 \text{ lb.}$$

Stresses at Trunnion Section B-B (See Figure 3.9.5-1)

The cross-section Area, $A_{B\text{-}B}$, is,

$$A_{B\text{-}B} = \pi/4\ (12^2 - 8^2) = 62.83 \text{ in}^2$$

Area Moment of Inertia, $I_{B\text{-}B}$, is,

$$I_{B\text{-}B} = \pi/64\ (12^4 - 8^4) = 816.81 \text{ in}^4$$

Therefore, the bending moment, $M_{B\text{-}B}$, is,

$$M_{B\text{-}B} = 88{,}500 \text{ lb} \times (3.25 \text{ in.} / 2) = 143{,}813 \text{ in-lb.}$$

The maximum shear stress due to bending for a hollow circular section, τ_{max}, is the following.

$$\tau_{max} = 2F_l / A_{B\text{-}B} = 2 \times 88{,}500 \text{ lb} / 62.83 \text{ in}^2 = 2{,}817 \text{ psi}$$

The maximum bending stress due to lateral load, σ_x, is,

$$\sigma_x = (M_{B\text{-}B} / I_{B\text{-}B}) \times (H_{B\text{-}B} /2)$$
$$= (143{,}813 \text{ in-lb} / 816.61 \text{ in}^4)\ (12 \text{ in.} / 2) = 1{,}057 \text{ psi.}$$

The stress intensity, *S.I.*, is then,

$$S.I. = [(\sigma_x^2 + 4(\tau_{max})^2]^{0.5} = [1{,}057^2 + 4(2{,}817)^2]^{0.5}$$
$$= 5{,}732 \text{ psi} < S_m$$

The stress intensity, S.I., calculated here is conservatively considered to be primary membrane stress, P_m, and is evaluated against its allowable stress, S_m, as per ASME B&PV Section III-NC [3].

$$S_m = 20{,}000 \text{ psi (for SA-182 Gr.F304 at 300° F)}$$

Stresses at Section C-C (See Figure 3.9.5-1)

Cross-section Area, $A_{C\text{-}C}$, is,

$$A_{C\text{-}C} = \pi/4\ (17.15^2 - 8^2) = 180.74 \text{ in}^2.$$

Area Moment of Inertia, $I_{C\text{-}C}$, is,

$$I_{C\text{-}C} = \pi/64\ (17.15^4 - 8^4) = 4{,}045 \text{ in}^4.$$

The bending moment, $M_{C\text{-}C}$, is then,

$$M_{C\text{-}C} = F \times L_{C\text{-}C}$$
$$= 88{,}500 \text{ lb} \times (8.75 \text{ in.} - 3.25 \text{ in.} / 2) = 630{,}563 \text{ in-lb.}$$

The maximum shear stress due to bending for a hollow circular section, τ_{max}, is the following.

$$\tau_{max} = 2\ F / A_{C\text{-}C} = 2 \times 88{,}500 \text{ lb} / 180.74 \text{ in}^2 = 979 \text{ psi.}$$

The maximum bending stress due to lateral load, σ_x, is,

$$\sigma_x = (M_{C\text{-}C} / I_{C\text{-}C}) \times (H_{C\text{-}C} /2) + F_a / A_{C\text{-}C}$$
$$= (630{,}563 \text{ in-lb} / 4{,}045 \text{ in.}^4)\ (17.15\text{in.} / 2) = 1{,}337 \text{ psi}$$

The stress intensity, *S.I.*, is,

$$S.I. = [(\sigma_x^2 + 4(\tau_{max})^2]^{0.5}$$
$$= [1{,}337^2 + 4(979)^2]^{0.5} = 2{,}371 \text{ psi} < S_m$$

B. DW (1*g* vertical) + 1*g* Vertical

At the top and bottom trunnions the *g*-load per trunnion is:

2.0*g* (vertical) / 2 sides / 2 set trunnions = 0.5*g* vertical per trunnion

The lateral load at each bottom trunnion, F_1 is the following.

$$F_1 = 250{,}000\text{lb} \times 0.5g = 125{,}000 \text{ lb.}$$

Stresses are calculated from Case A by multiplying with a factor 125,000/88,500 = 1.4124

Stresses at trunnion Section B-B (See Figure 3.9.5-1)

Maximum Stress Intensity, *S.I.*, is,

$$S.I. = 1.4124 \times 5{,}732 = 8{,}096 \text{ psi.} < S_m$$

Stresses at trunnion Section C-C (See Figure 3.9.5-1)

Maximum Stress Intensity, *S.I.*, is,

$$S.I. = 1.4124 \times 2{,}371 = 3{,}349 \text{ psi.} < S_m$$

C. DW (1*g* vertical) + 1*g* Transverse

At the top and bottom trunnions the *g*-loads per trunnion are:

1.0*g* (transverse) / 1 side / 2 set trunnions = 0.5*g* transverse per trunnion.
1.0*g* (vertical) / 2 sides / 2 set trunnions = 0.25*g* vertical per trunnion

Lateral load at each bottom trunnion, F_1, is,

$$F_1 = 250{,}000\text{lb} \times 0.25 = 62{,}500 \text{ lb}$$

Axial Load at bottom trunnion, F_2, is,

$$F_2 = 250{,}000\text{lb} \times 0.5 = 125{,}000 \text{ lb}$$

Stresses at trunnion Section B-B (See Figure 3.9.5-1)

Therefore, the bending moment, $M_{B\text{-}B}$, is,

$$M_{B\text{-}B} = 62{,}500 \text{ lb} \times (3.25 \text{ in.} / 2) = 101{,}563 \text{ in-lb.}$$

The maximum shear stress due to bending for a hollow circular section, τ_{max}, is the following.

$$\tau_{max} = 2F_1 / A_{B\text{-}B} = 2 \times 62{,}500 \text{ lb} / 62.83 \text{ in}^2 = 1{,}989 \text{ psi.}$$

The maximum normal stress, σ_x, is,

$$\begin{aligned}\sigma_x &= \text{max. bending stress due to lateral load + normal stress due to axial load}\\ &= (M_{B\text{-}B} / I_{B\text{-}B}) \times (H_{B\text{-}B} / 2) + F_2 / A_{B\text{-}B}\\ &= (101{,}563 \text{ in-lb} / 816.61 \text{ in}^4)\ (12 \text{ in.} / 2) + 125{,}000 \text{ lb} / 62.83 \text{ in}^2\\ &= 746 + 1989 = 2{,}735 \text{ psi.}\end{aligned}$$

The stress intensity, *S.I.*, is,

$$\begin{aligned}S.I. &= [(\sigma_x^2 + 4(\tau_{max})^2]^{0.5} = [2{,}735^2 + 4(1{,}989)^2]^{0.5}\\ &= 4{,}828 \text{ psi} < S_m\end{aligned}$$

Stresses at Section C-C (See Figure 3.9.5-1)

The bending moment, $M_{C\text{-}C}$, is,

$$\begin{aligned}M_{C\text{-}C} &= F_1 \times L_{C\text{-}C}\\ &= 62{,}500 \text{ lb} \times (8.75 \text{ in.} - 3.25 \text{ in.} / 2) = 445{,}313 \text{ in-lb.}\end{aligned}$$

The maximum shear stress due to bending for a hollow circular section, τ_{max}, is the following.

$$\tau_{max} = 2F / A_{C\text{-}C} = 2 \times 62{,}500 \text{ lb} / 180.74 \text{ in}^2 = 692 \text{ psi.}$$

The maximum normal stress, σ_x, is,

$$\begin{aligned}\sigma_x &= \text{max. bending stress due to lateral load + normal stress due to axial load}\\ &= (M_{C\text{-}C} / I_{C\text{-}C}) \times (H_{C\text{-}C} / 2) + F_a / A_{C\text{-}C}\\ &= (445{,}313 \text{ in-lb} / 4{,}045 \text{ in}^4)\ (17.15 \text{ in.} / 2) + 125{,}000 \text{ lb} / 180.74 \text{ in}^2\\ &= 944 + 692 = 1{,}636 \text{ psi.}\end{aligned}$$

The stress intensity, *S.I.*, is,

$$\begin{aligned}S.I. &= [(\sigma_x^2 + 4(\tau_{max})^2]^{0.5}\\ &= [1{,}636^2 + 4(692)^2]^{0.5} = 2{,}143 \text{ psi} < S_m\end{aligned}$$

D. DW + 0.5*g* Axial + 0.5*g* Vertical + 0.5*g* Transverse

At the top and bottom trunnions the *g*-loads per trunnion are:

0.5*g* (axial) / 2 sides / 2 set trunnions = 0.125*g* axial per trunnion
0.5*g* (transverse) / 1 side / 2 set trunnions = 0.25*g* transverse per trunnion
1.5*g* (vertical) / 2 sides / 2 set trunnions = 0.375*g* vertical per trunnion

The vector sum of 0.375*g* vertical and 0.125*g* axial = $[0.375^2 + 0.125^2]^{1/2}\, g = 0.395g$

Lateral Load at each bottom trunnion, F_1, is,

$$F_1 = 250{,}000\text{lb} \times 0.395g = 98{,}750 \text{ lb}$$

Transverse Load at bottom trunnion, F_2, is,

$$F_2 = 250{,}000\text{lb} \times 0.25g = 62{,}500 \text{ lb}$$

Where, the load, F_2, acts as an axial load on the bottom trunnion.

Stresses at trunnion Section B-B (See Figure 3.9.5-1)

The bending moment, $M_{B\text{-}B}$, is,

$$M_{B\text{-}B} = 98{,}750 \text{ lb} \times (3.25 \text{ in.} / 2) = 160{,}469 \text{ in-lb.}$$

The maximum shear stress due to bending for a hollow circular section, τ_{max}, is the following.

$$\tau_{max} = 2F_1 / A_{B\text{-}B} = 2 \times 98{,}750 \text{ lb} / 62.83 \text{ in}^2 = 3{,}143 \text{ psi.}$$

The maximum normal stress, σ_x, is,

σ_x = max. bending stress due to lateral (F_1) load + normal stress due to F_2 load
$= (M_{B\text{-}B} / I_{B\text{-}B}) \times (H_{B\text{-}B} /2) + F_2 / A_{B\text{-}B}$
$= (160{,}469 \text{ in-lb} / 816.61 \text{ in.}^4)\ (12 \text{ in.} / 2) + 62{,}500 \text{ lb} / 62.83 \text{ in}^2.$
$= 1{,}179 + 995 = 2{,}174$ psi.

The stress intensity, *S.I.*, is,

$$S.I. = [(\sigma_x^2 + 4(\tau_{max})^2]^{0.5} = [2{,}174^2 + 4(3{,}143)^2]^{0.5}$$
$$= 6{,}651 \text{ psi.} < S_m$$

Stresses at Section C-C (See Figure 3.9.5-1)

The bending moment, $M_{C\text{-}C}$, is,

$$M_{C\text{-}C} = F_1 \times L_{C\text{-}C}$$
$$= 98{,}750 \text{ lb} \times (8.75 \text{ in.} - 3.25 \text{ in.} / 2) = 703{,}594 \text{ in-lb.}$$

The maximum shear stress due to bending for a hollow circular section, τ_{max}, is the following.

$$\tau_{max} = 2F_1 / A_{C\text{-}C} = 2 \times 98{,}750 \text{ lb} / \ 180.74 \text{ in}^2 = 1{,}093 \text{ psi.}$$

The maximum normal stress, σ_x, is,

$$\sigma_x = \text{max. bending stress due to lateral load + normal stress due to axial load}$$
$$= (M_{C\text{-}C} / I_{C\text{-}C}) \times (H_{C\text{-}C} /2) + F_2 / A_{C\text{-}C}$$
$$= (703{,}594 \text{ in-lb} / 4{,}045 \text{ in.}^4) (17.15 \text{ in.} / 2) + 62{,}500 \text{ lb} / 180.74 \text{ in.}^2$$
$$= 1{,}492 + 346 = 1{,}838 \text{ psi.}$$

The stress intensity, $S.I.$, is,

$$S.I. = [(\sigma_x^2 + 4(\tau_{max})^2]^{0.5}$$
$$= [1{,}838^2 + 4(1{,}093)^2]^{0.5} = 2{,}856 \text{ psi.} < S_m$$

3.9.5.7 Summary of Computed Stresses

The calculated maximum trunnion stresses are summarized in Table 3.9.5-1 and compared with their corresponding allowable stresses.

3.9.5.8 Conclusions

Table 3.9.5-1 shows that all calculated trunnion stresses are less than their corresponding allowable stresses. Therefore, the NUHOMS®-OS187H Transfer Cask top and bottom trunnions are structurally adequate to withstand loads during lifting and transfer operations.

3.9.5.9 References

1. "Special Lifting Devices for Shipping Containers Weighing 10,000 Pounds or More", ANSI N14.6, 1993.

2. American Society of Mechanical Engineers, ASME Boiler and Pressure Vessel Code, Section II, Part D, 1998, including 2000 addenda.

3. American Society of Mechanical Engineers, ASME Boiler and Pressure Vessel Code, Section III, Division 1, Subsection NC, 1998, including 2000 addenda.

Table 3.9.5-1
Summary of Computed and Allowable Trunnion Stresses

Case Number	Load	Maximum Stress		Allowable (ksi)
		Type	Magnitude (ksi)	
1	Lifting 6*g*	Shear	19.9	43.3 (2)
		Tensile	29.8	43.3 (2)
2	Lifting (1) 10*g*	Shear	33.2	94.2 (4)
		Tensile	49.6	94.2 (4)
3	Handling DW + 1.0g Axial	P_m	5.7	20.0 (3)
		$P_m + P_b$	5.7	20.0 (3)
4	Handling DW + 1.0*g* Vertical	P_m	8.1	20.0 (3)
		$P_m + P_b$	8.1	20.0 (3)
5	Handling DW + 1.0*g* Transverse	P_m	4.8	20.0 (3)
		$P_m + P_b$	4.8	20.0 (3)
6	Handling DW + 0.5*g* Axial + 0.5*g* Vertical + 0.5*g* Transverse	P_m	6.7	20.0 (3)
		$P_m + P_b$	6.7	20.0 (3)

Notes:
(1) Stresses in the trunnions are obtained by direct ratio from 6*g* load.
(2) Yield stress, S_y, for top trunnion material SA-182-FXM19 at 300° F per ANSI N14.6 [1] criterion.
(3) Design Stress Intensity, S_m, for bottom trunnion material SA-182-F304 at 300° F per ASME Section III-NC [3] criterion. Conservatively, $P_m + P_b$ is compared with S_m.
(4) Ultimate stress, S_u, for trunnion material SA-182-FXM19 at 300° F per ANSI N14.6 [1] criterion.

Figure Withheld Under 10 CFR 2.390

Figure 3.9.5-1
OS187H Transfer Cask Bottom Trunnion (Top View)

Figure Withheld Under 10 CFR 2.390

Figure 3.9.5-2
OS187H Transfer Cask Top Trunnion (Top View)

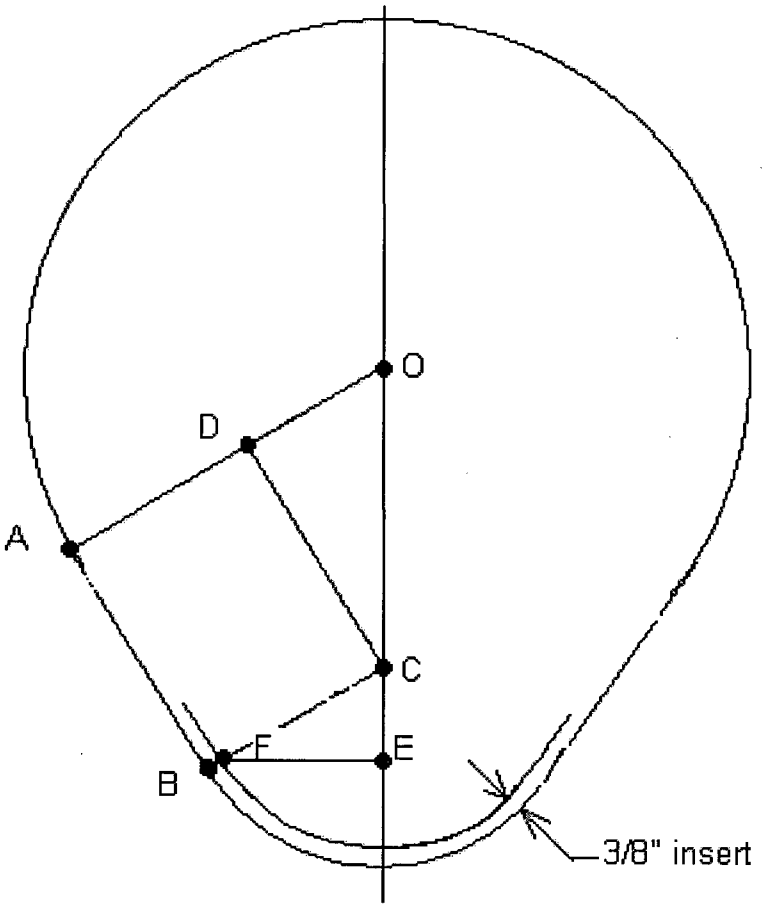

Figure 3.9.5-3
Opening in the Lifting Yoke Arm Geometry

APPENDIX 3.9.6
OS187H TRANSFER CASK SHIELD PANEL STURCTURAL ANALYSIS

TABLE OF CONTENTS

3.9.6 OS187H TRANSFER CASK SHIELD PANEL STURCTURAL ANALYSIS.. 3.9.6-1

3.9.6.1 Introduction 3.9.6-1

3.9.6.2 Material Properties 3.9.6-1

3.9.6.3 Component Weights 3.9.6-2

3.9.6.4 Stress Criteria 3.9.6-2

3.9.6.5 Load Cases 3.9.6-3

3.9.6.6 Stress Calculations 3.9.6-3

3.9.6.7 Conclusions 3.9.6-7

3.9.6.8 References 3.9.6-8

LIST OF TABLES

3.9.6-1 Summary of Computed and Allowable Neutron Shield Shell Stresses

LIST OF FIGURES

3.9.6-1 Neutron Shield Shell Finite Element Model

3.9.6-2 Neutron Shield Shell Finite Element Model, Top Plate Region

3.9.6-3 Neutron Shield Shell Finite Element Model, Bottom Plate Region

3.9.6-4 Neutron Shield Shell Finite Element Model, 3*g* Lifting Boundary Conditions

3.9.6-5 3*g* Lifting Stress Intensity Distribution

3.9.6-6 Neutron Shield Shell Finite Element Model, Transfer Loads Boundary Conditions

3.9.6-7 Transfer Loads Stress Intensity Distribution

3.9.6-8 Cold Ambient Environment Temperature Distribution

3.9.6-9 Hot Ambient Environment Temperature Distribution

4.9.6-10 Transfer Loads plus Cold Ambient Condition Stress Intensity Distribution

4.9.6-11 Transfer Loads plus Hot Ambient Condition Stress Intensity Distribution

3.9.6 OS187H TRANSFER CASK SHIELD PANEL STRUCTURAL ANALYSIS

3.9.6.1 Introduction

The purpose of this appendix is to present the evaluation of the stresses in the NUHOMS®-OS187H Transfer Cask neutron shield shell due to all applied loads during fuel loading and transfer operations.

A finite element model was built for the structural analysis of the outer neutron shield shell, end closure, central plates and structural shell. These components were modeled with the ANSYS Solid PLANE42 elements with axisymmetric option. The top and bottom closure plate welds were also modeled with PLANE42 elements. Double nodes were created at the central plate and shell intersections. These nodes were coupled to simulate the weld effect. Figures 3.9.6-1, 3.9.6-2 and 3.9.6-3 show the overall finite element model and its details. The same finite element model is used for all loading conditions.

3.9.6.2 Material Properties

The transfer cask shell is assumed to be at 300° F uniform temperature during transfer operations. This assumption is conservative based on the thermal evaluations performed in Chapter 4.

All shell components are constructed from stainless steel SA-240, Grade 304. The following mechanical and thermal material properties taken from Reference 1 are used in the analysis:

Material	Temp. °F	S_u (ksi)	S_y (ksi)	S_m (ksi)	E (10^6 psi)	α (10^{-6}) (in/in/°F)	Conductivity (Btu/hr-in-°F)	Density (lb/in^3)
SA-240 Stainless Steel 304	70	75.0	30.0	20.0	28.3	8.5	0.7217	0.29
	200	71.0	25.0	20.0	27.6	8.9	0.775	0.29
	300	66.2	22.4	20.0	27.0	9.2	0.8167	0.29
	400	64.0	20.7	18.7	26.5	9.5	0.8667	0.29

3.9.6.3 Component Weights

The weight of the NUHOMS®-OS187H Transfer Cask neutron shield shell, including the cylindrical shell, the top and bottom support rings, and the 15 central support rings is 4,288 lb. The weight of the neutron shield shell water is 8,458 lb (the transfer component weights are tabulated in Section 3.2). However, for conservatism, a weight of 8,500 lb. is used for the weights of water in this analysis.

For the transfer cask in the vertical orientation, the inertial force due to water weight is applied as pressure in the following way.

The weight of the neutron shield water, W is 8,500 lb. The maximum hydrostatic pressure at the bottom of the neutron shield shell, W_h, is,

$$W_h = 62.4 \text{ lb/ft}^3 \times 177.24 \text{ in} / 12^3 = 6.4 \text{ psi. ... say } 6.5 \text{ psi}$$

This hydrostatic pressure is linear with the axial height of the shield shell and is 0 psi at the top.

In addition to the water weight pressure, an additional internal uniform pressure of 40 psig is used in all load cases.

3.9.6.4 Stress Criteria

All load cases are analyzed and results evaluated to the requirements of ASME Code, Subsection NC [2] as normal condition (Level A) load cases. According to Reference 2, the maximum allowable membrane (P_m) and membrane plus bending ($P_m + P_b$) stress intensities for normal conditions are S_m and 1.5 S_m respectively. Also, average pure shear is limited to 0.6 S_m. The maximum primary plus secondary stress is limited to 3.0 S_m.

The transfer cask inner shell and structural shell are constructed from SA-240, Type 304 stainless steel. Therefore, the maximum allowable membrane and membrane plus bending stress intensities (at 300° F) are as follows:

Stress Category	Stress Criteria	Maximum Allowable Stress
P_m	S_m	20.0ksi.
$P_m + P_b$	$1.5S_m$	30.0 ksi.
$P_m + P_b + Q$	3.0 S_m	60.0 ksi.
Pure Shear	$0.6S_m$	12.0 ksi.

3.9.6.5 Load Cases

The following load cases are considered. When transfer the loaded cask to ISFSI, the transfer loads are 1g axial, 1g transverse, and 1g vertical. For conservatism, a bounding 2g axial + 2g transverse + 2g vertical is used for stress calculations.

Load Case	Applied Load
3*g* Lifting (Cask Vertical)	40 psi. pressure + hydrostatic pressure + 3*g* longitudinal
Transfer Loads (Cask Horizontal)	40 psi. pressure + water pressure + 2*g* longitudinal + 2*g* vertical + 2*g* transverse 40 psi. pressure + water pressure + 2*g* longitudinal + 2*g* vertical + 2*g* transverse + Cold Thermal 40 psi. pressure + water pressure + 2*g* longitudinal + 2*g* vertical + 2*g* transverse + Hot Thermal

3.9.6.6 Stress Calculations

3.9.6.6.1 3*g* Lifting Load Case

The pressure at the bottom plate due to the 3*g* lifting load for water = 3 × 6.5 = 19.5 psi

The ANSYS elastic stress run is made by applying a 40 psi internal pressure and a 19.5 psi hydrostatic pressure. The loading and boundary conditions are shown in Figure 3.9.6-4. A 3g vertical acceleration is applied to account for the inertia loads. As shown in Figure 3.9.6-4, an internal pressure of 59.5 psi. (40 psi. + 19.5 psi.) is applied at the bottom of the shield shell. This pressure tapers linearly to 40 psi at the top.

The resulting stress intensity distribution in the various shell components is shown in Figure 3.9.6-5. It is seen that the maximum nodal stress intensity in the shell model is 24,123 psi. This maximum stress occurs in weld between the bottom plate and cylinder. These stresses are linearized through the shell thickness and presented in Table 3.9.6-1.

3.9.6.6.2 Transfer Load Condition

During transfer operations, the cask is in the horizontal position and the neutron shield shell is subjected to 40 psi internal pressure and transfer handling loads (2*g* vertical + 2*g* lateral + 2*g* axial).

The vertical and lateral loads are combined in the following way.

$$g_{transverse} = (2.0^2 + 2.0^2)^{1/2} = 2.83g$$

The stress due to the 2.83*g* inertia load conservatively assumes that the weight of the shell structure (4,288 lb.) and water (8,500 lb.) are uniformly distributed only over the 177.24 inch length and a 60° arch. Therefore, the equivalent pressure applied to the outer shell is,

$$p_{vl} = [(4{,}288 + 8{,}500) \times 2.83] / [2\,\pi\,(45.913)(177.24)] \times (360°/60°) = 4.25 \text{ psi. ... say 5 psi}$$

Again, the 5 psi load on the 60° sector is conservatively assumed to act on the full 360°. This pressure is added to 40 psi. pressure and applied to the cylinder.

For 2*g* axial acceleration, the pressure due to the water inertial load on the top plate is,

$$p_a = 8{,}500 \times 2.0 / [\pi \times (45.913^2 - 41.35^2)] = 13.6 \text{ psi. ... say 14 psi}$$

Therefore, a pressure of 54 psi. (40 + 14) is applied to the top plate. Also, there is a 40 psi. pressure applied to the bottom plate.

An ANSYS elastic stress run is made by applying the above calculated pressures to the finite element model. The boundary conditions are shown in Figure 3.9.6-6. The resulting stress intensity distribution is shown in Figure 3.9.6-7. It is seen that the maximum nodal stress intensity in the shell model is 20,137 psi. This maximum stress occurs in the outer shell near the bottom plate weld. These stresses are linearized through the shell thickness and presented in Table 3.9.6-1.

3.9.6.6.3 Thermal Analyses

The thermal analysis of the neutron shield shell model is conducted for both cold and hot environmental conditions. Steady-state ANSYS thermal analyses of the model are conducted to obtain the nodal temperatures by impressing the temperatures as the boundary conditions for both cold and hot conditions. Two-dimensional thermal elements (PLANE55) are used in the analyses. Temperature dependent thermal material properties are also used in the analysis

The resulting temperature distributions for cold and hot ambient cases are shown in Figures 3.9.6-8 and 3.9.6-9, respectively.

3.9.6.6.4 Thermal Stress Analyses

Elastic stress analyses of the shield shell structure are conducted in order to evaluate the transfer plus thermal loads. The loads and boundary conditions of model are shown in Figure 3.9.6-6. The nodal temperature distribution from the above thermal analyses results is applied to obtain the thermal stresses in the model.

The nodal stress intensity distribution is plotted Figures 3.9.6-10 for cold condition, and in Figure 3.9.6-11 for 115° F hot ambient case. The critical stress intensities are summarized in Table 3.9.6-1.

It is seen from these figures that the maximum thermal stress intensities are generated in the cold ambient case. The maximum nodal stress intensity in the shell model is 26,045 psi. This maximum stress occurs in the outer shell near the bottom plate weld. Cold and hot stresses are linearized through the shell thickness, and the maximum stresses are summarized and evaluated in Table 3.9.6-1.

3.9.6.6.5 Weld Stresses at Center Support Plates

The center support plates are attached to the cask structural shell by 3/16 inch fillet (3-12) stitch-welds, and to the outer neutron shield cylinder by 1 inch × 0.12 inch plug welds (24 plug welds for each plate). It is seen from stress intensity distribution in Figure 3.9.6-10 that the maximum stress intensity (13,417 psi) occurs during the transfer load plus cold ambient load case. The maximum stressed center support plate is located close to the bottom end closure plate. The maximum weld stresses are also expected to occur at this plate. The following fillet and plug weld stresses are calculated from the nodal forces.

Fillet Weld Stresses

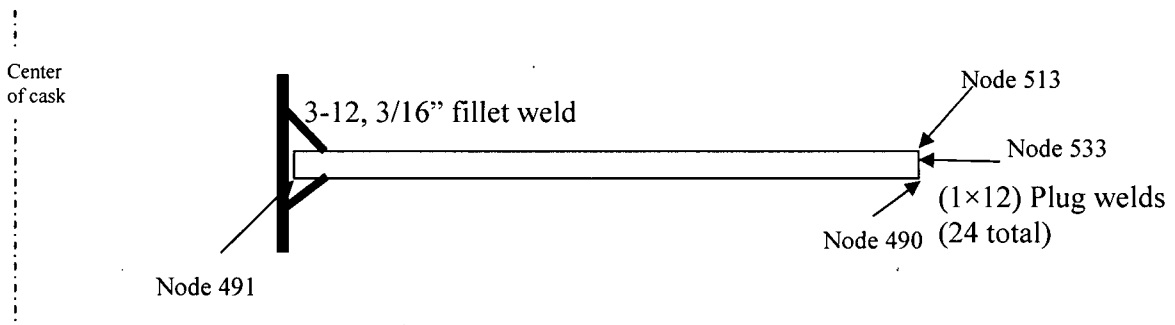

The maximum nodal forces at node 491 (from ANSYS result file) are:

$$F_x = 124{,}800 \text{ lb.} \qquad F_y = -11{,}840 \text{ lb.}$$

The fillet weld tensile/shear area, A_f is,

$$A_f = 3/12\ [\pi(81.7) \times 3/16 \text{ x } 2] = 24.06 \text{ in}^2$$

Therefore, the tensile stress, σ_f is,

$$\sigma_f = 124{,}800 / 24.06 = 5{,}187 \text{ psi}$$

And the shear stress, τ_f, is,

$$\tau_f = 11{,}840 / 24.06 = 492 \text{ psi}$$

The maximum stress intensity, $S.I._f$, is,

$$S.I._f = [(5{,}187)^2 + 4 \times (492^2)]^{0.5} = 5{,}280 \text{ psi,}$$

Which is less than the allowable stress, $S_m = 20.0$ ksi. The maximum shear stress, τ_{fmax}, is,

$$\tau_{fmax} = [(5{,}187/2)^2 + 492^2]^{0.5} = 2{,}640 \text{ psi}$$

Which is less than the allowable shear stress, $0.6S_m = 0.6(20.0) = 12.0$ ksi.

Plug Weld Stress

The maximum forces in the plug weld are the following.

Node	F_x (lb.)	F_y (lb.)
533	0	0
513	-110,100	-130,700
490	59,850	123,800
Total	**-50,250**	**-6,900**

The fillet weld shear area, A_b is,

$$A_b = 24 \text{ plugs} \times (1.0 \times 0.12) = 2.88 \text{ in}^2$$

Therefore, the tensile stress, σ_b is,

$$\sigma_b = 50{,}250/2.88 = 17{,}448 \text{ psi}$$

And the shear stress,τ_b, is,

$$\tau_b = 6{,}900/2.88 = 2{,}396 \text{ psi}$$

The maximum stress intensity, $S.I._b$, is,

$$S.I._b = [(17{,}448)^2 + 4\times(2{,}396^2)]^{0.5} = 18{,}094 \text{ psi}$$

Which is less than the allowable stress, $S_m = 20.0$ ksi. The maximum shear stress, $\tau_{b\max}$, is,

$$\tau_{b\max} = [(17{,}448/2)^2 + 2{,}396^2]^{0.5} = 9{,}047 \text{ psi}$$

Which is less than the allowable shear stress, $0.6S_m = 0.6(20.0) = 12.0$ ksi.

3.9.6.7 Conclusions

Based on the results of the analysis, it is concluded that the outer shell structure is structurally adequate for the specified transfer loads.

3.9.6.8 References

1. American Society of Mechanical Engineers, ASME Boiler and Pressure Vessel Code, Section II, Part D, 1998, including 2000 addenda.

2. American Society of Mechanical Engineers, ASME Boiler and Pressure Vessel Code, Section III, Division 1, Subsection NC, 1998, including 2000 addenda.

Table 3.9.6-1
Summary of Calculated and Allowable Neutron Shield Shell Stresses

Load Case	Stress Category	Maximum Stress (ksi)	Allowable Stress (ksi)
3*g* Lifting	P_m	9.11	20.0
	$P_m + P_b$	21.47	30.0
Transfer Load	P_m	1.52	20.0
	$P_m + P_b$	15.99	30.0
	$P_m + P_b + Q$ (Cold)	21.21	60.0
	$P_m + P_b + Q$ (Hot)	20.6	60.0

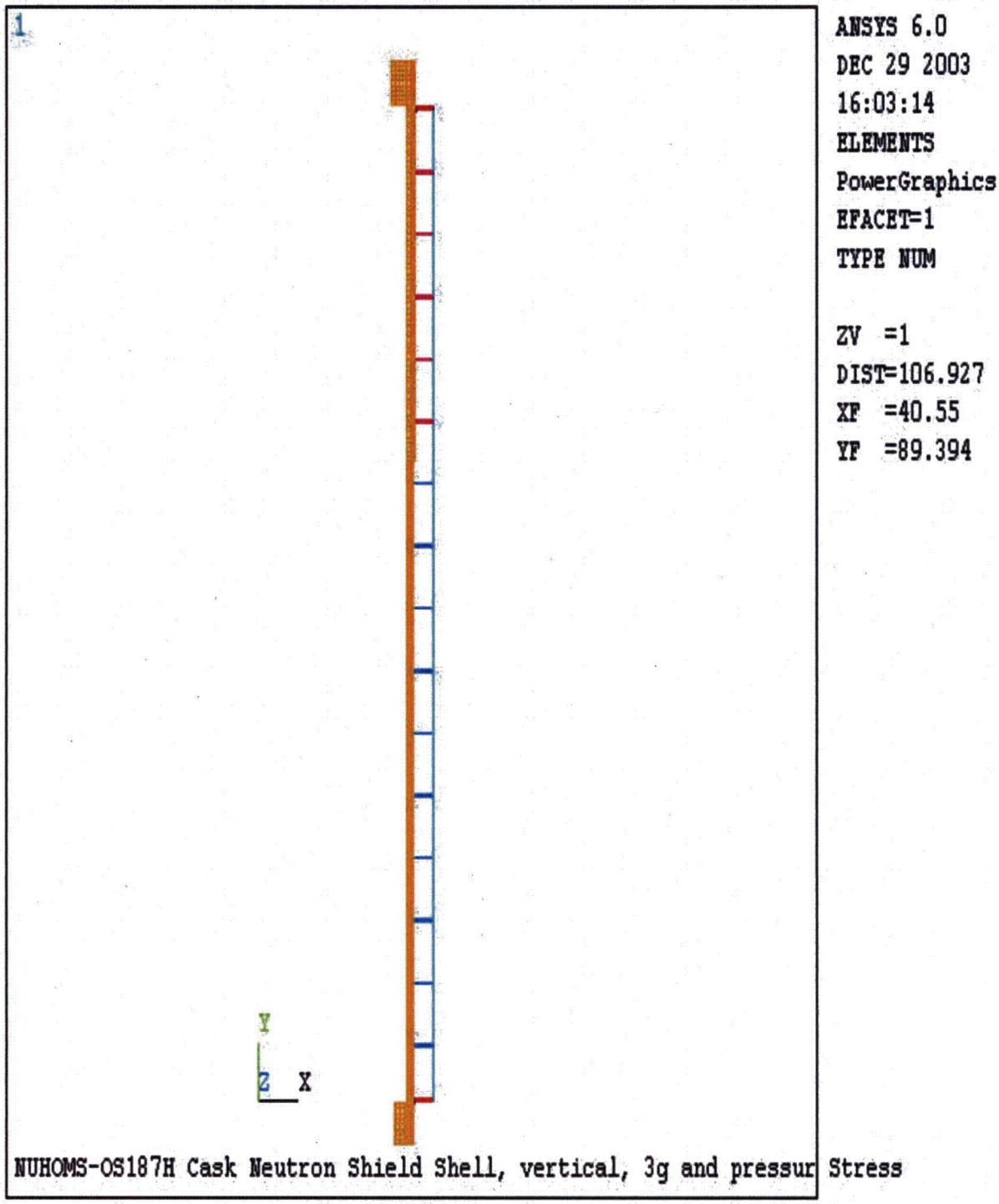

Figure 3.9.6-1
Neutron Shield Shell Finite Element Model

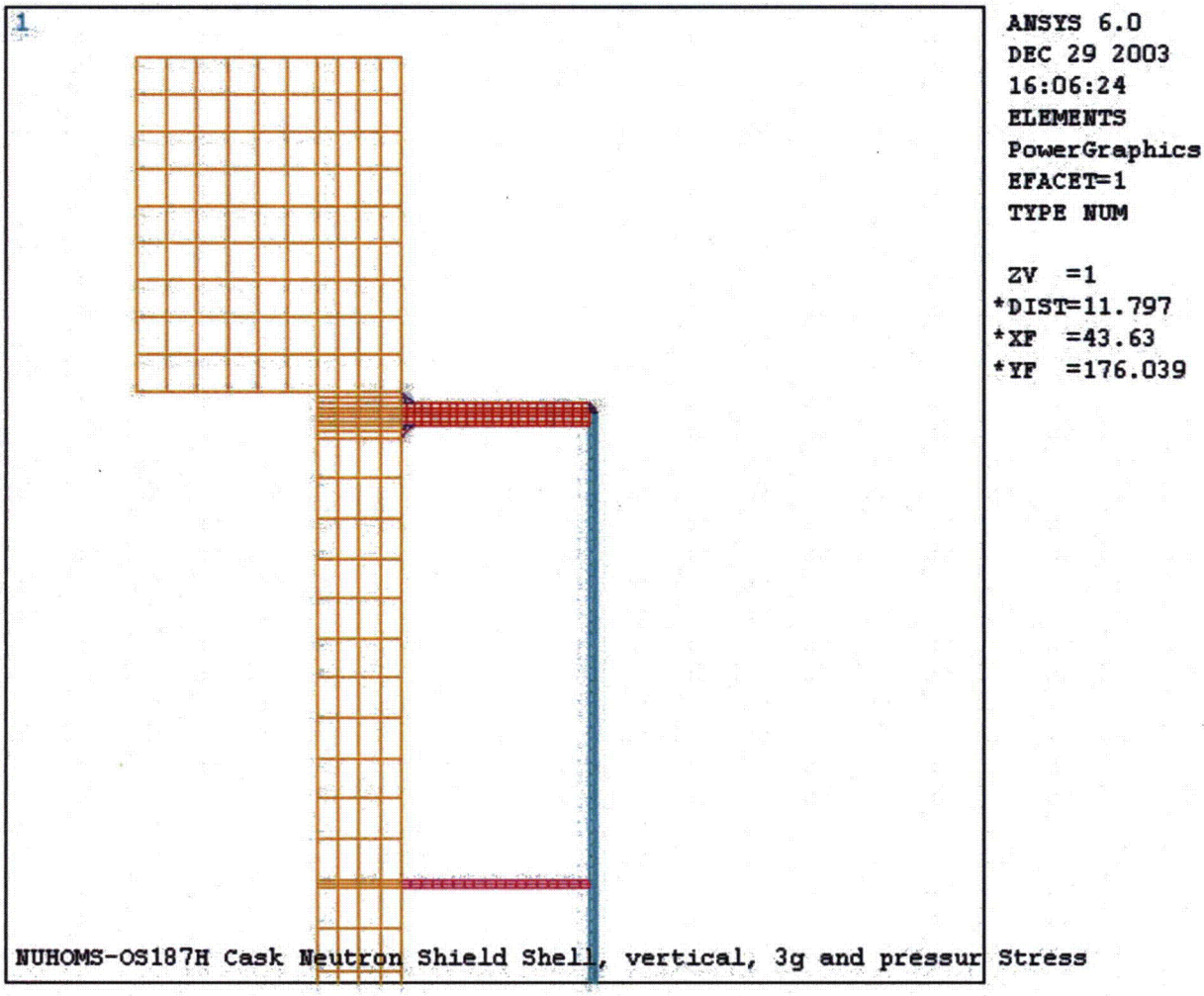

Figure 3.9.6-2
Neutron Shield Shell Finite Element Model, Top Plate Region

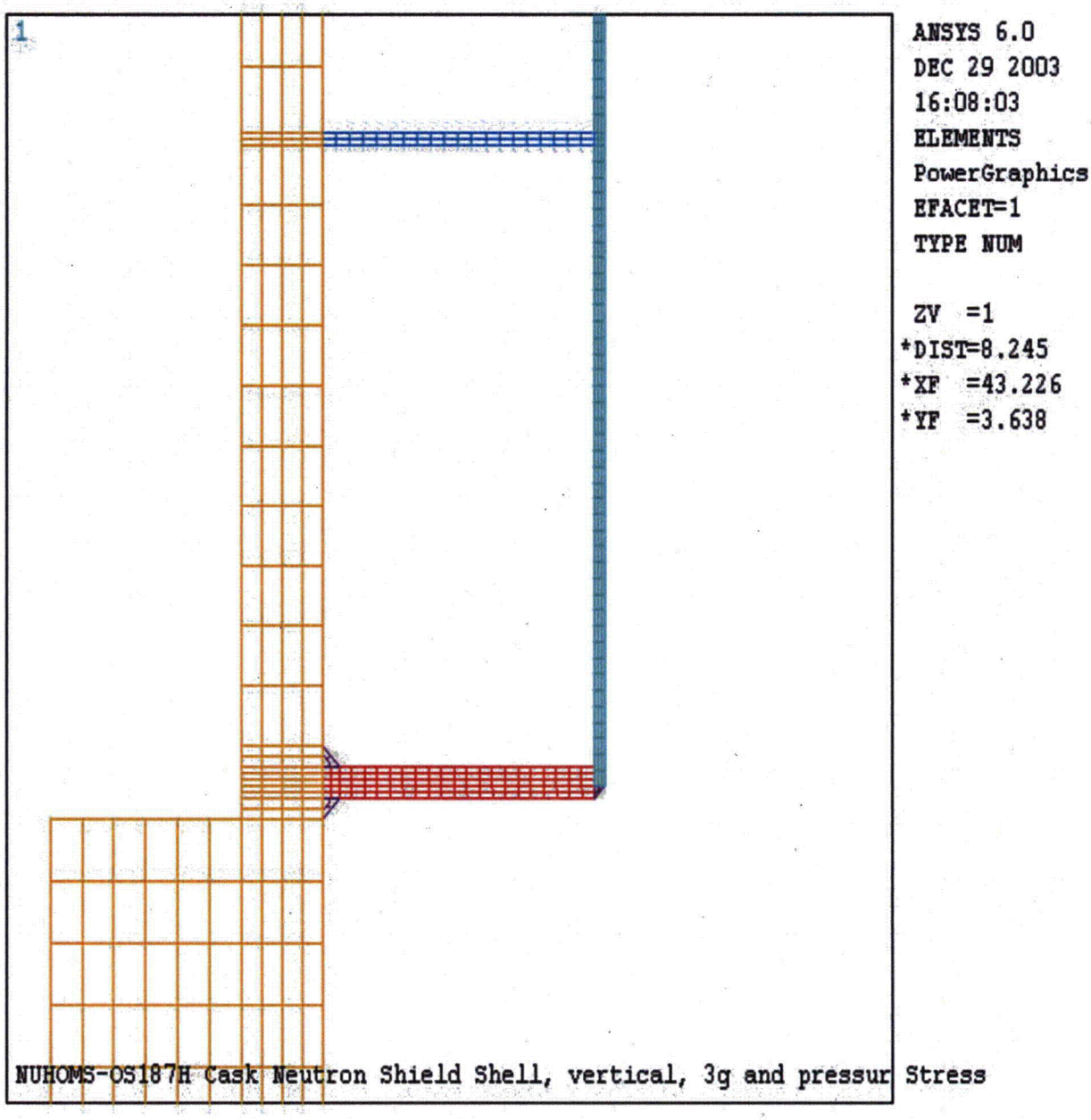

Figure 3.9.6-3
Neutron Shield Shell Finite Element Model, Bottom Plate Region

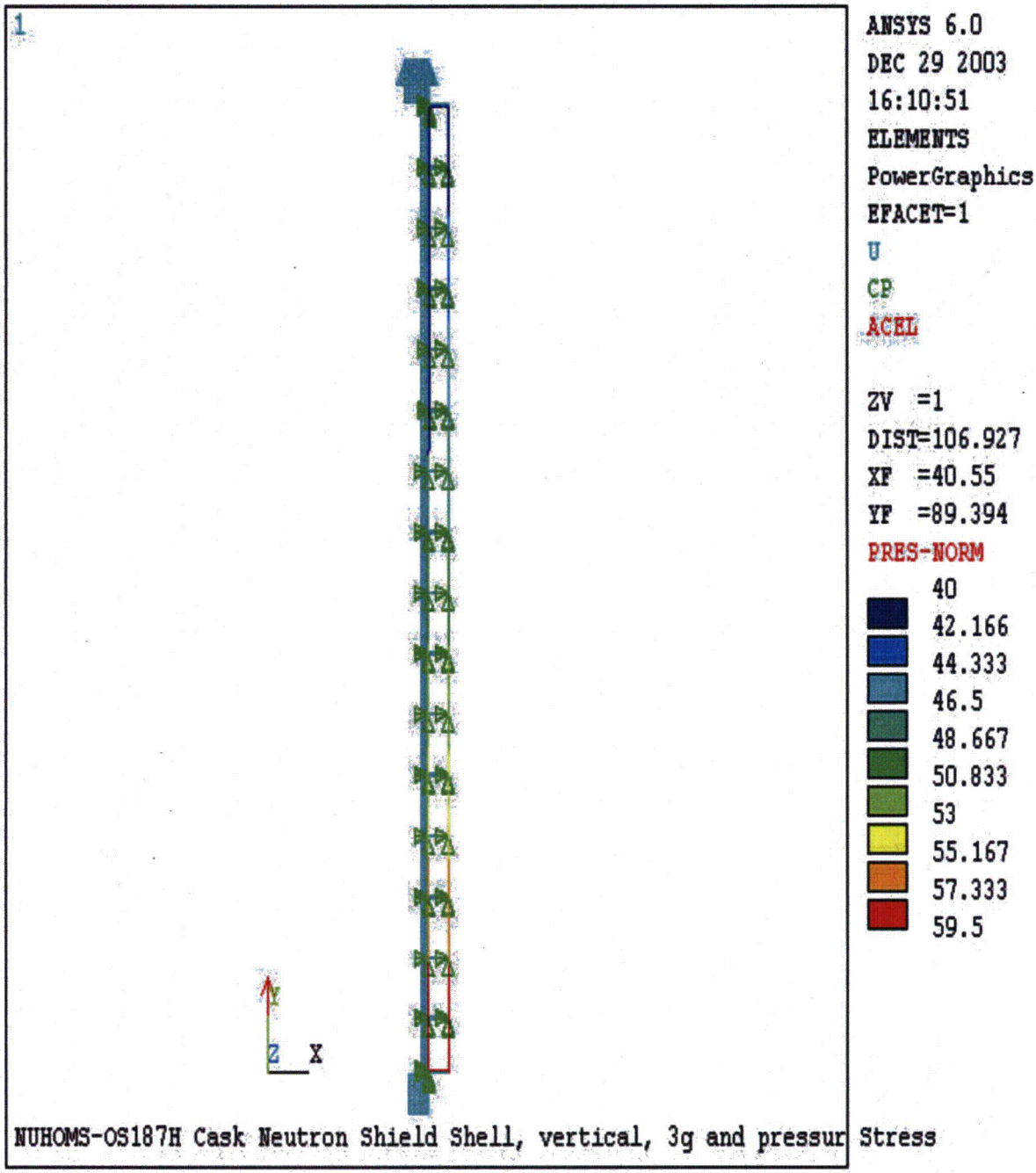

Figure 3.9.6-4
Neutron Shield Shell Finite Element Model, 3*g* Lifting Boundary Conditions

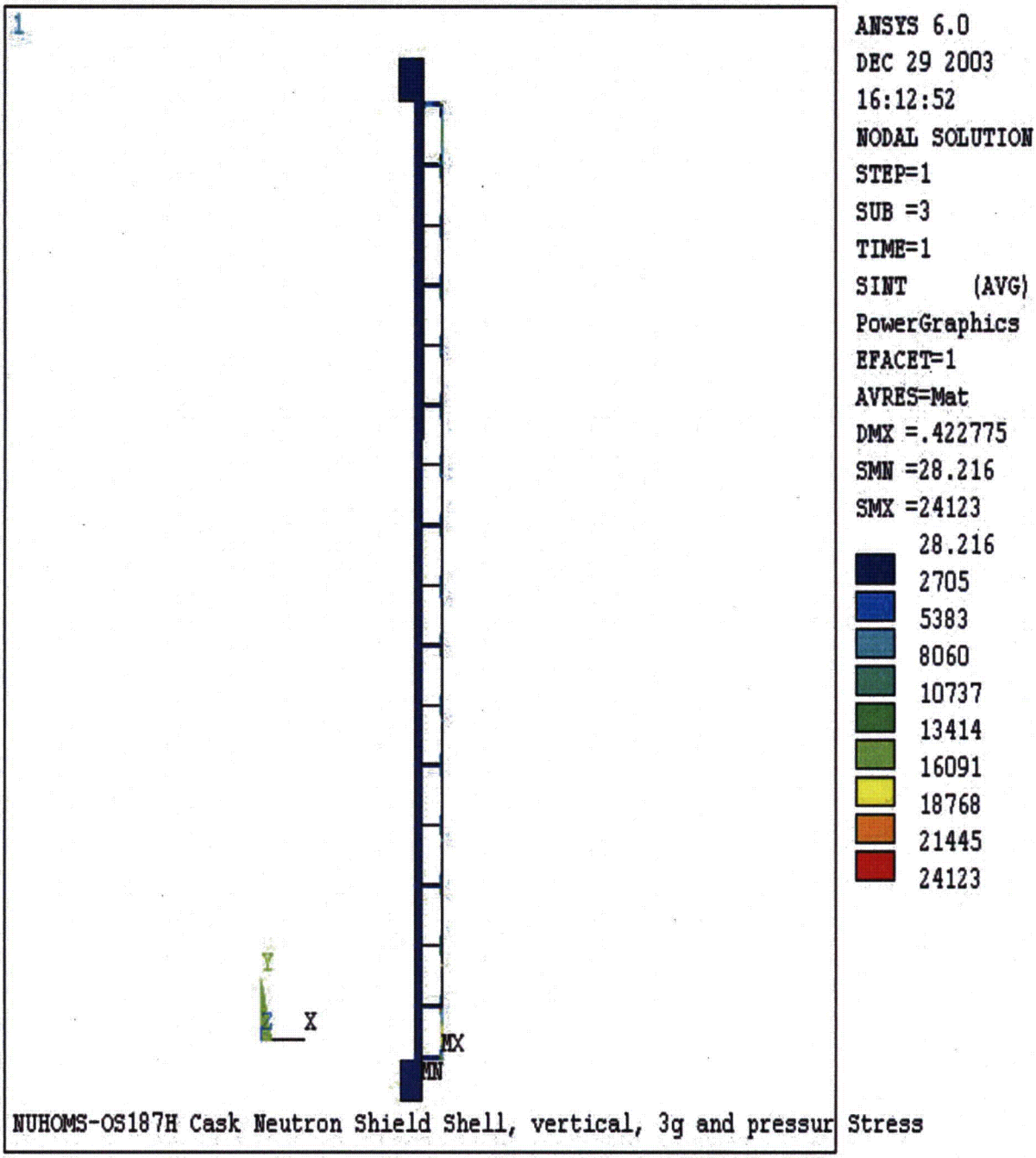

Figure 3.9.6-5
3g Lifting Stress Intensity Distribution

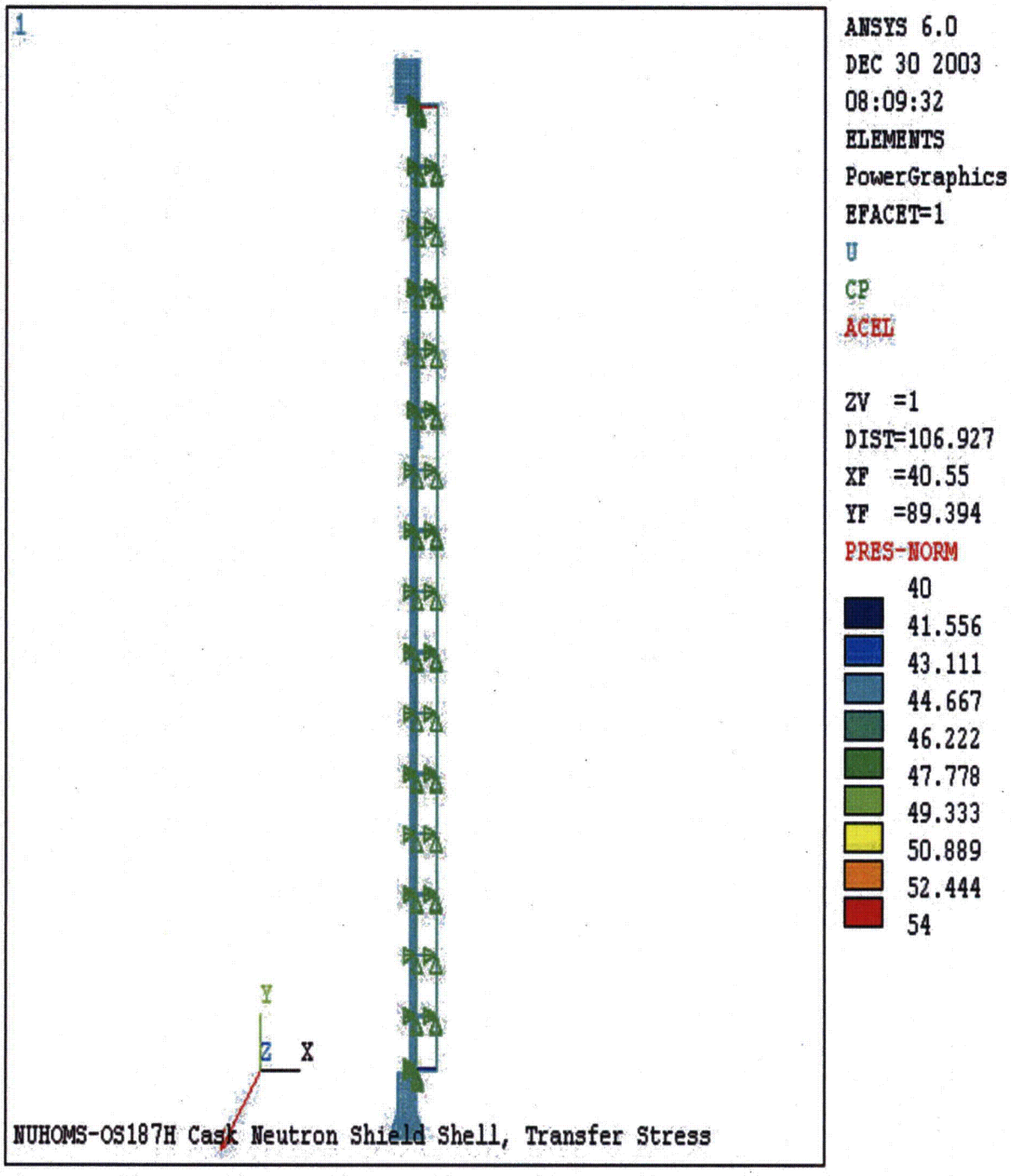

Figure 3.9.6-6
Neutron Shield Shell Finite Element Model, Transfer Loads Boundary Conditions

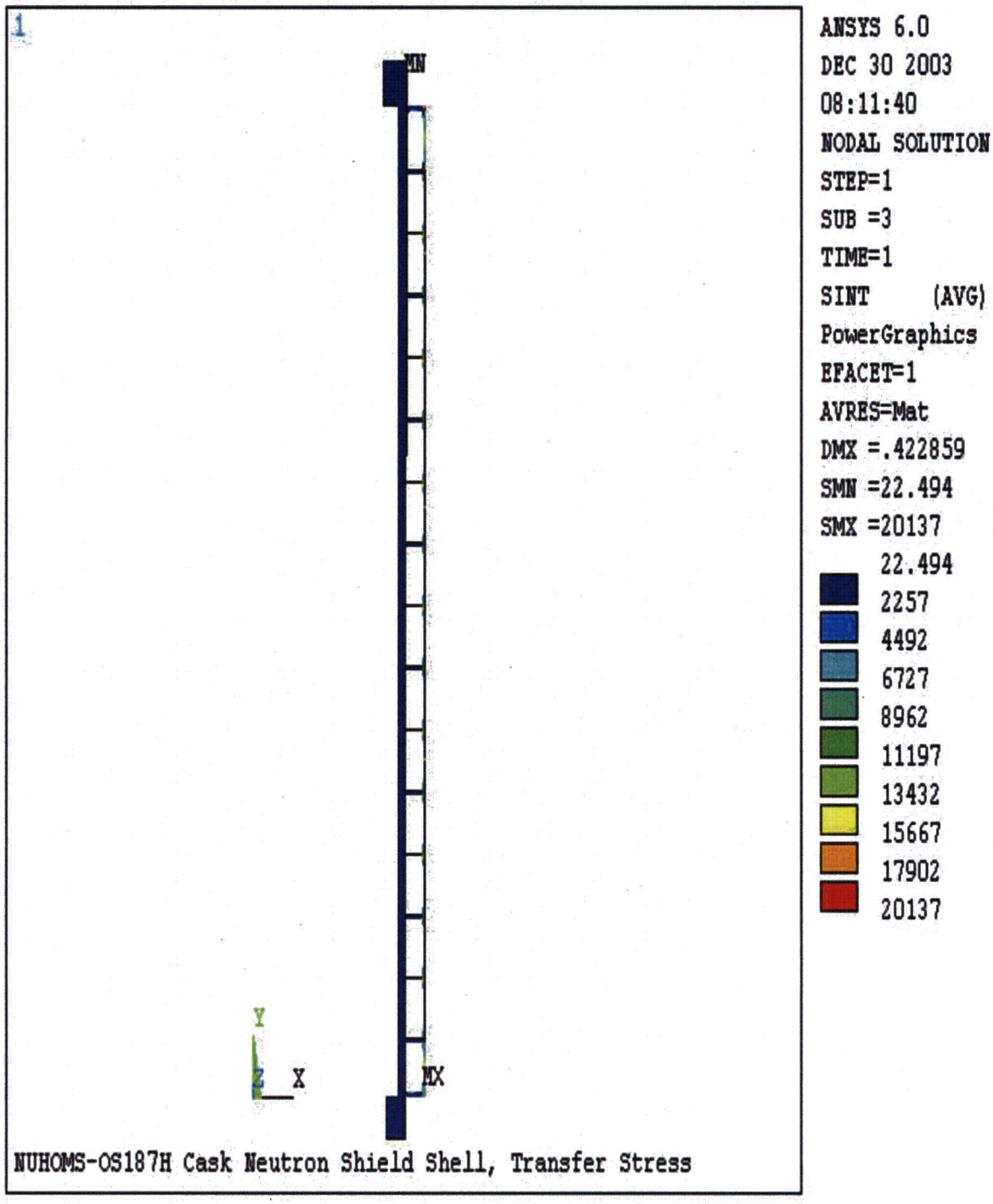

Figure 3.9.6-7
Transfer Loads Stress Intensity Distribution

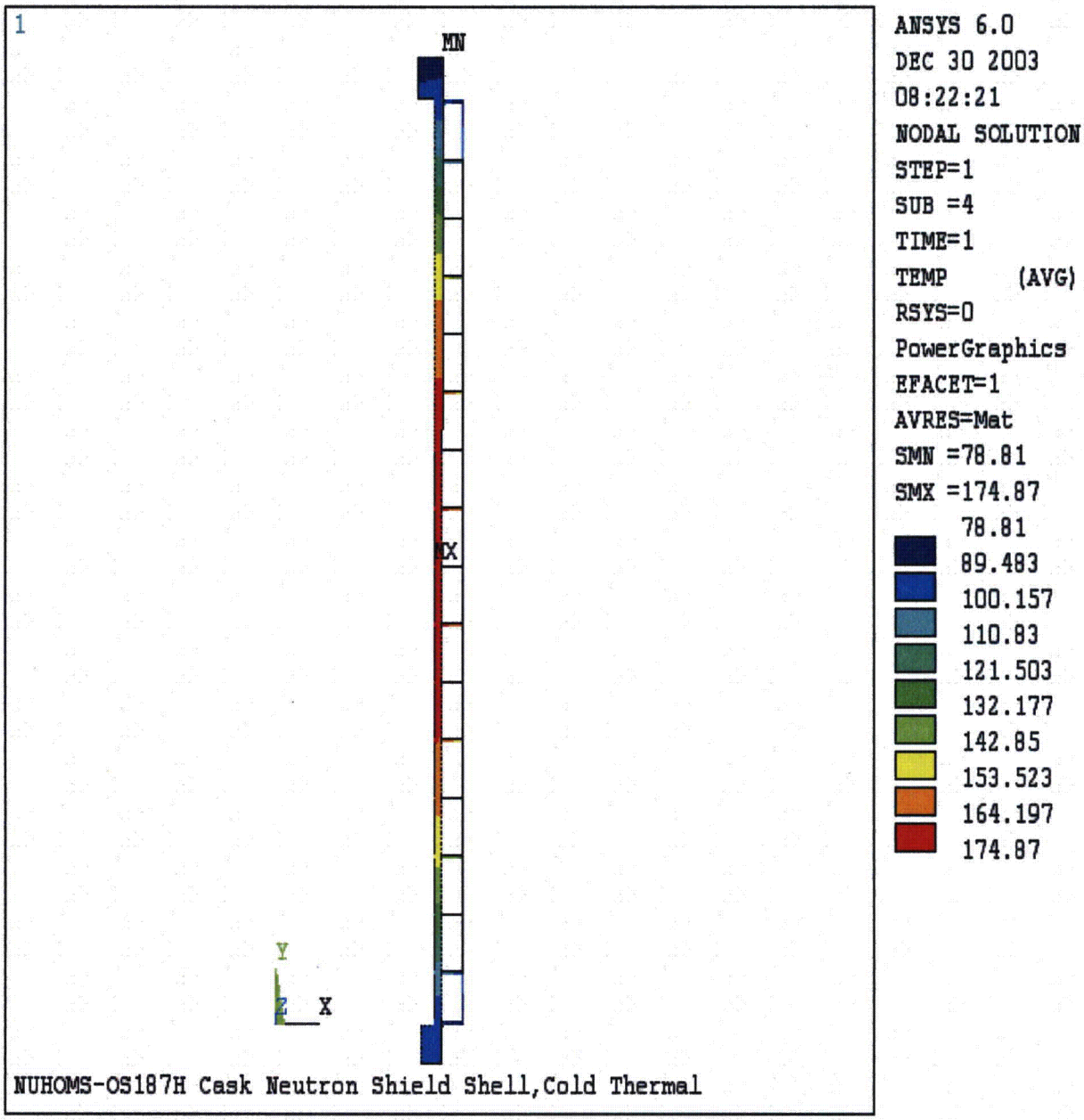

Figure 3.9.6-8
Cold Ambient Environment Temperature Distribution

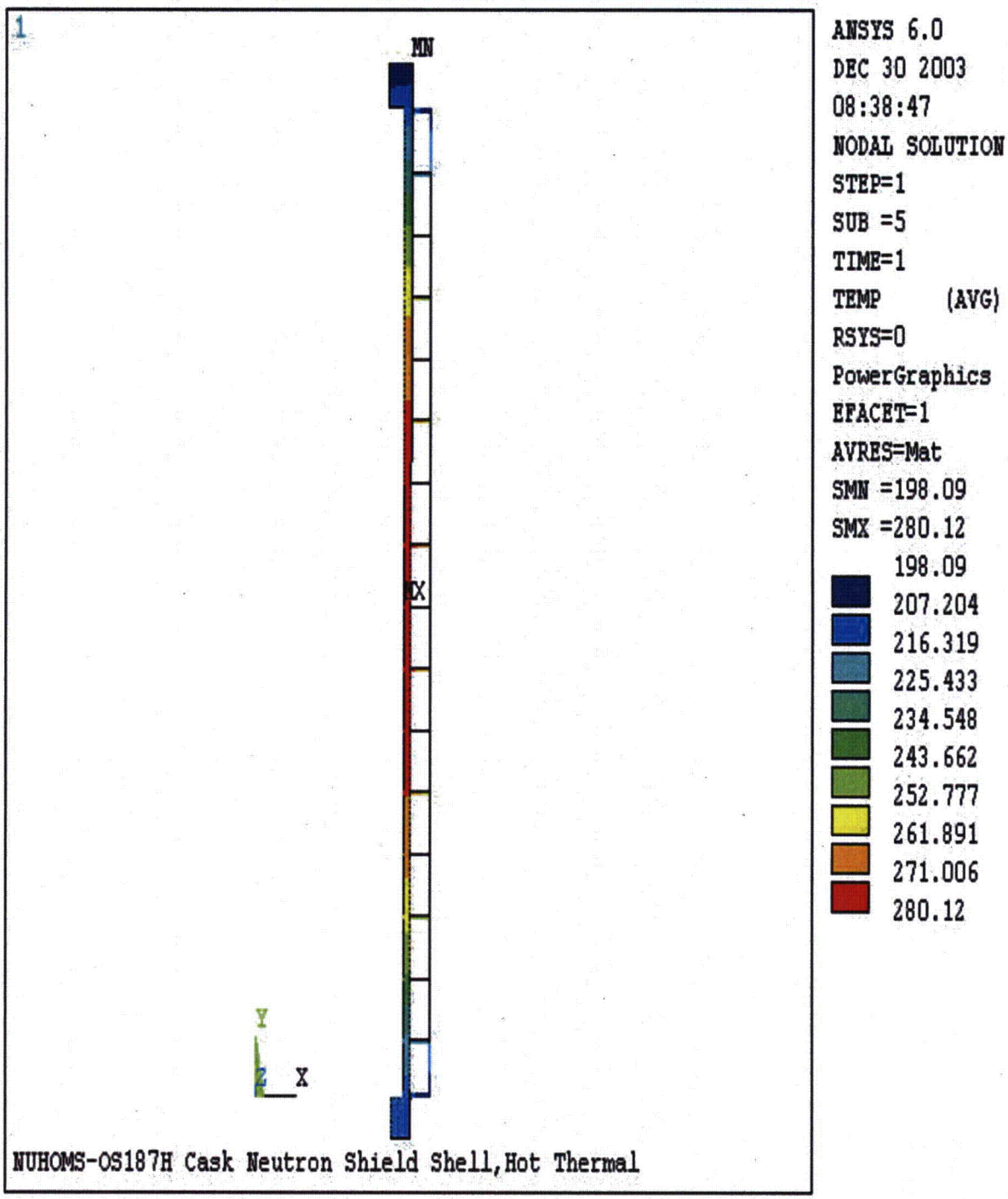

Figure 3.9.6-9
Hot Ambient Environment Temperature Distribution

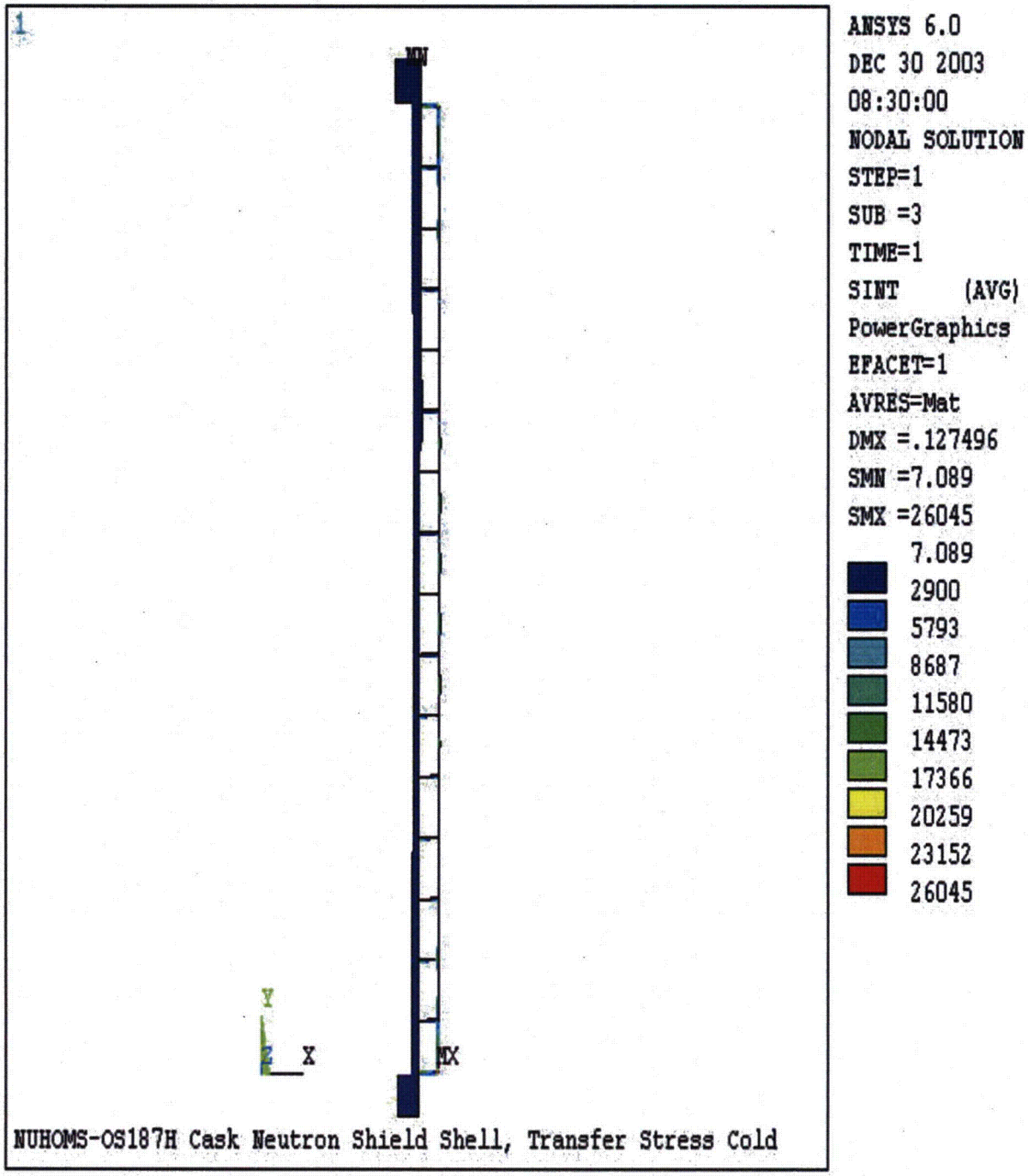

Figure 3.9.6-10
Transfer Loads plus Cold Ambient Condition Stress Intensity Distribution

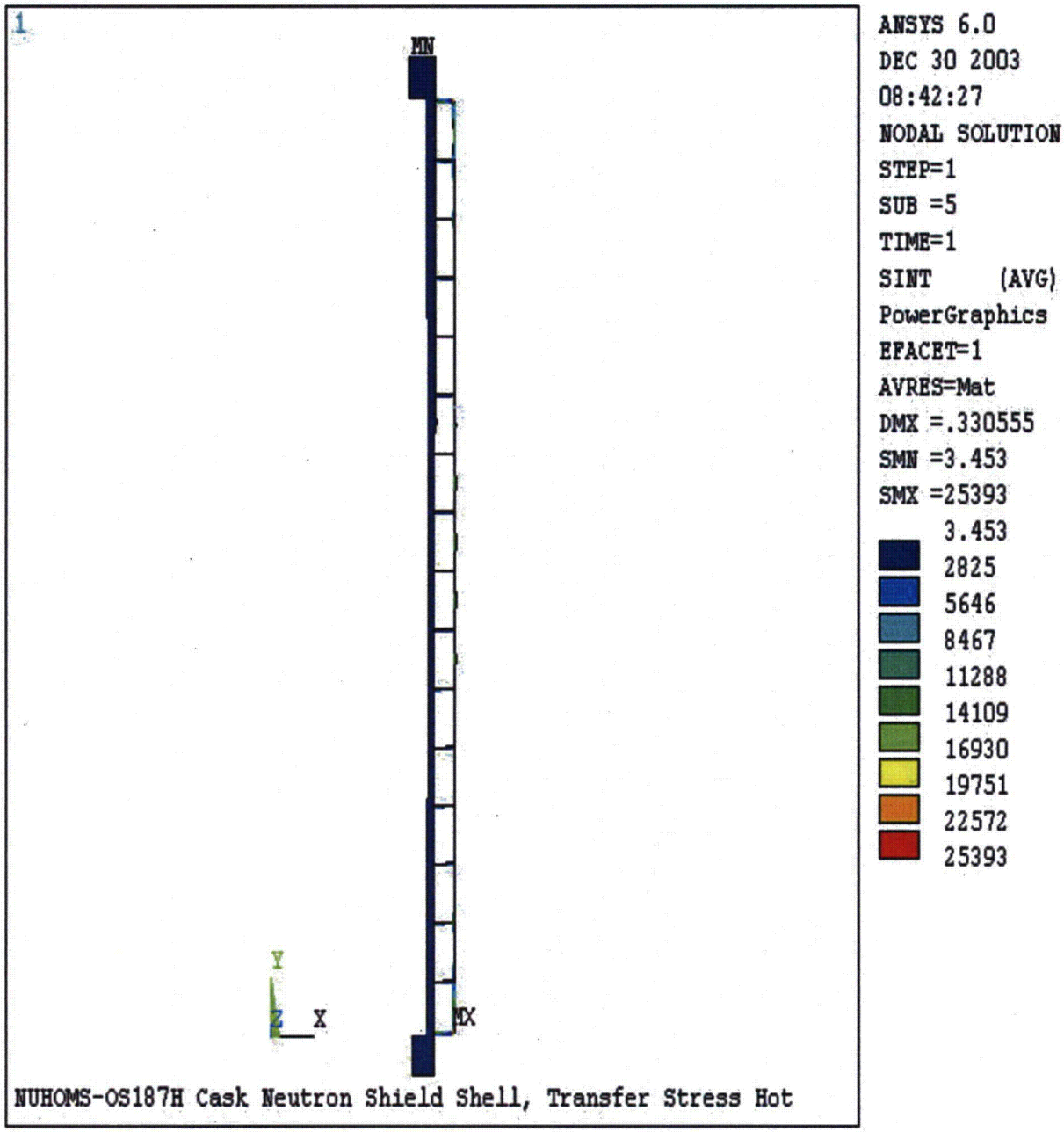

Figure 3.9.6-11
Transfer Loads plus Hot Ambient Condition Stress Intensity Distribution

APPENDIX 3.9.7
OS187H TRANSFER CASK IMPACT ANALYSIS

TABLE OF CONTENTS

3.9.7 OS187H TRANSFER CASK IMPACT ANALYSIS 3.9.7-1
3.9.7.1 Introduction 3.9.7-1
3.9.7.2 Material Properties 3.9.7-1
3.9.7.3 Component Weights 3.9.7-2
3.9.7.4 Geometry and Nomenclature 3.9.7-2
3.9.7.5 Ultimate Capacity of Slab 3.9.7-3
3.9.7.6 End Drop Impact Analysis 3.9.7-4
3.9.7.7 Side Drop Impact Analysis 3.9.7-6
3.9.7.8 Corner Drop Impact Analysis 3.9.7-8
3.9.7.9 Conclusions 3.9.7-9
3.9.7.10 References 3.9.7-10

LIST OF TABLES

3.9.7-1 Spreadsheet for 80 inch Side Drop Impact Load Calculations (Using Non-Linear *S* vs. *g* relationship)

3.9.7-2 C. G. Over Corner Drop – *L* Calculations

3.9.7-3 C. G. Over Corner Drop – Area Calculations

3.9.7-4 C. G. Over Corner Drop – Energy Calculations

LIST OF FIGURES

3.9.7-1 Force vs. Displacement – End Drop (see Reference 1, Figure 14)

3.9.7-2 *S* vs. *g* Curve for 80 inch Side Drop

3.9.7-3 Geometry of C. G. Over Corner Drop

3.9.7-4 Geometry of C. G. Over Corner Drop (continued)

3.9.7-5 Geometry of the C. G. Over Corner Drop – Area Calculation (continued)

3.9.7-6 C. G. Over Corner Drop – *L* Dimension Calculation

3.9.7 OS187H TRANSFER CASK IMPACT ANALYSIS

3.9.7.1 Introduction

The purpose of this appendix is to present the evaluation of the peak decelerations of NUHOMS® OS187H Transfer Cask during impact, subsequent to the hypothetical accident drop onto the concrete pad/soil system during transfer operations. The hypothetical accident condition drop consists of 80 inch end drop, side drop and center of gravity (C.G.) over corner drop. The 80 inch end drop and CG over corner drop are not credible events under 10CFR72 storage and transfer operations. However, these analyses are included to support credible accidents under 10CFR50. The fuel cladding integrity has not been demonstrated for these accident scenarios. An additional safety review by the user is required to demonstrate fuel cladding integrity under 10CFR50.

For the impact analysis, the transfer cask is assumed rigid as compared to the flexibility of the concrete slab/soil system. The methodology described in Reference 1 is used in this evaluation.

The cask is approximated by a cylinder 197.07 inches long and 81.7 inches in diameter. The effect of the outer shield shell, which is very thin relative to the main structural body of the transfer cask, is neglected. Also, small variations around top cover and cylinder are neglected. The stiffness variation due to the neglected items of the transfer cask is negligible.

The OS187H Transfer Cask is assumed to impact a 36 inch thick concrete pad, with #11 rebar on 12" spacing, at top and bottom of the pad, and 2" coverage.

3.9.7.2 Material Properties

The following material properties, taken from Reference 1, are assumed to model the design basis concrete pad and soil foundation.

E_c = Concrete elastic modulus = 3.6×10^6 psi.
σ_u = Ultimate concrete strength = 4,000 psi.
E_s = Sub-soil modulus = 60,000 psi. (higher value gives higher g load)
S_y = Rebar yield strength = 60,000 psi.
ν_c = Poisson's ratio of concrete = 0.17
ν_s = Poisson's ratio of soil = 0.49

3.9.7.3 Component Weights

The 32PTH DSC and OS187H Transfer Cask component weights are tabulated in Section 3.2. The following component weights relevant to this analysis are summarized below.

Empty Canister Weight = 28.19 kips
Fuel Basket Weight = 29.85 kips
Fuel Assembly Weight (32) = 50.72 kips
Transfer Cask Weight = 119.95 kips

Total Weight, W = 228.71 kips.

For conservative estimating the g load, a lower weight, 226.9 kips, is used for the impact analysis (lower weight gives higher g load).

3.9.7.4 Geometry and Nomenclature

The technical data used for transfer cask and concrete slab/soil system are:

W = Weight of cask = 226,900 lbs
R = Cask outer radius = 81.7/2 = 40.85 in
A = cask foot print area = π $(40.85)^2$ = 5,242.4 in^2
L = cask length = 197.07 in.
E_c = Concrete elastic modulus = 3.6×10^6 psi
σ_u = Ultimate concrete strength = 4,000 psi
υ_c = Poisson's ratio of concrete = 0.17
h_c = Concrete pad thickness = 36 inches
S_y = Rebar yield strength = 60,000 psi
E_s = Sub-soil modulus = 60,000 psi (high value of E_s gives higher g load)
υ_s = Poisson's ratio of soil = 0.49
A_s = Rebar (#11) area = $\pi/4$ $(1.41)^2$ = 1.56 in^2

3.9.7.5 Ultimate Capacity of Slab

The ultimate bending capacity of reinforced cement concrete slab, M_u, is computed based on a 1 foot wide pad with a thickness of 36 in., #11 Rebar @ 12 inch spacing and a 2 inch cover. For a 36 inch thick concrete slab, the steel in compression zone is assumed to have no effect and is neglected.

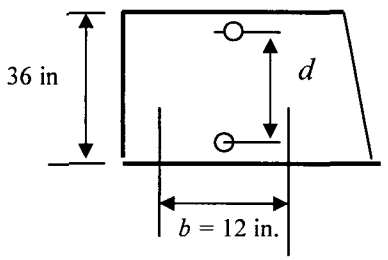

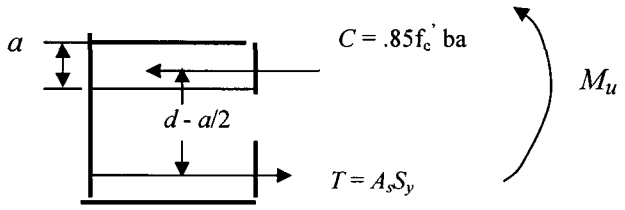

Average depth of steel, d, is the following.

$d = 36 - 4 - 1.41 = 30.59$ in

Therefore,

$C = T = A_sS_y = 0.85f_c' ba$

$a = A_sS_y / 0.85f_c' b = 1.56 \times 60{,}000 / 0.85 \times 4000 \times 12 = 2.294$ in

$M_u = A_sS_y (d - a/2) = 1.56 \times 60{,}000 (30.59 - 2.294/2) = 2.7559 \times 10^6$ in-lb/ft width of slab

3.9.7.6 End Drop Impact Analysis

The results of EPRI NP-7551 report [1] are presented in terms of a target hardness number, S. In general this is given by the following.

$$S = \frac{M_u \sigma_u A}{W^2 \delta_e}$$

Where,

M_u = Ultimate moment capacity of 1 foot section of slab = 2.7559×10^6 in-lb/ft
σ_u = Ultimate concrete strength = 4,000 psi
A = Area of impact surface = 5,242.4 in^2
W = Weight of cask = 226,900 lbs
δ_e = Deflection of cask under weight of cask (1g), in

The deflection, δ_e, is given as:

$$\delta_e = \frac{W}{2Rk}\left(1 - e^{-\beta R}\cos(\beta R)\right)$$

Where,

$$k = \frac{\pi E_s}{1-\upsilon_s^2} = \frac{\pi(60{,}000)}{1-0.49^2} = 248{,}053 \text{ psi/in}$$

$$\beta = \left(\frac{E_s}{4D_c}\right)^{1/4} = \left(\frac{60{,}000}{4 \times 14{,}413 \times 10^6}\right)^{1/4} = 0.03194$$

$$D_c = \frac{E_c h^3}{12(1-\upsilon_c^2)} = \frac{3.6(10)^6(36)^3}{12(1-0.17^2)} = 14{,}413 \times 10^6 \text{ in-lbs}$$

Therefore,

$$\delta_e = \frac{226{,}900}{2 \times 40.85 \times 248{,}053}\left(1 - e^{-0.03194 \times 40.85}\cos 0.03194 \times 40.85\right) = 0.0104 \text{ in}$$

Then,

$$S = \frac{M_u \sigma_u A}{W^2 \delta_e} = \frac{2.7559 \times 10^6 \times 4{,}000 \times 5{,}242.4}{226{,}900^2 \times 0.0104} \approx 10.793 \times 10^4$$

Conservatively using upper bound of Figure 28 from Reference 1 for an 80 inch drop height, the peak force is 49*g* (× weight). To calculate the maximum deformation of the concrete, the force-deformation curve (Figure 3.9.7-1) is obtained by interpolating the data shown on Figure 14 of the EPRI report [1]. From Figure 3.9.7-1, the displacement at the end of elastic phase is about 0.4 inch and elastic-plastic displacement is about 1.0 inch.

We now use energy method to compute final deformation. Using the force – displacement plot on Figure 3.9.7-1 (interpolating $S = 107{,}930$). It is assumed that displacements beyond 1 inch are fully plastic.

Let x be the final plastic deformation. Then, the energy absorbed by target, E_{ab}, is equal to the Area under the Curve (see Figure 3.9.7-1). Therefore,

$$E_{ab} = W\,[(27.5\times0.4/2) + (27.5 + 39.0)/2\,(0.66 - 0.44) + (39.0 + 48.3)/2\,(1.0 - 0.66) + 49(x - 1.0)]$$

The potential energy of the drop, E_{drop}, is,

$$E_{drop} = W\,[H + x + 1] = W\,[81 + x]$$

Equating $E_{ab} = E_{drop}$, gives the following.

$$5.5 + 8.65 + 14.84 + 49x - 49 = 81 + x$$

$$\Rightarrow x = 2.10 \text{ in}$$

Therefore, the total displacement is,

Displacement = 1.0 + 2.10 = 3.10 in

3.9.7.7 Side Drop Impact Analysis

The side drop analysis is conducted in the same manner as for the end drop, except that the expression for δ_e varies, and the target area changes as the depth of penetration increases. Using Reference 1 to evaluate δ_e, we get,

$$I_c = \frac{Lh^3}{12} = 197.07 \times \frac{36^3}{12} = 766{,}208 \text{ in}^4$$

$$\beta = \left(\frac{E_s}{4E_c I_c}\right)^{1/4} = \left(\frac{60{,}000}{4 \times 3.6 \times 10^6 \times 766{,}208}\right)^{1/4} = 0.00859 \text{ in}^{-1}$$

$$k = E_s = 60{,}000 \text{ lb/in}^2$$

$$\delta_e = \frac{W\beta}{2k} = \frac{226{,}900 \times 0.00859}{2 \times 60{,}000} = 0.01624 \text{ in}$$

$$S = \frac{M_u \sigma_u A}{W^2 \delta_e} = \frac{2.7559 \times 10^6 \times 4{,}000 \times A}{226{,}900^2 \times 0.01624} = 13.18464A$$

The following sketch shows the geometry of the transfer cask side drop

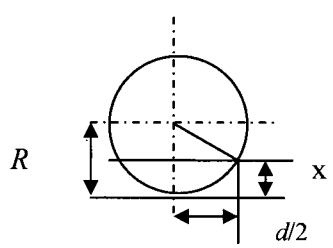

Where,

$$d/2 = [R^2 - (R - x)^2]^{0.5} = [2Rx - x^2]^{0.5}$$

The impact surface area, A, as a function of the penetration depth is,

$$A = 2 \times 197.07\,[81.7\,x - x^2]^{0.5} = 394.14 \times [81.7\,x - x^2]^{0.5}$$

$$S = 13.18464\,A$$

The following data is obtained from Figure 28 of Reference 1.

Target Hardness, *S*	Acceleration, *g*
0	6
10,000	17.5
20,000	25.0
30,000	29.8
40,000	33.5
50,000	37.0
60,000	40.0
70,000	43.3
80,000	46.0
90,000	47.8
100,000	49.0

This S vs. g curve is plotted in Figure 3.9.7-2. A spread sheet solution is carried out by incrementing x (penetration depth) to obtain the absorbed energy equal to drop energy. The following steps are carried out on the spreadsheet:

1. Select x
2. Compute Area, $A = 394.14 \times [81.7\,x - x^2]^{0.5}$
3. Compute $S = 13.18464\,A$
4. Obtain g from Figure 3.9.7-2 for computed S
5. Compute Force, $F = W \times g$
6. Compute Energy Increment, $\Delta E = [1/2(F_i + F_{i-1})]\,(x_i - x_{i-1})$
7. Add ΔE to the previous to obtain current total absorbed energy
8. Compute total drop energy $= W\,(80 + x)$
9. Keep incrementing x until total absorbed energy is equal to the drop energy.

The resulting spreadsheet for the side drop impact is given on Table 3.9.7-1.

From Table 3.9.7-1, it is seen that, when the target deformation is 2.46 inches, the total absorbed energy is approximately equal to the drop energy. The *g* load at this deformation is 44*g*.

3.9.7.8 Corner Drop Impact Analysis

The C. G. over corner drop is performed in a similar manner as the side drop. For the corner drop, both δ_e and impact area are a function of the penetration depth into the target.

$$\delta_e = \frac{W\beta}{2k} = \frac{226{,}900 \times \beta}{2 \times 60{,}000} = 1.8908\beta$$

And

$$\beta = \left(\frac{E_s}{4E_c I_c}\right)^{1/4} = \left(\frac{60{,}000}{4 \times 3.6 \times 10^6}\right)^{1/4} \times \left(\frac{1}{I_c}\right)^{1/4} = \frac{0.254}{I_c^{1/4}}$$

$$I_c = \frac{Lh^3}{12} = L \times \frac{36^3}{12} = 3{,}888L$$

The geometry relations used to evaluate of the impact area as a function of the deformation into the target are shown in Figures 3.9.7-3 to 3.9.7-6. The area, A, as a function of deformation is shown in Figure 3.9.7-5. Table 3.9.7-3 tabulates the results of the 'area vs. deformation' calculations, using a small ANSYS input file.

The next quantity that is needed is the deflection, δ_e. This deflection will occur as a result of only a small portion of the transfer cask being in contact with the target surface, with the area increasing as δ_e increases. The above L dimension calculation is developed in Figure 3.9.7-6.

$$L = 2\left[\left(\frac{2R\delta_e}{\cos 67.48°}\right) - \left(\frac{\delta_e^2}{\cos^2 67.48°}\right)\right]^{1/2} \quad \text{(See Fig. 3.9.7-3 for drop angle calculation)}$$

$$= 2\left[213.316\delta_e - 6.8166\delta_e^2\right]^{1/2}$$

To solve for *L*, iteratively, this is done in the spreadsheet given in Table 3.9.7-2. Which give

$$\delta_e = 0.03922, \quad L = 5.7815 \text{ in}$$

Using Reference 1, the target hardness number, S, is

$$S = \frac{M_u \sigma_u A}{W^2 \delta_e} = \frac{2.7559 \times 10^6 \times 4{,}000 \times A}{226{,}900^2 \times 0.03922} = 5.4594A$$

A spread sheet solution is carried out by incrementing Δ (penetration depth as shown in Figure 3.9.7-3) to obtain the Absorbed Energy that is equal to Drop Energy. The following steps are carried out in the spreadsheet:

1. Select Δ
2. Obtain Area, A, from Table 3.9.7-3
3. Compute $S = 5.4594\,A$
4. Obtain g from Figure 3.9.7-2
5. Compute Force, $F = W \times g$
6. Compute Energy Increment, $\Delta E = [1/2(F_i + F_{i\text{-}1})]\,(\Delta_i - \Delta_{i\text{-}1})$
7. Add ΔE to the previous to obtain current total absorbed energy
8. Compute total drop energy = $W\,(80 + x)$
9. Keep incrementing x till total absorbed energy is equal to the drop energy

The spreadsheet is given on Table 3.9.7-4. It is seen from this table that at a target deformation of 6.5 inches, the total absorbed energy is equal to the drop energy and the g load for this deformation is 15.9g.

3.9.7.9 Conclusions

The following table summarizes the results of the analysis described above.

Drop Orientation	Peak Deceleration (gs)	Target Penetration Depth (in.)
End Drop	49	3.10
Side Drop	44	2.5
Corner Drop	15.9	6.5

3.9.7.10 References

1. "Structural Design of Concrete Storage Pads for Spent Fuel Casks", EPRI NP-7551, August 1991 by Rashid, Nickell and James.

Table 3.9.7-1
Spreadsheet for 80 inch Side Drop Impact Load Calculations
(Using Non-Linear *S* vs. *g* relationship)

x	*A*	*S*	*g*	*F*	Δ*E*	Energy Absorbed	Drop Energy
0	0	0	0	0	0	0	18,152,000
0.5	2511.4	33,112	31.0	7,033,900	1,758,475	1,758,475	18,265,450
1	3540.7	46,683	36.0	8,168,400	3,800,575	5,559,050	18,378,900
1.5	4323.0	56,997	39.0	8,849,100	4,254,375	9,813,425	18,492,350
2	4976.2	65,609	42.0	9,529,800	4,594,725	14,408,150	18,605,800
2.1	5095.9	67,187	42.5	9,643,250	958,653	15,366,803	18,628,490
2.2	5212.5	68,725	42.9	9,734,010	968,863	16,335,666	18,651,180
2.3	5326.3	70,225	43.2	9,802,080	976,804	17,312,470	18,673,870
2.4	5437.4	71,690	43.5	9,870,150	983,612	18,296,082	18,696,560
2.42	5459.3	71,979	43.7	9,915,530	197,857	18,493,938	18,701,098
2.44	5481.2	72,267	43.8	9,938,220	198,538	18,692,476	18,705,636
2.46	**5502.9**	**72,554**	**43.9**	**9,960,910**	**198,991**	**18,891,467**	**18,710,174**
2.5	5546.0	73,123	44.0	9,983,600	398,890	19,290,357	18,719,250
2.51	5556.8	73,264	44.1	10,006,290	99,949	19,390,307	18,721,519
2.52	5567.5	73,405	44.15	10,017,635	100,120	19,490,426	18,723,788
2.53	5578.2	73,546	44.2	10,028,980	100,233	19,590,659	18,726,057
2.54	5588.8	73,687	44.24	10,038,056	100,335	19,690,995	18,728,326
2.55	5599.5	73,827	44.28	10,047,132	100,426	19,791,421	18,730,595

Table 3.9.7-2
C. G. Over Corner Drop – *L* Calculations

$L_{initial}$	I_c	β	δ_e	L_{final}
6	23328	0.020552	0.0388606	5.75475522
5.9	22939.2	0.020639	0.0390243	5.766842939
5.8	22550.4	0.020727	0.0391914	5.779163276
5.7	22161.6	0.020818	0.0393622	5.791724835
5.75	22356	0.020772	0.0392763	5.785413347
5.76	22394.88	0.020763	0.0392593	5.784158456
5.77	22433.76	0.020754	0.0392422	5.782906012
5.78	22472.64	0.020745	0.0392253	5.781656007
5.781	22476.53	0.020744	0.0392236	5.78153114
5.7815	**22478.47**	**0.020744**	**0.0392227**	**5.781468716**

Table 3.9.7-3
C. G. Over Corner Drop – Area Calculations

Δ	Δ_{CL}	α_{max}	α_{min}	Area, A
0.5	-15.146	37.942	36.529	19.361
1	-14.646	38.150	35.323	54.494
1.5	-14.146	38.357	34.117	99.620
2	-13.646	38.564	32.911	152.613
2.5	-13.146	38.772	31.705	212.213
3	-12.646	38.979	30.500	277.544
3.5	-12.146	39.186	29.294	347.950
4	-11.646	39.394	28.088	422.905
4.5	-11.146	39.601	26.882	501.977
5	-10.646	39.808	25.676	584.796
5.5	-10.146	40.015	24.470	671.043
6	-9.646	40.223	23.264	760.435
6.5	-9.146	40.430	22.058	852.716
7	-8.646	40.637	20.852	947.656
7.5	-8.146	40.845	19.646	1045.042
8	-7.646	41.052	18.440	1144.679
8.5	-7.146	41.259	17.234	1246.381
9	-6.646	41.467	16.028	1349.978
9.5	-6.146	41.674	14.822	1455.306
10	-5.646	41.881	13.617	1562.209
10.5	-5.146	42.089	12.411	1670.539
11	-4.646	42.296	11.205	1780.153
11.5	-4.146	42.503	9.999	1890.915
12	-3.646	42.710	8.793	2002.689
12.5	-3.146	42.918	7.587	2115.347
13	-2.646	43.125	6.381	2228.761
13.5	-2.146	43.332	5.175	2342.808
14	-1.646	43.540	3.969	2457.364
14.5	-1.146	43.747	2.763	2572.310
15	-0.646	43.954	1.557	2687.526
15.5	-0.146	44.162	0.351	2802.894
16	0.354	44.369	-0.855	2918.295
16.5	0.854	44.576	-2.060	3033.611
17	1.354	44.784	-3.266	3148.725
17.5	1.854	44.991	-4.472	3263.517
18	2.354	45.198	-5.678	3377.868
18.5	2.854	45.406	-6.884	3491.655
19	3.354	45.613	-8.090	3604.757
19.5	3.854	45.820	-9.296	3717.048
20	4.354	46.027	-10.502	3828.400

Table 3.9.7-4
C. G. Over Corner Drop – Energy Calculations

Δ	*AREA, A*	*S*	*g*	*Force, F*	*Energy Inc.*	*Total energy*	*Drop Energy*
0.00	0	0	-	0	0	0	18,152,000
0.50	19.361	105.70	14.04	3,186,193	796,548	796,548	18,265,450
1.00	54.494	297.50	14.12	3,203,602	1,597,449	2,393,997	18,378,900
1.50	99.620	543.87	14.22	3,225,961	1,607,391	4,001,388	18,492,350
2.00	152.613	833.18	14.33	3,252,219	1,619,545	5,620,933	18,605,800
2.50	212.213	1158.55	14.46	3,281,750	1,633,492	7,254,425	18,719,250
3.00	277.544	1515.23	14.61	3,314,122	1,648,968	8,903,393	18,832,700
3.50	347.950	1899.60	14.76	3,349,007	1,665,782	10,569,175	18,946,150
4.00	422.905	2308.81	14.92	3,386,147	1,683,789	12,252,964	19,059,600
4.50	501.977	2740.49	15.10	3,425,327	1,702,869	13,955,833	19,173,050
5.00	584.796	3192.64	15.28	3,466,364	1,722,923	15,678,755	19,286,500
5.50	671.043	3663.49	15.47	3,509,099	1,743,866	17,422,621	19,399,950
6.00	760.435	4151.52	15.66	3,553,392	1,765,623	19,188,244	19,513,400
6.50	**852.716**	**4655.32**	**15.86**	**3,599,117**	**1,788,127**	**20,976,371**	**19,626,850**
7.00	947.656	5173.63	16.07	3,646,159	1,811,319	22,787,690	19,740,300
7.50	1045.042	5705.30	16.28	3,694,413	1,835,143	24,622,833	19,853,750
8.00	1144.679	6249.26	16.50	3,743,783	1,859,549	26,482,382	19,967,200

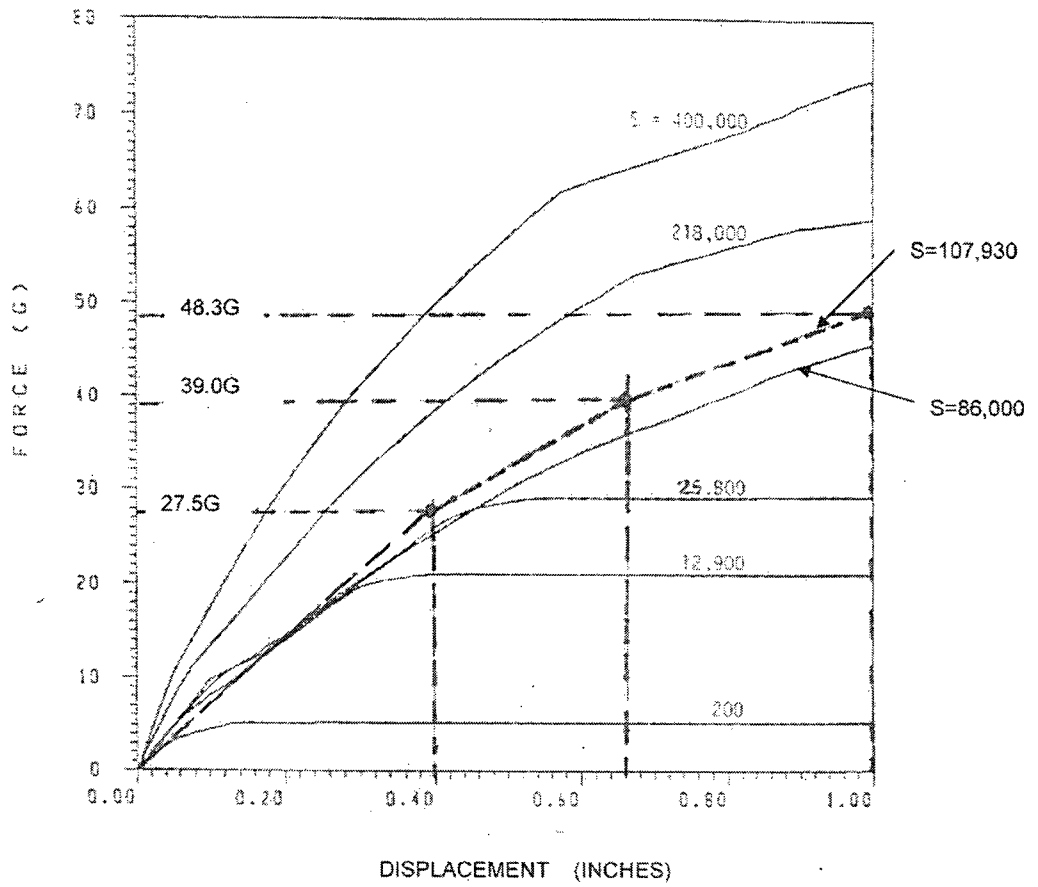

Figure 3.9.7-1
Force vs. Displacement – End Drop
(see Reference 1, Figure 14)

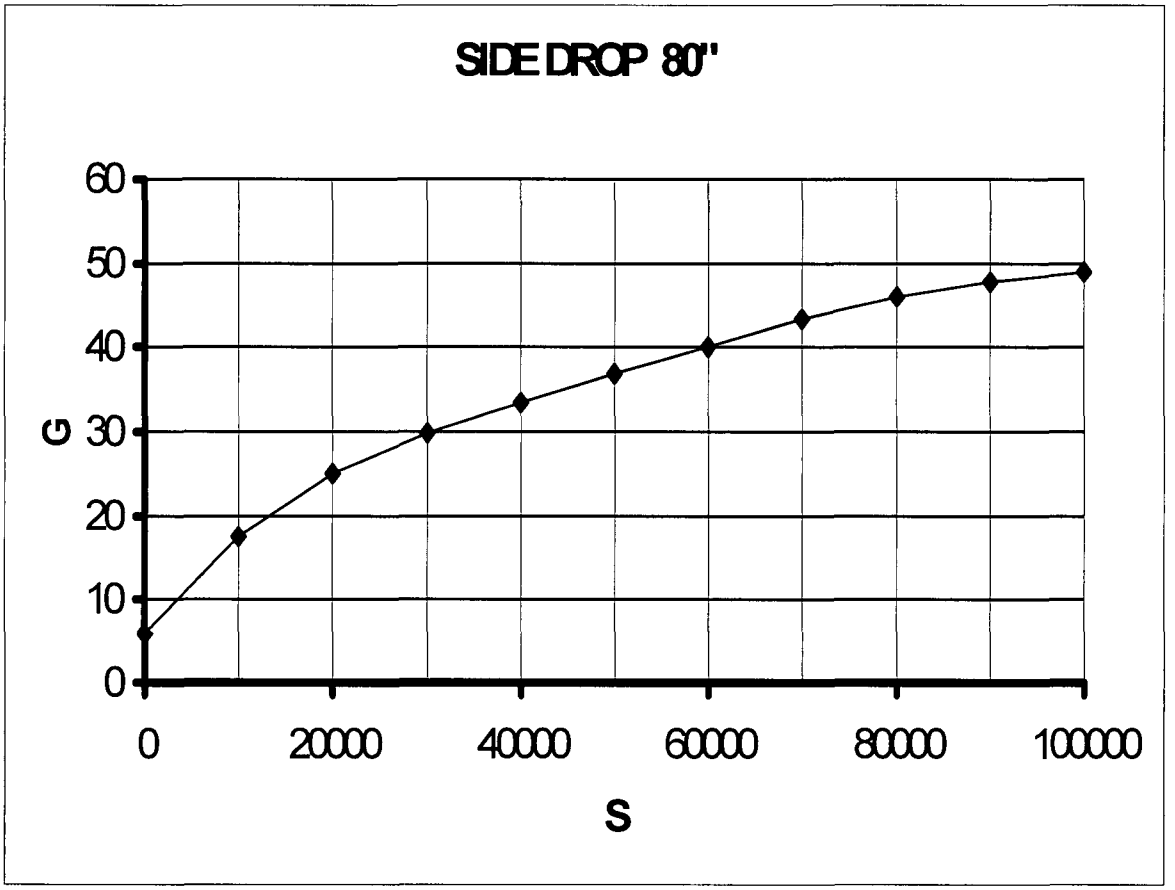

Figure 3.9.7-2
S vs. g Curve for 80 inch Height Side Drop

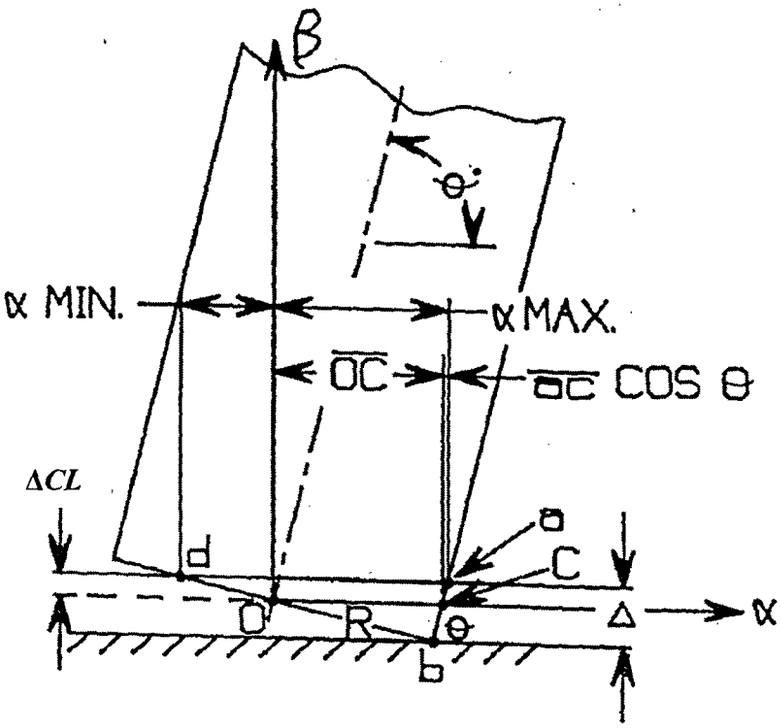

$$\sin\theta = \frac{R}{oc} \qquad \cos\theta = \frac{bc}{oc} \qquad \theta = \tan^{-1}\left(\frac{197.07}{81.7}\right) = 67.48°$$

$$bc = oc\cos\theta = R\left(\frac{\cos\theta}{\sin\theta}\right)$$

$$ac = ab - bc = \frac{\Delta}{\sin\theta} - R\left(\frac{\cos\theta}{\sin\theta}\right)$$

$$ad = \frac{ab}{\cos\theta} = \frac{\Delta}{\sin\theta\cos\theta}$$

$$\Delta CL = \Delta - bc\sin\theta = \Delta - R\cos\theta$$

$$\alpha_{max} = oc + ac\cos\theta = \frac{R}{\sin\theta} + ac\cos\theta$$

$$= \frac{R}{\sin\theta} + \Delta CL\left(\frac{\cos\theta}{\sin\theta}\right)$$

$$\alpha_{min} = ad - \alpha_{max} = \frac{\Delta}{\sin\theta\cos\theta} - \frac{R}{\sin\theta} - \Delta CL\left(\frac{\cos\theta}{\sin\theta}\right)$$

$$= \Delta CL\left(\frac{1}{\sin\theta\cos\theta} - \frac{\cos\theta}{\sin\theta}\right)$$

Figure 3.9.7-3
Geometry of C. G. Over Corner Drop

The area of the impact surface is obtained by first writing the equation for the intersection curves between the cylinder and plane surfaces. We set up the following coordinate systems with the origin at the bottom center of the cask.

By transforming coordinates:

$$\alpha = x \sin\theta + z \cos\theta \qquad x = \alpha \sin\theta - \beta \cos\theta$$
$$\beta = -x \cos\theta + z \sin\theta \qquad z = \alpha \cos\theta + \beta \sin\theta$$

The equation for a cylinder is,

$$x^2 + y^2 = R^2$$

Or by transforming coordinates,

$$\alpha^2 \sin^2\theta - 2\alpha\beta \sin\theta \cos\theta + \beta^2 \cos^2\theta + y^2 = R^2$$

By setting the intersection of this surface with target surface, $\beta = \Delta CL$, the equation of the intersection curve becomes the following.

$$\alpha^2 \sin^2\theta - 2\Delta CL \sin\theta \cos\theta + \Delta CL^2 \cos^2\theta + y^2 = R^2$$

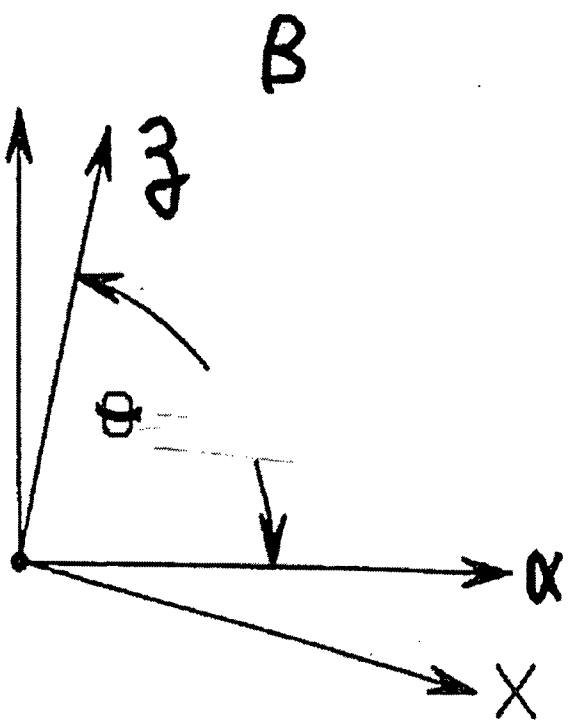

Figure 3.9.7-4
Geometry of C. G. Over Corner Drop (continued)

The area, A, as a function of the deformation is calculated by integrating the following.

$$\alpha^2 \sin^2\theta - 2\alpha\Delta CL \sin\theta \cos\theta + \Delta CL^2 \cos^2\theta + y^2 = R^2$$

$$A = 2 \int_{\alpha\,\min}^{\alpha\,\max} y d\alpha$$

Where y is given in above equation.

This is numerically integrated using 100 divisions and the trapezoidal rule. The results are tabulated in Table 3.9.7-4.

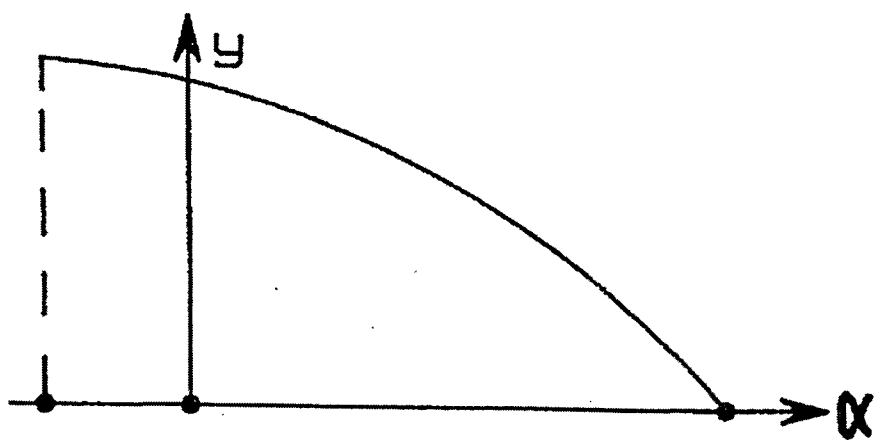

Figure 3.9.7-5
Geometry of the C. G. Over Corner Drop - Area Calculation (continued)

$$L = 2\left[\left(\frac{2R\delta_e}{\cos\theta}\right) - \left(\frac{\delta_e^2}{\cos^2\theta}\right)\right]^{1/2}$$

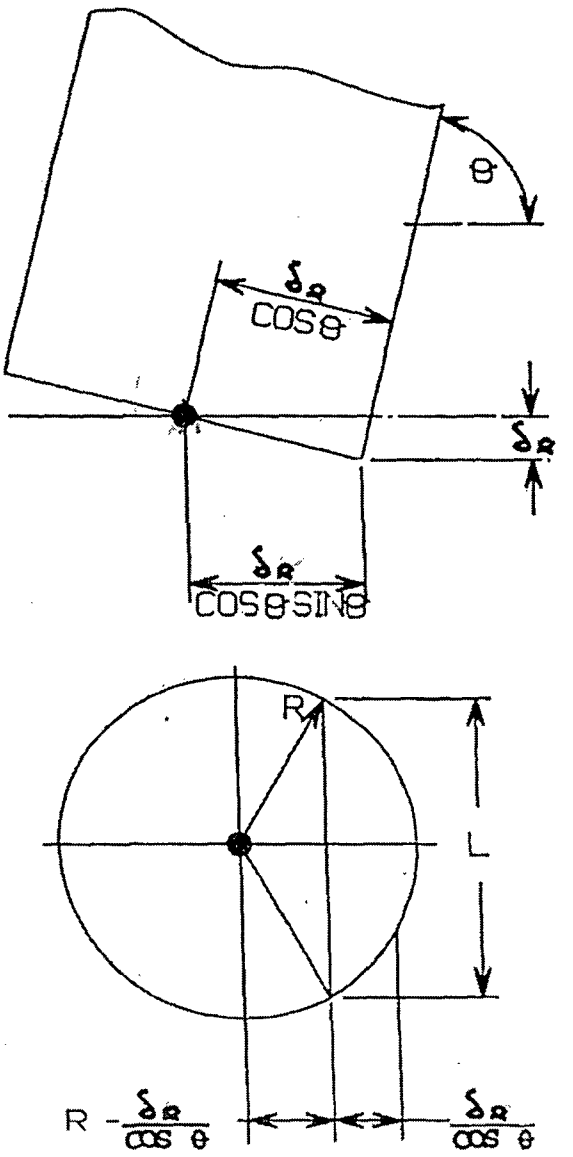

Figure 3.9.7-6
C. G. Over Corner Drop – *L* Dimension Calculation

APPENDIX 3.9.8
DAMAGED FUEL CLADDING STRUCTURAL EVALUATION

TABLE OF CONTENTS

3.9.8 DAMAGED FUEL CLADDING STRUCTURAL EVALUATION 3.9.8-1

3.9.8.1 Introduction 3.9.8-1
3.9.8.2 Design Input / Data 3.9.8-2
3.9.8.3 Loads 3.9.8-3
3.9.8.4 Evaluation Criteria 3.9.8-5
3.9.8.5 Evaluation Methodology 3.9.8-6
3.9.8.6 Trailer Acceleration from 0 mph to 5 mph during Transfer 3.9.8-8
3.9.8.7 Trailer Decceleration from 0 mph to 5 mph during Transfer 3.9.8-11
3.9.8.8 Normal Loading Condidtion during Insertion/Retrieval of DSCa into/from HSM 3.9.8-13
3.9.8.9 Off-Normal Jammed Canister Loading during Insertion of DSC into HSM 3.9.8-14
3.9.8.10 One Foot End Drop Damaged Fuel Evaluation 3.9.8-15
3.9.8.11 One Foot Side Drop Damaged Fuel Evaluation 3.9.8-16
3.9.8.12 Conclusions 3.9.8-20
3.9.8.13 Derivation of Fuel Assembly Material Properties 3.9.8.21
3.9.8.14 DELETED 6.9.8.24
3.9.8.15 References 6.9.8.29

LIST OF TABLES

3.9.8-1 WE and WES 15x15 - K_I Calculation using Fracture Geometry #2

3.9.8-2 WE 17x17 - K_I Calculation using Fracture Geometry #2

3.9.8-3 MK BW 17x17 - K_I Calculation using Fracture Geometry #2

3.9.8-4 WEV 17x17 - K_I Calculation using Fracture Geometry #2

3.9.8-5 WEO 17x17 - K_I Calculation using Fracture Geometry #2

3.9.8-6 CE 14x14 - K_I Calculation using Fracture Geometry #2

3.9.8-76 Summary - Maximum Fuel Rod Stresses and Stress Ratios

3.9.8-87 Summary - Computed Fuel Tube Stress Intensity Factors and Ratios

3.9.8-98 Derivation of Tensile Force (T) and Applied Moment (M) Relationship for a Circular Tube

3.9.8-10 Tire Stiffness Calculation

LIST OF FIGURES

3.9.8-1 Fracture Geometry #1: Ruptured Section

3.9.8-2 Fracture Geometry #2: Through-Wall Circumferential Crack in Cylinder Under Bending

3.9.8-3 Stress Intensity Factor Solutions For Several Specimen Configuration

3.9.8-4 Temperature Vs Tensile and Yield Strength for Low Burn up Fuel

3.9.8-5 Temperature Vs Tensile Yield Strength for High Burn up Fuel

3.9.8-6 DELETED

3.9.8-7 DELETED

3.9.8-8 DELETED

3.9.8-9 DELETED

3.9.8-10 DELETED

3.9.8-11 DELETED

3.9.8-12 DELETED

3.9.8-13 DELETED

3.9.8-14 DELETED

3.9.8 DAMAGED FUEL CLADDING STRUCTURAL EVALUATION

3.9.8.1 Introduction

The purpose of this appendix is to demonstrate structural integrity of the damaged fuel cladding in the NUHOMS® 32PTH DSC following normal and off-normal loading conditions of storage and onsite transfer (required for Part 72 License) and normal condition of offsite transport (required for Part 71 License).

In this appendix, the damaged fuel is defined as: "damaged PWR fuel assemblies are fuel assemblies containing missing or partial fuel rods or fuel rods with known or suspected cladding defects greater than hairline cracks or pinhole leaks. The extent of cladding damage in the fuel rods is to be limited such that a fuel pellet is not able to pass through the damaged cladding during handling and retrievability is assured following Normal/Off-Normal conditions".

This appendix evaluates stresses in the fuel cladding associated with normal and off-normal conditions of on-site transfer/storage and off-site transport. It also presents a fracture mechanics assessment of the cladding using conservative assumptions regarding defect size geometry and amount of oxidation in the cladding material. These evaluations demonstrate the structural integrity of the damaged fuel cladding under normal and off-normal conditions.

The NUHOMS® 32PTH DSC is designed to store 32 intact fuel assemblies, or no more than 16 damaged and the remainder intact, for a total of 32 standard PWR fuel assemblies per canister. All the fuel assemblies, intact or damaged, consist of PWR fuel assemblies with Zircaloy cladding. Damaged fuel assemblies may only be stored in the center compartments of the NUHOMS® 32PTH DSC, as shown in Chapter 2, Figure 2-2.

3.9.8.2 Design Input / Data

The design inputs, taken from References [2] and [12], are modified to include the reduction in cladding thickness due to oxidation. They are documented in the following table.

Fuel Assembly Type	WE & WES 15x15	WE 17x17	MK BW 17x17	WEV 17x17	WEO 17x17	CE 14x14	Notes
Fuel Assembly Weight (lb)	1,555	1,575	1,575	1,575	1,575	1,450	(1,2)
No. of Rods	204	264	264	264	264	176	(1)
Active Fuel Length (in)	144.0	144.0	144.0	144.0	144.0	137.0	(1)
No. of Internal Spacers	6	6	6	6	6	7	(3)
Max. Fuel Rod Span (in)	27.0	25.0	25.0	25.0	25.0	17.0	(5)
Fuel Rod OD (in)	0.4193	0.3713	0.3713	0.3713	0.3573	0.4373	(1,4)
Clad Thickness (in)	0.0216	0.0198	0.0213	0.0198	0.0198	0.0253	(1,4)
Fuel Pellet OD (in)	0.3659	0.3225	0.3195	0.3225	0.3088	0.3765	(1)
Fuel Tube Area (in^2)	0.0270	0.0219	0.0234	0.0219	0.0210	0.0327	
Fuel Tube M.I. (in^4)	5.35E-04	3.39E-04	3.60E-04	3.39E-04	3.00E-04	6.97E-04	
Fuel Rod Weight (lb)	7.62	5.97	5.97	5.97	5.97	8.24	(6)
Irradiated Yield Stress (psi)	69,500	69,500	69,500	69,500	69,500	69,500	(7)
Young's Modulus (psi)	10.6E6	10.6E6	10.6E6	10.6E6	10.6E6	10.6E6	(8)

Notes:
1. Data are obtained from Chapter 2, Table 2-1.
2. The fuel assembly weight includes BPRA weight.
3. The number of internal spacers is obtained from (Ref 12).
4. Include 0.00270 in thickness reduction to account for maximum oxide thickness.
5. Maximum fuel rod span is obtained from (Ref 12) and have been rounded up to whole number.
6. Fuel rod weight = Fuel Assembly Weight / No. of Rods.
7. Data are obtained from Figure 3.9.8-5 at 725 °F temperature.
8. Data is obtained from (Ref 3).

3.9.8.3 Loads

3.9.8.3.1 Part 72 Normal and Off-normal Condition Loads

The damaged fuel inside the DSC is subjected to following normal and off normal condition Part 72 loads:

- Dead Weight
- Internal Pressure
- Thermal
- Transfer Load (Inertia Loads associated with moving the DSC from the fuel loading area to the ISFSI site), which consists of 1g in the longitudinal, 1g in the transverse and 1g in the vertical direction.
- HSM Loading/Unloading (Normal loads associated with inserting the DSC into and retrieving the DSC from the HSM)
- Jammed Canister Load (Off normal loads associated with jamming the DSC during DSC insertion into the HSM)

The stresses due to the dead weight are insignificant. No internal pressure is assumed for the damaged fuel. The cladding is assumed to be able to expand due to thermal loads and thus no thermal-induced stresses are considered. However, the temperature of the cladding is considered for selection of allowable stresses at temperature. Therefore, the structural integrity of the damaged fuel is evaluated in this appendix only for the Transfer/Handling loads (DSC Loading/transfer to ISFSI, HSM Loading/Unloading, and Jammed Canister Load conditions).

3.9.8.3.2 Part 71 Normal Condition Loads

The structural integrity of the fuel cladding for the normal condition Part 71 load is evaluated only for the one-foot side drop condition in this application. The one-foot end drop and vibratory loads will be addressed in the 10CFR71 application.

Note that for the normal and accident off-site transport drops, the impact limiters are attached at both ends of the horizontal loaded cask.

THIS PAGE INTENTIONALLY BLANK

3.9.8.4 Evaluation Criteria

The retrievability of the damaged fuel in the NUHOMS® 32PTH DSCs is assured if the damaged fuel cladding retains its structural integrity when subjected to normal and off normal loads. Per the damaged fuel definition in Section 3.9.8.1, the damaged fuel rods loaded in the 32PTH DSCs may have cladding defects greater than hairline cracks or pinhole leaks. However, under normal and off-normal loads, the original defects (such as cracks or pinholes) should not change significantly so that the damaged fuel can be retrieved.

The damaged fuel cladding needs to meet the following criteria to ensure their structural integrity and thus be retrievable:

- Fuel cladding stresses under normal and off-normal load conditions are less than the irradiated yield strength of the cladding material.
- Stability of the cladding tube is maintained (i.e., no buckling occurs).
- The stress intensity factor, K_I, of the fuel cladding tube geometry considering through-wall flaw is less than experimentally determined fracture toughness, K_{IC}, considering temperature and irradiation effects.

3.9.8.5 Evaluation Methodology

The onsite transfer of the fuel is accomplished using the OS 187H or Standard Transfer Cask loaded on a transfer trailer that is 10' 6" wide [8]. The transfer trailer has four axles with eight (8) 235/75 R17.5 SLR 184 tires per axle (total of 32 tires). The measured tire stiffness per tire is 1500 lbs/in [1].

During the on-site transfer operation, the trailer either accelerates from 0 initial velocity to a maximum velocity of 5 MPH [8] or decelerates from a maximum velocity of 5 MPH to 0 final velocity. Therefore, during the transfer operation the gap between the fuel assemblies and the DSC top or bottom plugs may close if friction is overcome. The kinetic energy during impact of the fuel assemblies' mass on the top or bottom plugs is absorbed as strain energy through the cask, skid, trailer, and ultimately in the tires, acting as springs.

The structural integrity of the fuel assembly is evaluated by using the principle of conservation of energy. Thus, for a spring/mass system the kinetic energy of the mass is equal to the strain energy absorbed by the spring at the time of impact.

Therefore: $(1/2)\, M*V^2 = (1/2)\, K*X^2$

Where:

M = Mass of the system ($lb.sec^2/in$) = W/g
W = Weight of the system (lbs)
g = Acceleration due to gravity = 386.4 in/sec^2
V = Velocity of the system (in/sec)
K = Stiffness of the spring (lbs/in)
F = Force acting on the mass and the spring (lbs)
X = Displacement of the spring (in) = F/K

Substituting F/K for X in the above equation and solving for F gives the force acting on the mass as:

$$F = (K*M)^{1/2} * V$$

Therefore, the equivalent g load acting on the mass = F/W

For the fuel rod once the force of impact (F) is known the stress may be computed knowing the area of cross section (A) of the cladding.

The following basic equations of kinematics relating distance, velocity, acceleration and time are used in this appendix:

$$s = u*t + (1/2)*a*t^2$$
$$v = u + a*t$$

where,

s = distance (in)

u = initial velocity (in/sec)
v = final velocity (in/sec)
a = acceleration or deceleration (in/sec ^{2})
t = time (sec)

The structural integrity of the damaged fuel rods is evaluated for the following five loading events:

- Damaged fuel rod assemblies subjected to 1g acceleration when the trailer accelerates from 0 initial velocity to constant velocity of 5 mph [8] during onsite transfer.
- Damaged fuel rod assemblies subjected to 1g deceleration when the trailer decelerates from 5 mph [8] constant velocity to 0 final velocity during onsite transfer.
- Normal condition of loading during insertion or extraction of the DSC into or from the HSM for storage.
- Off normal jammed canister loading during insertion or extraction of the DSC into the HSM for storage.
- Damaged fuel rod assemblies subjected to 1-foot drops during normal condition of off site transport.

For each of the above five loading events, the integrity of the damaged fuel assemblies is evaluated in the following sections.

3.9.8.6 Trailer Acceleration from 0 mph to 5 mph during Transfer

During onsite transfer of the cask from the fuel building to the ISFSI the loaded trailer picks up the velocity from 0 mph to 5 mph (88 in/s). The fuel assemblies inside the canister are subjected to a maximum postulated 1g (386.4 in/s^2) equivalent axial transfer load [1]. The maximum speed during this event is 5 mph and any sudden load on the fuel assemblies is transferred from the fuel assemblies to the cask, the support skid, the trailer, the rubber tires and to the road bed. The maximum transfer acceleration is +/- 1g.

Under the hot condition, the maximum gap between the fuel assemblies and the DSC plug = d (in)

Substituting in the kinematics equation $s = s_o + u_o t + a*t^2/2 = d$

Where:

Initial displacement, $s_o = 0$

Initial velocity, $u_o = 0$

Acceleration, $a = (1-0.3)\ g = 0.7g$

Where, 0.3 is the friction coefficient between the fuel assembly grid straps and the fuel compartment [9].

$g = 386.4$ in/s ^{2}

Solving for t

$$t = \{(2)*\ (d)\ /\ (0.7g)^{1/2}$$

At contact with top shield plug the velocity of the fuel assembly is

$$v = (0.7g)\ (t)$$

The contact force on the fuel assembly is equal to: $F = (K*M)^{1/2} * (v)$

Where:

M = total mass of the fuel assemblies = (W*n)/g
W = Weight of each fuel assembly
n = number of fuel assemblies/canister = 32
K= k*32 lb/in, where k = stiffness of each of 32 rubber tires
k = stiffness of each tire is computed as follows:

Tire pressure = 135 psi,

For **235** (tire width mm)/**75** (height to width ratio in %) **R 17.5** (rim diameter inch) **SLR184** tires:

Tire width = (235 mm)/(25.4mm/in) = 9.25 in

Height of the tire = 75% of 9.25 in = 6.94 in

Diameter of the tire = (17.5 in) + 2*6.94 in = 31.4 in

Total loaded trailer weight = weight of (loaded cask +trailer + skid +ram)

Loaded Cask Weight (with impact limiters) = 250,000 lbs. (conservative, see Chapter 3, Section 3.2.3)

Weight (trailer + skid + ram) = 39,700(trailer)+ 26,500(skid)+ 6,400(ram) [1]
= 72,600 lb

Total Load = 250,000 + 72,600 = 322,600 lb

Load per tire = (322,600 lb)/(32 tires) = 10,081 lb

Area of contact of the tire = (10,081 lbs/135 psi) = 74.7 in ^{2}

Length of compression of the tire = 74.7 in^2 / 9.25 in = 8.08 in

Therefore, deflection of the tire = $(31.4/2) - \{(31.4/2)^2 - (8.08/2)^2\}^{1/2} = 0.5287$ in

Tire stiffness/tire = (10,081 lb)/(0.5287 in) = 19,068 lb/in

Total tire stiffness for 32 tires = (19,068)(32) = 6.1×10^5 lb/in

As per Table 3.9.8-9, the measured tire stiffness = 1500 x 32 = 4.8×10^4 lb/in

Conservatively, use tire stiffness of 6.1×10^5 lb/in

The force in the fuel assemblies is $F = (K*M)^{1/2} * (v)$

Therefore, load per assembly = F / 32 lb

Equivalent g load in the fuel rods = F / 32 / W

The axial stress in the rod is = F / Fuel Tube Area

Using the methodology described above, the fuel tube axial stresses for the prescribed condition are computed and presented in the following table.

Fuel Assembly Type	WE & WES 15x15	WE 17x17	MK BW 17x17	WEV 17x17	WEO 17x17	CE 14x14
Total Fuel Weight (lb)	1,555	1,575	1,575	1,575	1,575	1,450
Fuel Tube Area (in^2)	0.0270	0.0219	0.0234	0.0219	0.0210	0.0327
gap (in) (1)	6.0	6.0	6.0	6.0	6.0	6.0
t (s)	0.211	0.211	0.211	0.211	0.211	0.211
v (in/s)	56.97	56.97	56.97	56.97	56.97	56.97
M ($lb\text{-}s^2/in$)	128.8	130.4	130.4	130.4	130.4	120.1
W (lb)	48.6	49.2	49.2	49.2	49.2	45.3
No. of Fuel Assemblies	32	32	32	32	32	32
K, lb/in	610,000	610,000	610,000	610,000	610,000	610,000
F (lb)	504,946	508,183	508,183	508,183	508,183	487,600
Force / Assembly (lb)	15,780	15,881	15,881	15,881	15,881	15,237
No of Rod / Assembly	204	264	264	264	264	176
Force / Rod (lb)	77.4	60.2	60.2	60.2	60.2	86.6
Equivalent g load	10.1	10.1	10.1	10.1	10.1	10.5
Axial Stress (lb)	2,865	2,747	2,571	2,747	2,864	2,648

Note:

(1) The gap between the fuel assembly and the DSC end component is conservatively assumed to be 6" (the actual length is around 2 in.).

The axial stresses in the fuel rods are compressive stresses, and they are significantly less than the irradiated yield stress of the cladding material = 69,500 psi (Figure 3.9.8-5). Therefore, the fuel rods will maintain their structural integrity when subjected to the trailer acceleration during transfer.

3.9.8.7 Trailer Deceleration from 5 mph to 0 mph during Transfer

During onsite transfer of the cask from the fuel building to the ISFSI the loaded trailer travels at a maximum constant velocity of 5 mph (88 in/s). Any sudden loads, which may occur during an emergency stop, are transferred from the road bed through the rubber tires, the trailer, the support skid, and the cask to the fuel assemblies. The fuel assemblies inside the canister are subjected to maximum postulated 1g (386.4 in/s ^{2}) equivalent axial transfer load [7]. Therefore, the maximum transfer acceleration is +/- 1g.

The initial velocity is v_i = 88 in/s, the deceleration, g = 386.4 in/s ^{2}

The maximum velocity at impact of the fuel assemblies on the inner bottom cover plate is

v = 88 in/sec - v_f (due to friction) - v_d (due to deceleration)

Where, v_f is a function of work done by the force due to friction (F_f).

Therefore, $(M^* v_f^2)/2 = F_f * d$

Where:

M = mass of the fuel assemblies

F_f = M*g*0.3 (where the coefficient of friction between grid straps and canister is 0.3 [9])

d = gap between fuel assembly and the DSC plug

$v_f = \{(2*F_f*d)/M)\}^{1/2}$

Conservatively assume that cask is tied to the trailer so that it does not move.

v_d is calculated as follows:

Substituting in the kinematics equation $s = s_o + ut + a*t^2/2$ (Section 3.9.8.5)

$s_o = 0$, u = 88 in/sec, Acceleration, a = 386.4 in/s ^{2} and solving for 't'

$v_d = u + a*t$

Conservatively, ignoring v_d (change in velocity due to deceleration), at contact with the inner bottom cover plate of the DSC the velocity of the fuel assembly is

$v = 88 - v_f$

The contact force on the fuel assembly = $F = (K*M)^{1/2} * (v)$

Where:

M = total mass of the fuel assemblies = (W*n)/g

W = maximum weight of each fuel assembly

n = number of fuel assemblies/canister = 32

K= conservatively use tire stiffness of 6.1 x 10^5 lb/in (Section 3.9.8.6)

F = (M * K)1/2 *v

Therefore, load per assembly = F / 32
Equivalent g load in the fuel rods = F / 32 / W.
The axial stress in the rod is = F / Fuel Tube Area.

Using the methodology described above, the fuel tube axial stresses for the prescribed condition are computed and presented in the following table.

Fuel Assembly Type	WE & WES 15x15	WE 17x17	MK BW 17x17	WEV 17x17	WEO 17x17	CE 14x14
Total Fuel Weight (lb)	1,555	1,575	1,575	1,575	1,575	1,450
Fuel Tube Area (in^2)	0.0270	0.0219	0.0234	0.0219	0.0210	0.0327
gap (in) (1)	6.0	6.0	6.0	6.0	6.0	6.0
M ($lb\text{-}s^2/in$)	128.8	130.4	130.4	130.4	130.4	120.1
W (lb)	48.6	49.2	49.2	49.2	49.2	45.3
F_f (lb)	14,928	15,120	15,120	15,120	15,120	13,920
v_f, (in/s)	37.3	37.3	37.3	37.3	37.3	37.3
v, (in/s)	50.7	50.7	50.7	50.7	50.7	50.7
K, lb/in	610,000	610,000	610,000	610,000	610,000	610,000
F (lb)	449,390	452,271	452,271	452,271	452,271	433,952
Force / Assembly (lb)	14,043	14,133	14,133	14,133	14,133	13,561
No of Rod / Assembly	204	264	264	264	264	176
Force / Rod (lb)	68.8	53.5	53.5	53.5	53.5	77.1
Equivalent g load	9.0	9.0	9.0	9.0	9.0	9.4
Axial Stress (lb)	2,550	2,445	2,288	2,445	2,549	2,356

Note:
(1) The gap between the fuel assembly and the DSC end component is conservatively assumed to be 6".

The axial stresses in the fuel rods are compressive stresses, and they are significantly less than the irradiated yield strength of the cladding material = 69,500 psi (Figure 3.9.8-5). Therefore, the fuel rods will maintain their structural integrity when subjected to the trailer deceleration during transfer.

3.9.8.8 Normal Loading Condition during Insertion / Retrieval of DSC into / from HSM

The insertion or retrieval of the DSC into the HSM is a highly controlled procedure, and the process is conducted slowly. For normal loading condition, the maximum ram push force for DSC insertion and grapple pull force for DSC retrieval are 80 kips and 60 kips, respectively. These applied forces are monitored and controlled. The acceleration/deceleration resulting from the procedure will be small and bounded by the transfer acceleration and deceleration as reported in Sections 3.9.8.6 and 3.9.8.7, respectively.

3.9.8.9 Off-Normal Jammed Canister Loading during Insertion of DSC into HSM

The insertion or retrieval of the DSC into the HSM is a highly controlled procedure, and the process is conducted slowly. For off-normal jammed canister loading condition, the maximum ram push for DSC insertion and grapple pull force for DSC retrieval are both 80 kips. This applied force is monitored and controlled. Similar to the normal loading condition, the acceleration/deceleration resulting from the procedure will be small and bounded by the transfer acceleration and deceleration as reported in Sections 3.9.8.6 and 3.9.8.7, respectively.

3.9.8.10 One Foot End Drop Damaged Fuel Evaluation

The structural integrity of the fuel cladding due to the one-foot end drop loading condition will be analyzed in the 10CFR71 application.

3.9.8.11 One Foot Side Drop Damaged Fuel Evaluation

Note: The one-foot side drop analysis contained in this section has not been reviewed by the NRC staff because it is not needed to support a 10 CFR Part 72 certification. Therefore, the NRC staff expects the one-foot side drop and the one-foot end drop and vibratory loading conditions to be addressed in the 10 CFR Part 71 application.

During off site transport (Part 71) the damaged fuel assemblies need to be evaluated for 1 foot side drop. The transport operation is carried out using the MP 187H Cask, with the DSC and the impact limiters in the horizontal position.

The maximum g load acting on the damaged fuel rods under 1 foot side drop load = 30g. The damaged fuel rod structural integrity under 1 foot side drop load is assessed by computing the bending stress in the rod and comparing it with the yield stress of the cladding material. The fracture assessment of the damaged fuel rod structural integrity is made by using two fracture geometries (ruptured sections) as described below.

It is assumed that the damaged fuel tube is burst at the spacers (supports) location, which is the location of maximum bending moment. The loading assumed is on the opposite side of the rod at the burst location. The following two geometries, used for the fracture evaluation of the damaged fuel rods, are based on these assumptions.

Fracture Geometry #1: The first geometry is shown in Figure 3.9.8-1. In this damage mode the fuel tube is assumed to bulge from diameter D to diameter W ($W \geq D$) and rupture to a hole of diameter (2a) at the bulge location. It is assumed that (2a/w) = 0.5 for this geometry.

Fracture Geometry #2: The second geometry is shown in Figure 3.9.8-2. The stress intensities factors for this geometry are determined using the solution for a tube with a crack subjected to pure bending moment given in Reference 13. This evaluation is based on a crack length to diameter ratio of 0.47 (or $2a/D_m$=0.47).

The basis for the 0.5 (ruptured hole to tube diameter ratio) for fracture geometry #1 and 0.47 (crack length to tube diameter ratio) for fracture geometry #2 are the experimental tests on "as received" Zircalloy fuel tubes with measured burst temperatures of up to 909°C, which showed flaw opening to diameter ratios of 0.4 to 0.5 [16].

3.9.8.11.1 Structural Integrity Evaluation with Fracture Geometry #1

The fracture geometry #1 (Ruptured Section) is shown in Figure 3.9.8-1. With reference to Figure 3.9.8-1, the methodology for computing the stress intensity factor K_I is as follows:

Fuel rod OD = D
Oxidized Clad Thickness = t
Average radius, R = (D-t)/2

I = net tube MI.

Span Length = S

Assume (2a/W) = 0.5, where 2a = ruptured hole diameter,

W = bulged fuel tube diameter ≥ D.

Stress Intensity Factor, $K_I = (Y)(P*a^{1/2})/(t*W)$, [Reference 14, Fig. 8.7(c)]

Where:

Y = 2.11 {established using (2a/W) = 0.5 (for Forman et al. case) in Figure 3.9.8-3 }

P = average tensile force at the crack which is expressed as a function of moment on the cross section as:

$= (2MR^2t)/I$ (See Table 3.9.8-8)

$W = \pi R$

$M = 0.1058(W_s*S^2)$ (See Appendix 2 of Reference 3)

W_s = 30g Fuel Rod Weight / Length

Bending Stress = MD / 2I

Using the methodology described above, the stress intensity factors, K_I, for the prescribed condition are computed and presented in the following table.

Fuel Assembly Type	WE & WES 15x15	WE 17x17	MK BW 17x17	WEV 17x17	WEO 17x17	CE 14x14
Fuel Rod OD, D (in)	0.4193	0.3713	0.3713	0.3713	0.3573	0.4373
Clad Thickness, t (in)	0.0216	0.0198	0.0213	0.0198	0.0198	0.0253
Average Radius, R (in)	0.1989	0.1758	0.1750	0.1758	0.1688	0.2060
Fuel Tube M.I. (in^4)	5.35E-04	3.39E-04	3.60E-04	3.39E-04	3.00E-04	6.97E-04
Span Length, S (in)	27.0	25.0	25.0	25.0	25.0	17.0
(2a/W)	0.5	0.5	0.5	0.5	0.5	0.5
Y	2.11	2.11	2.11	2.11	2.11	2.11
W (in)	0.62	0.55	0.55	0.55	0.53	0.65
Fuel Assembly Weight (lb)	1,555	1,575	1,575	1,575	1,575	1,450
No. of Rods	204	264	264	264	264	176
Active Fuel Length (in)	144.0	144.0	144.0	144.0	144.0	137.0
1-Foot Side Drop Equivalent g load	30	30	30	30	30	30
W_s (lb/in)	1.59	1.24	1.24	1.24	1.24	1.80
Moment, M (kip. in)	0.12	0.08	0.08	0.08	0.08	0.06
Bending Stress (psi)	47,990	45,040	42,390	45,040	48,950	17,300
P (kip)	0.391	0.297	0.298	0.297	0.309	0.170
K_I (ksi $in^{1/2}$)	24.2	21.3	19.9	21.3	22.6	8.8

The computed stress intensity factor is compared with experimentally obtained plane strain fracture toughness, K_{IC} of irradiated Zircaloy cladding material as reported in [15].

Reference15 reports a K_{IC} = 35 ksi $in^{1/2}$ at approximately 300°F which is greater than highest computed stress intensity factor, K_I of 24.2 ksi $in^{1/2}$ presented in the above table.

Therefore, the structural integrity of the damaged fuel rods, which are conservatively assumed to rupture as shown in Figure 3.9.8-1, will be maintained.

3.9.8.11.2 Structural Integrity Evaluation with Fracture Geometry #2

This geometry is shown in Figure 3.9.8-2. Stress intensity factors are computed for a crack in a fuel tube subjected to a uniform bending moment (M) using formulae given in Reference 13. As per Reference 13, page 472:

$$K_I = \sigma (\pi * R_m * \theta)^{1/2} F(\theta)$$

where,

$$F(\theta) = 1 + 6.8*(\theta/\pi)^{3/2} - 13.6*(\theta/\pi)^{5/2} + 20.0*(\theta/\pi)^{7/2}$$

σ = Bending Stress due to Uniform Moment 'M'

R_m = Average radius of the fuel tube

2θ = Angle which the crack makes at the center of the tube

K_I = Stress Intensity Factor at the crack

The K_I is computed for all the different fuel assemblies, and the results for all the fuel assemblies are presented in Table 3.9.8-1, 3.9.8-2, 3.9.8-3, 3.9.8- 4 and 3.9.8-5.

Based on the computed K_I using Fracture Geometries #1 & #2, a summary of the comparisons is presented as follows:

	Fracture Geometry #1 K_I	Fracture Geometry #2 K_I
WE & WES 15x15	24.2	33.8
WE 17x17	21.3	29.9
MK BW 17x17	19.9	28.0
WEV 17x17	21.3	29.9
WEO 17x17	22.6	31.8
CE 14x14	8.8	12.4

3.9.8.12 Conclusions

The maximum computed stresses in the fuel rods and their ratios to the irradiated yield stress of the cladding material are summarized in Table 3.9.8-6. From Table 3.9.8-6, it can be concluded that stresses for all load cases considered are significantly less than the yield stress of the Zircaloy cladding material (computed stresses are 4% to 49% of the yield stress).

It is important to note that, the stresses in the fuel rods for all analyzed normal and off normal load cases are compressive stresses (less than the critical buckling stress), except for the 1-foot transport condition side drop load.

For the 1-foot side drop it is demonstrated by using fracture mechanics procedures (by comparing computed stress intensity factors to critical crack initiation fracture toughness in Table 3.9.8-7), that the damaged fuel rods will maintain their structural integrity.

This calculation demonstrates that the fuel cladding in the NUHOMS® 32PTH DSC will retain its structural integrity when subjected to normal condition of storage and on site transfer loads. The fuel cladding will also maintain its integrity when subjected to a one-foot side drop during offsite transport. The fuel cladding integrity during the one-foot end drop and transport vibratory loads will be demonstrated in the 10CFR71 application. Therefore, the retrievability of the fuel assembly is assured when subjected to storage and transfer normal and off normal loads.

3.9.8.13 Derivation of Fuel Assembly Material Properties

Material property for low burnup fuel

The material properties used for the fuel cladding structural analysis is based on the LLNL report "Dynamic Impact Effects on Spent Fuel Assemblies" [3] and is for low burnup fuel. The material properties used for the drop analysis at elevated temperature are obtained from the following methodology.

Yield Strength of cladding: The yield stress vs. temperature is taken from Table 5 of [3, page 12] and is depicted in Figure 3.9.8-4. Since the relation between the yield strength vs. temperature is linear, the yield strength at higher temperature is obtained by extending the curve.

S_y = 81,500 psi (725°F)
S_y = 80,500 psi (750°F)

Tensile Strength of cladding: The tensile strength corresponding to the yield strength at the temperatures is obtained from Figure 5 of [3, page 17] and is also depicted in Figure 3.9.8-4.

S_u = 92,000 psi (725°F)
S_u = 91,800 psi (750°F)

Material property for high burnup fuel

Information Withheld Under 10 CFR 2.390

Information Withheld Under 10 CFR 2.390

In order to calculate the actual thickness of the cladding needed to be reduced, the oxide thickness accumulation needed to be corrected. A Pilling-Bedworth factor of 1.75 [18, page 426] is used in Chapter 3 calculation and is repeated as follows.

$(120/1.75) \times 10^{-6} \times 39.372 = 0.0027$ in.

Information Withheld Under 10 CFR 2.390

Information Withheld Under 10 CFR 2.390

3.9.8.14 THIS PAGE INTENTIONALLY BLANK

THIS PAGE INTENTIONALLY BLANK

THIS PAGE INTENTIONALLY BLANK

THIS PAGE INTENTIONALLY BLANK

THIS PAGE INTENTIONALLY BLANK

3.9.8.15 References

1. Transnuclear Calculation No. NUH24PTH.0209 Rev. 0, "NUHOMS® 24PTH Damaged Fuel Cladding Structural Evaluation to Demonstrate the Retrievability of the Fuel Subject to Normal and Off-Normal Loads".
2. Transnuclear, Inc., "Design Criteria Document (DCD) for the NUHOMS®-32PTH System for Transportation and Storage," NUH32PTH.0101, Revision 0.
3. UCID – 21246, "Dynamic Impact Effects on Spent Fuel Assemblies," Lawrence Livermore National Laboratory, October 20, 1987.
4. Transnuclear Calculation No. 10494-6, Rev. 0, "NUHOMS-32PTH DSC, Transfer Cask, and 'Under Hook' Nominal Weight Calculation".
5. ANSI N14.23, "Draft American National Standard Design Basis for Resistance to Shock and Vibration of Radioactive Material Packages Greater than One Ton in Truck Transport", May 1980.
6. NRC -12 , SAND76-0427, NUREG766510, "Shock and Vibration Environments for Large Shipping Containers on Rail Cars and Trucks", June 1977.
7. Transnuclear Inc., "Final Safety Analysis Report for Standard NUHOMS® Horizontal Modular Storage System for Irradiated Nuclear Fuel," Document No. NUH-003, Revision 6
8. Transnuclear, Inc., "Technical Specification for the NUHOMS® 10' - 6" Wide Cask Transfer Trailer," Report No. NUH-07-106, Revision 3.
9. Baumeister, T., "Mark's Standard Handbook for Mechanical Engineers," McGraw-Hill Book Company, 8th Edition.
10. Transnuclear Calculation No. 10494-20, Rev. 0, "NUHOMS-32PTH Thermal Analysis of DSC in HSM for the Normal, Off-Normal, and Accident Storage Conditions".
11. Transnuclear Calculation No. 10494-46, Rev. 0, "NUHOMS-32PTH Thermal Expansions".
12. OCRWM Database, "Characteristics of spent fuel, high level waste, and other radioactive wastes which may require long term isolation" Appendix 2A, Volume 3 of 6, DOE/RW-0184, December 1987.
13. "The Stress Analysis of Cracks Handbook" Third Edition by Hiroshi Tada et al., ASME press.
14. R.W. Hertzberg," Deformation and Fracture Mechanics of Engineering Material" John Wiley & Sons, New York, 1976.

15. T.J. Walker, et al., "Variation of Zircaloy Fracture Toughness in Irradiation" Zirconium in Nuclear Applications, ASTM STP 551, American Society for Testing and Materials, 1974, pp. 328-354.

16. Light-Water Reactor Safety Research Program: Quarterly Progress Report July-September 1976, Section III, "Mechanical Properties of Zircaloy Containing Oxygen", Figs III-29 to III-32, ANL-75-72 (September 1975).

17. EPRI Technical Report 1003218 "Hot Cell Examination of ZIRLO PWR Fuel, Irradiated to 70 GWd/MTU", December 2003.

18. Van Swam, L. F., Strasser A. A., Cook J. D., Burger J. M., "Behavior of Zircaloy-4 and Zirconium Linear Zircaloy-4 Cladding at High Burnup" Proceedings of the 1997 International Topical Meeting on LWR Fuel Performance, Portland, Orgon March 2-6, 1997.

19. North Anna Power Station UFSAR, rev. 40, 13/30/04.

20. John F. Harvey "Theory and Design of Modern Pressure Vessel" Second edition.

21. NUREG/CR-0497 "A handbook of Materials Properties for Use in the Analysis of Light Water Reactor Fuel Rod Behavior, MATPRO-Version 11" February 1979.

Table 3.9.8-1

WE & WES 15x15 - K_I Calculation using Fracture Geometry #2

OD (in) =	0.4193
t (in) =	0.0216
R / t =	9.71
Rm (in) =	0.1989
M (kip-in) =	0.12
Theta (radian) =	0.47
I (in^4) =	5.34E-04
Bending Stress (ksi) =	47.99
E (ksi) =	10,600

Theta (rad)	Theta/pi	Half Length (in)	F(Theta)	K_I (ksi $in^{1/2}$)
0.05	0.0159	0.0099	1.0132	8.6
0.10	0.0318	0.0199	1.0363	12.4
0.15	0.0477	0.0298	1.0646	15.6
0.20	0.0637	0.0398	1.0966	18.6
0.25	0.0796	0.0497	1.1312	21.5
0.30	0.0955	0.0597	1.1677	24.3
0.35	0.1114	0.0696	1.2058	27.1
0.40	0.1273	0.0795	1.2450	29.9
0.45	0.1432	0.0895	1.2853	32.7
0.47	0.1496	0.0935	1.3017	33.8
0.51	0.1623	0.1014	1.3348	36.2
0.52	0.1655	0.1034	1.3432	36.7
0.55	0.1751	0.1094	1.3686	38.5
0.60	0.1910	0.1193	1.4117	41.5
0.65	0.2069	0.1293	1.4557	44.5
0.70	0.2228	0.1392	1.5009	47.6

Table 3.9.8-2

WE 17x17 - K_I Calculation using Fracture Geometry #2

OD (in) =	0.3713
t (in) =	0.0198
R / t =	9.38
Rm (in) =	0.1758
M (kip-in) =	0.08
Theta (radian) =	0.47
I (in^4) =	3.39E-04
Bending Stress (ksi) =	45.04
E (ksi) =	10,600

Theta (rad)	Theta/pi	Half Length (in)	F(Theta)	K_I (ksi $in^{1/2}$)
0.05	0.0159	0.0088	1.0132	7.6
0.10	0.0318	0.0176	1.0363	11.0
0.15	0.0477	0.0264	1.0646	13.8
0.20	0.0637	0.0352	1.0966	16.4
0.25	0.0796	0.0439	1.1312	18.9
0.30	0.0955	0.0527	1.1677	21.4
0.35	0.1114	0.0615	1.2058	23.9
0.40	0.1273	0.0703	1.2450	26.4
0.45	0.1432	0.0791	1.2853	28.9
0.47	0.1496	0.0826	1.3017	29.9
0.51	0.1623	0.0896	1.3348	31.9
0.52	0.1655	0.0914	1.3432	32.4
0.55	0.1751	0.0967	1.3686	34.0
0.60	0.1910	0.1055	1.4117	36.6
0.65	0.2069	0.1142	1.4557	39.3
0.70	0.2228	0.1230	1.5009	42.0

Table 3.9.8-3

MK BW 17x17 - K_I Calculation using Fracture Geometry #2

OD (in) =	0.3713
t (in) =	0.0213
R / t =	8.72
Rm (in) =	0.1750
M (kip-in) =	0.08
Theta (radian) =	0.47
I (in^4) =	3.60E-04
Bending Stress (ksi) =	42.39
E (ksi) =	10,600

Theta (rad)	Theta/pi	Half Length (in)	F(Theta)	K_I (ksi $in^{1/2}$)
0.05	0.0159	0.0088	1.0132	7.1
0.10	0.0318	0.0175	1.0363	10.3
0.15	0.0477	0.0263	1.0646	13.0
0.20	0.0637	0.0350	1.0966	15.4
0.25	0.0796	0.0438	1.1312	17.8
0.30	0.0955	0.0525	1.1677	20.1
0.35	0.1114	0.0613	1.2058	22.4
0.40	0.1273	0.0700	1.2450	24.7
0.45	0.1432	0.0788	1.2853	27.1
0.47	0.1496	0.0823	1.3017	28.0
0.51	0.1623	0.0893	1.3348	30.0
0.52	0.1655	0.0910	1.3432	30.4
0.55	0.1751	0.0963	1.3686	31.9
0.60	0.1910	0.1050	1.4117	34.4
0.65	0.2069	0.1138	1.4557	36.9
0.70	0.2228	0.1225	1.5009	39.5

Table 3.9.8-4

WEV 17x17 - K_I Calculation using Fracture Geometry #2

OD (in) =	0.3713
t (in) =	0.0198
R / t =	9.38
Rm (in) =	0.1758
M (kip-in) =	0.08
Theta (radian) =	0.47
I (in^4) =	3.39E-04
Bending Stress (ksi) =	45.04
E (ksi) =	10,600

Theta (rad)	Theta/pi	Half Length (in)	F(Theta)	K_I (ksi $in^{1/2}$)
0.05	0.0159	0.0088	1.0132	7.6
0.10	0.0318	0.0176	1.0363	11.0
0.15	0.0477	0.0264	1.0646	13.8
0.20	0.0637	0.0352	1.0966	16.4
0.25	0.0796	0.0439	1.1312	18.9
0.30	0.0955	0.0527	1.1677	21.4
0.35	0.1114	0.0615	1.2058	23.9
0.40	0.1273	0.0703	1.2450	26.4
0.45	0.1432	0.0791	1.2853	28.9
0.47	0.1496	0.0826	1.3017	29.9
0.51	0.1623	0.0896	1.3348	31.9
0.52	0.1655	0.0914	1.3432	32.4
0.55	0.1751	0.0967	1.3686	34.0
0.60	0.1910	0.1055	1.4117	36.6
0.65	0.2069	0.1142	1.4557	39.3
0.70	0.2228	0.1230	1.5009	42.0

Table 3.9.8-5

WEO 17x17 - K_I Calculation using Fracture Geometry #2

OD (in) =	0.3573
t (in) =	0.0198
R / t =	9.02
Rm (in) =	0.1688
M (kip-in) =	0.08
Theta (radian) =	0.47
I (in^4) =	3.00E-04
Bending Stress (ksi) =	48.95
E (ksi) =	10,600

Theta (rad)	Theta/pi	Half Length (in)	F(Theta)	K_I (ksi $in^{1/2}$)
0.05	0.0159	0.0084	1.0132	8.1
0.10	0.0318	0.0169	1.0363	11.7
0.15	0.0477	0.0253	1.0646	14.7
0.20	0.0637	0.0338	1.0966	17.5
0.25	0.0796	0.0422	1.1312	20.2
0.30	0.0955	0.0506	1.1677	22.8
0.35	0.1114	0.0591	1.2058	25.4
0.40	0.1273	0.0675	1.2450	28.1
0.45	0.1432	0.0759	1.2853	30.7
0.47	0.1496	0.0793	1.3017	31.8
0.51	0.1623	0.0861	1.3348	34.0
0.52	0.1655	0.0878	1.3432	34.5
0.55	0.1751	0.0928	1.3686	36.2
0.60	0.1910	0.1013	1.4117	39.0
0.65	0.2069	0.1097	1.4557	41.8
0.70	0.2228	0.1181	1.5009	44.8

Table 3.9.8-6

CE 14x14 - K_I Calculation using Fracture Geometry #2

OD (in) =	0.4373
t (in) =	0.0253
R / t =	8.64
Rm (in) =	0.2060
M (kip-in) =	0.06
Theta (radian) =	0.47
I (in^4) =	6.97E-04
Bending Stress (ksi) =	17.30
E (ksi) =	10,600

Theta (rad)	Theta/pi	Half Length (in)	F(Theta)	K_I (ksi $in^{1/2}$)
0.05	0.0159	0.0103	1.0132	3.2
0.10	0.0318	0.0206	1.0363	4.6
0.15	0.0477	0.0309	1.0646	5.7
0.20	0.0637	0.0412	1.0966	6.8
0.25	0.0796	0.0515	1.1312	7.9
0.30	0.0955	0.0618	1.1677	8.9
0.35	0.1114	0.0721	1.2058	9.9
0.40	0.1273	0.0824	1.2450	11.0
0.45	0.1432	0.0927	1.2853	12.0
0.47	0.1496	0.0968	1.3017	12.4
0.51	0.1623	0.1051	1.3348	13.3
0.52	0.1655	0.1071	1.3432	13.5
0.55	0.1751	0.1133	1.3686	14.1
0.60	0.1910	0.1236	1.4117	15.2
0.65	0.2069	0.1339	1.4557	16.3
0.70	0.2228	0.1442	1.5009	17.5

Table 3.9.8-7

Summary - Maximum Fuel Rod Stresses and Stress Ratios

Normal and Off Normal Load Case	Maximum (1) Stress (psi)	Stress (2) Ratio
On site Transport and Transfer Operations	2,865	0.04
One-foot Side Drop (Part 71)	48,950	0.70

Notes:
(1) Maximum stress for all fuel assemblies.
(2) Stress ratio = maximum stress / 69,500 (yield stress for Zircaloy cladding).

Table 3.9.8-8

Summary - Computed Fuel Tube Stress Intensity Factors and Ratios

Fracture Geometry	Max K_I (1) (ksi $in^{1/2}$)	K_{IC} (2) (ksi $in^{1/2}$)	Ratio Max K_I / K_{IC}
Geometry #1	24.2	35.0	0.69
Geometry #2	33.8	35.0	0.97

Notes:

1. Maximum K_I for all fuel assemblies.
2. K_{IC} = Crack initiation fracture toughness (plane strain fracture toughness).

Table 3.9.8-9

Derivation of Tensile Force (T) and Applied Moment (M) Relationship for a Circular Tube

Consider a circular tube of average radius "R", thickness "t" subjected to a bending moment "M".

At angle "θ" from the neutral axis (N/A), for a segment of the tube with angle "dθ"

Area = A = t*R*dθ,

Tensile stress = σ = (M*R*Sinθ)/I

Where, I = moment of inertia of the section

Therefore,

Tensile Force =ΔP = (M*R*Sin θ/I) *(t*R*dθ)

Total Tensile Force = P = ∫ (M*R*Sinθ/I) *(t*R*dθ)

Where, limits of integral are from angle "θ = 0" to angle "θ = π"

Therefore, $P = (M*R^2 *t / I) \int \text{Sin}\theta \, d\theta$

$= (M*R^2 *t / I) [- \text{Cos}\theta]^{\pi}_{0}$

$= 2*M*R^2 *t / I$

Table 3.9.8-9 (continued)

Derivation of Tensile Force (T) and Applied Moment (M) Relationship for a Circular Tube

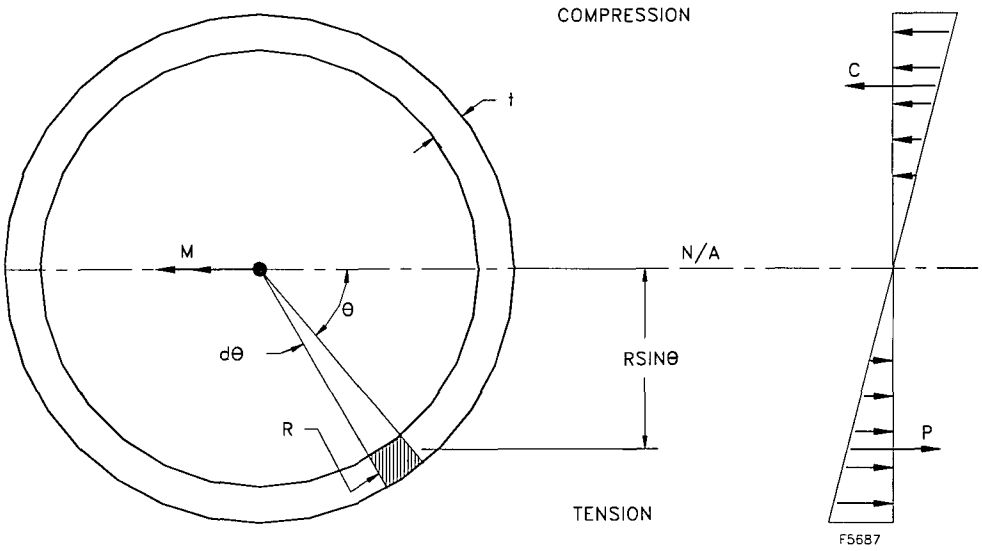

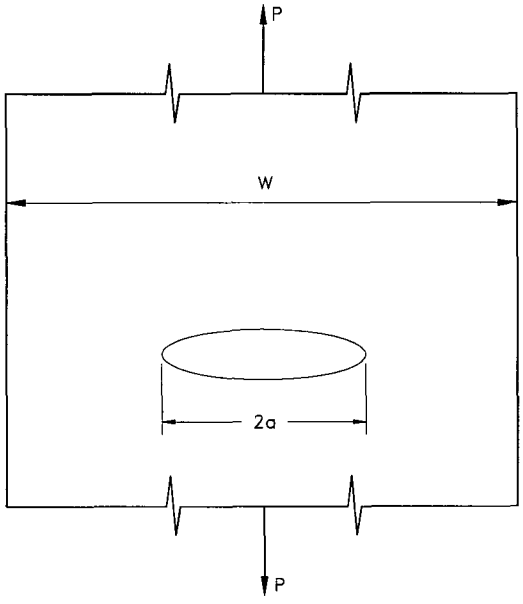

M = Applied moment
P = Resultant tensile force
R = Average radius of fuel tube
t = Thickness of fuel tube
I = Moment of inertia of fuel tube
2a = Crack width

$W = \pi R$

$P = \frac{2MR^2t}{I}$

Table 3.9.8-10

Tire Stiffness Calculation

The on-site transfer trailer has four axles with eight 235/75R 17.5 SLR 184 tires per axle (total of 32 tires). The tire stiffness is estimated based on tire measurements as follows:

For 235 (tire width in mm)/75 (height-to-width ratio in %) R 17.5 (rim diameter in inches) SLR184:
Tire width 235mm/25.4mm/in =9.25 inch

Height of tire = 75% of 9.25= 6.94 inch

Tire diameter = 17.5+2*6.94= 31.4 inch.

From trailer tire measurements:

	a (height) - in	b (width) - in	c (ground top) - in
A (front right tire)	6.5	7.4	30.0
B (front left tire)	7.3	7.4	30.8
C (rear right tire)	4.8	7.3	31.3
D (rear left tire)	4.0	7.2	31.4

Tire pressure: 140-145 psi

Trailer weight: 39,700 lbs.

Skid weight: 26,500 lbs

RAM weight: 6,400 lbs.

Average c dimension at front= (30+30.8)/2=30.4 inches

Average c dimension at rear = (31.3+31.4)/2=31.4 inches

Tire height: 33 inches, at approximately 145 psi pressure

Weight per tire (excluding RAM weight): 66,200/32=2070 lbs/tire

Weight per tire (assuming RAM weight is distributed on 8 tires): 6400/8= 1600 lb/tire

Front 8 tires: 2070+1600=3670 lbs/tire.

Table 3.9.8-10 (continued)

Tire Stiffness Calculation

All other tires: 2070 lbs/tire

Stiffness is determined as:

K_{front} = 3670/(33-30.4)=1411 lbs/in

$K_{all\ others}$ = 2070/(33-31.4)=1294 lbs/in

Use K/tire =1500 lbs/inch.

Total stiffness = 32x 1500= 4.8E 4 lbs/in

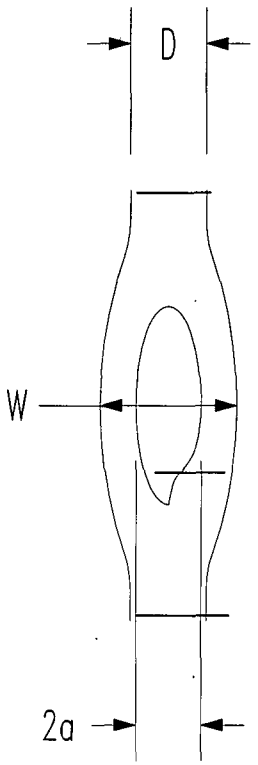

Figure 3.9.8-1

Fracture Geometry #1 - Ruptured Section

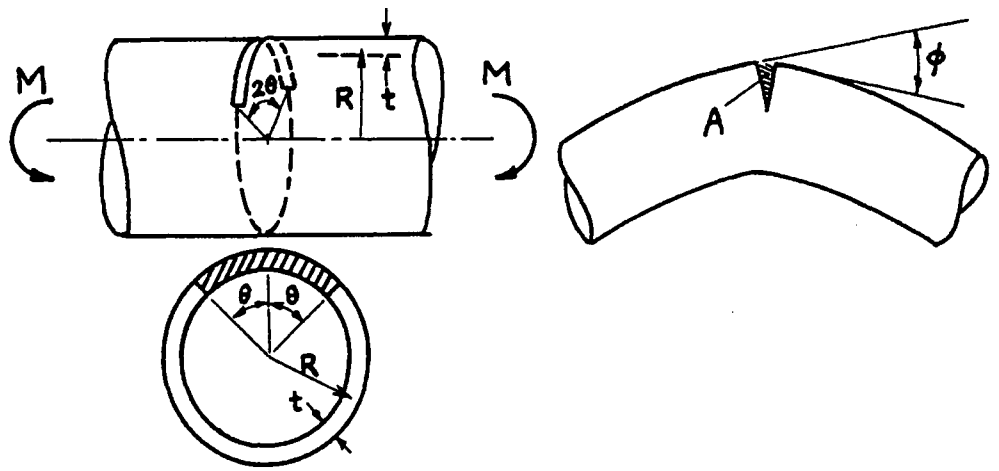

$$\underline{R/t \simeq 10} \qquad \left(\theta < 110^\circ\right)$$

$$\sigma = M/\left(\pi R^2 t\right)$$

$$K_I = \sigma\sqrt{\pi(R\theta)} \cdot F(\theta)$$

$$F(\theta) = 1 + 6.8\left(\frac{\theta}{\pi}\right)^{3/2} - 13.6\left(\frac{\theta}{\pi}\right)^{5/2} + 20.0\left(\frac{\theta}{\pi}\right)^{7/2}$$

Figure 3.9.8-2

Fracture Geometry #2: Through-Wall Circumferential Crack in Cylinder under Bending

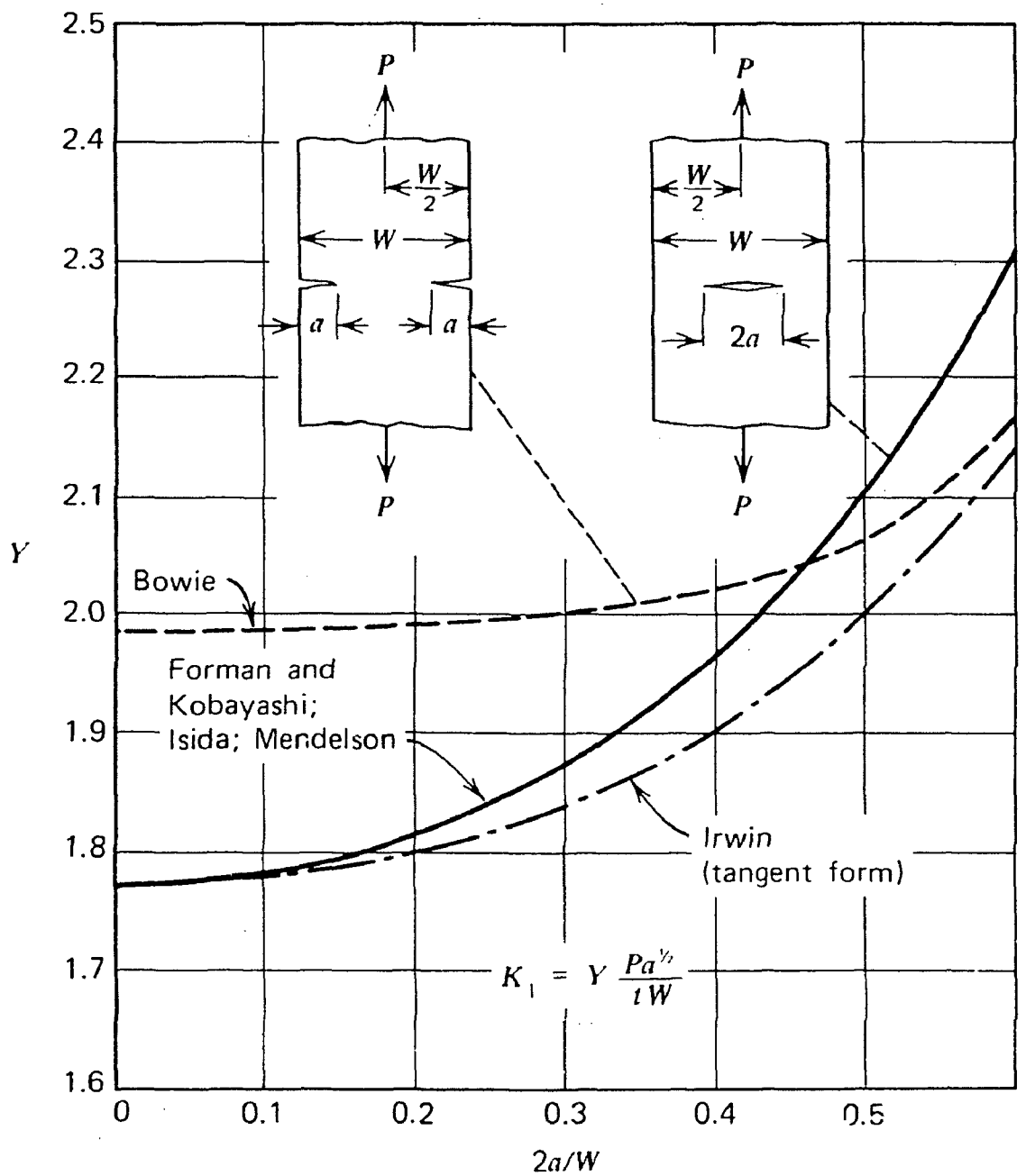

Figure 3.9.8-3

Stress Intensity Factor Solutions: For Several Specimen Configurations

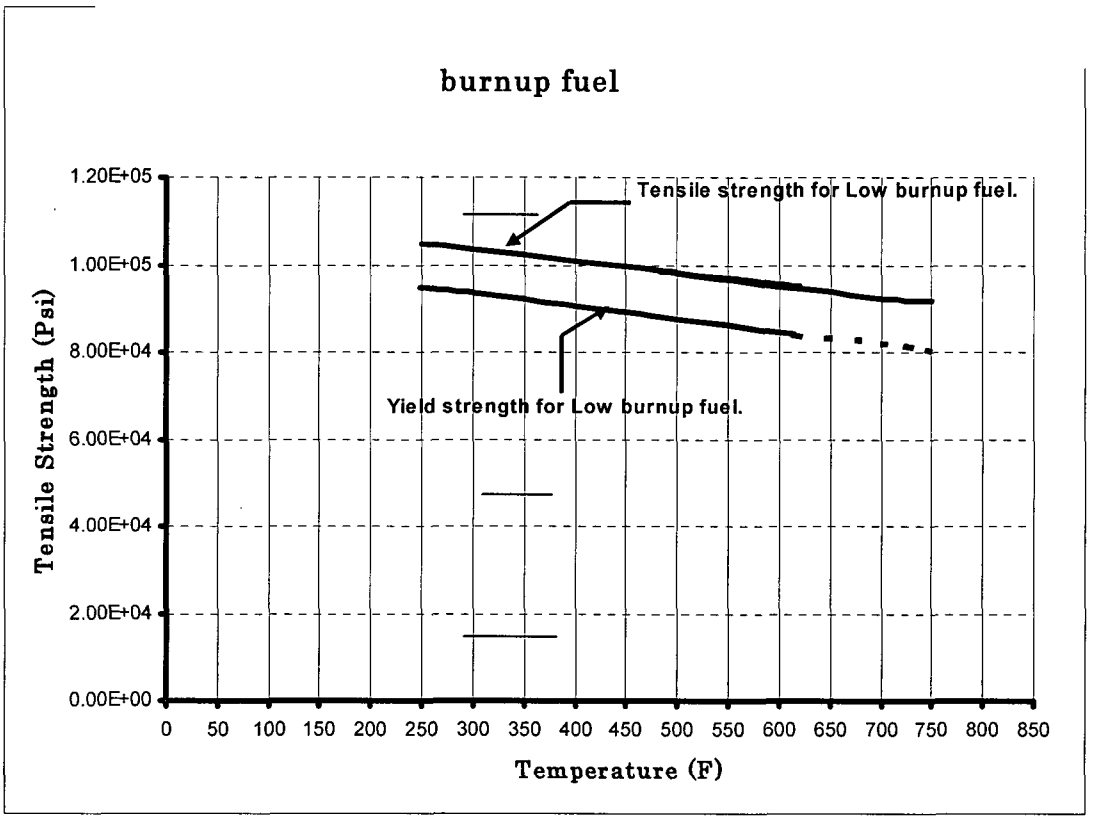

Yield Strength (Low Burn Up)	Temp F
9.49E+04	248
9.44E+04	264
9.39E+04	284
9.33E+04	304
9.24E+04	334
9.14E+04	369.
9.01E+04	415
8.81E+04	486
8.44E+04	615
8.15E+04	725
8.05E+04	750

Tensile Strength (Low Burn Up)	Temp F
1.05E+05	250
9.52E+04	615
9.85E+04	486
9.20E+04	725
9.18E+04	750

Figure 3.9.8-4

Temperature Vs Tensile and Yield Strength for Low Burn up Fuel

Proprietary Information Withheld Under 10 CFR 2.390

Figure 3.9.8-5

Temperature Vs Tensile and Yield Strength for High Burn up Fuel

APPENDIX 3.9.9
HSM-H STRUCTURAL ANALYSIS

TABLE OF CONTENTS

3.9.9 HSM-H STRUCTURAL ANALYSIS 3.9.9-1
3.9.9.1 Introduction 3.9.9-1
3.9.9.2 General Description of the HSM-H 3.9.9-1
3.9.9.3 Material Properties 3.9.9-3
3.9.9.4 Component Weights 3.9.9-4
3.9.9.5 Design Criteria 3.9.9-5
3.9.9.6 Load Cases 3.9.9-8
3.9.9.7 Finite Element Models 3.9.9-13
3.9.9.8 Normal Operation Structural Analysis 3.9.9-16
3.9.9.9 Off-Normal Operation Structural Analysis 3.9.9-18
3.9.9.10 Accident Condition Structural Analysis 3.9.9-20
3.9.9.11 Load Combinations 3.9.9-27
3.9.9.12 Conclusions 3.9.9-28
3.9.9.13 References 3.9.9-29

LIST OF TABLES

3.9.9-1 Summary of HSM-H Component Design Loadings

3.9.9-2 Summary of 32PTH DSC Support Structure Design Loadings

3.9.9-3 HSM-H Concrete Load Combinations

3.9.9-4 Ultimate Capacities of Concrete Components

3.9.9-5 Structural Design Criteria for DSC Support structure

3.9.9-6 HSM-H Support Steel Structure Load Combinations

3.9.9-7 Design Pressure for Tornado Wind Loading

3.9.9-8 Maximum HSM-H Concrete Component Forces and Moment for Normal & Off-Normal Loads

3.9.9-9 Summary of Thermal Forces and Moments in the HSM-H Concrete Components

3.9.9-10 Maximum HSM-H Concrete Component Forces and Moments for Accident Loads

3.9.9-11 Comparison of Highest Combined Shear Forces/Moments with the Capacities

3.9.9-12 Maximum/Minimum Forces/Moments in the Rail Components in the Local System

3.9.9-13 Maximum/Minimum Forces/Moments in the Rail Extension Plates in the Local System

3.9.9-14 Maximum/minimum Axial Forces in the Cross member Components

3.9.9-15 Rail component Results

3.9.9-16 Extension Plates and Cross Members Results

LIST OF FIGURES

3.9.9-1 Analytical Model of W12x96 Beam with Slotted, Nitronic and Stiffener Plates

3.9.9-2 Analytical Model of the HSM-H for Mechanical Load Analysis

3.9.9-3 Analytical Model of the 32PTH DSC Support Structure

3.9.9-4 Analytical Model of the HSM-H for Thermal Load Analysis

3.9.9-5 Symbolic Notations of Force and Moment Capacities

3.9.9-6 Components of Support Structure

3.9.9 HSM-H STRUCTURAL ANALYSIS

3.9.9.1 Introduction

The purpose of this appendix is to present the structural evaluation of the HSM-H due to all applied loads during storage loading operations.

The design of the HSM-H for 32PTH DSC is the same as the HSM-H which is under NRC review as Amendment 8 to CoC 1004 for 24PTH DSC. Analyses performed for HSM-H with 24PTH DSC used bounding values to envelop both 24PTH DSC and 32PTH DSC.

The HSM-H module design for 32PTH canister is identical to the HSM-H design for 24PTH canister except the following modifications:

1. The module for the 32PTH canister is designed such that the center line of the loaded 32PTH canister is approximately four inches higher compared to that of the 24PTH canister.

2. The diameter of the door openings in the front and rear of the front wall are approximately four inch and two inch larger for the 32PTH canister compared to those of the 24PTH canister.

3. The transfer cask docking surface in the module for the 32PTH canister transfer cask is approximately half inch wider compared to the cask docking surface for the 24PTH canister transfer cask.

4. The diameters of the front inner circular steel plate and rear circular concrete block of the shielded door for the 32PTH canister are approximately four inch and two inch larger compared to those of the 24PTH canisters.

5. For the 32PTH design the spacers at the canister stop plate of the module will be provided similar to the 24PTH short cavity design.

Analyses performed for HSM-H with 24PTH DSC used bounding values to envelop both 24PTH DSC and 32PTH DSC. The structural evaluation provided in this appendix is identical as the information provided in Amendment 8 to CoC 1004 for 24PTH DSC. Amendment 8 reference sections are indicated in this appendix for cross reference.

3.9.9.2 General Description of the HSM-H

The HSM-H is a free standing reinforced concrete structure designed to provide environmental protection and radiological shielding for the 32PTH DSC. Each HSM-H provides a self contained modular structure for the storage of a 32PTH DSC containing up to 32 PWR spent fuel

assemblies. The HSM-H provides heat rejection from the spent fuel decay heat by a combination of radiation, conduction and convection. Schematic sketch of the HSM-H showing the different components is provided in Chapter 1, Figure 1-1. The drawings in Chapter 1, Section 1.5 provide the principal dimensions and design parameters of the HSM-H.

The HSM-H is a reinforced concrete structure comprised of a base unit, where the 32 PTH DSC is stored and a roof unit that serves to provide environmental protection and radiation shielding. These two units are assembled together to form a single module.

The HSM-H modules may be prefabricated off-site, then transported to the ISFSI site and installed on a reinforced concrete basemat. The HSM-H is placed next to, and in contact with, adjacent module(s) to form a continuous single or double row arrays.

The 32PTC is supported inside the HSM-H by the DSC support structure. The DSC support structure (rail support assembly) is comprised of two rail sections, two slotted plates and two rail support plates. The rail support assembly provides support for the DSC during storage and act as a sliding surface during DSC insertion and retrieval.

The air inlet vents are extending through the front on both sides of the front wall. The front wall and the rear wall of the base unit provide support for the rails and the rail extension flanges. The roof unit rests on the front, rear and side walls of the base unit. The air outlet vents are provided in the roof unit.

The HSM-H front standard door is a composite door, which consists of a rectangular steel face plate at the front attached to a circular thick steel plate and a circular reinforced concrete block at the rear. The rectangular steel face plate of the door is attached to the front wall concrete using four bolts anchored through four embedments. The alternate circular door is similar to the standard door except that the front face is a circular steel plate. The circular steel plate of the door is attached to the front wall concrete by four clamps which are located at the 45° line in each quadrant of the door. The clamps consist of four "L" shaped clips which are bolted to the front wall concrete through four embedments. The door provides missile protection and shielding for the DSC.

The concrete door provides missile protection and shielding. End shield walls are provided at the ends of a module array to provide the required missile and shielding protection. Similarly, an additional shield wall is used at the rear of the module for single module rows.

The side heat shields of the HSM-H consist of three panels. Each panel consists of optional anodized aluminum fins mounted on the stainless steel base plates. The base plates are provided with aluminum backing plates on the surface facing the concrete. The top louvered heat shield under the roof consists of seven panels. Each panel has two stainless steel mounting bars. Horizontal louvers are mounted on these bars. The heat shields provide thermal protection for the HSM-H concrete.

During DSC insertion/retrieval operations, the transfer cask is docked with the HSM-H docking surface and mechanically secured to the embedment provided in the front wall. The embedments are equally spaced on either side of the HSM-H access opening.

The drawings in Chapter 1, Section 1.5 provide the principal dimensions and design parameters of the HSM-H. The dimension differences between the HSM-H to be used for storing the 32PTH canister and 24PTH canister are listed in the following tables.

TN drawing No. 10494-72-104

HSM-H		
Dimension	System Type	
	For 32PTH Canister	For 24PTH Canister [13]
A	8' – 10"	8' – 6"
B	Ø 5' – 11 5/8"	Ø 5' – 9"
C	Ø 7' – 5"	Ø 7' – 1 1/2"

TN drawing No. 10494-72-107

HSM-H		
Dimension	System Type	
	For 32PTH Canister	For 24PTH Canister [13]
A	34.88"	33.60"

TN drawing No. 10494-72-108

HSM-H		
Dimension	System Type	
	For 32PTH Canister	For 24PTH Canister [13]
A	8' – 1 1/2"	7' – 10"
B	Ø 7' – 3"	Ø 6' – 11 1/2"
C	Ø 5' – 8 5/8"	Ø 5' – 6"
D	Ø 7' – 7 1/4"	Ø 7' – 3 3/4"
E	Ø 1' – 10 1/2"	Ø 1' – 10 1/2"

3.9.9.3 Material Properties

The temperature dependent material properties for concrete and reinforcing steel are provided in Chapter 3, Tables 3-6, 3-7 and 3-7A. The material properties of the Type 304 Stainless Steel rails are identical to the ASME Code properties listed in Chapter 3, Table 3-5.

3.9.9.4 Component Weights

The following table summarizes the weight of the loaded HSM-H.

Component Description	CALCULATED WEIGHT (kips)
32PTH DSC Empty Weight	58.04
32 PWR Spent Fuel Assemblies	50.72
Total Loaded DSC Weight (Dry)	**108.76**
HSM-H Single Module Weight (Empty)	306.1
HSM-H Single Module Weight (Loaded)	**414.86**

3.9.9.5 Design Criteria

Codes and Standards

The reinforced concrete HSM-H, including the 32PTH-DSC support structures, are important to safety NUHOMS® HD system components. Consequently, they are designed and analyzed to perform their intended functions under the extreme environmental and natural phenomena specified in 10CFR 72.122 [1] and ANSI 57.9 [2]. These include tornado, wind, seismic, and flood design criteria.

The following table summarizes Codes and Standards for design and fabrication of these components.

Component	Code of Construction
HSM-H and 32PTH DSC Support Structures	- ACI 349-97 (Concrete); ACI 308-97 (construction) - AISC Ninth Edition (Structural Steel) - AWS D1.1-98 (Structural Welds) - ASCE 7-95 (Loads) - ANSI 57.9-84 (Loads & Load Combinations)

Loadings

The loadings are listed in Tables 3.9.9-1 & 3.9.9-2 and discussed in details in Section 3.9.9.6.

Loading Criteria

The ultimate strength method of ACI 349 [3] is used for the design of the HSM-H reinforced concrete structural components. Required reinforcement is provided to meet the minimum flexural and shear reinforcement requirements of ACI 349 and to ensure that the provided design strength exceeds that required for the factored design loads specified in Table 3.9.9-3.

The following relationships from the ACI code are used to compute capacities of the concrete components:

Ultimate Moment Capacity (M_u)

$$M_u = \phi M_n = \phi A_s f_y (d-a/2)$$

where $a = (A_s f_y)/(0.85 f_c' b)$

Ultimate Tension Capacity (P_{tu})

$P_{tu} = \phi A_{st} f_y$

$\phi = 0.9$

$A_{st} = 2A_s$ (The reinforcement in two opposite faces are assumed to be same)

Ultimate Compression Capacity (P_{cu})

$P_{cu} = \phi P_n = 0.8\phi[0.85 f_c' (A_g - A_{st}) + f_y A_{st}]$

$A_{st} = 2A_s, \quad \phi = 0.7$

Ultimate In-Plane Shear Capacity (V_{ui})

$V_{ui} = \phi A_g (2\sqrt{f_c'} + \rho_n f_y)$

$\phi = 0.85$, $\rho_n = (2A_s/bT)$

Ultimate Out-Plane Shear Capacity (V_{uo})

$V_{uo} = \phi 2 \sqrt{f_c'} (bd)$

$\phi = 0.85$

where:

ϕ = Strength reduction factor

A_s = Area of reinforcing steel in tension

A_{st} = Total area of the reinforcing steel

A_g = Gross area of concrete section

fy = Yield strength of reinforcing steel

f_c' = Compressive strength of concrete

d = Distance of the top fiber of concrete from the center of the rebar

b = Width of the section = 12"

T = Depth of the section

The computed shear and moment capacities for all the concrete components of the HSM-H, calculated based on the preceding equations from ACI 349 [3] are provided in Table 3.9.9-4.

The capacities calculated in Table 3.9.9-4 for the accident condition consider a 10% reduction in compressive strength of the concrete and yield strength of the reinforcing rebar materials due to concrete temperatures exceeding 350°F.

The required steel strength, S, and required shear strength, S_v for critical sections of steel structure are calculated in accordance with the requirements of AISC Allowable Stress Design (ASD) method [4].

In addition to deadweight and normal and off normal handling loads, the steel support structure components are subjected to the normal operating thermal loads (TN), off-normal operating thermal loads (TO) and accident thermal loads (TA), which cause additional stresses. However, the steel support structure is protected from design wind load (WW), Tornado wind and missile impact loads (WT) and Flood loads (FL) by the concrete components of the HSM-H. Therefore, these loads do not cause stresses in the steel support structure.

The corresponding structural design criteria for the DSC support structure are summarized in Table 3.9.9-5 and 3.9.9-6.

3.9.9.6 Load Cases

3.9.9.6.1 HSM-H Normal Loads (*Section P.2.2.5.2.1 from CoC 1004 Amendment #8)*

(A) Dead Loads (DW)

Dead load includes the weight of the HSM-H concrete structure and the steel structure (the DSC weight is considered as a live load rather than a dead load).

The dead load is varied by +5% from the estimated value to simulate the most adverse loading condition in accordance with ANSI-57.9 [2].

(B) Live Loads (LL)

Live loads include the roof design basis snow and ice load of 110 psf conservatively derived from ASCE 7-95 [5]. A total live load of 200 psf (which includes snow and ice load) is used to envelope all postulated live loading, including such items as ladders, handrails, conduits, etc. added for personnel protection. In addition, the normal handling loads (RO), and off-normal handling loads (RA), and the DSC weight are treated as live loads for the concrete component evaluation.

In accordance with ANSI-57.9 [2], the live load is varied between 0% and 100% of the estimated load to simulate the most adverse conditions for the structure.

(C) Normal Operating Thermal Loads (TN)

The normal thermal loads on HSM-H include the effects of design basis internal heat load (40.8 kW maximum heat load) generated by the canister plus the effects of normal ambient conditions (0°F and 100°F).

(D) Normal Handling Loads (RO)

The most significant normal operational loading condition for the HSM-H components is the sliding of the DSC from the TC into the HSM-H. Friction forces are developed between the sliding surfaces of the DSC, the TC and the HSM-H support rails. Normal operation assumes the canister is sliding over the support structure due to a hydraulic ram force of up to 80,000 lbs (insertion) and 60,000 lbs (extraction) applied to the DSC base. It is assumed that the 80 or 60 kips load is resisted by an axial load (40 or 30 kips) in each support rail and front embedments. In addition the DSC weight is applied as a distributed load on both the rails. The normal handling loads are considered as live loads for the design of the concrete components.

(E) Design Basis Wind Load (WW)

Conservatively, this load case is assumed to be enveloped by tornado generated wind load (WT) described in Section 3.9.9.6.3.

3.9.9.6.2 HSM-H Off-Normal Loads (*Section P.2.2.5.2.2 from CoC 1004 Amendment #8)*

(A) Off-Normal Operating Thermal Loads (TO)

This load case is the same as the normal thermal load but with an ambient temperature range from -40°F to 117°F. The temperature distribution for the extreme ambient conditions is used in the analysis for the concrete and steel component evaluation.

(B) Off-Normal Handling Loads (RA)

This load case assumes that the TC is not accurately aligned with respect to the HSM-H resulting in binding of the DSC during a transfer operation causing the hydraulic pressure in the ram to increase. The ram force is limited to a maximum load of 80 kips during insertion and 80 kips during retrieval. Therefore, for the steel support structure, the off-normal jammed canister load (RA) is defined as an axial load on one rail of 80 kips during insertion and 80 kips during retrieval, plus a vertical load of one half the DSC weight (on both rails) at the most critical location. The off-normal operating handling loads are considered as live loads for the design of the concrete components.

3.9.9.6.3 HSM-H Accident Loads (*Section P.2.2.5.2.3 from CoC 1004 Amendment #8)*

(A) Accident Thermal Loads (TA)

The postulated accident thermal event occurs due to blockage of either the air inlet or outlet vents under off-normal ambient temperatures range from –40°F to 117°F.

(B) Tornado Wind and Tornado Missiles (WT, WM)

The design basis tornado (DBT) wind intensities used for the HSM-H design are obtained from NRC Regulatory Guide 1.76 [6]. Region I intensities are utilized since they result in the most severe loading parameters. For this region, the maximum wind speed is 360 mph, the rotational speed is 290 mph and the maximum translational speed is 70 mph. The radius of the maximum rotational speed is 150 ft, the pressure drop across the tornado is 3 psi and the rate of pressure drop is 2 psi per second [6].

Determination of Forces on Structure

Tornado loads are generated for three separate loading phenomena:

- Pressure or suction forces created by drag as air impinges and flows past the HSM-H. These pressure or suction forces are due to tornado generated wind with maximum wind speed of 360 mph.
- Pressure or suction forces created by tornado generated pressure drop or differential pressure load of 3 psi.
- Impact, penetration and spalling forces created by tornado-generated missiles impacting on the HSM-H.

The DBT velocity pressure is computed based on the following equation specified in ASCE 7-95 [5].

$$q_v = 0.00256\ K_z * K_{zt} * I * V^2 \text{ lb/sq ft}$$

Where:

K_z = velocity pressure exposure coefficient equal to 0.9 applied to the full HSM-H height of 18.5 ft for level C exposure (Table 6-3 of [5]).

K_{zt} = 1.0 for level C exposure and structures with height less than 30 ft. (Section 6.5.5 of [5]).

I = Importance Factor equal to 1.15 (Table 6-2 of [5]).
Since the generic design basis HSM-H dimensions are relatively small compared to 150 ft rotational radius of the DBT, the velocity value of combined rotational and translational wind velocity of 360 mph is conservatively used in the above equation to compute the DBT velocity pressure of 344 psf.

The design pressures for the tornado wind load are shown in Table 3.9.9-7.

Tornado Missiles

The determination of impact forces created by DBT generated missiles for the HSM-H is based on the criteria provided by NUREG-0800, Section 3.5.1.4, III.4 [7]. Accordingly, eight types of missiles are postulated:

1. The utility wooden pole, 13.5" diameter, 35' long missile weighing 1500 lbs at a horizontal velocity of 294 fps.
2. The armor piercing artillery shell 8" diameter, weighing 276 lbs at a horizontal velocity of 185 fps.
3. The steel pipe missile 12" diameter, Schedule 40, 30' long weighing 1500 lbs at a horizontal velocity of 205 fps.
4. The massive automobile missile weighing 4000 lbs at a horizontal velocity of 195 fps traveling through the air not more than 25 ft above the ground and having contact area of 20 square ft.
5. Wood plank missiles traveling end on, 200 lbs, traveling at 440 fps.
6. Steel Pipe 3" diameter, Sch 40, weighing 115 lbs, traveling at 268 fps.
7. Steel Pipe 6" diameter, Sch 40, 285 lbs, traveling at 230 fps.
8. Steel rod, 1" diameter, 3' long weighing 8 lbs traveling at 317 fps.

For the overall effects of a DBT missile impact, overturning and sliding of the HSM-H, the force due to the deformable massive missile impact is applied to the structure at the most adverse location. Conservation of momentum is assumed to demonstrate that sliding and/or tipping of the module will not result in an unacceptable condition for the module. The coefficient of restitution is assumed to be zero and the missile energy is transferred to the module to be dissipated as sliding friction, or an increase in potential energy due to raising the center of gravity. The force is evenly distributed over the impact area. The magnitude of the impact force for design of the local reinforcing is calculated in accordance with Bechtel Topical Report "Design of Structures for Missile Impact" [8].

For the local damage analysis of the HSM-H for DBT missiles, three governing missiles are used for the evaluation of concrete penetration, spalling, scabbing and perforation thickness. The modified National Defense Research Committee (NDRC) empirical formula is used for this evaluation as recommended in NUREG-0800, Section 3.5.3 [7]. The results of these evaluations are reported in Chapter 11.

(C) Flood Load (FL) *(Section P.2.2.2 from CoC 1004 Amendment #8)*

Flooding of the NUHOMS® ISFSI greater than 0.46 m (1'-6") above grade results in blockage of the HSM inlet vents. Flooding of the NUHOMS® ISFSI greater than 1.7 m (5'-8") above grade results in wetting of the DSC. Greater flood heights result in submersion of the DSC and blockage of the HSM outlet vents.

The DSC and HSM are conservatively designed for an enveloping design basis flood, postulated to result from natural phenomena such as a tsunami, and seiches, as specified by 10CFR72.122(b). For the purpose of this bounding generic evaluation, a 15 m (50 foot) flood height and water velocity of 4.6 m/sec (15 fps) is used. The HSM-H is evaluated for the effects of a water current of 4.6 m/sec (15 fps) impinging upon the side of a submerged HSM-H. The DSC is subjected to an external pressure equivalent to a 15 m (50 foot) head of water.

The calculated effects of the enveloping design basis flood are included in the load combinations and reported stresses presented in Section 3.9.9.10.3. The plant specific design basis flood (if the possibility for flooding exists at a particular ISFSI site) should be evaluated by the licensee and shown to be enveloped by the flooding conditions used for this generic evaluation of the NUHOMS® DSC and HSM-H.

(D) Seismic Load (EQ) *(Section P.2.2.3 from CoC 1004 Amendment #8)*

The design basis response spectra of NRC Regulatory Guide 1.60 [9] are selected as the design earthquake for qualifying different component of HSM-H. A damping value of seven percent of damping is used for the concrete structure [12]. The response spectra are anchored to a maximum ground acceleration of 0.3g for the horizontal component and 0.2g for the vertical component. The results of the frequency analysis of the HSM-H structure (which includes a simplified model of the DSC) yield a lowest frequency of 23.2 Hz in the transverse direction and 28.4 Hz in the longitudinal direction. The lowest vertical frequency exceeds 33 Hz. Thus, based on the R.G. 1.60 response spectra amplifications, the corresponding seismic accelerations used for the design of the HSM-H are 0.37g and 0.33g in the transverse and longitudinal directions respectively and 0.20g in the vertical direction. The corresponding accelerations applicable to the DSC are 0.41g and 0.36g in the transverse and longitudinal directions, respectively, and 0.20g in the vertical direction. The seismic analysis of the HSM-H is further discussed in Section 3.9.9.10.

3.9.9.6.4 Combined Load Criteria *(Section P.2.2.5 from CoC 1004 Amendment #8)*

A summary of the design loads for the HSM-H System is provided in Tables 3.9.9-1 and 3.9.9-2. These tables also present the applicable codes and standards for development of these loads. Table 3.9.9-3 and 3.9.9-6 summary the load combination requirements of the HSM-H module design. These tables comply with the requirements of 10CFR72.122, and ANSI 57.9.

3.9.9.7 Finite Element Model

3.9.9.7.1 ANSYS Finite Element Model of the Rail Assembly

Description of the Rail Assembly

The HSM-H support structure consists of two rail assemblies, each at 30 degrees from the vertical center line of the DSC. Four cross members connect the two rail assemblies (at the time they are shop fabricated) by four gusset plates welded to the rail web and the flanges. However, after the rail assemblies are installed at the ISFSI site, and before the DSC is loaded, the two outer most end cross members are removed. The steel support structure supports the DSC stored inside the module. Each rail assembly of the DSC support structure consists of the following components:

1. W 12x96 Rail Section 187" long made up off ASTM A992 material and with twelve (12) 6" diameter holes for airflow cooling of the DSC. The depth of the section is 12.71", thickness of the web is 0.55", width of the flange is 12.16" and thickness of the flange is 0.9" (Ref. 4).

2. A 1" thick slotted plate made up of A572 Grade 50 material with slots at angle of 30 degree to normal to the plate axis. The slot thickness range from 0.5" inside to 0.75" outside.

3. A 3/16" thick support plate made up of nitronic 60 (RC 29-35) material which provide a smooth support for the DSC to slide.

4. A rail extension flange which consists of 1" thick flange plate (A572, Grade 50 material), and 3/16" thick rail support extension plate (nitronic 60 material).

The rail extension flange is attached to a 1-1/4" thick embeded base plate (A36 material)by four bolts.

Finite Element Model of the Rail Assembly

A three dimensional finite element model of the rail section, slotted plate, rail support plate and rail extension flange was developed for the computer program ANSYS [10]. The rail flanges, slotted plate, rail support plate and extension flanges were modeled using SOLID 73 element. Each element has 8 nodes with six degrees of freedom (three translational and three rotational) per node. The web of the W section and the stiffeners were modeled using Shell 63 element. In order to establish compatability of the degrees of freedom between solid and plate elements, the ANSYS option for actvating realistic in-plane rotational stiffeness (Allman rotational stiffeness, KEYOPT(3)=2) is used for the plate elements. The model is inclined by 30 degrees from the vertical. A plot of the partial model (front end) is shown in Figure 3.9.9-1.

The model is completely restrained at the bottom end of the extension flange and supported vertically and transversely approximately 6" from the end to simulate the weld between the

extension flange and the base plate. The model also is supported in the vertical and transverse directions at approximately 12" on either side of the W section at the bottom flange (to simulate the simple support condition of the concrete pedestalls at the front and rear walls).

Finite element analysis of the above rail assembly model was performed to compute the maximum displacements of the model, subjected to unit load normal to rail axis in and out of plane of the curb and in the axial direction. The equivalent beam element properties such as area (A), moment of inertia about the major axis (I_{x-x}) and moment of inertia about the minor axis (I_{y-y}) are determined by equating the maximum deflection of the beam to displacement obtained from the finite element model.

3.9.9.7.2 ANSYS Finite Element Model of the HSM-H Combined Concrete and Steel Structure for Structural Analysis

The structural analysis of an individual module provides a conservative estimate of the response of the HSM-H structural elements under various static and dynamic loads for any HSM-H array configuration. Therefore, analytical models of a single free standing HSM-H is developed in this section for the computer program ANSYS [10]. The frame and shear wall action of the HSM-H concrete components are considered to be the primary structural system resisting the loads. The analytical models are evaluated for normal operating, off-normal and postulated accident loads acting on the HSM-H.

A three dimensional finite element model of the HSM-H which includes all the concrete components (rear wall, front wall, two side walls and the roof) was developed for the computer program ANSYS [10]. The eight node brick element type SOLID 73 element was used to model the concrete structure. Four layers of brick elements were used to model the concrete components. Each node of the eight node brick element has six degrees of freedom. The DSC was modeled using the beam elements (ANSYS element type BEAM4). The rails and the lateral bracing between the rails (Cross beams) were also modeled using beam elements with appropriate stiffness The mass of the DSC was lumped at the nodes representing the DSC using lumped mass elements (ANSYS element type MASS21). Plots of the model which includes the concrete structure and the support structure are shown in Figures 3.9.9-2. A plot of the support structure model (which includes the DSC, rails and the cross beams) is shown in Figure 3.9.9-3.

The material properties used in the DSC support structure model are provided in Chapter 3. The DSC support structure model is attached to the concrete at several locations (four locations at the rear shelf, four locations in the front shelf and two locations on the front wall opening. Each node of the support structure has three translational and three rotational degree of freedoms. The rails are supported such that they are completely restrained at the front extension plate locations and free to rotate in all three directions and free to translate only in axial direction at the other supports in the rear and the front shelf locations.

The DSC support structure analytical model is incorporated into the HSM-H analytical model. The various normal, off-normal and accident loads are applied to the analytical model and

internal forces and moments were computed in different members by performing a linear elastic finite element analysis.

The node coupling option of ANSYS was used to represent the appropriate connection between the different concrete components of the HSM-H model. The connections of the support structure to the concrete structure were modeled also using the node coupling option.

For the analysis performed in this calculation, due to applied loading, the model is assumed neither to uplift from the basemat (because of its dead weight) nor to slide on the basemat (because of friction). Therefore, the model is restrained vertically at all nodes on the bottom of the model, and also restrained laterally and axially at all nodes on the bottom of the model to prevent rigid body movement.

3.9.9.7.3 ANSYS Finite Element Model of the HSM-H for Thermal Stress Analysis

The thermal stress analysis of the HSM-H was performed using the three dimensional finite element model (developed for ANSYS) which includes the concrete and support steel components. The eight node brick elements of type SOLID73 were used to model the concrete structure. Four layers of brick elements were used to model the concrete components. Each node of the brick element has three translational and three rotational degrees of freedom. The connections between the HSM-H concrete structure and the door are designed such that free thermal growth is permitted in the door, when the HSM-H is subjected to thermal loads. Because of the free thermal growth, the door does not induce stresses in the concrete components of the HSM-H. Therefore, the analytical model of the HSM-H for thermal stress analysis of the concrete components does not include the door. The ANSYS model used to perform thermal stress analysis of the concrete and support steel components is shown in Figures 3.9.9-4. Conservatively, the roof and the base unit are coupled in this model. However, the DSC beam model is uncoupled from the support steel beam model.

The model base is restrained at one set of end nodes (in axial and lateral directions) and friction forces are applied in the axial and lateral directions at the opposite set of end nodes. For the thermal load analysis all the nodes at the base are restrained in the vertical direction.

3.9.9.8 Normal Operation Structural Evaluation

The evaluation of the HSM-H for 32PTH DSC is the same as the HSM-H which is under NRC review as Amendment 8 to CoC 1004 for 24PTH DSC [13]. Analyses performed for HSM-H with 24PTH DSC used bounding values to envelop both 24PTH DSC and 32PTH DSC. Following table shows how the bounding loads are used for structural evaluation of the HSM-H.

	Weight	Thermal
24PTH DSC (loaded weight)	93.7 kips	40.8 kw
32PTH DSC (loaded weight)	108.76 kips	34.8 kw
Weight used for HSM-H structural evaluation to envelop both 24PTH & 32PTH	110.0 kips (max.) (1) 72.0 kips (min.) (2)	
Thermal load used for HSM-H structural evaluation to envelop both 24PTH & 32PTH		40.8 kw

Notes:
1. Maximum weight is used for structural evaluation of the HSM-H.
2. Minimum weight is used for stability evaluation of the HSM-H.

The following table shows the normal operating loads for which the HSM-H components are designed. The table also lists the individual NUHOMS® HSM-H components which are affected by each loading.

Load Type	Affected Component	
	DSC Support Structure	HSM-H
Dead Weight	X	X
Normal Thermal	X	X
Normal Handling	X	X
Live Loads		X

The reinforced concrete and the support steel structure of the HSM-H are analyzed for the normal, off-normal, and postulated accident conditions using finite element models described in Section 3.9.9.7. These models are used to evaluate concrete and support structure forces and moments due to dead load, live load, normal thermal loads, and normal handling loads. The methodology used to evaluate the effects of these normal loads is addressed in the following paragraphs.

(A) HSM-H Dead Load (DW) Analysis (Section P.3.6.1.4(A) from CoC 1004 Amendment #8)

Dead loads are applied to the analytical model by application of 1.05g where g is the gravitational acceleration in the vertical direction (386.4 in/sec^2). The 5% variation in the dead

load is in accordance with ANSI/ANS 57.9. The results of the HSM-H concrete components dead load analysis are presented in Table 3.9.9-8.

(A) HSM-H Live load (LL) Analysis (Section P.3.6.1.4(B) from CoC 1004 Amendment #8)

Live load analysis is performed by applying 200 psf pressure on the roof and the DSC weight as a distributed load on the support structure. The normal handling load of 80 kips during DSC insertion and 60 kips during DSC retrieval is included as a live load for the concrete component evaluation. The results of the HSM-H concrete components live load analysis are presented in Table 3.9.9-8.

(B) HSM-H Normal Operating Thermal (TN) Stress Analysis *(Section P.3.6.1.4(C) from CoC 1004 Amendment #8)*

Normal operating thermal stress analysis of the concrete and steel support structure is performed for the enveloping thermal load case which is 40.8 kW heat load with ambient temperature of 100°F. An additional thermal load case with -40°F ambient and 40.8 kW heat load is also considered as a bounding case for the end module in an array of HSM-H. The thermal tests of the HSM-H documented in [15] showed that the HSM-H thermal analysis methodology as described in Chapter 4 conservatively predicts HSM-H component temperatures. The HSM-H thermal stress analysis was performed using thermal profiles and maximum temperatures that bounds those reported in Chapter 4. The results of the HSM-H concrete components thermal load analysis are presented in Table 3.9.9-9.

(C) HSM-H Operational Handling Load (RO) Analysis (Section P.3.6.1.4(D) from CoC 1004 Amendment #8)

The operation handling loads of 80 kips during DSC insertion and 60 kips during DSC retrieval are applied to the rail support structure in the axial direction. In addition, the DSC weight is applied as a distributed load on both rails of the HSM-H.

The normal operating handling loads are considered as live loads for the design of the concrete components. The results of the HSM-H concrete components operational handling load analysis are presented in Table 3.9.9-8.

(D) HSM-H Design Basis Wind Load (WW) Analysis (Section P.3.6.1.4(E) from CoC 1004 Amendment #8)

The DSC support structure and DSC inside the HSM-H are not affected by wind load. The concrete structure forces and moments due to design basis wind load are bounded by the result of tornado generated wind load discussed in Section 3.9.9.10. Therefore, no separate analysis is performed for this case.

The results of the HSM-H concrete components design basis wind load analysis are presented in Table 3.9.9-8.

3.9.9.9 OFF-Normal Operation Structural Analysis

This section describes the design basis off-normal events for the HSM-H modules and presents analyses which demonstrate the adequacy of the design safety features of the HSM-H modules.

The following table shows the off-normal operating loads for which the HSM-H components are designed.

Load Type	Affected Component	
	DSC Support Structure	HSM-H
Off-Normal Thermal	X	X
Off-Normal Handling	X	X

For an operating NUHOMS® HD system, off-normal events could occur during fuel loading, transfer cask handling, trailer towing, canister transfer and other operational events. Two off-normal events are defined which bound the range of off-normal conditions. The limiting off-normal events are defined as a jammed DSC during loading or unloading from the HSM-H and the extreme ambient temperatures of -40°F (winter) and +117°F (summer). These events envelope the range of expected off-normal structural loads and temperatures acting on the HSM-H. ANSYS finite element models described in Section 3.9.9.7 are used to evaluate concrete and support structure forces and moments due to these loads.

(A) HSM-H Off-Normal Thermal Loads (TO) Analysis (*Section P.3.6.2.3 (A) from CoC 1004 Amendment #8)*

This load case is the same as the normal thermal load but with an ambient temperature range from -40°F to 117°F. The temperature distributions for the extreme ambient conditions are used in the analysis for the concrete component evaluation. The results of the HSM-H concrete components thermal load analysis are presented in Table 3.9.9-9.

(B) HSM-H Off-Normal Handling Loads (RA) Analysis (*Section P.3.6.2.3 (B) from CoC 1004 Amendment #8)*

This load case assumes that the transfer cask is not accurately aligned with respect to the HSM-H resulting in binding of the DSC during a transfer operation causing the hydraulic pressure in the ram to increase. The ram force is limited to a maximum load of 80 kips during insertion and 80 kips during retrieval. Therefore, for the steel support structure, the off-normal jammed canister load (RA) is defined as an axial load on one rail of 80 kips during insertion and 80 kips during retrieval, plus a vertical load of one half the DSC weight (on both rails) at the most critical

location. The off-normal operating handling loads are considered as live loads for the design of the concrete components.

The results of the HSM-H concrete components for off-normal load analysis are presented in Table 3.9.9-8.

3.9.9.10 Accident Condition Structural Analysis

The design basis accident events specified by ANSI/ANS 57.9-1984, and other credible accidents postulated to affect the normal safe operation of the NUHOMS® HSM-H are addressed in this section.

In the following sections, each accident condition is analyzed to demonstrate that the requirements of 10CFR72.122 are met and that adequate safety margins exist for the HSM-H design. The resulting accident condition stresses in the HSM-H components are evaluated and compared with the applicable code limits set forth in Section 3.9.9.5. Load combination results for the HSM-H are presented in Section 3.9.9.11. The postulated accident conditions addressed in this section include:

- Tornado winds and tornado generated missiles (WT, WM)
- Design basis earthquake (EQ)
- Design basis flood (FL)
- Block Vent Thermal (TA)

ANSYS finite element models described in Section 3.9.9.7 are used to evaluate concrete and support structure forces and moments due to these loads.

3.9.9.10.1 Tornado Winds/Tornado Missile (WT, WM) (Section P.3.7.1 from CoC 1004 Amendment #8)

Stability and stress analyses are performed to determine the response of the HSM-H to tornado wind pressure loads. The stability analyses are performed using manual calculation methods to determine sliding and overturning response of the HSM-H array. A single HSM-H with both the end and the rear shield walls is conservatively selected for the analyses. The stress analyses are performed using the ANSYS finite element model of a single HSM-H to determine design forces and moments. These conservative generic analyses envelop the effects of wind pressures on the HSM-H array. Thus, the requirements of 10CFR 72.122 are met.
In addition, the HSM-H is evaluated for tornado missiles.

Effect of DBT Wind Pressure Loads on HSM-H

The HSM-H is qualified for maximum DBT generated design wind loads of 234 lb/ft^2 and 148 lb/ft^2 on the windward and leeward HSM-H walls (Table 3.9.9-7), respectively and a pressure drop of 3 psi.

A single stand-alone HSM-H is protected by shield walls on either side and at the rear. For an HSM-H array, the critical module is on the windward end of the array. This module has an end shield wall to protect the module from tornado missile impacts. The shield wall is also subjected to the 234 lb/ft^2 windward pressure load. The leeward side of the same end module in the array

has no appreciable suction load due to the presence of the adjacent module. The 148 lb/ft^2 suction load is applicable to the end shield wall on the opposite end module in the array. A suction of 207 lb/ft^2 is also applied to the roof of each HSM-H in the array.

For the stress analyses, the DBT wind pressures are applied to the HSM-H as uniformly distributed loads. The rigidity of the HSM-H in the transverse direction, due to frame and shear wall action of the HSM-H, is the primary load transfer mechanism assumed in the analysis. The bending moments and shear forces at critical locations in the HSM-H concrete components are calculated by performing an analysis using the ANSYS analytical model of the HSM-H. The resulting moments and shear forces are shown in Table 3.9.9-10 and are included in the HSM-H load combination results reported in Section 3.9.9.11.

For conservatism, the design basis operating wind pressure loads are assumed to be equal to those calculated for the DBT in the formulation of HSM-H load combination results.

A stability analysis is performed to evaluate the effects of overturning and sliding due to the postulated DBT. A single, freestanding HSM-H with end shield walls and rear shield wall is used for this analysis.

The pressure drop has no effect on the HSM-H, since the HSM-H is an open structure, due to the presence of the inlet and outlet vents.

HSM-H Overturning Analysis *(Section P.3.7.1.1.1 from CoC 1004 Amendment #8)*

For the DBT wind overturning analysis, the overturning moment and the resulting stabilizing moments are calculated.

A lower bound estimate of the stabilizing moment (M_{st}) for the windward module is:

M_{st} = Wd = 18,824 k-in.

Where:
- W = 362 K, [Lower bound weight of HSM-H (290 kips) + Lowest envelope of any DSC weight (72 kips)]
- d = 52 in., Horizontal distance between center of gravity of HSM-H to the outer edge of the module.

and the overturning moment (M_{ot}) for the windward module due to DBT wind pressure is:

M_{ot} = $[(W_1) A_w h/2 + W_3 A_r d]12$

Where:
- W_1 = 0.148 K/ft.^{2}, Wind load, leeward wall
- h = 18.5 ft, Wall height
- W_3 = 0.207 K/ft.^{2}, Wind uplift on roof
- A_r = 199.9 ft.^{2}, Roof area
- A_w = 382.4 ft.^{2}, Wall area
- d = 4.34 ft., Half of the transverse dimension of the roof

Therefore: M_{ot} = 8437.0 K-in.

Because the overturning moment is smaller than the stabilizing moment, the freestanding HSM-H will not overturn. The resulting factor of safety against overturning effects for the DBT wind loads is > 2.23.

HSM-H Sliding Analysis *(Section P.3.7.1.1.2 from CoC 1004 Amendment #8)*

To evaluate the potential for sliding of a single, freestanding HSM-H, the sliding force generated by the postulated DBT wind pressure is compared to the sliding resistance provided by friction between the base of the HSM-H and the ISFSI basemat.

The force (F_{sl}) required to slide the end module in an array is:

$$F_{sl} = [W - W_3 A_r]\mu$$

Where: μ = 0.6, coefficient of friction
W, W_3 and A_r are defined above.

Substituting gives:

$$F_{sl} = 192.4 \text{ K}$$

The sliding force (F_{hw}) generated by DBT wind pressure for a single HSM-H is:

$$F_{hw} = (W_1 + W_2) A_W$$

Where: W_2 = 0.234 k/ft^2 wind load, windward wall
W_1, and A_w are as defined above.

Substituting gives:

$$F_{hw} = 146.1 \text{ K}$$

Because the horizontal force generated by the postulated DBT is smaller than the force required to slide the end module in an HSM-H array, the HSM-H will not slide. The factor of safety against sliding of the HSM-H due to DBT wind loads is 1.32.

3.9.9.10.2 Earthquake (Seismic) *(Section P.3.7.2 from CoC 1004 Amendment #8)*

The peak horizontal ground acceleration of 0.30g and the peak vertical ground acceleration of 0.20g are utilized for the design basis seismic analysis of the HSM-H components.
Based on NRC Reg. Guide 1.61 [12], a damping value of three (3) percent is used for the DSC seismic analysis. Similarly, a damping value of seven (7) percent for DSC support steel and concrete is utilized for the HSM-H. An evaluation of the frequency content of the loaded HSM-H is performed to determine the amplified accelerations associated with the design basis seismic response spectra for the NUHOMS® HSM-H and DSC.

HSM-H Seismic Evaluation (*Section P.3.7.2.3 from CoC 1004 Amendment #8)*

Seismic Loads (EQ)

As described in Section 3.9.9.6.3, the design basis accelerations for the HSM-H are 0.3g in the horizontal directions and 0.2g in the vertical direction. These seismic accelerations are amplified based on the results of the frequency analysis of the HSM-H, as documented in Section 3.9.9.6.3. The resulting amplified accelerations are 0.37g and 0.33g in the transverse and longitudinal directions, respectively and 0.20g in the vertical direction. For conservatism, a value of 0.37g is used for both horizontal directions in the seismic analysis of the HSM-H.

Seismic Stress Analysis

An equivalent static analysis of the HSM-H is performed using the ANSYS model described in Section 3.9.9.7 and the seismic accelerations of 0.37g horizontally (longitudinal and transverse directions) and 0.2g vertically. These amplified accelerations are determined based on the frequency analysis of the HSM-H.

The responses for each orthogonal direction are combined using the SRSS method.
The seismic analysis results are shown in Table 3.9.9-10 and are incorporated in the loading combination C4C (Table 3.9.9-3) and C4S (Table 3.9.9-6) for the concrete and support structure components, respectively.

HSM-H Seismic Overturning Analysis

The following conservative analysis is performed to show that a single freestanding HSM-H with an end shield wall (in an array of two or more loaded modules) will not overturn due to seismic loads. Overturning about the long axis (i.e., in the short direction of the module) is considered.

Stabilizing moment = $M_{st} = (W_{hsm} + W_{dsc})\ b/2$
Overturning moment = $M_{ot} = (W_{hsm}\ 0.4a_{v1}+W_{dsc}0.4a_{v2})b/2+W_{hsm}\ d_1a_{h1}+W_{dsc}d_2a_{h2}$
(100% of horizontal acceleration is combined with 40% of vertical acceleration, Ref. [11])

Where:

W_{hsm}	=	310 K, Weight of the HSM-H (conservatively assumed)
W_{dSC}	=	110 K, Weight of DSC (conservatively assumed)
b/2	=	52 in, Horizontal distance from CG to corner(half width of the HSM-H)
d_1	=	123.45 in, Height of CG of HSM-H without the DSC
d_2	=	106 in, Height of the DSC center line
a_{v1}	=	0.20g, HSM-H peak vertical seismic acceleration
a_{v2}	=	0.20g, DSC peak vertical seismic acceleration
a_{h1}	=	0.37g, HSM-H peak horizontal seismic acceleration
a_{h2}	=	0.43g, DSC peak horizontal seismic acceleration (conservatively assumed)
M_{st}	=	21,840 K-in
M_{ot}	=	20,921 K-in

Because stabilizing moment is greater than the overturning moment the HSM-H will not overturn during the seismic event.

HSM-H Seismic Sliding Analysis

The friction force resisting sliding = $F_{st} = W_{hsm}(1-0.4*a_{v1})+W_{dsc}(1-0.4*a_{v2})]\mu$

The applied horizontal seismic force = $F_{hs} = [W_{hsm}a_{h1}+W_{dsc}a_{h2}]$

Where: μ = coefficient of friction between concrete HSM-H base on concrete basemat = 0.6.

W_{hsm}, W_{dsc}, a_{v1}, a_{v2}, a_{h1}, a_{h2} are defined above.

F_{st} = 231.8K
F_{hs} = 162.0K

The force required to slide the HSM-H is larger than the resulting lateral seismic force and therefore, the loaded HSM-H will not slide.

3.9.9.10.3 Flood Load (FL) *(Section P.3.7.3 from CoC 1004 Amendment #8)*

Since the source of flooding is site specific, the exact source, or quantity of flood water, should be established by the licensee. However, for this generic evaluation of the HSM-H, bounding flooding conditions are specified that envelop those that are postulated for most plant sites. As described in Section 3.9.9.6.3, the design basis flooding load is specified as a 50 foot static head of water and a maximum flow velocity of 15 feet per second. Each licensee should confirm that this represents a bounding design basis for their specific ISFSI site.

HSM-H Flooding Analysis

Because the HSM-H is open to the atmosphere, static differential pressure due to flooding is not a design load.

The maximum drag force, F, acting on the HSM-H due to a 15 fps flood water velocity is calculated as follows:

Where:

F	=	$(v^2/2g)\ C_D\ A\ \rho_\omega$ [14]
v	=	15 fps, Flood water velocity
C_D	=	2.0, Drag coefficient for flat plate
A	=	18.5 ft^2/ft, HSM-H area per foot length
ρ_w	=	62.4 $lb./ft.^3$, Flood water density
F	=	Drag force (lb.)

$g = 32.2\ ft./s^2$ = Acceleration due to gravity

The resulting flood induced load is: F = 8.07 K/ft.

The following four flood load cases are considered:

Case 1: Flood water flow from front of HSM-H to rear of HSM-H
Case 2: Flood water flow from rear of HSM-H to front of HSM-H
Case 3: Flood water flow from left side of HSM-H to right side
Case 4: Flood water flow from right side of HSM-H to left side

Flood water flow from front of HSM-H to rear or rear of HSM-H to front (Cases 1 and 2)

Front/Rear wall, F_w = 8070*9' 8" = 78010 lbs
Conservatively, the total drag load on the front concrete components of the HSM-H is applied as a normal pressure load of magnitude (78010)/(18'6"*9'8"*144) = 3.1 psi.

Flood water flow in left side of HSM-H to right side or right side of HSM-H to left (Cases 3 and 4)

Side walls, F_w = 8070*20'8" = 166780 lbs

Conservatively, the total drag load on the left side concrete components of the HSM-H is applied as a normal pressure load of magnitude (166780)/(18'6"*20'8"*144) = 3.1 psi.

ANSYS finite element model described in Section 3.9.9.7 is used for the structural evaluation. The results for flood load case are obtained by enveloping results from above 4 load cases and shown on Table 3.9.9-10.

HSM-H Overturning Analysis

The factor of safety against overturning for the postulated flooding conditions is calculated using the stabilizing moment for a single HSM-H (with shield walls included) by summing moments about the bottom outside corner of a free-standing HSM-H. A net weight of 253.7 kips for a loaded HSM-H plus 100.4 kips for the upstream end shield wall, including buoyancy effects, is used to calculate the stabilizing moment that resists the overturning moment applied to the HSM-H by the flood water drag force. The stabilizing moment is:

$$M_{st} = 253.7 \times 52 + 100.4 \times 18$$

$$= 15{,}000 \text{ K-in.}$$

The maximum drag force due to the postulated water current velocity of 15 fps is 8.07 k/ft (see calculation above). The overturning moment due to the postulated flood current is based on drag

forces acting on a minimum of two modules in an array. The overturning moment is estimated as:

$$M_{ot} = 0.5 \times 8.07 \text{ K/ft.} \times 20.67 \text{ ft.} \times (18.5 \times 12/2)$$

$$= 9{,}258 \text{ K-in.}$$

The factor of safety (F.S.) against overturning for a freestanding HSM-H due to the postulated design basis flood water velocity is given by:

F.S. = 15,000 / 9,258 = 1.62

Therefore, a minimum of two (2) HSM-Hs adjacent to each other are required to prevent overturning.

HSM-H Sliding Analysis

The factor of safety against sliding of a freestanding HSM-H due to the maximum postulated flood water velocity of 15 fps is calculated using methods similar to those described above. The effective weight of the HSM-H including the DSC and end shield wall acting vertically downward, less the effects of buoyancy acting vertically upward is 354 K. The friction force resisting sliding of the HSM-H is equal to the product of the net weight of the HSM-H and the DSC and the coefficient of friction for concrete placed against another concrete surface such as that between the HSM-H and basemat, which is 0.6 [3]. Therefore, the force resisting sliding of the HSM-H is 0.6 x 354 or 212.5 kips. The drag force acting on a HSM-H (considering a minimum of two modules in an array) is 0.5 x 8.07 kips/ft x 20.67 = 83.4 kips total acting on the side wall of a single HSM-H, due to a flood velocity of 15 fps. The resulting factor of safety against sliding of a free standing HSM-H due to the design basis flood water velocity is 2.55. Therefore, a minimum of two (2) HSM-Hs adjacent to each other are required to prevent sliding.

3.9.9.10.4 Blocked Vent Thermal (TA) *(Section P.3.7.6 from CoC 1004 Amendment #8)*

This accident conservatively postulates the complete blockage of the HSM-H ventilation air inlet and outlet openings on the HSM-H side walls.

Since the NUHOMS® HSM-Hs are located outdoors; there is a remote probability that the ventilation air inlet and outlet vent openings could become blocked by debris. The NUHOMS® design features such as the perimeter security fence and the redundant protected location of the air inlet and outlet vent openings and the screens reduces the probability of occurrence of such an accident. Nevertheless, for this conservative generic analysis, such an accident is postulated to occur and is analyzed.

The postulated accident thermal event occurs due to blockage of either the air inlet or outlet vents under off-normal ambient temperatures range from –40°F to 117°F. The results of the HSM-H concrete components blockage thermal load analysis are presented in Table 3.9.9-9.

3.9.9.11 Load Combination

Concrete Components

To determine the required strength (internal axial forces, shear forces, and bending moments) for each HSM-H concrete component, linear elastic finite element analyses are performed for the normal, off-normal, and accident loads using the analytical models described in Section 3.9.9.7 for mechanical and thermal loads.

The individual load analysis results of the HSM-H concrete structure are presented in Table 3.9.9-8, 9 and 3.9.9-10. The load combination results for each component are presented in Table 3.9.9-11 for the load combinations defined in Table 3.9.9-3. The notations for the components of forces and moments and the concrete component planes in which capacities are computed are shown in Figure 3.9.9-5. The HSM-H concrete components thermal stresses used in the load combination results, summarized in Table 3.9.9-11, are based on thermal results that bound those reported in Chapter 4. All load combination results are below the computed section capacities.

Support Steel Structure

The support rails, rail stiffener plates, extension plates and cross members of the DSC support structure, shown in Figure 3.9.9-6 are evaluated using the allowable stress design method of the AISC Manual of Steel Construction [4]. The load combination results for each of these components are provided in Table 3.9.9-12 to 14. The maximum temperature used in the stress analysis of the support steel bounds the maximum temperature reported in Chapter 4.

The support rail stress comparison results are presented in Table 3.9.9-15. The extension plate and cross member stress comparison results are presented in Table 3.9.9-16.

HSM-H Shield Door

The shield door is free to grow in the radial direction when subjected to thermal loads. Therefore, there will be no stresses in the door due to thermal growth. The dead weight, tornado wind, differential pressure and flood loads cause insignificant stresses in the door compared to stresses due to missile impact load. Therefore, the door is evaluated only for the missile impact load. The computed maximum ductility ratio for the door is less than 1 (compared to the allowable ductility of 20).

For the door anchorage, the controlling load is tornado generated differential pressure drop load. The maximum tensile force per bolt (four door attachment bolts), is 9.0 kips. This is less than the allowable of 10.8 kips. The concrete pull-out strength is conservatively estimated as 24 kips which is greater than the ultimate capacity of the four bolts, thus satisfying the ductility requirements of the ACI Code.

HSM-H Heat Shield

The top heat shield (louvers) consists of seven panels. Each panel has two stainless steel mounting bars. The aluminum louvers are mounted on the mounting bars. Each mounting bar is suspended from the roof by two threaded rods. The natural lateral frequency of a typical rod is conservatively estimated to be 9.0 Hz. The combined axial and bending stress in the hanger rods is 34.63 ksi. The allowable axial and bending stress is 84.3 ksi.

The side heat shields consists of three panels. Each panel is suspended from the roof by two threaded rods, and supported laterally and longitudinally by four rods. The maximum axial plus bending stress in the lateral and longitudinal support rods is 83.7 ksi. The allowable axial and bending stress is 84.3 ksi. The maximum temperature used in the stress analysis of the heat shields bounds the maximum temperatures reported in Chapter 4.

HSM-H Seismic Retainers

The seismic retainer consists of a capped tube steel embedment located within the bottom center of the round access opening of the HSM-H, and a tube steel retainer assembly that drops into the embedment cavity after DSC transfer is complete. The drop-in retainer extends approximately 4" above the rail to provide axial restraint of the DSC. The maximum seismically induced shear load in the retainer is 61 kips. The maximum shear stress in the retainer is 15.25 ksi. The allowable shear stress is 17.8 ksi.

3.9.9.12 Conclusions

The load categories associated with normal operating conditions, off-normal conditions and postulated accident conditions are described and analyzed in previous sections. The load combination results for HSM-H components important to safety are also presented. Comparison of the results with the corresponding design capacity shows that the design strength of the HSM-H is greater than the strength required for the most critical load combination.

3.9.9.13 References

1. Title 10, Code of Federal Regulations, Part 72 (10CFR72), "Licensing Requirements for the Storage of Spent Fuel in the Independent Spent Fuel Storage Installation," U.S. Nuclear Regulatory Commission, August 31, 1988.

2. ANSI/ANS 57.9-1984, "Design Criteria for an Independent Spent Fuel Storage Installation (Dry Storage Type)," American Nuclear Society.

3. "Code Requirements for Nuclear Safety Related Concrete Structures," ACI 349-97, American Concrete Institute, Detroit, MI.

4. "Manual of Steel Construction," American Institute of Steel Construction, Ninth Edition, 1990.

5. American Society of Civil Engineers, ASCE 7-95, "Minimum Design Loads for Buildings and Other Structures" (formerly ANSI A58.1).

6. "Design Basis Tornado for Nuclear Power Plants," Regulatory Guide 1.76, U.S. Atomic Energy Commission, April 1974.

7. "Missiles Generated by Natural Phenomenon," Standard Review Plan, NUREG-0800, U.S. Nuclear Regulatory Commission

8. Bechtel Topical Report, "Design of Structures for Missile Impact," BC-TOP-9-A, Revision 2, September 1974.

9. Regulatory Guide 1.60, "Design Response Spectra for Seismic Design of Nuclear Power Plants," U.S. Atomic Energy Commission, Revision 1, December 1973.

10. ANSYS Engineering Analysis System, Users Manual for ANSYS Rev. 5.6 and 7.0, Swanson Analysis Systems, Inc., Houston, PA.

11. "Structural Analysis and Design of Nuclear Plant Facilities," ASCE Publication No. 58.

12. Regulatory Guide 1.61, "Damping Values for Seismic Design of Nuclear Power Plants", U.S. Atomic Energy Commission, October 1973.

13. Amendment No. 8 to NUHOMS® CoC 1004, addition of 24PTH DSC to Standardized NUHOMS® System.

14. "Fluid Mechanics", Raymond C. Binder, 4th Edition, Prentice-Hall, Inc.

15. "Thermal testing of the NUHOMS® Horizontal Storage Module, Model HSM-H", Transnuclear Report No. E-21625,Rev 1

Table 3.9.9-1
Summary of HSM-H Component Design Loadings

Component	Design Load Type	Design Parameters	Applicable Codes
HSM-H Module	Dead Load (DW)	150 pcf concrete structure and weight of support steel structure	ANSI 57.9-1984 [2]
	Live Load (LL)	200 psf (including snow and ice load) on the roof DSC weight (110 kips)	ANSI-57.9-1984 [2] ASCE 7-95 [5]
	Normal Operating Temperature (TN) Off-Normal Operating Temperature (TO)	Normal: Ambient air temperature 0°F -100°F Off Normal: Ambient air temperature -40°F to 117°F	ANSI 57.9-1984 [2]
	Normal Handling Loads (RO)	Hydraulic ram load of 80,000 lb.(DSC HSM insertion) 60,000 lb (DSC HSM extraction) on the rails	ANSI 57.9-1984 [2]
	Design Basis Wind Load (WW)	Conservatively assumed to be same as tornado generated wind load.	ASCE 7-95 [5]
	Off-Normal Handling Loads (RA)	Hydraulic ram load of: 80,000 lb (DSC insertion) 80,000 lb (DSC extraction) on each rail, one rail at a time.	ANSI-57.9-1984 [2]
	Accident Temperature (TA)	Ambient air temperature of –40°F and 117°F with inlet and outlet vents blocked.	10CFR72.122(n) [1]
	Tornado Wind Load (WT)	Maximum wind speed of 360 mph and a pressure drop of 3 psi	ASCE 7-95 [5] NRC Regulatory Guide 1.76 [6]
	Tornado Missile Load (WM)	See Section T.2.2.1.3 for missiles considered.	NUREG-0800 Section 3.5.1.4 [7]
	Flood (FL)	Maximum water height: 50 ft. Maximum velocity of water 15'/sec.	10CFR72.122(b) [1]
	Seismic (EQ)	Horizontal ground acc: 0.30g Vertical ground acc.: 0.20g	NRC Reg. Guides 1.60 & 1.61 [9] and [12]

Table 3.9.9-2
Summary of 32PTH DSC Support Structure Design Loadings

Component	Design Load Type	Design Parameters	Applicable Codes
32PTH DSC Support Structure	Live Load (LL)	DSC weight (110 kips)	ANSI-57.9-1984 [2]
	Normal Operating Temperature (TN) Off-Normal Operating Temperature (TO)	Normal: Ambient air temperature 0°F -100°F Off Normal: Ambient air temperature -40°F to 117°F	ANSI 57.9-1984 [2]
	Normal Handling Loads (RO)	Hydraulic ram load of 80,000 lb.(DSC insertion) 60,000 lb (DSC extraction) on the rails	ANSI 57.9-1984 [2]
	Off-Normal Handling Loads (RA)	Hydraulic ram load of: 80,000 lb (DSC insertion) 80,000 lb (DSC extraction) on each rail. One rail at a time.	ANSI-57.9-1984 [2]
	Accident Temperature (TA)	Ambient air temperature of –40°F and 117°F with inlet and outlet vents blocked.	10CFR72.122(n) [1]
	Seismic (EQ)	Horizontal ground acc: 0.30g Vertical ground acc.: 0.20g	NRC Reg. Guides 1.60 & 1.61 [9] and [12]

Table 3.9.9-3
HSM-H Concrete Load Combinations

Load Combination No.	Combination Identifier	Load Combination
C1C	COMB1C	U > 1.4*DW+1.7*(LL+RO)
C2C	COMB2C	U > 1.05*DW+1.275*(LL+TN+WW)
C3C	COMB3C	U > 1.05*DW + 1.275*(LL+TN+RA)
C4C	COMB4C	U > DW+LL+TN+EQ
C5C	COMB5C	U > DW+LL+TN+WT
C6C	COMB6C	U > DW+LL+TN+FL
C7C	COMB7C	U > DW+LL+MAX(TO and TA)

Note: For definition of individual load cases see Table 3.9.9-1

Table 3.9.9-4
Ultimate Capacities of Concrete Components

Component	Thermal Condition	V_{ui}(1) Kips/ft	V_{uo1}(1) Kips/ft	V_{uo2}(1) kips/ft	M_{u1}(1) Kip-in/ft	M_{u2}(1) kip-in/ft
Rear Wall (upper)	Normal	75.2	14.5	14.5	298.2	298.2
	Accident	69.6	13.8	13.8	273.8	273.8
Rear Wall (lower)	Normal	96.8	36.2	36.2	757.9	757.9
	Accident	90.1	34.3	34.3	696.3	696.3
Side Walls (upper)	Normal	55.4	14.8	14.8	196.9	196.9
	Accident	50.5	14.0	14.0	180.8	180.8
Side Walls (lower)	Normal	64.0	23.4	23.4	314.6	314.6
	Accident	58.7	22.2	22.2	289.0	289.0
Roof	Normal	177.6	59.1	59.1	2375.0	2375.0
	Accident	162.4	56.1	56.1	2181.7	2181.7
Front Wall (upper)	Normal	174.7	56.3	56.3	2257.3	2257.3
	Accident	159.6	53.4	53.4	2073.5	2073.5
Front Wall (lower)	Normal	192.1	73.6	73.6	2963.4	2963.4
	Accident	176.0	69.8	69.8	2722.4	2722.4

NOTES:

(1) V_{ui} = Minimum of ultimate in plane shear capacities in planes 1 and 2.

Vuo1 = Minimum Ultimate out of plane shear capacity in plane 1

Vuo2 = Minimum Ultimate out of plane shear capacity in plane 2

Mu1 = Minimum Ultimate moment capacity in plane 1

Mu2 = Minimum Ultimate moment capacity in plane 2

Table 3.9.9-5
Structural Design Criteria for DSC Support Structure

Allowable Stress (S)	
Stress Type	Stress Value
Tensile	0.60 S_y
Compressive	(See Note 1)
Bending	0.60 S_y(2)
Shear	0.40 S_y
Interaction	(See Note 3)

Notes:

(1) Equations E2-1 or E2-2 of the AISC Specification (Ref. 4) are used as appropriate.

(2) For properly braced non-compact sections, for other cases see AISC Specification Chapter F.

(3) Interaction equations per the AISC Specification are used as appropriate.

(4) S_y = Yield strength of the material

Table 3.9.9-6
HSM-H Support Steel Structure Load Combinations

Load Combination No.	Combination Identifier	Load Combination
C1S	COMB1S	(1.5S or 1.4 S_v) > DW+LL+TN[(1), (2)]
C2S	COMB2S	S > DW+RO[(3), (4)]
C3S	COMB3S	1.3S > DW+TN+RA[(3), (4)]
C4S	COMB4S	(1.6S or 1.4S_v) > DW+LL+TN+EQ[(2)]
C5S	COMB5S	(1.7S or 1.4S_v) > DW+LL+MAX (TO and TA)[(2)]

Notes:

(1) This normal operating load combination applies to DSC storage condition.
(2) DSC weight is included as live load (LL) for this condition; the DSC spans between end supports
(3) These load combinations represent normal and off-normal handling conditions.
(4) DSC weight is included as a direct load on the rail.

Table 3.9.9-7
Design Pressures for Tornado Wind Loading

HSM-H Wall Orientation(1)	Velocity Pressure (psf)	Pressure Coefficient(2)	Max/Min Design Pressure (psf)
Front	344	+0.68	234
Left	344	-0.60	-207
Rear	344	-0.43	-148
Right	344	-0.60	-207
Roof	344	-0.60	-207

Notes:

1. Wind direction assumed to be from front. Wind load from other directions may be found by rotating table values to desired wind directions.
2. Pressure coefficient = guest factor (0.85) x max/min pressure coefficient from Figure 6-3 of reference 5.

Table 3.9.9-8
Maximum NUHOMS® HSM-H Concrete Component Forces and Moment for Normal and Off-Normal Loads

Load Case	Concrete Component	Forces/Moments			
		Shear, V_{01} (kips/ft)	Shear, V_{02} (kips/ft)	Moment, M_1 (kip-in/ft)	Moment, M_2 (kip-in/ft)
Dead Load (DW)	Rear Wall	1.20	0.60	5.40	20.10
	Side Wall	4.40	2.80	24.80	20.40
	Front Wall	5.30	5.10	75.30	190.80
	Roof	2.80	3.50	45.20	136.20
Live Load (LL)	Rear Wall	1.40	0.60	6.70	20.10
	Side Wall	1.20	0.80	8.50	9.60
	Front Wall	30.20	23.80	344.60	510.60
	Roof	0.90	1.30	16.00	47.20
Operational Handling Load (RO)	Rear Wall	Included in Live Load (LL)			
	Side Wall				
	Front Wall				
	Roof				
Off-Normal Handling Load (RA)	Rear Wall	Included in Live Load (LL)			
	Side Wall				
	Front Wall				
	Roof				
Design Wind Load (WW)	Rear Wall	4.88	2.20	81.50	124.88
	Side Wall	27.00	10.87	190.50	135.00
	Front Wall	12.75	12.12	179.00	289.12
	Roof	3.25	2.50	135.50	80.88

Table 3.9.9-9
Summary of Thermal Forces and Moments in the HSM-H Concrete Components

Thermal Case	Concrete Component	Forces/Moments			
		Shear, V_{o1} (1) (kips/ft)	Shear, V_{o2} (1) (kips/ft)	Moment, M_1 (2) (kip-in/ft)	Moment, M_2 (2) (kip-in/ft)
Normal Thermal (TN)	Rear Wall	4	6	104	228
	Side Wall	7	7	185	71
	Front Wall	30	23	1318	2025
	Roof	6	5	111	234
Off-Normal Thermal (TO)	Rear Wall	4	5	100	207
	Side Wall	6	6	160	67
	Front Wall	30	23	1315	1938
	Roof	6	5	93	233
Accident Thermal (TA)	Rear Wall	9	19	140	272
	Side Wall	92	32	184	340
	Front Wall	41	38	1772	3325
	Roof	11	24	404	830

Notes:
1. V_{o1} and V_{o2} are out of plane shear
2. M_1 and M_2 are out of plane moment

Table 3.9.9-10
Maximum HSM-H Concrete Component Forces and Moments for Accident Loads

Load Case	Concrete Component	Forces/Moments			
		Shear, V_{01}(1) (kips/ft)	Shear, V_{02}(1) (kips/ft)	Moment, M_1(2) (kip-in/ft)	Moment, M_2(2) (kip-in/ft)
Earthquake (EQ)	Rear Wall	4.71	1.31	23.92	89.41
	Side Wall	7.30	5.47	49.13	64.12
	Front Wall	17.71	13.37	133.16	498.61
	Roof	3.05	1.83	230.46	75.03
Flood (FL)	Rear Wall	6.34	3.42	146.03	106.63
	Side Wall	49.04	19.28	340.62	248.39
	Front Wall	20.5	17.57	309.27	351.48
	Roof	3.05	1.83	230.46	75.03
Tornado Wind (WT)	Rear Wall	4.88	3.81	151.94	124.88
	Side Wall	51.75	21.25	349.75	259.50
	Front Wall	16.62	13.94	295.69	289.12
	Roof	5.75	4.25	248.06	112.25

Notes:
(1) V_{01} and V_{02} are out of plane shears.
(2) M_1 and M_2 are out of plane moments.

Table 3.9.9-11
Comparison of Highest Combined Shear Forces/Moments with the Capacities

Component	Load Comb.(1)	Quantity	V_1 kips/ft	V_{01} kips/ft	V_{02} kips/ft	M_1 kip-in/ft	M_2 kip-in/ft
Rear Wall (Upper)	Comb 1c thru 6c	Computed	14.52	7.71	9.16	147.35	267.10
		Capacity	75.2	14.5	14.5	298.2	298.2
		Ratio	**0.19**	**0.53**	**0.63**	**0.49**	**0.90**
	Comb 7c	Computed	18.44	11.37	6.08	131.14	264.5
		Capacity	69.6	13.8	13.8	273.8	273.8
		Ratio	**0.26**	**0.82**	**0.44**	**0.48**	**0.97**
Rear Wall (Lower)	Comb 1c thru 6c	Computed	17.34	9.48	13.25	159.40	167.70
		Capacity	96.8	36.2	36.2	757.9	757.9
		Ratio	**0.18**	**0.26**	**0.37**	**0.21**	**0.22**
	Comb 7c	Computed	9.49	6.40	20.84	154.30	251.80
		Capacity	90.1	34.3	34.3	696.3	696.3
		Ratio	**0.11**	**0.19**	**0.61**	**0.22**	**0.36**
Side Walls (Upper)	Comb 1c thru 6c	Computed	18.92	12.05	13.19	177.76	163.10
		Capacity	54.4	14.8	14.8	196.9	196.9
		Ratio	**0.35**	**0.82**	**0.89**	**0.90**	**0.83**
	Comb 7c	Computed	22.37	12.08	9.10	120.24	91.05
		Capacity	50.5	14.0	14.0	180.8	180.8
		Ratio	**0.44**	**0.86**	**0.265**	**0.67**	**0.50**
Side Walls (Lower)	Comb 1c thru 6c	Computed	36.17	22.33	21.12	308.10	261.55
		Capacity	63.0	23.4	23.4	314.6	314.6
		Ratio	**0.57**	**0.95**	**0.91**	**0.98**	**0.83**
	Comb 7c	Computed	19.28	21.12	15.34	97.25	180.24
		Capacity	58.7	22.2	22.2	289.0	289.0
		Ratio	**0.33**	**0.95**	**0.69**	**0.34**	**0.63**
Roof	Comb 1c thru 6c	Computed	13.18	9.44	28.73	487.01	1022.49
		Capacity	174.6	59.1	59.10	2475.0	2375.0
		Ratio	**0.08**	**0.16**	**0.49**	**0.21**	**0.43**
	Comb 7c	Computed	7.69	11.48	28.38	386.48	897.67
		Capacity	162.4	56.1	56.10	2181.7	2181.70
		Ratio	**0.05**	**0.21**	**0.51**	**0.18**	**0.41**
Front Wall (Upper)	Comb 1c thru 6c	Computed	41.82	44.83	37.00	1393.19	1895.08
		Capacity	174.7	56.3	56.3	2257.3	2317.3
		Ratio	**0.24**	**0.80**	**0.66**	**0.62**	**0.84**
	Comb 7c	Computed	32.63	48.95	26.29	1853.0	1906.74
		Capacity	159.6	53.4	53.4	2073.5	2073.5
		Ratio	**0.20**	**0.92**	**0.49**	**0.89**	**0.92**
Front Wall (Lower)	Comb 1c thru 6c	Computed	29.29	30.43	37.83	1783.50	836.92
		Capacity	189.0	73.6	73.6	2963.4	2963.4
		Ratio	**0.16**	**0.42**	**0.52**	**0.60**	**0.28**
	Comb 7c	Computed	48.04	45.95	41.38	1908.90	507.22
		Capacity	176.0	69.8	69.8	2722.4	2722.4
		Ratio	**0.27**	**0.66**	**0.59**	**0.70**	**0.19**

Note:
1. Com 1c thru 6c includes normal thermal. Com 7c includes accident thermal (see Table 3.9.9-3)

Table 3.9.9-12
Maximum/Minimum Forces/Moments in the Rail Components in the Local System

Load Combination		F_x Kips	F_y Kips	F_z Kips	M_x kip-in	M_y kip-in	M_z Kip-in
C1S	MAX	0.0	33.0	65.2	63.5	231.1	213.7
	MIN	0.0	-41.0	-61.3	-52.4	-1146.7	-236.2
C2S	MAX	38.5	39.8	77.0	0.22	428.2	247.8
	MIN	-28.9	-39.8	-60.9	-0.32	-1137.6	-247.8
C3S	MAX	86.5	30.7	89.6	63.6	592.7	199.4
	MIN	-86.5	-38.1	-63.0	-52.4	-1422.4	-230.4
C4S	MAX	22.3	38.2	102.1	63.6	562.5	-267.6
	MIN	-22.3	-46.3	-98.3	-52.4	-1869.0	-290.2
C5S	MAX	0.	49.6	82.1	183.7	264.8	267.3
	MIN	0.	-54.1	-80.9	-159.3	-143.4	-267.1

Table 3.9.9-13
Maximum/Minimum Forces/Moments in the Rail Extension Plates in the Local System

Load Combination		F_x Kips	F_y Kips	F_z Kips	M_x kip-in	M_y kip-in	M_z Kip-in
C1S	MAX	0.0	0.85	-0.25	2.7	6.8	13.8
	MIN	0.0	-4.0	-0.73	-2.7	-4.3	-45.9
C2S	MAX	40.0	2.6	-0.4	0.1	5.3	26.1
	MIN	-30.0	-2.6	-0.5	-0.1	-2.6	-26.1
C3S	MAX	80.0	0.8	-0.2	2.7	7.2	13.6
	MIN	-79.9	-3.9	-0.8	-2.8	-4.2	-44.9
C4S	MAX	38.5	1.5	-0.0	2.7	9.3	17.0
	MIN	-38.5	-4.7	-1.0	-2.8	-5.8	-53.2
C5S	MAX	0.1	1.02	0.34	9.4	12.3	18.2
	MIN	0.1	-7.6	-1.5	-9.5	-9.7	-94.7

Table 3.9.9-14
Maximum/Minimum Axial Forces in the Cross Member Components

Load Combination		F_x Kips
C1S	MAX	6.2
	MIN	5.2
C2S	MAX	8.1
	MIN	5.8
C3S	MAX	5.2
	MIN	2.6
C4S	MAX	6.2
	MIN	5.2
C5S	MAX	7.1
	MIN	5.1

Table 3.9.9-15
Rail Component Results

Load Comb.	Interaction Ratio(1)	Shear Stress Ratio(2)	Stiffener Plate Stress Ratio(3)
C1S	0.35	0.67	0.19
C2S	0.58	0.84	0.00
C3S	0.58	0.93	0.22
C4S	0.51	0.96	0.18
C5S	0.40	0.63	0.55

Notes:

(1) Axial and bending stresses are computed using axial (F_x) and bending moment (M_y, M_z) results from Table 3.9.9-12. Interaction ratios are based on appropriate equations from Chapter H of AISC [4].

(2) Shear stresses are computed using shear forces (F_y, F_z) from Table 3.9.9-12. Shear stress ratio is the computed shear stress/shear stress allowable.

(3) Flexural stresses in the stiffener plates are computed using torsional moment (M_x) result from Table 3.9.9-12. Stiffener plate stress ratio is the bending stress in the plate/bending allowable stress.

Table 3.9.9-16
Extension Plates and Cross Members Results

Load Comb.	Extension Plates Interaction Ratio(1)	Cross Members Stress Ratio(2)
C1S	0.77	0.25
C2S	0.77	0.32
C3S	0.71	0.21
C4S	0.60	0.25
C5S	0.71	0.33

Notes:

(1) Axial and bending stresses are computed using axial (F_x) and bending moment (M_y, M_z) results from Table 3.9.9-13. Interaction ratios are based on appropriate equations from Chapter H of AISC [4].

(2) Axial stresses in the cross members are computed using axial (F_x) force results from Table 3.9.9-14. Cross member stress ratio is the axial stress in the member/axial allowable stress.

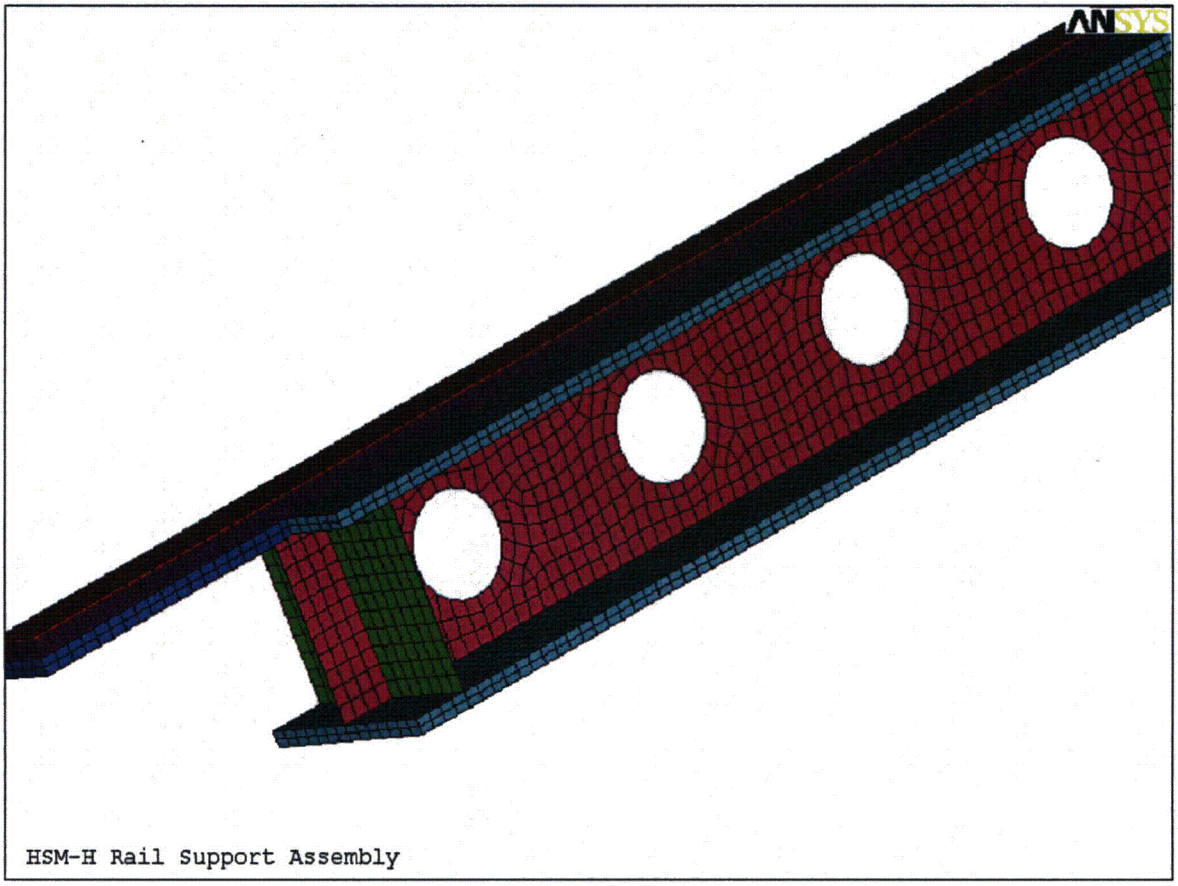

Figure 3.9.9-1
Analytical Model of the W12x96 Beam with Slotted, Nitronic and Stiffener Plates

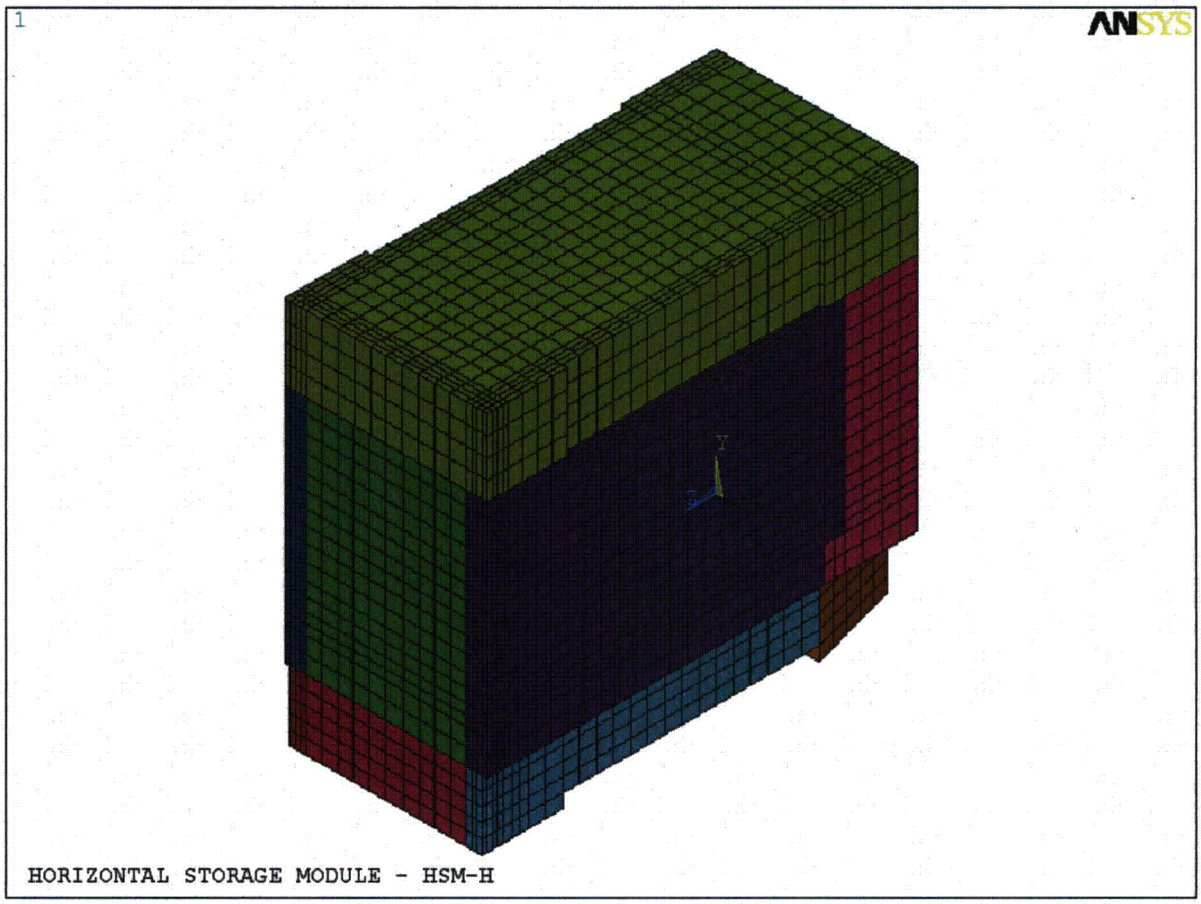

Figure 3.9.9-2
Analytical Model of the HSM-H for Mechanical Load Analysis

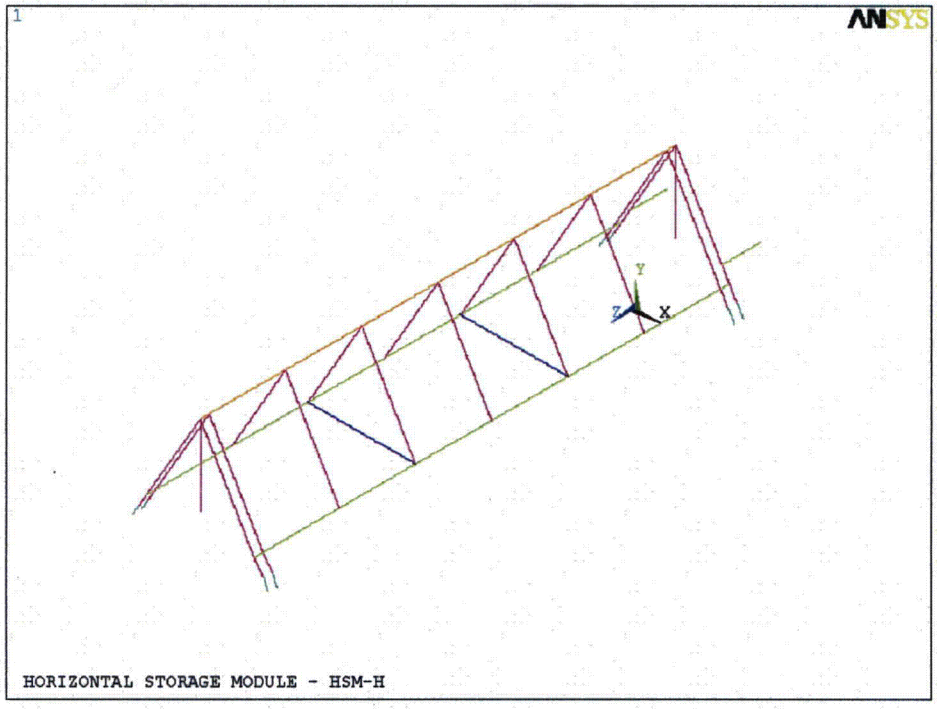

Figure 3.9.9-3
Analytical Model of the 32PTH DSC Support Structure

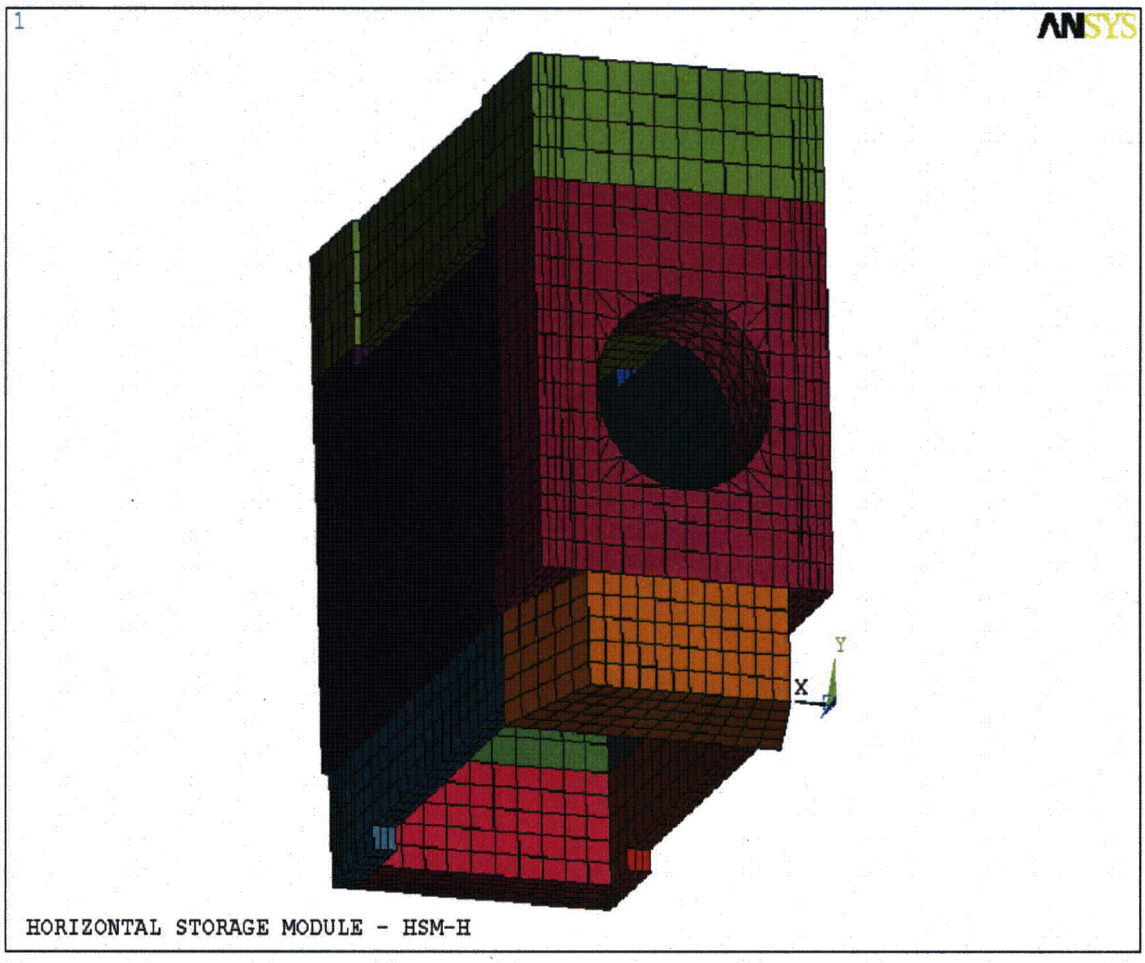

Figure 3.9.9-4
Analytical Model of the HSM-H for Thermal Load Analysis

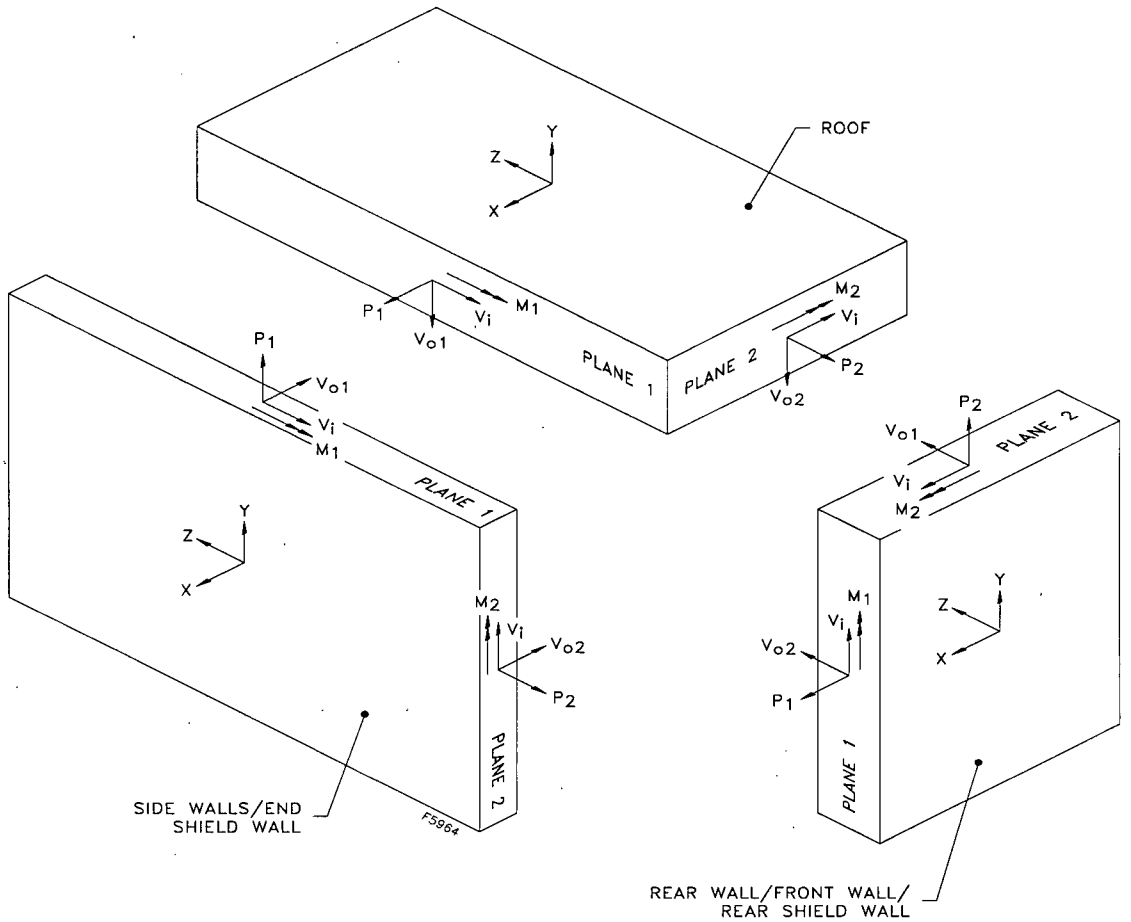

Figure 3.9.9-5
Symbolic Notations of Force and Moment Capacities
(Also for Computed Forces and Moments)

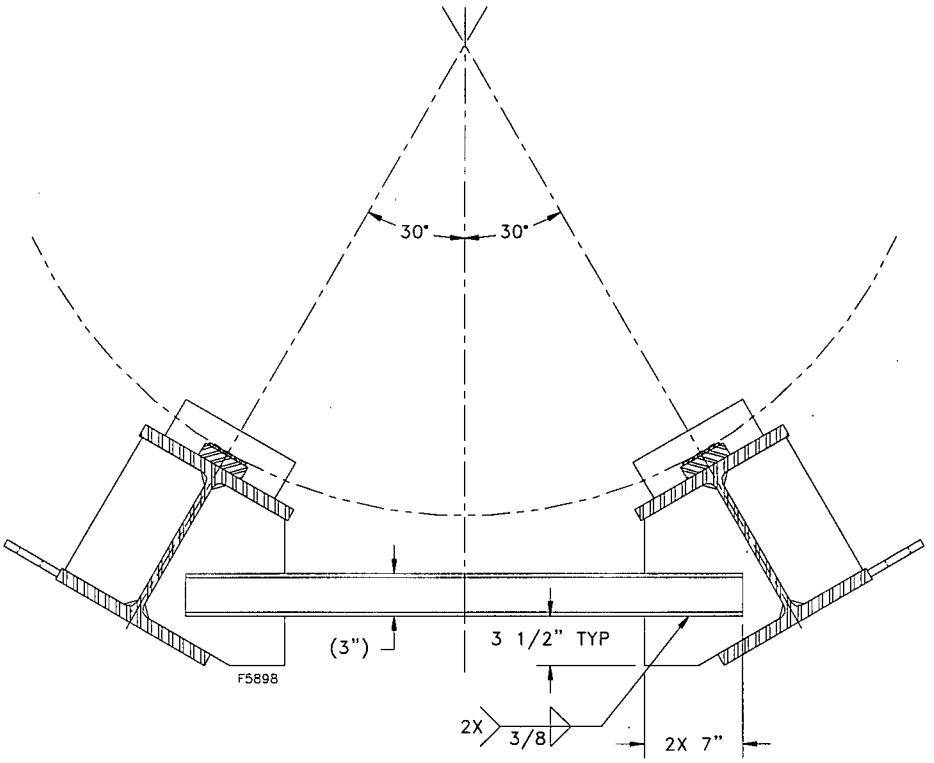

DSC SUPPORT STRUCTURE

Figure 3.9.9-6
Components of Support Structure

APPENDIX 3.9.10

TABLE OF CONTENTS

Page

3.9.10 OS187H TRANSFER CASK DYNAMIC IMPACT ANALYSIS 3.9.10-1

3.9.10.1 Introduction 3.9.10-1
3.9.10.2 Analysis Software 3.9.10-1
3.9.10.3 Validation of the LS-DYNA Impact Analysis 3.9.10-2
3.9.10.4 OS187H Transfer Cask Impact Analysis 3.9.10-8
3.9.10.5 Summary of g-Loads for OS187H Transfer Cask Body and Lid Bolt Stress Analysis 3.9.10-14
3.9.10.6 References 3.9.10-16

LIST OF FIGURES

3.9.10-1 Finite Element Model of "GENERIC" Storage Cask, Side Drop and Tip Over Onto Concrete Pad And Soil (Reproduced From LLNL Report)
3.9.10-2 TN-32 Cask Tipover Analysis Finite Element Model
3.9.10-3 TN-32 Cask Tipover Analysis Finite Element Model (Enlarged view of the TN-32 Cask)
3.9.10-4 TN-32 Transfer Cask Deformed Shape – Mode 1
3.9.10-5 TN-32 Transfer Cask Deformed Shape – Mode 2
3.9.10-6 OS187H Transfer Cask Side Drop Dynamic Impact Finite Element Model
3.9.10-7 OS187H Transfer Cask Side Drop Dynamic Impact Finite Element Model (Enlarged view of the Transfer Cask)
3.9.10-8 OS187H Transfer Cask CG Over Corner Drop Dynamic Impact Finite Element Model
3.9.10-9 OS187H Transfer Cask CG Over Corner Drop Dynamic Impact Finite Element Model (Enlarged View of the Transfer Cask)
3.9.10-10 OS187H Transfer Cask Finite Element Model without the Internals
3.9.10-11 OS187H Transfer Cask Internals Finite Element Model
3.9.10-12 OS187H Transfer Cask Side Drop Nodal Sections Analyzed
3.9.10-13 OS187H Transfer Cask CG Over Corner Drop Nodal Sections Analyzed
3.9.10-14 OS187H Transfer Cask Finite Element Model used for Modal Analysis, Elements
3.9.10-15 OS187H Transfer Cask Finite Element Model used for Modal Analysis, Boundary Conditions
3.9.10-16 OS187H Transfer Cask Deformed Shape – Mode 2
3.9.10-17 OS187H Transfer Cask Deformed Shape – Mode 3

3.9.10-18 OS187H Transfer Cask Deformed Shape – Mode 4
3.9.10-19 OS187H Transfer Cask, Side Drop, Lid Section Acceleration Time History
3.9.10-20 OS187H Transfer Cask, Side Drop, Middle Section Acceleration Time History
3.9.10-21 OS187H Transfer Cask, Side Drop, Maximum Effective Stress Distribution
3.9.10-22 OS187H Transfer Cask, CG Over Corner Drop, Lid Section Axial Acceleration Time History
3.9.10-23 OS187H Transfer Cask, CG Over Corner Drop, Maximum Effective Stress Distribution

APPENDIX 3.9.10

OS187H TRANSFER CASK DYNAMIC IMPACT ANALYSIS

3.9.10.1 Introduction

The purpose of this calculation is to determine the rigid body accelerations for the NUHOMS®-OS187H Transfer Cask during the hypothetical accident condition 80 inch free drop during fuel transfer. The drop orientations analyzed in this appendix are the 80 inch side drop (10CFR72) and the 80 inch corner drop (10CFR50).

The rigid body transfer cask accelerations are predicted numerically by the LS-DYNA 3D explicit nonlinear dynamic analysis finite element solver, Version 970 [1]. The methodology used in performing this analysis is based on work conducted at the Lawrence Livermore National Laboratory, where an analysis methodology is developed and validated through comparisons with test data [2][3]. Validation of the dynamic impact analyses presented herein is achieved through comparison of a previous TN-32 Dry Storage Cask Tipover Analysis with a similar analysis performed by Lawrence Livermore National Labs (LLNL). The results of these analyses are used as input to the detailed static analyses for the cask body presented in Appendix 3.9.2.

The results of these analyses are also used as input to the static analyses of the cask internal basket and canister structures (presented in Appendix 3.9.1) by including dynamic application factors (See Appendix 3.9.11).

3.9.10.2 Analysis Software

The LS-DYNA [1] finite element program was used for the analyses presented in this Appendix. Model generation was performed using the ANSYS [4] finite element program. Data filtering was performed using the LS-PREPOST software supplied with LS-DYNA.

LS-DYNA is a general purpose, explicit finite element program used to model the nonlinear dynamic response of three-dimensional models. Applications of LS-DYNA include crash worthiness, sheet metal forming, high velocity impact, explosive phenomena, drop tests, etc.

ANSYS is a general purpose program capable of solving structural, mechanical, electrical, electromagnetic, electronic, thermal, fluid, and biomedical problems. It has extensive preprocessing (model generation), solution, postprocessing, and graphics capabilities.

3.9.10.3 Validation of the LS-DYNA Impact Analysis

In order to validate the accuracy of the HUNOMS®-OS187H Transfer Cask impact analysis, a tipover analysis of the TN-32 cask is performed and compared with the LLNL [2] results based on the TN-32 cask geometry.

The following table lists key dimensions and weights of the LLNL and Transnuclear TN-32 Model3.

	LLNL Model	TN-32 Model
Cask ID	68.75"	68.75"
Cask OD	87.75"	87.75"
Cask Cavity Length	163.25"	163.25"
Cask Overall Length	184"	184"
Weight Including Internals	232,000 lb	232,000 lb
Cask Material	Carbon Steel	Carbon Steel

These two models have the same geometry and weight, therefore it is a reasonable approach to use the TN-32 model to validate the accuracy of the LS-DYNA impact analysis.

LLNL Model

The finite element model of the LLNL model is described in the LLNL report [2]. A plot of the finite element model is shown in Figure 3.9.10-1 of this Appendix for reference.

TN-32 Model

The finite element model of the TN-32 is developed in a similar manner to those models represented in LLNL report. The cask and basket meshes are simplified and totally independent of each other with surface-to-surface contact elements transferring load between the two components. Contact surfaces are also used between the cask and concrete pad and between the concrete pad and the soil.

The TN-32 finite element model is made up of four components: cask body, cask internals, concrete and soil. Each of these components is modeled using 3-D 8-node brick elements. The finite element models were developed in ANSYS and transferred to LS-DYNA through the ANSYS-LS-DYNA interface. Modifications were made to the LS-DYNA input to add the material definition and state variables since they are not available through the ANSYS translator. The geometries of the cask and basket have been simplified since the purpose of the analysis is to predict the rigid body response of the cask. Features on the cask such as the trunnions, neutron shield and weather cover are neglected in terms of stiffness but their weight is lumped into the density of the cask. Figures 3.9.10-2 and 3.9.10-3 illustrate the finite element model of the cask, basket, concrete, and soil. Mesh sizes in this analysis are in reasonable agreement with those represented in LLNL report [2]. The concrete material is modeled with all elements having a constant length of 10 inches since the concrete material law can be dependent on mesh size.

TN-32 Material Properties

The material properties required to perform the analysis include modulus of elasticity, E, Poison's Ratio, ν, and material density (ρ) for the cask body, basket, concrete, and soil. The concrete pad requires a more detailed material model since all of the significant nonlinear deformations occur in the concrete. Material properties used for the concrete and soil are based on those developed at Lawrence Livermore National Labs [2].

All material properties are taken at room temperature. This is considered conservative because the cask loaded with spent fuel will typically reach temperatures higher than room temperature, and the lower modulus of elasticity at higher temperatures tends to soften the impact and consequently lower the computed g-loads.

TN-32 Cask Material

The same modulus of elasticity used in the LLNL report is used for the TN-32 tipover analysis. The density of the cask was adjusted to match the mass properties of those entities not explicitly modeled. The material properties used for the casks are as follows:

$E = 30 \times 6$ psi
$\nu = 0.3$
$\rho = 0.865 \times 10^{-3}$ lb-sec^2/in^4

Note that the density of each cask has been adjusted so that the weight of the TN-32 cask minus the basket and fuel is 166,200 lbs.

TN-32 Fuel and Basket Material

The fuel and basket were modeled as a set of hollow cylinders inside the cask walls (similar manner to those models represented in Reference [2]). The material properties of the fuel/basket were defined to match the correct weight and approximate the stiffness of the basket. The cask and basket finite element model meshes are totally independent of each other with surface-to-surface contact elements transferring load between the two components. Because the cask stiffness is so much greater than the basket stiffness this simplification is reasonable. The modulus of elasticity used for the basket is adjusted such that the fundamental frequency of the approximate basket matches the fundamental frequency of the detailed basket analysis. Material properties used for the basket are as follows:

$E = 8.1 \times 10^6$ psi
$\nu = 0.3$
$\rho = 0.863 \times 10^{-3}$ lb-sec^2/in^4

Again the density of the basket has been adjusted to account for the weight of the fuel. The weight of the basket plus fuel for TN-32 cask is 65,800 lbs.

Concrete Material

The concrete is modeled using material law 16 in LS-DYNA [1], which was developed specifically for granular type materials. The concrete data used in the analysis was originally designed by LLNL for the Shippingport Station Decommissioning Project in 1988. This model is also used in the LLNL [2] cask drop analysis. Material constants are implemented into Material Model 16, Mode II.B in LS-DYNA. The material represents 4,200 psi compressive strength concrete. A summary of the input used in the analysis is as follows.

$\rho = 2.09675\times10^{-4}$ lb sec^2 / in^4
$\nu = 0.22$
$a_0 = 1606$
$a_1 = 0.418$
$a_2 = 8.35\times10^{-5}$ psi^{-1}
$b_1 = 0$
$a_{0f} = 0.0$ psi
$a_{1f} = 0.385$

Effective Plastic Strain versus Scale Factor for Concrete Material

Effective Plastic Strain	Scale Factor, ν
0	0
0.00094	0.289
0.00296	0.465
0.00837	0.629
0.01317	0.774
0.0234	0.893
0.04034	1.0
1.0	1.0

The maximum principal stress tensile failure cutoff is set at 870 psi Strain rate effects are neglected in the analysis. Dilger [9] suggests that the major impact of strain rate effects is in the softening part of the stress-strain curve. Since the purpose of these analyses is primarily to predict the peak accelerations, we can neglect the strain rate effects on the material behavior.

The pressure-volume behavior of the concrete is modeled with the following tabulated pressure versus volumetric strain rate relationship using the equation of state feature in LS-DYNA [1].

Tabulated Pressure versus Volumetric Strain Rate for the Concrete Material

Volumetric Strain, ε	Pressure (psi)
0	0
-0.006	4,600
-0.075	5,400
-0.01	6,200
-0.012	6,600
-0.02	7,800
-0.038	10,000
-0.06	12,600
-0.0755	15,000
-0.097	18,700

An unloading bulk modulus of 700,000 psi is assumed to be constant at any volumetric strain, as was assumed in Reference [2].

One percent deformation is assumed in the concrete pad to account for the pad reinforcement. The one percent reinforcement is also used in the analyses presented in EPRI [10].

The material properties used for the reinforcing bar are as follows.

$E = 30\times10^6$ psi [2]
$\nu = 0.3$ [2]
$S_y = 30{,}000$ psi [2]
Tangent Modulus, $E_T = 30\times10^4$ psi [2]

Soil Material

The Lawrence Livermore National Labs report [2] indicates that the stiffness of the soil has little impact on the peak accelerations predicted in the cask. Thus for the purpose of the TN-32 impact analysis, the same soil model is assumed as that used in the Livermore report. The soil material properties assumed for the analysis are:

$E = 6{,}000$ psi [2]
$\nu = 0.3$ [2]
$\rho = 0.225\times10^{-3}$ lb-sec^2 / in^4 [2]

Boundary Conditions

A ½ model is also used in the TN-32 analysis, with symmetry boundary conditions used to simulate the full structure. Non-reflecting boundaries were used around the soil non-symmetry boundaries to prevent artificial stress waves from reflecting from the boundaries of the soil.

Damping Factor

The true damping characteristics of the cask impact event are very hard to quantify. Typical values for reinforced concrete structures subjected to dynamic loads are in the 5 to 10% range [11][12]. During the tipover drop events, the concrete, cask and soil absorb energy as a result of damping. Since the response of the concrete is nonlinear, a single damping ratio can not be defined. In order to define a relatively uniform damping ratio over a range of frequencies, damping is defined proportional to both the stiffness and mass matrices. Known as Rayleigh damping [16], two factors can be defined relative to mass and stiffness proportional damping to provide a range of damping. A uniform damping rate of 5% of critical is assumed between the frequencies of 50 and 1000 Hz in developing the initial damping coefficients. Since the damping ratio must be assumed, both an upper and lower bound ratio of damping is used in the preliminary analyses. However, based on the results presented in the LLNL report [2], the 6% critical damping results appear to be most realistic. The Damping ratio and parameters α and β used for the TN-32 Cask tipover verification analysis are summarized as follows.

Damping Ratio = 6%
$\alpha = 122$
$\beta = 1.5\times10^{-5}$

LS-DYNA Analysis and Results

For the TN-32 tipover verification analysis, an angular velocity is applied based on a non-mechanistic cask tipover accident. The center of rotation is set at the edge of the cask bottom located at the center of the coordinate system. LS-DYNA calculates the initial velocity components associated with each node for this rotational motion. The initial angular velocity applied to the TN-32 Cask model was 1.729 radian/sec.

LS-DYNA computes the nodal accelerations at 0.4 msec intervals. Therefore, by the Nyquist theorem, the frequency content of the nodal acceleration data, computed by LS-DYNA, ranges from zero Hz, up to the following maximum frequency, f_{max}.

$$f_{max} = \tfrac{1}{2}\times 1/(4\times10^{-4}) = 1{,}250 \text{ Hz}$$

The lowest natural frequencies of the TN-32 Cask model, which can be excited by an impact event, are much lower than this. These natural modes of the cask involve small displacements (and therefore low stresses) at frequencies higher than that of the rigid body motion of the cask. These high frequency accelerations mask the true rigid body motion of the cask, because both the low frequency rigid body acceleration and the high frequency natural vibration accelerations superimpose. The net acceleration is contained in the raw data computed by LS-DYNA. Therefore, filtering is necessary to remove these high frequency accelerations.

In order to estimate the natural frequencies of the cask model, a modal analysis is performed by using the ANSYS 3D finite element model. The weight densities are all changed to mass densities ($\rho_m = \rho_w$ /386.4).

The cask is oriented in the horizontal orientation and supported at the bottom. The cask finite element model and boundary conditions are shown in Figures 3.9.10-2 and 3.9.10-3.

The first two significant mode frequencies resulting from the ANSYS modal analysis are tabulated below:

Frequencies of the First Two Natural Modes of the TN-32 Cask Model

Mode Number	Frequency (Hz)
1	177.86
2	291.41

The mode shapes corresponding to these frequencies are plotted in Figures 3.9.10-4 and 3.9.10-5.

The averaged raw data for each cross section is filtered using a low pass Butterworth filter with a cutoff frequency of 350 Hz in order to recover the actual rigid body acceleration of the cask. The Butterworth filter used in this analysis is characterized by its large number of coefficients, small pass band ripple, and slow roll off. The cutoff frequency of 350 Hz is conservative, because it is higher than at least the first two dominant modes of the TN-32 Cask computed above (350 Hz also used in LLNL report for cutoff frequency). Therefore, the response predicted by the filtered results includes more dynamics than simply the rigid body motion of the transfer cask.

The results of the TN-32 tipover analyses provide reasonable agreement with LLNL results presented in LLNL report [2]. The following table compares the LLNL and Transnuclear TN-32 analysis results.

Comparison of LLNL Analysis and TN-32 Analysis

	LLNL LS-DYNA Analysis	Transnuclear LS-DYNA Analysis
Peak Acceleration (350 Hz Filter)	66.7 g	67 g
Duration of Pulse	0.003 sec	0.003 sec
Pulse Shape	Triangle	Triangle

3.9.10.4 OS187H Transfer Cask Impact Analysis

OS187H Transfer Cask Finite Element Model Description

The ANSYS finite element model of the OS187H Transfer Cask developed for the transfer cask stress analysis (Appendix 3.9.2) is simplified for use in the dynamic impact analysis. The OS187H Transfer Cask model consists of the transfer cask body, including the lead gamma shielding, the DSC, and the concrete pad and soil. Each of these components is modeled using 3D 8-node brick elements. Full Integration (Flanangan and Belytschko, 1981 [1]) with exact volume integration is used for all elements to reduce the risk of hourglassing problems.

The finite element models are developed with ANSYS and transferred to LS-DYNA through the use of an ANSYS macro. Modifications were made to the LS-DYNA input file to add the material definitions, non-reflecting boundaries and equation of state into LS-DYNA, since these input variables are not available through the ANSYS macro. Features of the transfer cask, such as the trunnions, neutron shield, and top neutron shield are neglected in terms of stiffness but their weight is lumped into the density of the transfer cask.

A simplified model of the DSC is placed inside the transfer cask in order to model the effect of the cask internals. Automatic surface to surface contact elements are placed between the external surface of the DSC and the internal surface of the transfer cask, between the transfer cask shells and lead gamma shielding, between the transfer cask outer surface and the concrete pad, and between the concrete pad and the soil.

The geometry of the transfer cask finite element model including the cask internals, concrete and base soil is shown in Figures 3.9.10-6 through 3.9.10-11. Figures 3.9.10-6 and 3.9.10-7 show the arrangement of the side drop impact analysis, and Figures 3.9.10-8 and 3.9.10-9 show the arrangement of the CG over corner drop impact analysis. Figure 3.9.10-10 is an enlarged view of the transfer cask without the internals, and Figure 3.9.10-11 is an enlarged view of the cask internals themselves.

Only ½ of the transfer cask, internals, concrete and soil are modeled, because the entire arrangement is symmetric about the *x-y* plane. The ½ slab of concrete modeled is 600 inches × 200 inches × 36 inches thick, and the ½ soil modeled is 1,200 inches × 400 inches × 500 inches deep.

Mesh sizes in this analysis are in reasonable agreement with those used in LLNL report [2]. The finite element sizes between the contact surfaces of the concrete and soil are refined to have better match (see Figure 3.9.10-3 for LLNL model and 3.9.10-7 for OS187H model).

OS187H Transfer Cask Material

The following material properties are used for the transfer cask body.

Stainless Steel (SA-240 Type 304)

$E = 28.3\times10^6$ psi [5]
$\nu = 0.3$
$S_y = 30.0$ ksi.[5]
Tangent Modulus, $E_T = 1.13\times10^5$ psi

The density of the transfer cask body is adjusted to account for the weight of unmodeled components, including the trunnions and outer radial neutron shield. The effective density is computed in the following way.

Weight of Transfer Cask = ½ × [119,891 lb (transfer cask weight) – 62,369 lb (lead weight)] = 28,761 lb

Volume of F.E.M. = 68,923.2 in^3 (from ANSYS model)

ρ_{eff} = 28,761 lb / 68,923.2 in^3 / (386.4 in/sec^2) = 1.080×10^{-3} lb-sec/in^4

Lead Gamma Shield Material

The following material properties are used for the transfer cask lead gamma shield.

Chemical Lead (ASTM B-29)

$E = 2.35\times10^6$ psi [5]
$\nu = 0.45$ [6]
$S_y = 1,140$ psi [8]
Tangent Modulus, $E_T = 8.93\times10^3$ psi

The density of the lead gamma shield is computed in the following way.

Weight of lead gamma shield = ½ × 62,369 lb = 31,184.5 lb

Volume of F.E.M. Lead = 75,358.5 in^3 (from ANSYS model)

ρ_{eff} = 31,184.5 lb / 75,358.5 in^3 / (386.4 in/sec^2) = 1.071×10^{-3} lb-sec/in^4

DSC (basket and canister) Material

The following material properties are used for the Dry Shielded Canister.

Stainless Steel (SA-240 Type 304)

$E = 28.3\times10^6$ psi
$\nu = 0.3$

The density of the DSC is adjusted so that the actual weight of the DSC is properly accounted for. The effective density is computed in the following way.

Weight of DSC = ½ × [28,191 lb (canister weight) + 29,854 lb (basket weight) + 50,720 lb (fuel weight)] = 54,382.5 lb

Volume of F.E.M. = 69,807.6 in^3 (from ANSYS model)

ρ_{eff} = 54,382.5 lb / 69,807.6 in^3 / (386.4 in/sec^2) = 2.016×10^{-3} lb-sec/in^4

Concrete Material

The same concrete material properties used in the LLNL and TN-32 analyses, presented in Section 3.9.10.3, are also used for OS187H transfer cask analysis.

Soil Material

The same soil material properties used in the LLNL and TN-32 analyses, presented in Section 3.9.10.3, are also used for OS187H transfer cask analysis.

Boundary Conditions

A ½ model is employed with symmetry boundary conditions used to simulate the full structure. Non-reflecting boundaries are used around the soil non-symmetry boundaries (bottom, left side, right side, and back) to prevent artificial stress waves from reflecting from the boundaries of the soil. Both dilatation and shear waves are damped as described in the LS-DYNA *BOUNDARY command [1].

Contact boundaries between the cask and DSC, cask and lead, cask and concrete, and concrete and soil are modeled using surface-to surface contact elements in LS-DYNA. These contacts are defined using part numbers defined by the ANSYS macro that transfers the ANSYS finite element to the LS-DYNA model. A description of the LS-DYNA surface-to-surface contact elements are provided in Reference [1].

Damping Factor

As described in the above LLNL and TN-32 impact analyses (Section 3.9.10.3), the true damping characteristics of the cask impact event are very hard to quantify. Typical values for reinforced concrete structures subjected to dynamic loads are in the 5 to 10% range. A 6% damping factor is used for the LLNL and TN-32 impact analyses, for conservatism a lower bound damping factor of 5% is used for OS187H transfer cask impact analysis.

OS187H Transfer Cask Model LS-DYNA Impact Analysis

Two accident condition drop scenarios are evaluated which are considered to bound all credible transfer cask drops during fuel transfer:

- 80 inch, 0° side drop, and
- 80 inch, 60° CG over corner drop

The cask outer surface is initially placed in contact with the concrete pad, and an initial velocity is applied to the cask, lead, and DSC, to simulate the non-mechanistic drop events. The initial velocity is computed by equating potential and kinetic energies.

V = potential energy = mgh

T = kinetic energy = $\frac{1}{2}mv^2$

$\Rightarrow mgh = \frac{1}{2}mv^2$

$\Rightarrow v = \sqrt{2gh} = \sqrt{2(386.4)(80)} = 248.644$ in /sec

With the above model, boundary conditions and initial conditions, the LS-DYNA program was run from $t_0 = 0$ seconds to $t_f = 0.04$ seconds for both the Side Drop and the C.G. Over Corner Drop runs. The time step was automatically chosen by the LS-DYNA program based on the minimum model element sizes.

Transfer Cask Sections Evaluated

The resulting nodal acceleration time histories, computed in the drop direction by LS-DYNA, are averaged over several cross sections of the transfer cask. For the side drop analysis, only the accelerations transverse to the transfer cask axis are computed since the resulting accelerations in the direction of the cask axis are negligible. For the CG over corner drop however, the accelerations in the drop direction are decomposed into accelerations in the longitudinal (parallel to the cask axis) and transverse directions, since significant impact accelerations are expected in both orthogonal directions. Different nodal sections are selected as appropriate for each drop orientation.

Figures 3.9.10-12 and 3.9.10-13 show the nodal sections analyzed for the side drop and CG over corner drop.

Raw Data Filtering

As described in the TN-32 model LS-DYNA analysis, the LS-DYNA computes the nodal accelerations at 0.4 msec intervals. Therefore, by the Nyquist theorem, the frequency content of the nodal acceleration data, computed by LS-DYNA, ranges from zero Hz, up to the following maximum frequency, f_{max}.

$$f_{max} = \frac{1}{2} \times 1/(4 \times 10^{-4}) = 1{,}250 \text{ Hz}$$

The lowest natural frequencies of the OS187H Transfer Cask, which can be excited by an impact event, are much lower than this. These natural modes of the transfer cask involve small displacements (and therefore low stresses) at frequencies higher than that of the rigid body motion of the transfer cask. These high frequency accelerations mask the true rigid body motion of the transfer cask, because both the low frequency rigid body acceleration and the high frequency natural vibration accelerations superimpose. The net acceleration is contained in the raw data computed by LS-DYNA. Therefore, filtering is necessary to remove these high frequency accelerations.

In order to estimate the natural frequencies of the OS187H transfer cask, a modal analysis is performed by using the ANSYS 3D finite element model described in Appendix 3.9.2 (page 3.9.2-13). The weight densities used in Appendix 3.9.2 file are all changed to mass densities ($\rho_m = \rho_w / 386.4$).

The cask is oriented in the horizontal orientation and supported at the bottom. The cask finite element model and boundary conditions are shown in Figures 3.9.10-14 and 3.9.10-15.

The first five mode frequencies resulting from the ANSYS modal analysis are tabulated below:

Frequencies of the First Five Natural Modes of the OS187H Transfer Cask

Mode Number	Frequency (Hz)
1	69.17
2	125.00
3	130.52
4	141.07
5	147.23

The mode shapes of Mode 2, 3, and 4 are plotted in Figures 3.9.10-16 through 3.9.10-18.

The averaged raw data for each cross section is filtered using a low pass Butterworth filter with a cutoff frequency of 180 Hz in order to recover the actual rigid body acceleration of the Transfer Cask. The Butterworth filter used in this analysis is characterized by its large number of coefficients, small pass band ripple, and slow roll off. The cutoff frequency of 180 Hz is conservative, because it is higher than at least the first five dominant modes of the OS187H Transfer Cask computed above. Therefore, the response predicted by the filtered results includes

more dynamics than simply the rigid body motion of the transfer cask.

Results of LS-DYNA Analyses

The following table lists the LS-DYNA side drop results.

Summary of Impact g Load Due to Side Drop

Transfer Cask Section (see Figure 3.9.10-12)	**G Load**
Lid Section	62.9g
Top Trunnion Section	55.8g
Middle Section	57.3g
Bottom Trunnion Section	46.9g
Bottom Plate Section	44.0g

Based on the Results shown in above table, the maximum acceleration in the OS187H Transfer Cask during the 80 inch accident condition side drop event is 62.9g and occurs in the transfer cask lid section. Also from this table, the highest acceleration in the region of the transfer cask where the DSC rests is 57.3g during an 80 inch side drop event.

Figure 3.9.10-19 and 3.9.10-20 show the acceleration time history of the transfer cask lid section and middle section. Figure 3.9.10-21 shows the maximum effective stress of the transfer cask during the side drop event as computed by LS-DYNA.

The following table lists the LS-DYNA CG over corner drop results.

Summary of Impact g Load Due to CG Over Corner Drop

Transfer Cask Section (see Figure 3.9.10-13)	**Axial Accelerations**
Lid Section	15.5g

This table shows that the maximum axial acceleration during an 80 inch CG over corner drop accident event is 15.5g. Figure 3.9.10-23 shows the axial acceleration time history of the transfer cask lid section. Figure 3.9.10-23 shows the maximum effective stress of the transfer cask during the CG over corner drop event as computed by LS-DYNA.

3.9.10.5 Summary of g-Loads for the OS187H Transfer Cask Body and Lid Bolt Stress Analyses

Based on the dynamic analysis results shown on the above table, the following table summarizes the g loads to be used for the stress analyses of the transfer cask body and lid bolts.

Component	Drop Orientation	Maximum G Load Computed by LS-DYNA	G Load used for Stress Evaluation
Cask Body	Side Drop	62.9	75
	Corner Drop	15.5(1)	75(1)
Lid Bolt	Corner Drop	15.5	21.65(2)

Note:
1. The transfer cask is transferred in a horizontal position held by the transfer trailer. In the axial direction it is possible to slide into the ground and incur a corner drop. The maximum stress resulting from DYNA corner impact analysis is plot in Figure 3.9.10-23 of this Appendix and also compared with ASME code allowable as described in item 5 below. Additionally, a conservative 75g end drop analysis of the cask body was also performed in Appendix 3.9.2.
2. A conservative 21.65g was used in the lid bolt corner drop analysis (Appendix 3.9.3, page 3.9.3-6).

The g loads used for the static stress analyses of the cask and lid bolts are reasonable and conservative for following reasons:

1. The casks of OS187H and LLNL/TN-32 are very similar in both geometry and weight. However, the OS187H (0.5" SS + 4.5" lead + 2.5" SS) is less rigid than the LLNL/TN-32 (9.5" thick CS shell). The less rigidity results in a lower calculated g load for the OS187H cask than for the LLNL/TN32 cask from LS-DYNA analyses.

2. Like LLNL/TN-32 models, the OS187H model does not include the outer shell and resin. In reality, these relatively soft components will deform and absorb energy during a drop and will slow down the rate of deceleration to produce a lower g load.

3. All material properties at room temperature are used in the LS-DYNA analyses. In reality, the transfer cask loaded with spent fuels will be at temperatures higher than room temperature. The modulus of elasticity for the cask material decreases while its temperature increases. The lower modulus of elasticity for the cask materials at the real temperatures will produce a lower impact g-load than that calculated in this analysis for the cask at room temperature.

4. During the drop accident, the g loads vary along the cask length from the minimum occurred at the bottom end to the maximum occurred at the top surface of the lid. However, a uniform 75 g load along the cask length is conservatively used in the cask static stress analysis. The maximum stress intensity in the cask structural shell is calculated to be 58.17 ksi (see Table 3.9.2-1 of Appendix 3.9.2, structural shell) from the static stress analysis.

5. Comparably, the maximum effective stress (Von Mises stress) in the cask structure shell is calculated to be 29.12 ksi (see Figure 3.9.10-21 of this Appendix) from the LS-DYNA dynamic analysis. This indicates that the static stress analysis using drop load of 75g is a very conservative approach, which produces about twice stress value of that produced by the dynamic LS-DYNA analysis.

5. Figure 3.9.10-23 shows the maximum effective stress (Von Mises stress) in transfer cask due to CG over corner drop from LS-DYNA analysis. The maximum effective stress at cask top cover plate is about 34.49 ksi, which is less than its allowable stress of 94.2 ksi (SA-240, Type XM 19 at 300°F). The maximum effective stress in the structural shell is about 24.0 ksi, which is less than its allowable stress of 66.2 ksi (SA-240, Type 304 at 300°F).

For g loads (including dynamic load factor) to be used for canister and basket structural analyses are described in Appendix 3.9.11.

3.9.10.6 References

1. LS-DYNA Keyword User's Manual, Volumes 1 & 2, Version 970, April 2003, Livermore Software Technology Corporation.

2. Witte, M. et. Al. Evaluation of Low-Velocity Impact Testing of Solid Steel Billet onto Concrete Pads and Application to Generic ISFSI Storage Cask for Tipover and Side Drop. Lawrence Livermore National Laboratory. UCRL-ID-126295, Livermore, California. March 1997.

3. NUREG 1CR-6608, UCRL-1D-12911," Summary and Evaluation of Low-Velocity Impact Tests of Solid Steel/Billet onto Concrete Pad" LLNL, February, 1998

4. ANSYS User's Manual, Rev 5.6.

5. American Society of Mechanical Engineers, ASME Boiler and Pressure Vessel Code, Section II, Part D, 1999, including 2000 addenda.

6. Baumeister & Marks, Standard Handbook for Mechanical Engineers. 7th Edition.

7. American Society of Mechanical Engineers, ASME Boiler and Pressure Vessel Code, Section II, Part A, 1998, including 1999 addenda.

8. A Survey of Strain Rate Effects for some Common Structural Materials Used in Radioactive Material Packaging and Transportation Systems, U.S. Energy Research and Development Administration, Battelle Columbus Laboratories, August 1976.

9. Dilger, etc. Ductility of Plain and Confined Concrete under Different Stain Rates. ACI journal, January-February, 1984.

10. Structural Design of Concrete Storage Pads for Spent Fuel Casks. Electric Power Research Institute, EPRI NP-7551, RP 2813-28, August 1991.

11. Matthiesen, R. B. Observations of Strong Motions from Earthquakes. ASCE Convention and Exposition, Portland, Oregon, April 1980.

12. Dove, R. C., Endebrock, E. G., Dunwoody, W. E., Bennet, J. G., Seismic Tests on Models of Reinforced-Concrete Category 1 Buildings, Structural Mechanics in Reactor Technology. SMIRT 8, Brussels, Belgium 1985.

13. ANSYS User's Manual, Rev 6.0.

14. Harris and Crede, Shock and Vibration Handbook, Second Edition, McGraw-Hill.

15. Methods for Impact Analysis of Shipping Containers, NUREG/CR-3966, UCID-20639, LLNL, 1987.

16. Clough and Penzien," Dynamics of Structures" McGraw-Hill, 2nd Edition, 1993

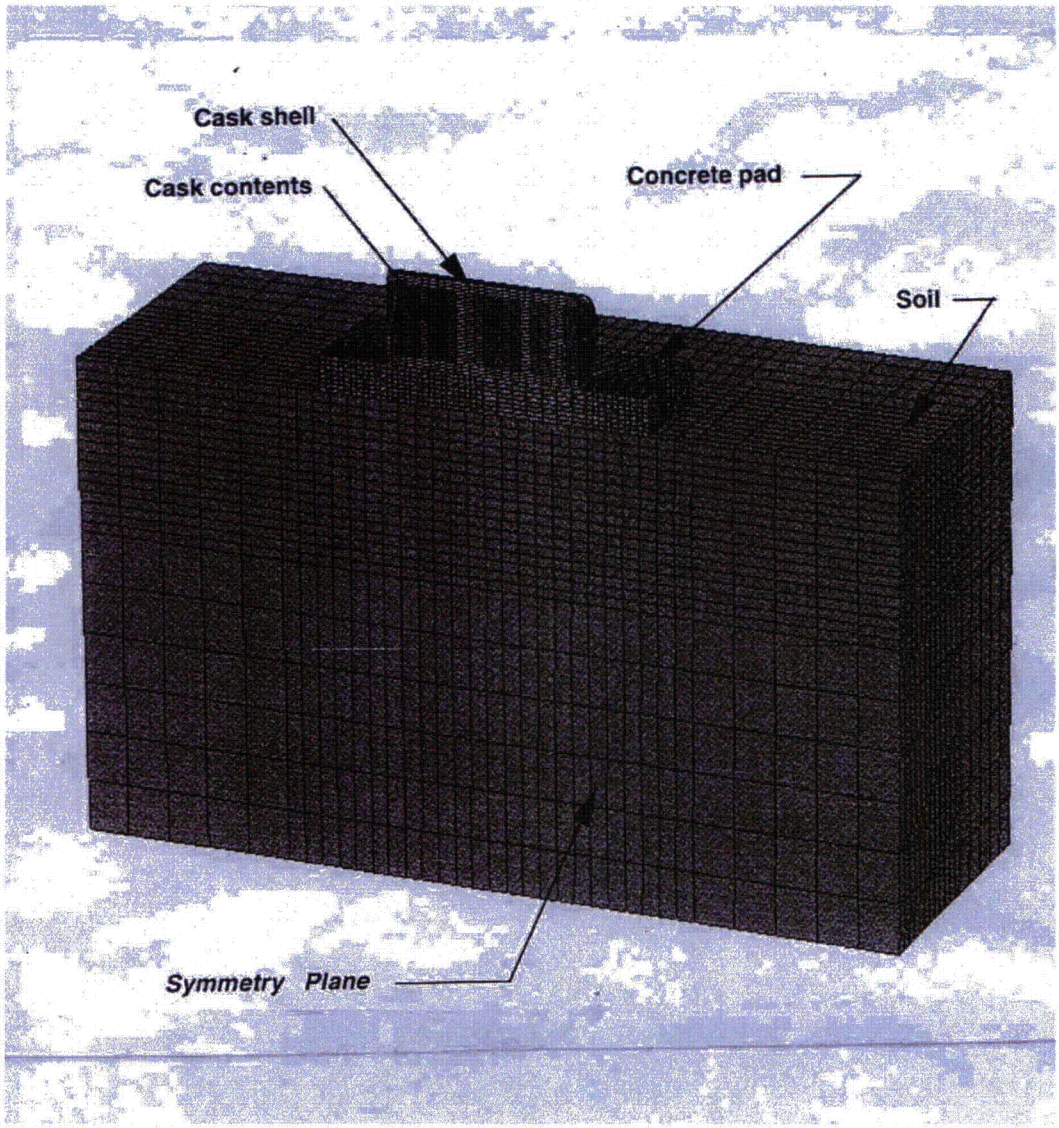

Figure 3.9.10-1
Finite Element Model of "GENERIC" Storage Cask, Side Drop and Tip Over Onto Concrete Pad And Soil (Reproduced From LLNL Report)

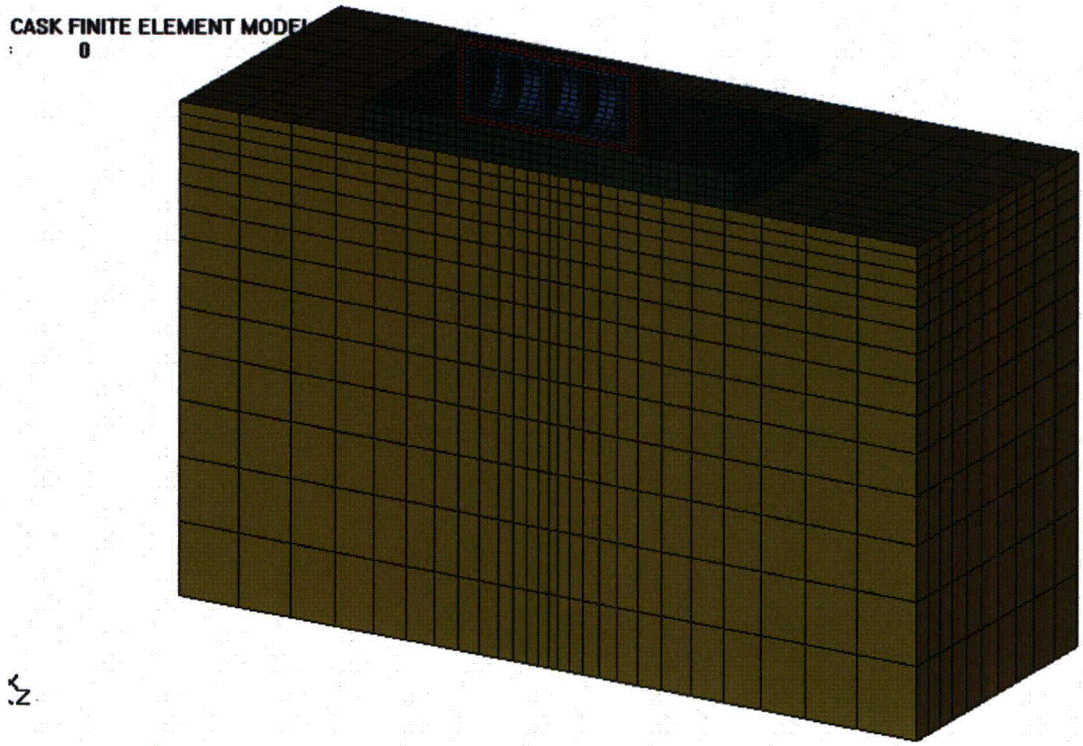

Figure 3.9.10-2
TN-32 Cask Tipover Analysis Finite Element Model

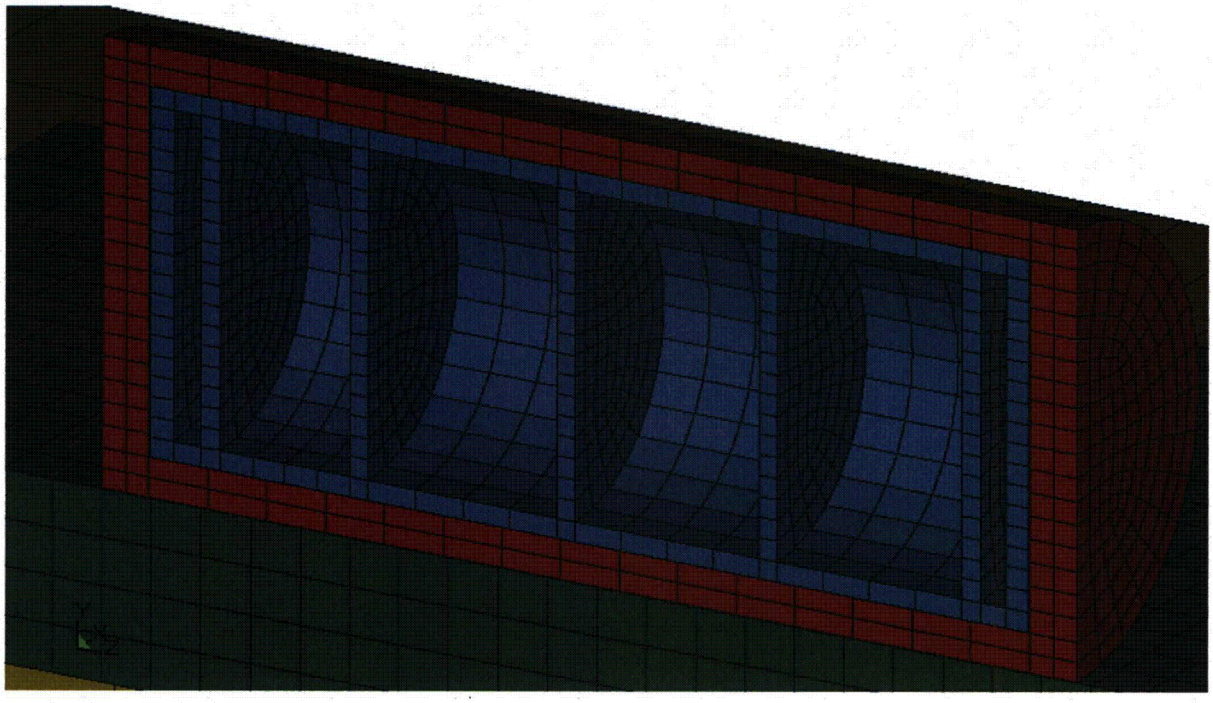

Figure 3.9.10-3
TN-32 Cask Tipover Analysis Finite Element Model (Enlarged view of the TN-32 Cask)

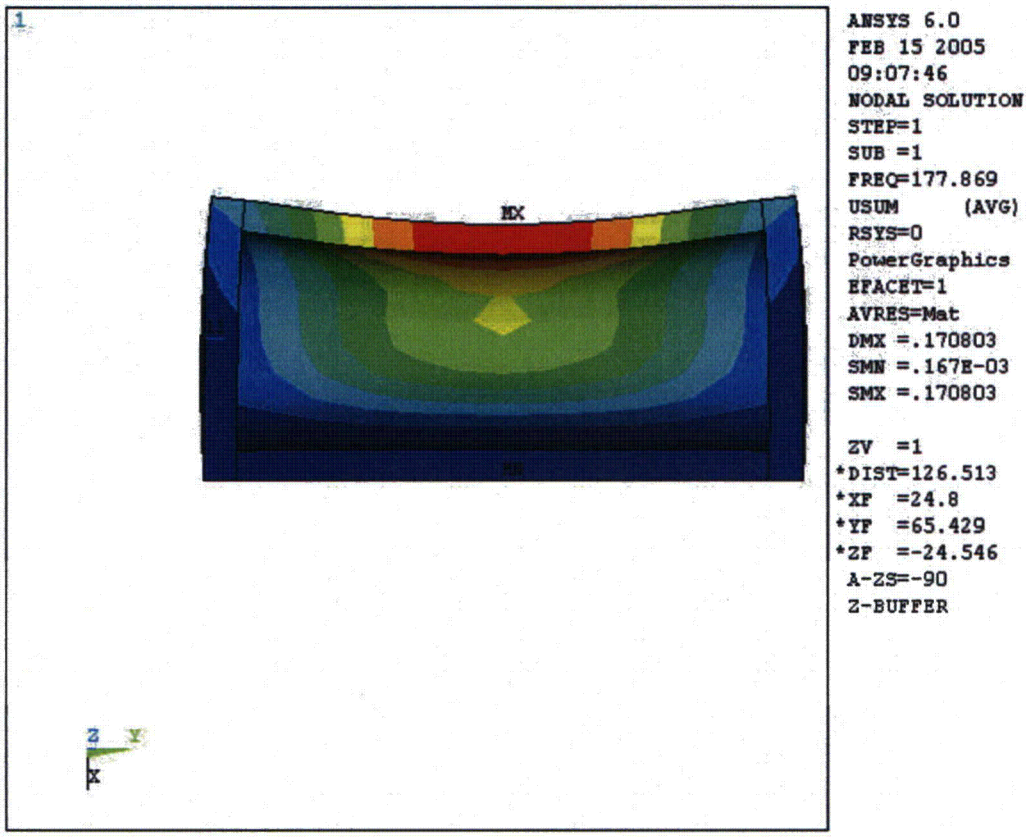

Figure 3.9.10-4
TN-32 Transfer Cask Deformed Shape-Mode 1

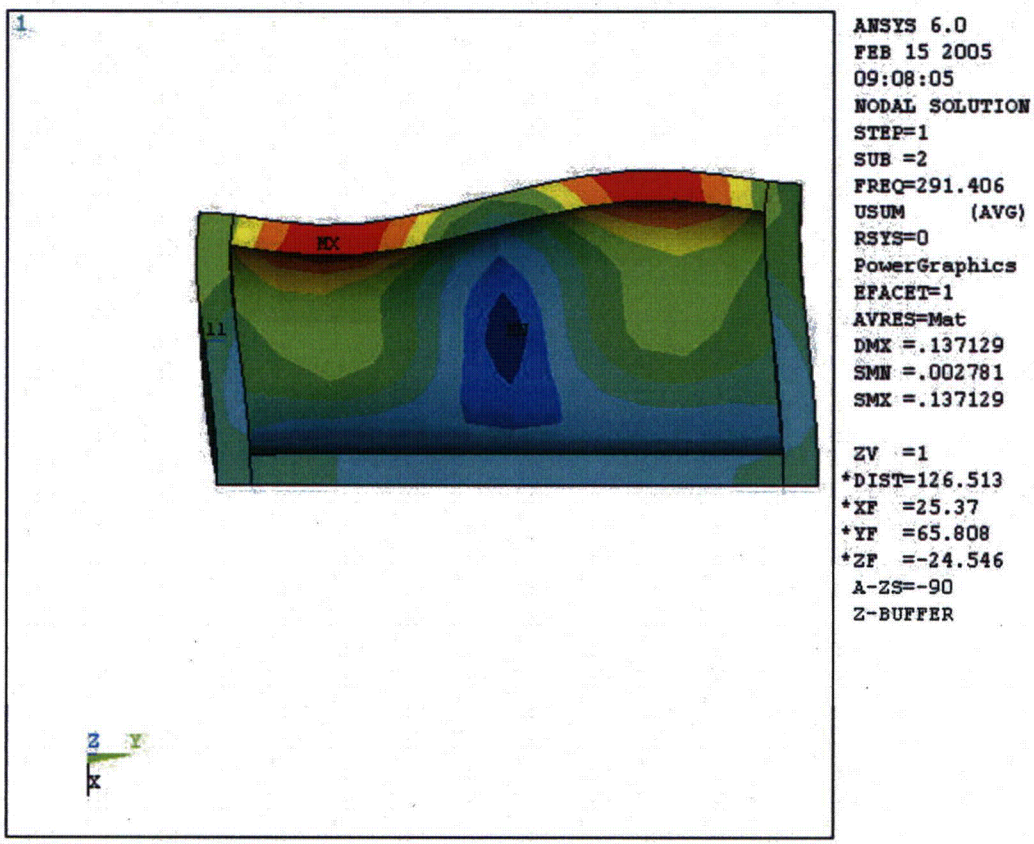

Figure 3.9.10-5
TN-32 Transfer Cask Deformed Shape-Mode 02

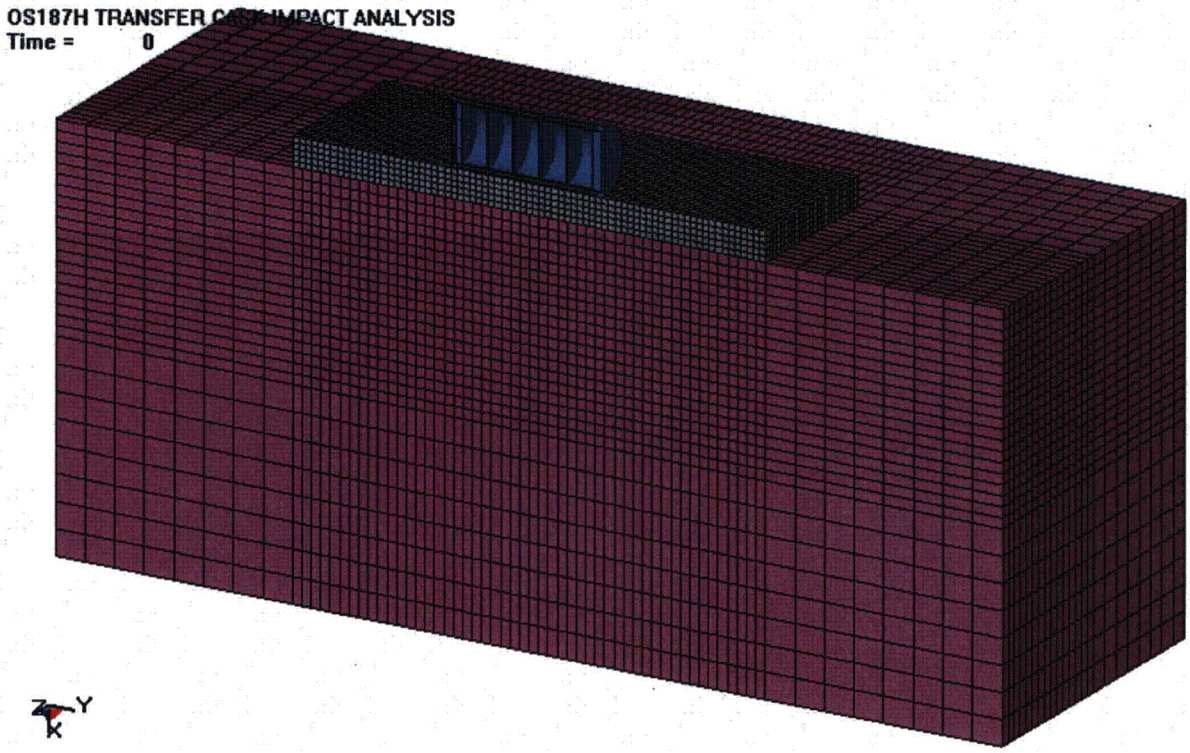

Figure 3.9.10-6
OS187H Transfer Cask Side Drop Dynamic Impact Finite Element Model

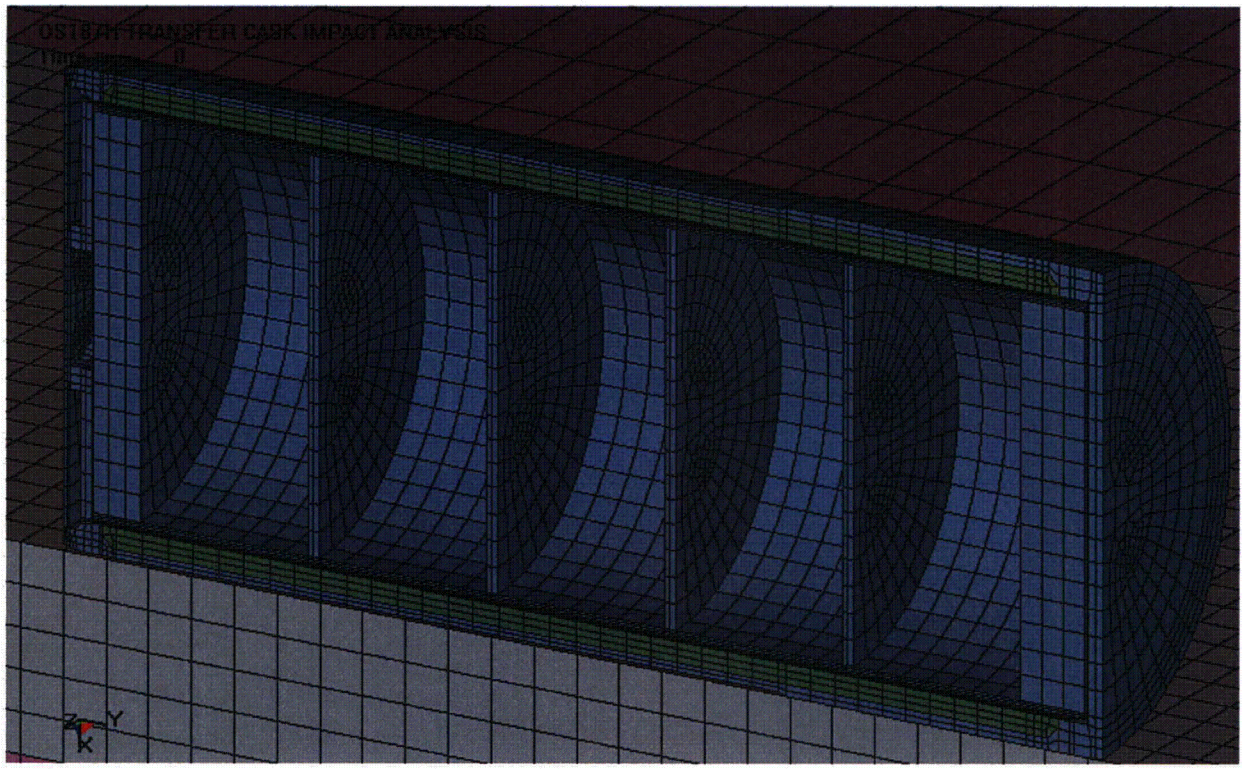

Figure 3.9.10-7
OS187H Transfer Cask Side Drop Dynamic Impact Finite Element Model
(Enlarged view of the Transfer Cask)

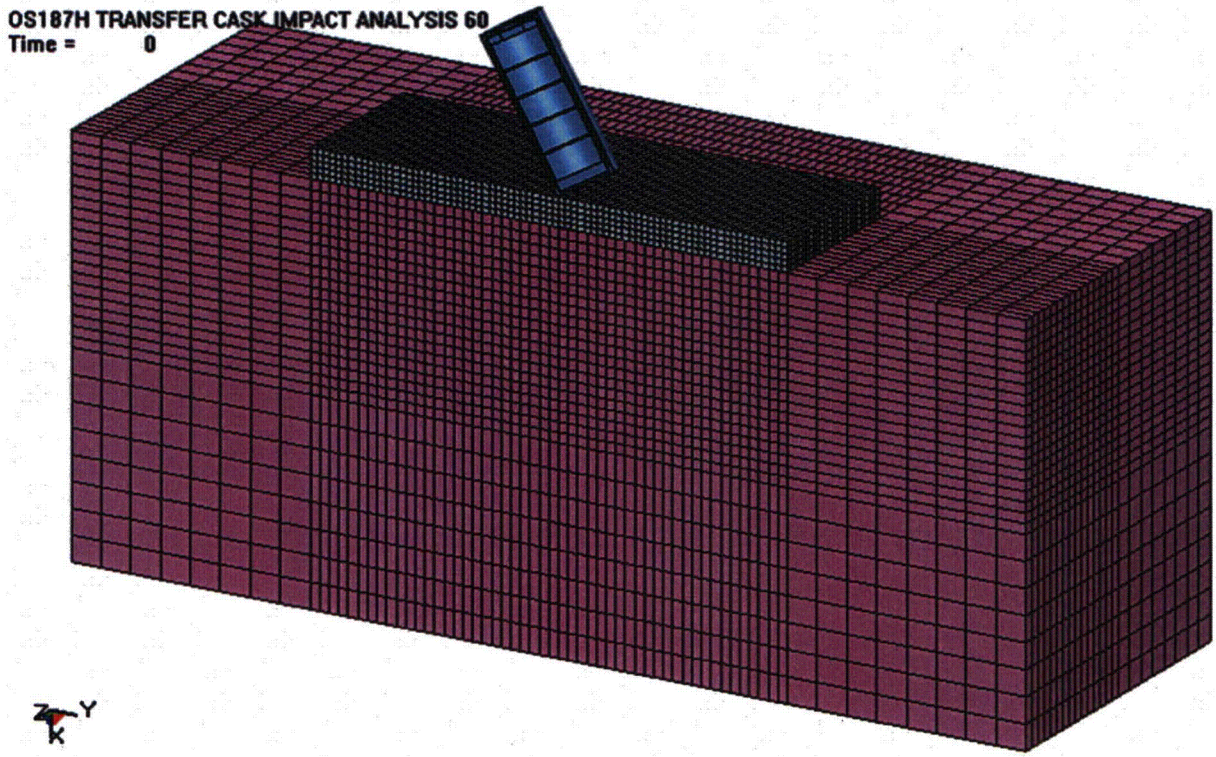

Figure 3.9.10-8
OS187H Transfer Cask CG Over Corner Drop Dynamic Impact Finite Element Model

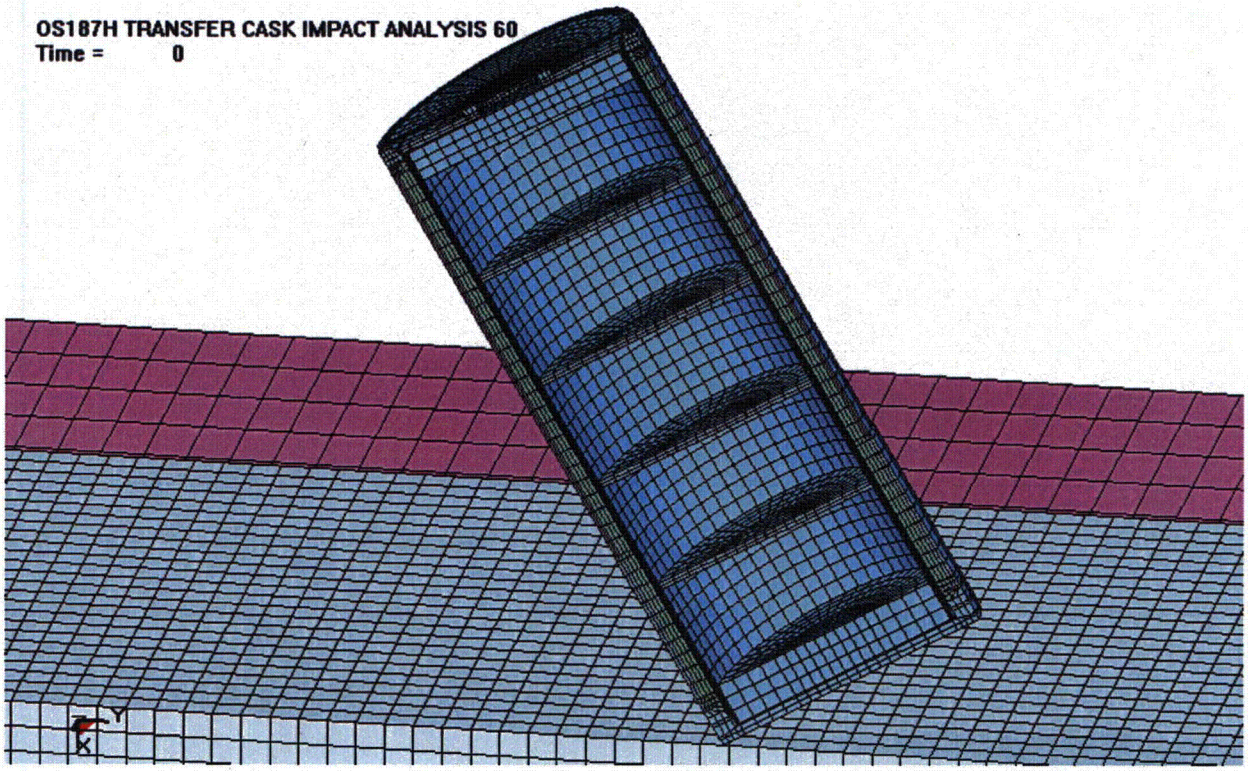

Figure 3.9.10-9
OS187H Transfer Cask CG Over Corner Drop Dynamic Impact Finite Element Model
(Enlarged View of the Transfer Cask)

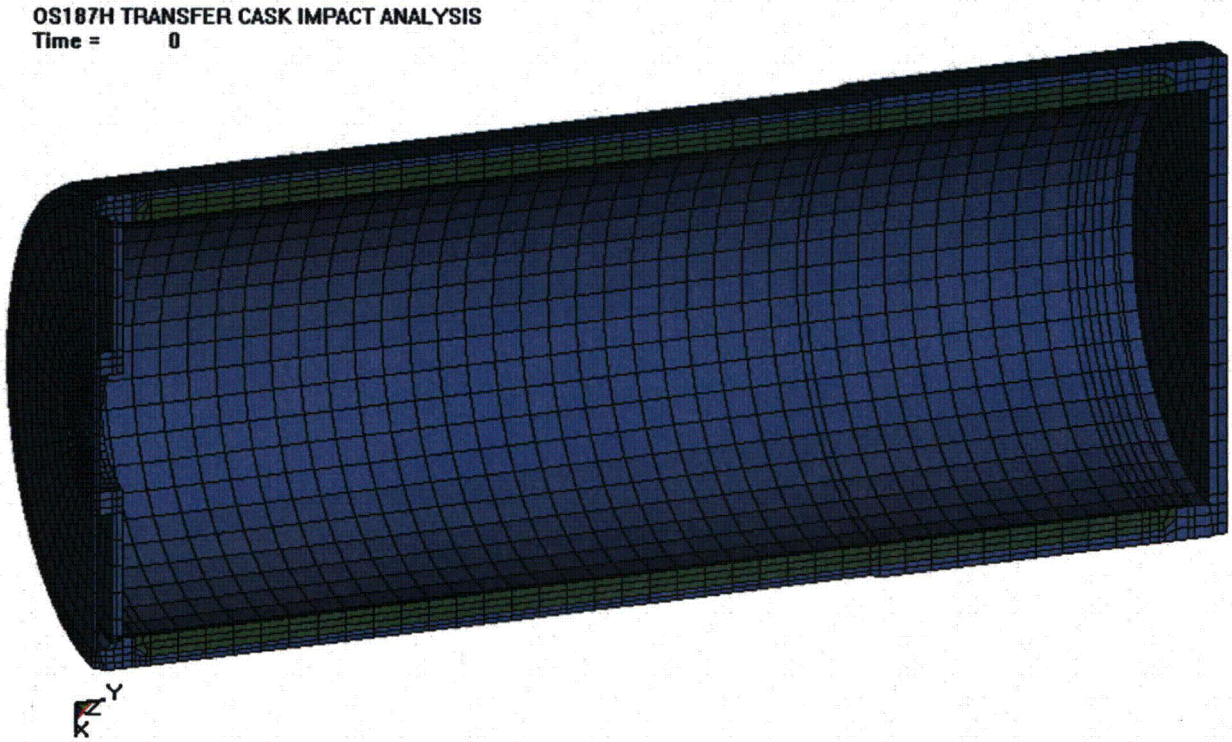

Figure 3.9.10-10
OS187H Transfer Cask Finite Element Model without the Internals

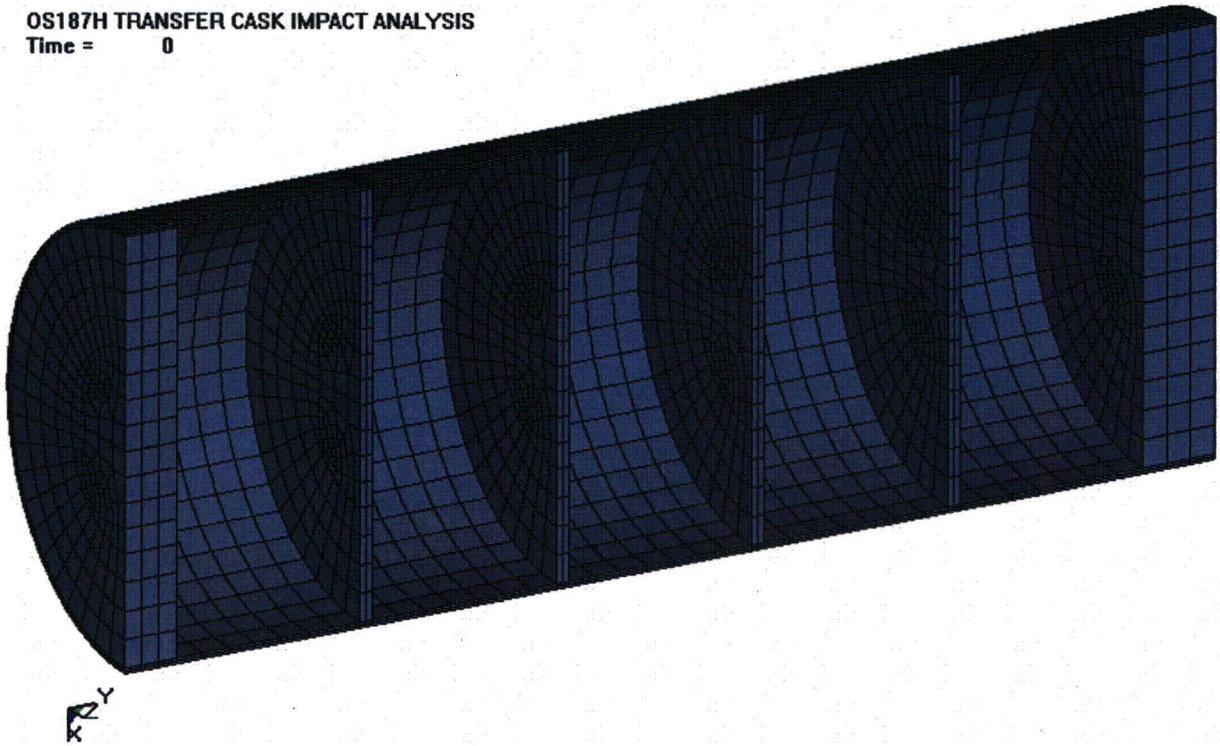

Figure 3.9.10-11
OS187H Transfer Cask Internals Finite Element Model

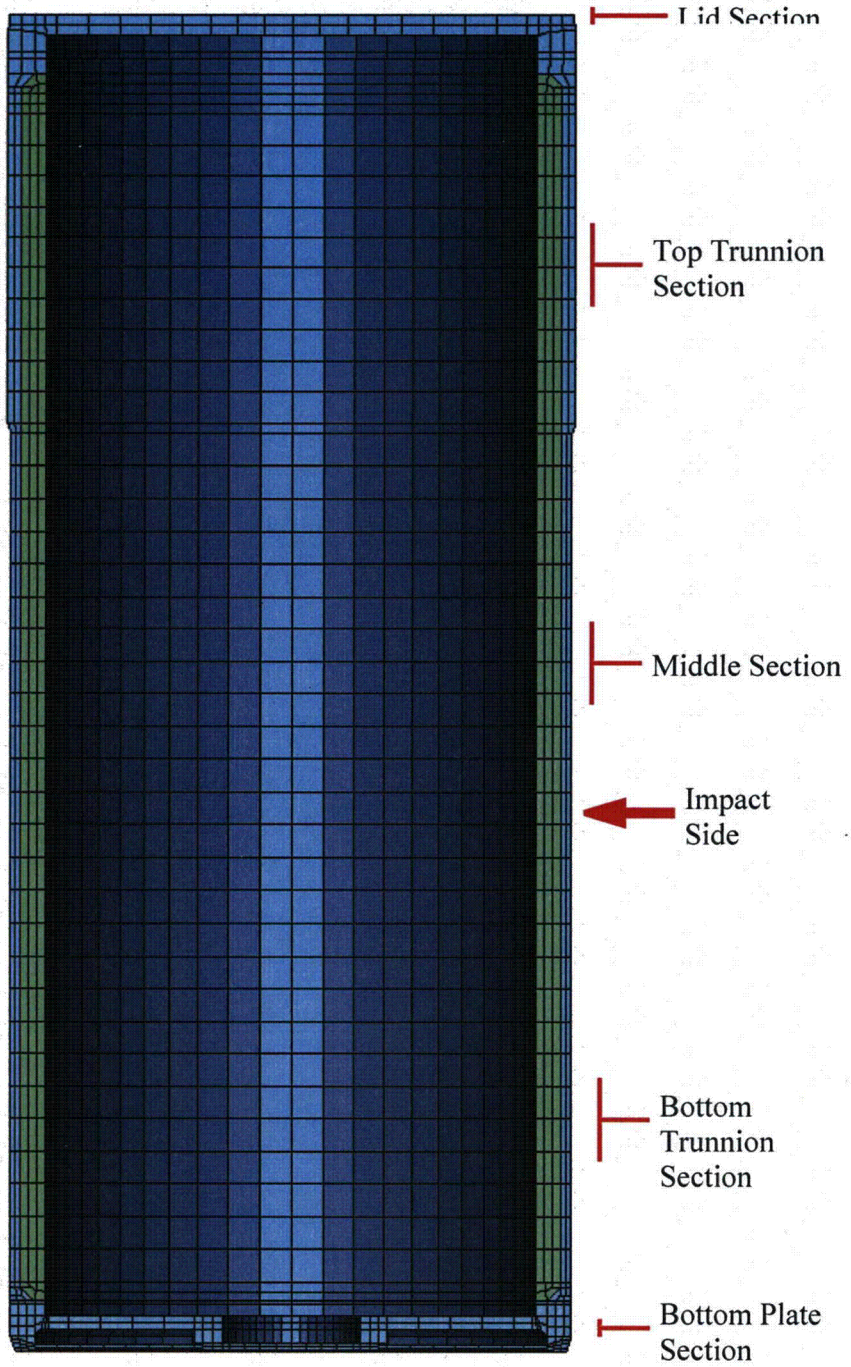

Figure 3.9.10-12
OS187H Transfer Cask Side Drop Nodal Sections Analyzed

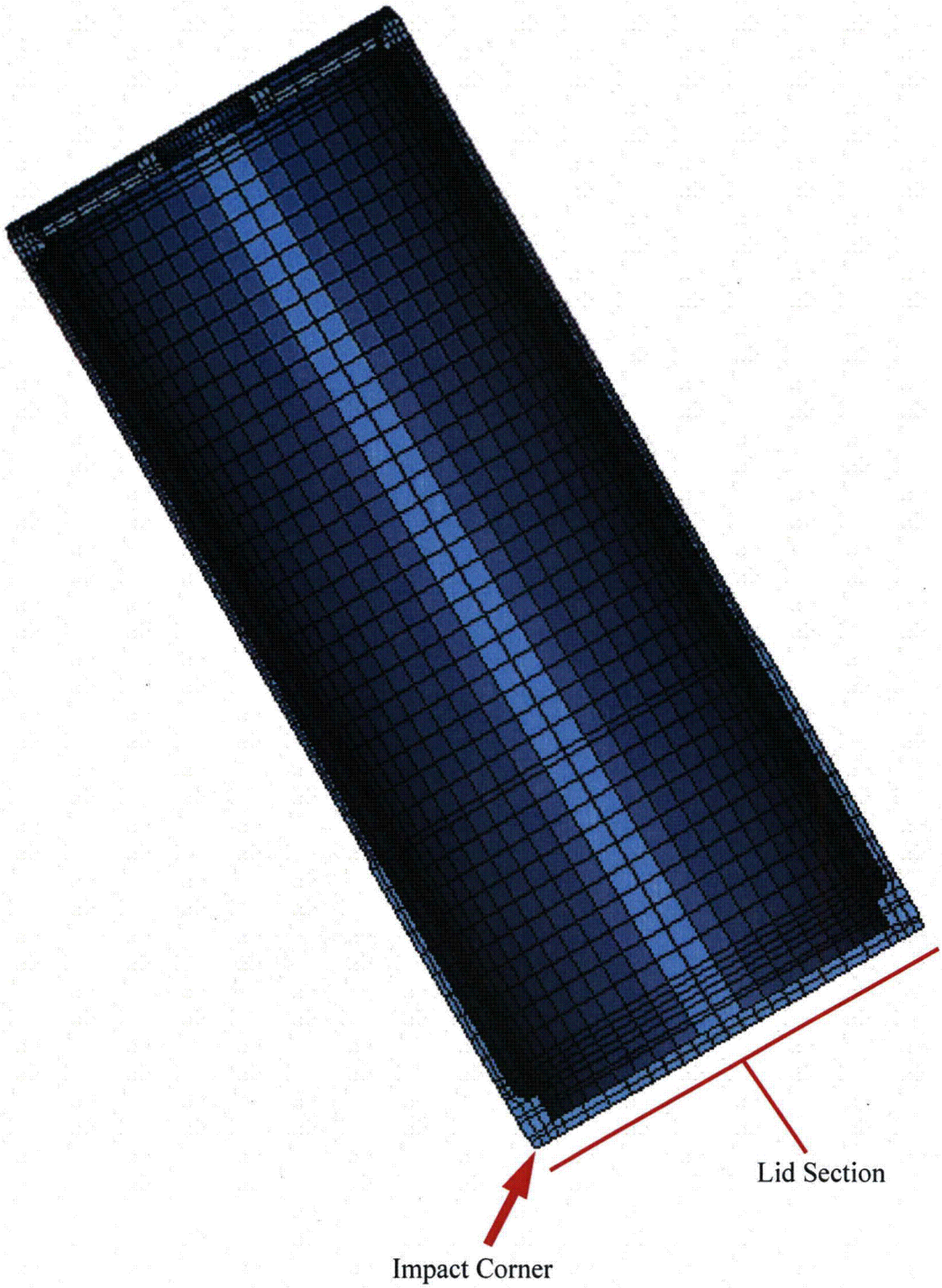

Figure 3.9.10-13
OS187H Transfer Cask CG Over Corner Drop Nodal Sections Analyzed

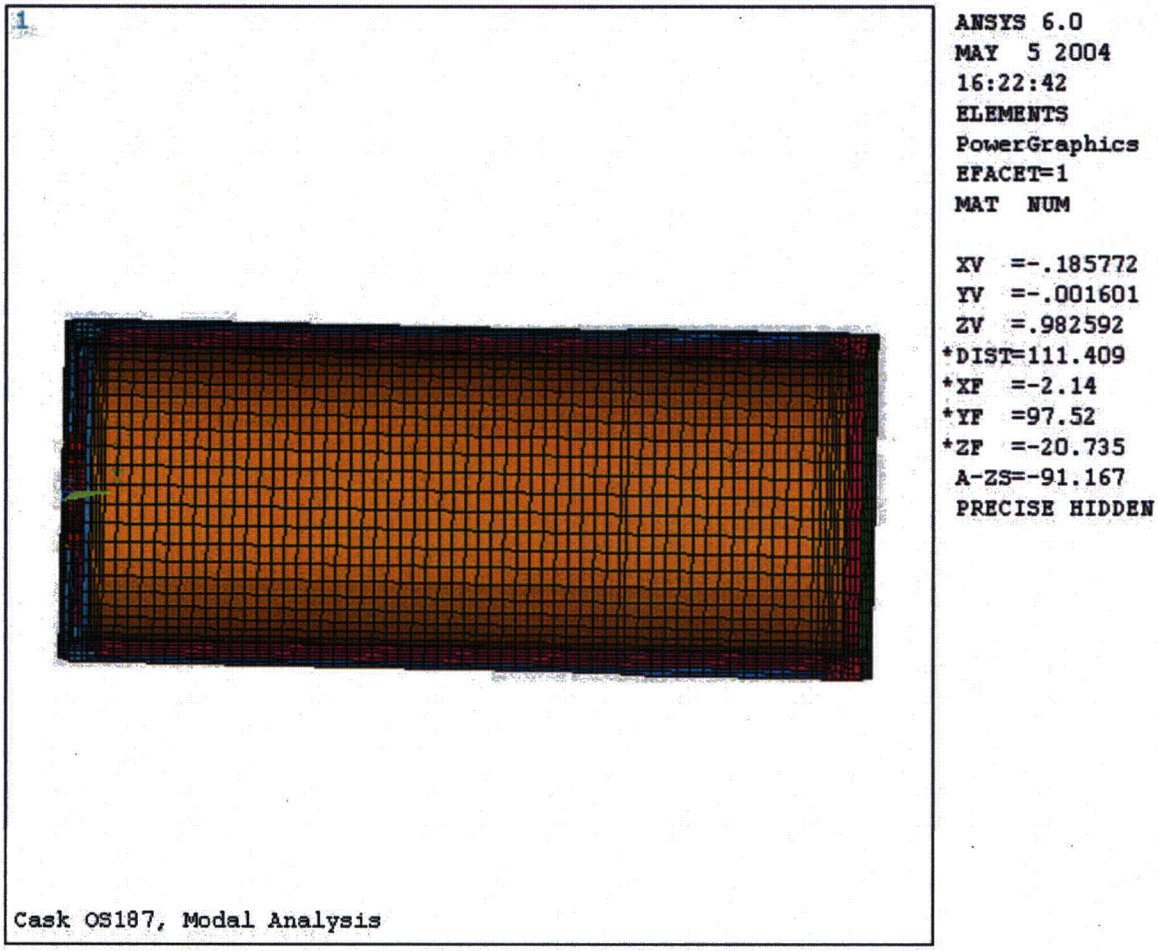

Figure 3.9.10-14
OS187H Transfer Cask Finite Element Model used for Modal Analysis, Elements

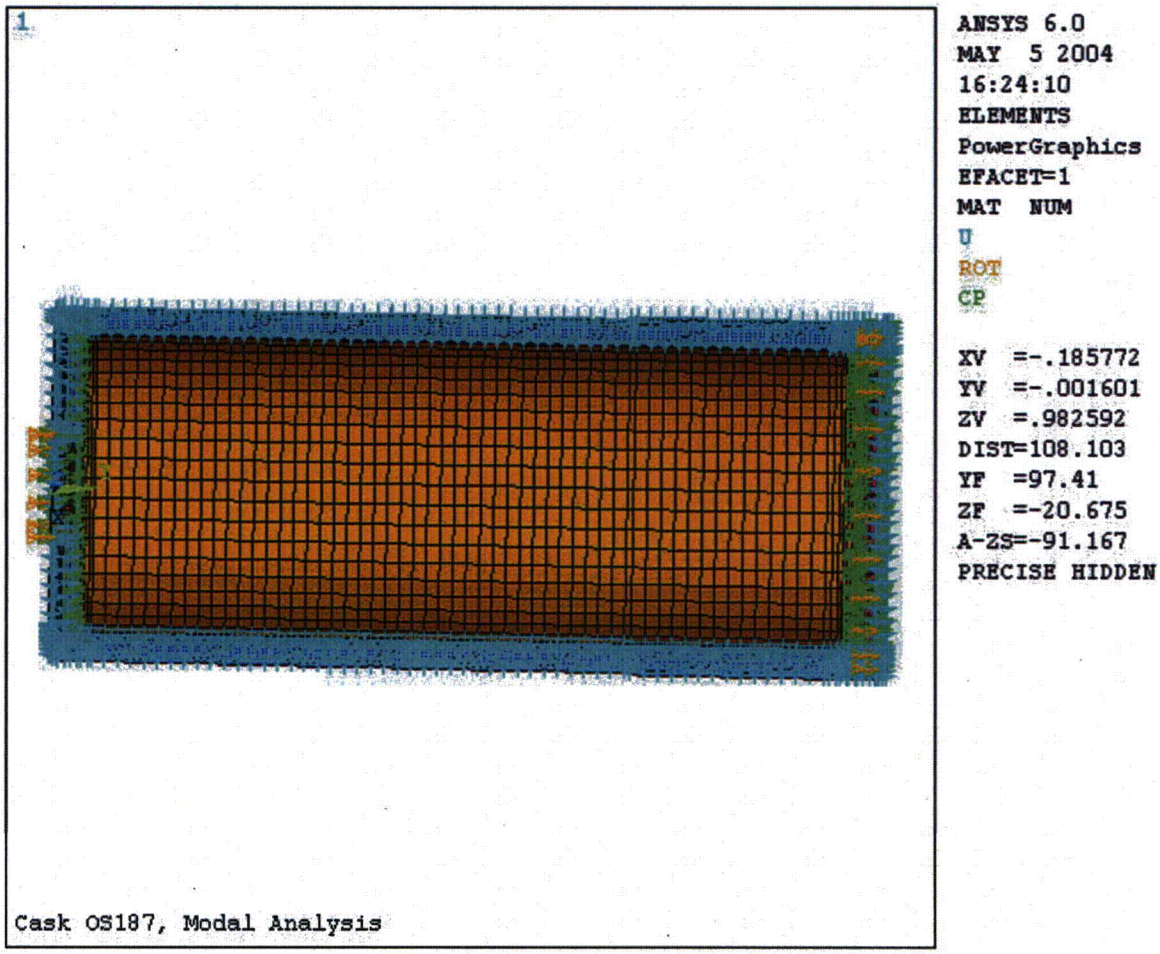

Figure 3.9.10-15
OS187H Transfer Cask Finite Element Model used for Modal Analysis, Boundary Conditions

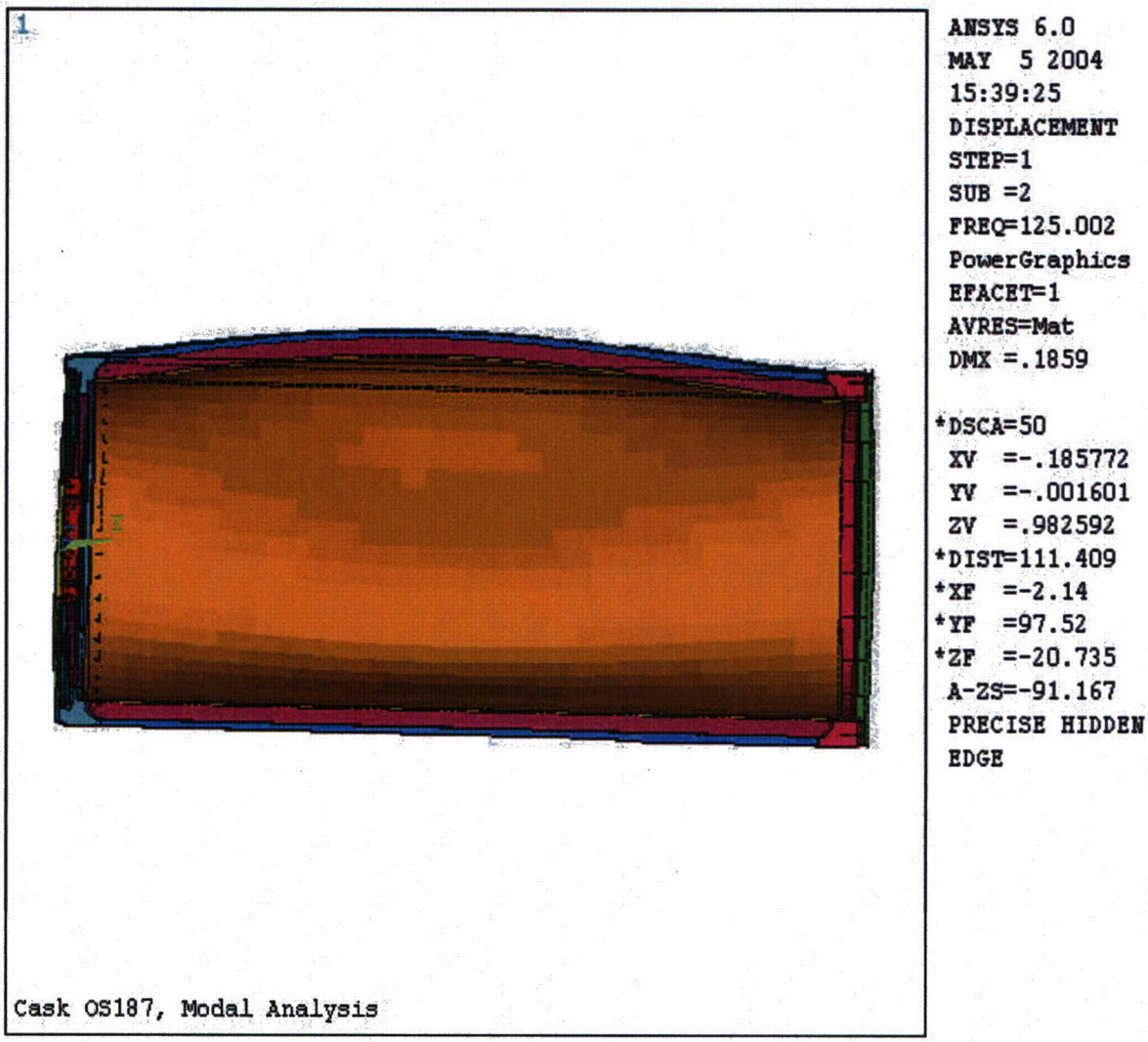

Figure 3.9.10-16
OS187H Transfer Cask Deformed Shape – Mode 2

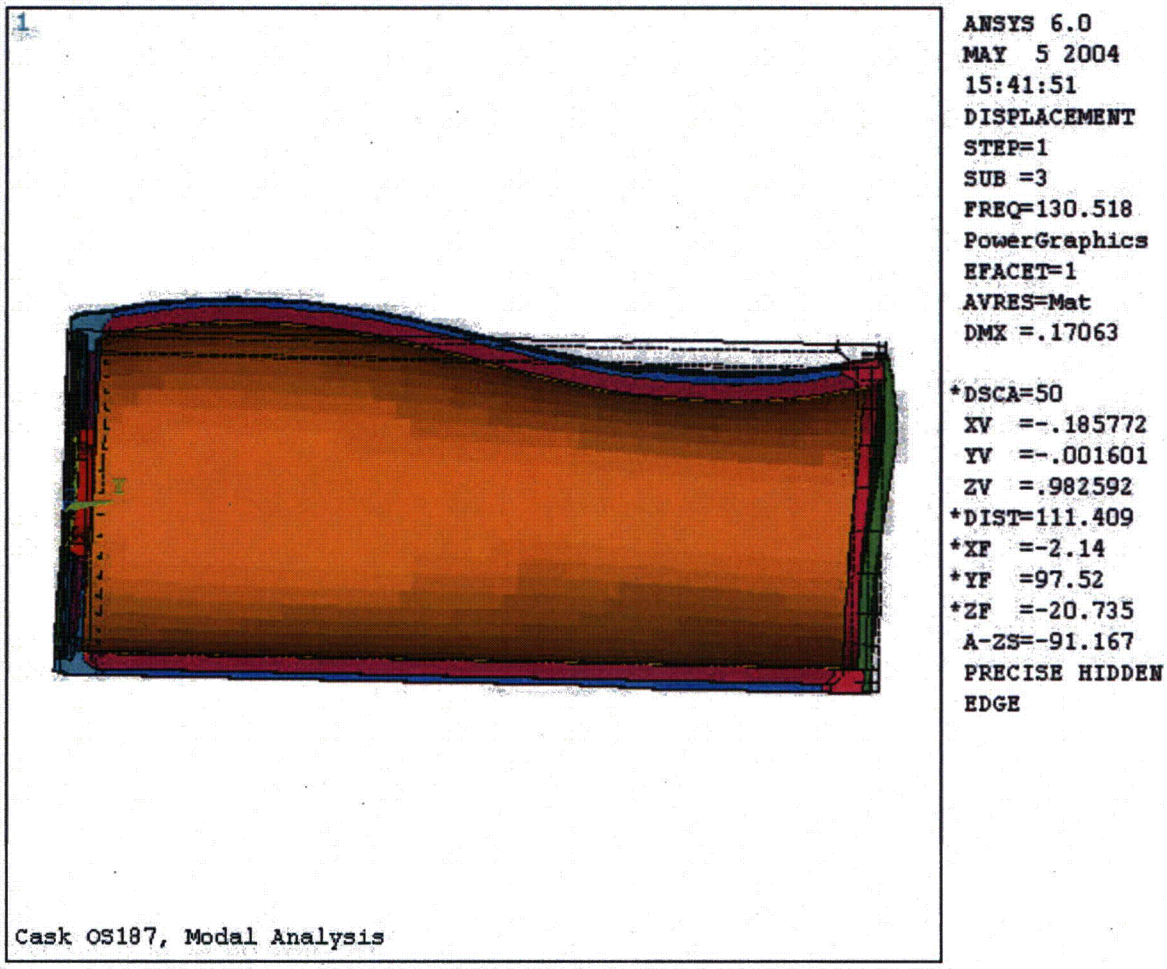

Figure 3.9.10-17
OS187H Transfer Cask Deformed Shape – Mode 3

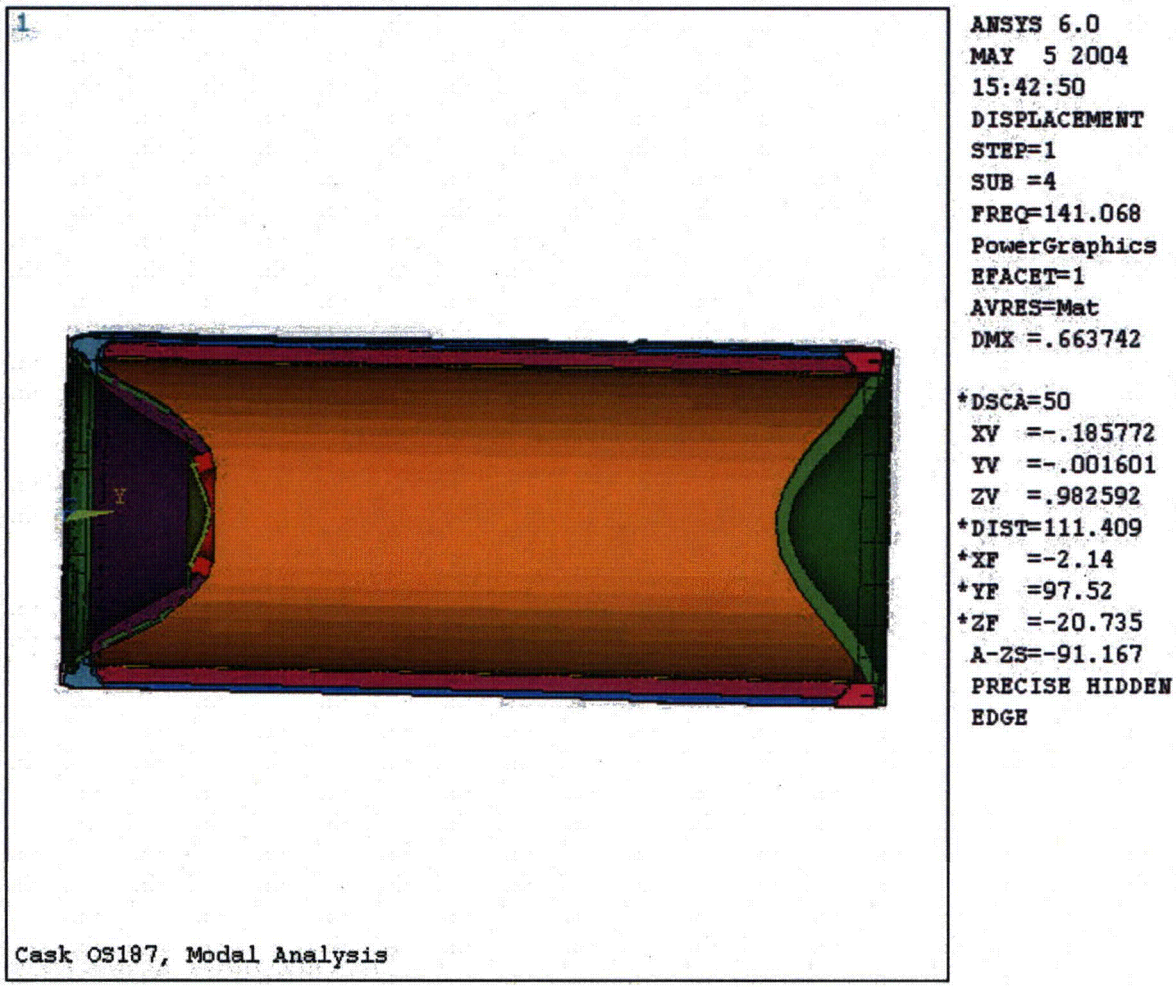

Figure 3.9.10-18
OS187H Transfer Cask Deformed Shape – Mode 4

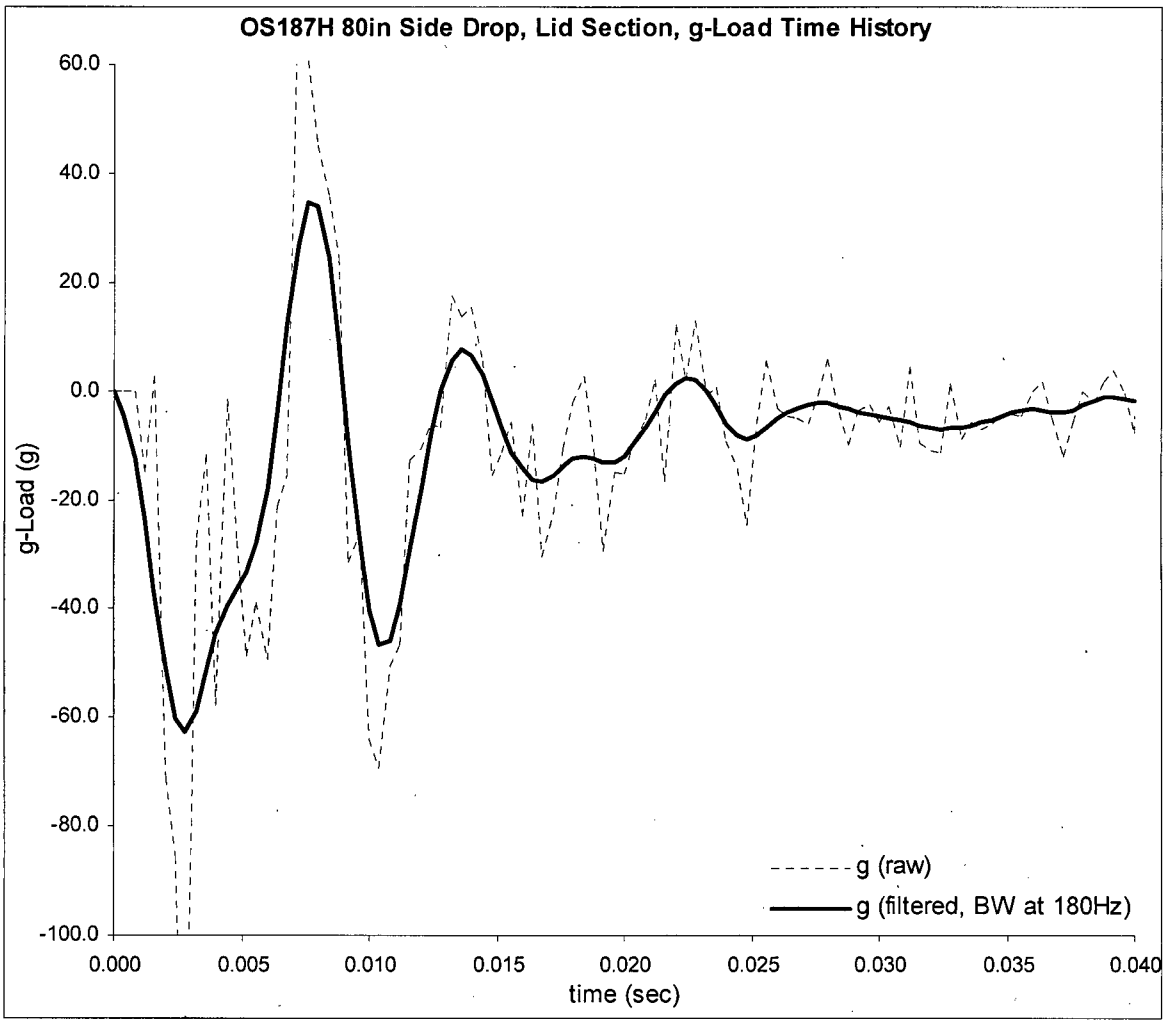

Figure 3.9.10-19
OS187H Transfer Cask, Side Drop,
Lid Section Acceleration Time History

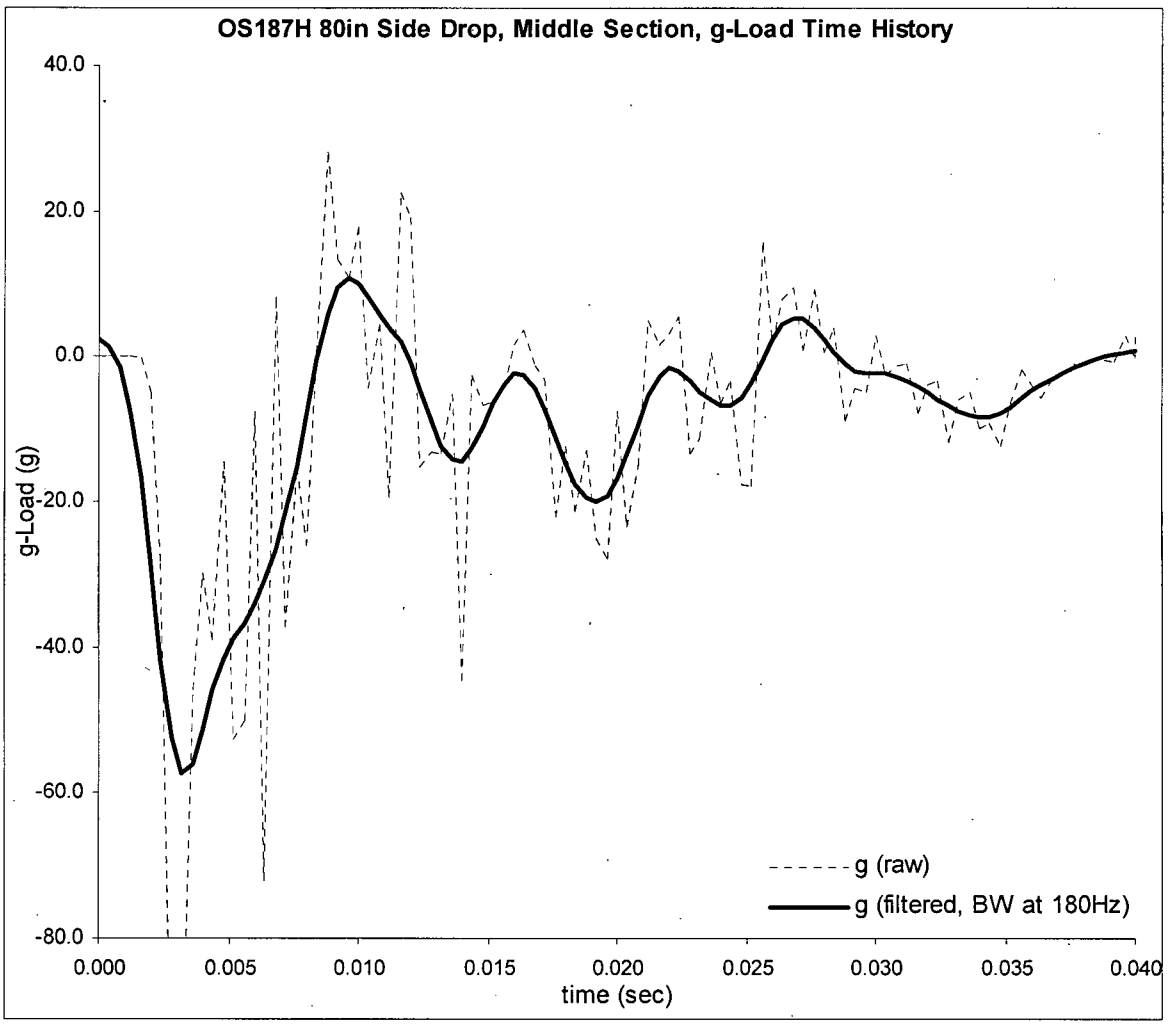

Figure 3.9.10-20
OS187H Transfer Cask, Side Drop,
Middle Section Acceleration Time History

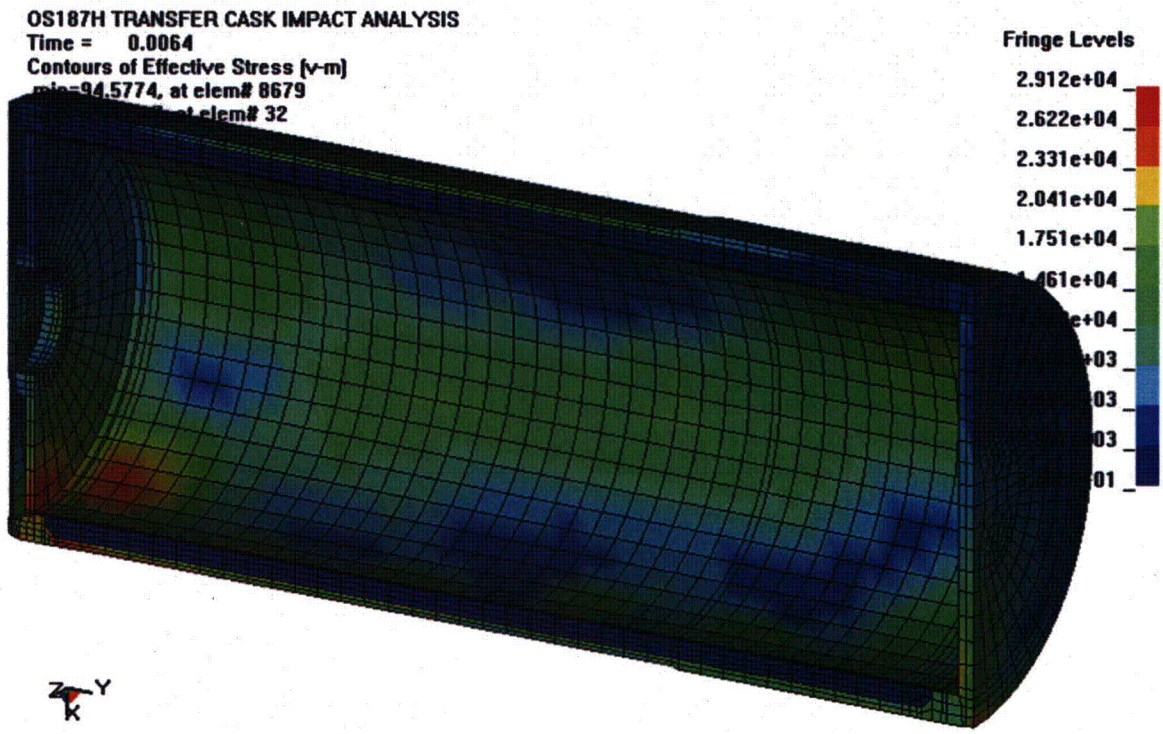

Figure 3.9.10-21
OS187H Transfer Cask, Side Drop,
Maximum Effective Stress Distribution

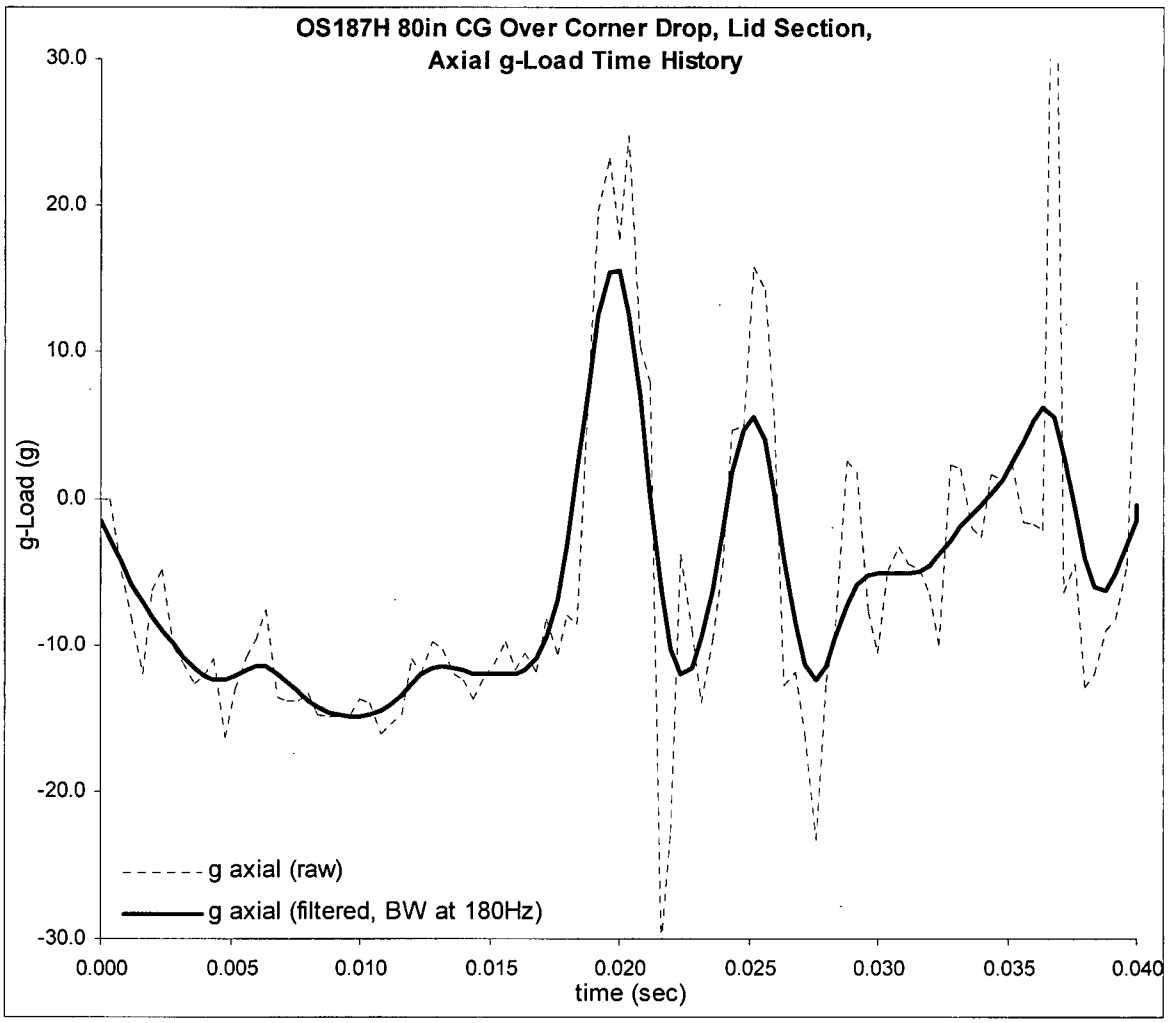

Figure 3.9.10-22
OS187H Transfer Cask, CG Over Corner Drop,
Lid Section Axial Acceleration Time History

Figure 3.9.10-23
OS187H Transfer Cask, CG Over Corner Drop,
Maximum Effective Stress Distribution